January 2018

# Calibration Of Calcic Pyroxenes For Interpreting Meteorite And Asteroid Spectra

Margaret Dievendorf

Follow this and additional works at: https://commons.und.edu/theses

CALIBRATION OF CALCIC PYROXENES FOR INTERPRETING METEORITE AND
ASTEROID SPECTRA


by


Margaret Elaine Dievendorf

Bachelor of Arts, Colgate University, 2013




A Thesis

Submitted to the Graduate Faculty

Of the

University of North Dakota
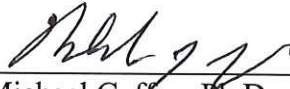
In partial fulfillment of the requirements


For the degree of

Master of Science


Grand Forks, North Dakota

December
2018
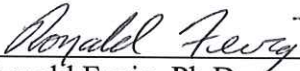
This thesis, submitted by Margaret Dievendorf in partial fulfillment of the requirements for the Degree of Master of Science from the University of North Dakota, has been read by the Faculty Advisory Committee under whom the work has been done and is hereby approved.

Michael Gaffey, Ph.D.

Edward Cloutis, Ph.D.

Ronald Fevig, Ph.D.

This thesis is being submitted by the appointed advisory committee as having met all of the requirements of the School of Graduate Studies at the University of North Dakota and is hereby approved.

Grant McGimpsey
Dean of the School of Graduate Studies

November 28, 2018
Date

iii

PERMISSION

Title        Calibration of Calcic Pyroxenes for Interpreting Meteorite and Asteroid Spectra

Department   Space Studies

Degree       Master of Science


In presenting this thesis in partial fulfillment of the requirements for a graduate degree from the University of North Dakota, I agree that the library of this University shall make it freely available for inspection.  I further agree that permission for extensive copying for scholarly purposes may be granted by the professor who supervised my thesis work or, in his absence, by the Chairperson of the department or dean of the School of Graduate studies.  It is understood that any financial gain shall not be allowed without my written permission.  It is also understood that due recognition shall be given to me and to the University of North Dakota in any scholarly use which may be made of any material in my thesis.

<div align="right">Margaret Dievendorf<br>10/5/2018</div>

# Table of Contents

# Table of Figures

ACKNOWLEDGEMENTS

To my parents, Chuck and Jane.

ABSTRACT


Calcic pyroxenes are a group of silicate minerals that are found in meteorite and asteroid spectra. I investigated the relationship of high-calcium clinopyroxenes in comparison with orthopyroxenes, pigeonites, mixtures, and the meteorite group of angrites to try to find any trends for spectral calibrations. I used spectra from HOSERLab, RELAB, and the USGS Spectral Library. The main band minima of pyroxenes in spectra are around 0.9 or 1 µm for band I and 1.15 or 2 µm for band II, with the former minima for type A clinopyroxenes and the latter for type B. Using sample minima found from both lowest reflectances and polynomial fittings, I graphed the different pyroxene features to view possible trends from band positions and calcium, iron, and magnesium abundances. The type B clinopyroxenes continued on previous trends found in the literature, having a stronger band position relationship for the iron and calcium contents than the type A clinopyroxene samples. However, their band position relationships with iron and calcium were much less linear than the orthopyroxenes, which has also been seen previously in the literature. The two main band minima found from the different methods were similar in band position for band I, while due to noise and slope, the band II features were more diverse. I also examined how calcic clinopyroxenes interacted in comparison to other minerals in mixtures. There did not appear to be a trend for the type A clinopyroxenes, although it was also complicated by the larger error in band positions from reddened slopes and faintness. When in mixtures with orthopyroxene and/or olivine there needed to be a large amount, usually around $\geq$ 70 % calcic pyroxene, before the minima could be found. Angrite spectra were also looked at

because they typically have a large amount of calcic clinopyroxene, including type A, although usually with larger amounts of titanium and aluminum. There were limited samples so I was unable to find any trends from them, but I investigated a set of mixtures from Cloutis et al. (2006a) and a set made for this study from HOSERLab that were made to resemble possible angrite and angrite parent-body spectra. From these, more data were available to show how a combined 1 μm feature from type A high-calcium pyroxene and olivine changes with differing amounts of both.

# Introduction

There are currently hundreds of thousands of known asteroids, with more being discovered each year. While most lie in the asteroid belt between Mars and Jupiter at 2.1-3.3 astronomical units (AU), a sizable population also surrounds the Earth, called Near-Earth Asteroids (NEAs). There are other smaller populations scattered between 1.52-5.2 AU (Gaffey et al. 1993b; Gaffey 1997; McSween 1999; Gaffey 2011). The largest asteroids are less than one thousand kilometers in diameter, while most are much smaller (Gaffey 2011). So far, scientific expeditions have sent spacecraft to orbit and fly by only twelve asteroids and rendezvous with two (Abe et al. 2006; Granahan 2011). Two new missions are coming up or are in progress: Hayabusa-2 and OSIRIS-REx (McSween 1999; Schweickart et al. 2003; Pinilla-Alonso et al. 2013; King et al. 2015). To find information on asteroids, scientists use remote sensing spectroscopy as a way to determine an asteroid's composition, mineralogy, and petrology (Gaffey 2011). This will continue to be an important investigative tool even with more asteroid rendezvous, as the number of asteroids known are too numerous to visit each individually (McSween 1999).

Knowing an asteroid's composition, mineralogy, and petrology is important for learning about the formation of life, potential asteroid mining locations, deflection of hazardous NEAs, and the formation of our solar system. One of the reasons is because of life in the universe, as certain asteroids contain organics and water which, through impacts, may have potentially contributed to life starting on Earth (Gaffey 1997-references Dreibus & Wanke 1989, Ahrens et al. 1989; McSween 1999; Gaffey 2011). The minerals I am looking at in asteroids and meteorites are anhydrous and have experienced varying amounts of heating, but there are more primitive, unmelted types that have undergone aqueous alteration. If asteroids were involved with

providing materials for starting life on Earth, then that also brings up the possibility of panspermia, which would have powerful implications for possible life throughout our solar system (McSween 1999).

Besides panspermia, there are the intriguing new mining possibilities on asteroids, leading to a potential new business sector. Many asteroids are very reachable, requiring less energy than going to the Moon (McSween 1999; Blaire 2000; Gaffey 2011). Even small asteroids tens of kilometers across have many metals and minerals on them that are not common or that cost a lot to extract on Earth (Gertsch et al. 1997; Blaire 2000; Gaffey 2011). By bringing them to Earth, the prices for these commodities would drop and destabilize; however, more people could afford them, possibly promoting infrastructure and technology advances (Gertsch et al. 1997; Blaire 2000). There is also the possibility of keeping these materials in space as a way to create in situ factories for producing spacecraft parts for future missions (Gertsch et al. 1997). Since lifting materials into space costs enormous amounts of money, having the potential to make some of the heavier pieces of equipment in space, such as in Low Earth Orbit, would be a possible lucrative business as well (Gertsch et al. 1997; Blaire 2000). As will be seen below, I have been mainly looking at pyroxenes, which are a type of chain silicate. While these among themselves may not have many uses for mining besides being some basic "industrial materials" or perhaps being used as radiation shields, they are still important for determining the make-up of asteroid mining candidates (Gertsch et al. 1997; Nesse 2012, p.211). Diopside, a type of high-calcium clinopyroxene, can also possibly be used in ceramics, such as for dental products (Nesse 2012, p.302).

Some of the theorized asteroid mining methods are being developed so that they could also potentially divert an asteroid that is heading towards the Earth. There have been large

impacts in the past, such as can be seen from Meteor Crater, the Tunguska event, and the Cretaceous-Tertiary extinction (McSween 1999; Schweickart et al. 2003; Gaffey 2011). These occur less frequently but still have non-negligible odds of happening. Schweickart et al. (2003) have the chances of a Tunguska-sized (60 meter-produced 3-5 Mt of energy) asteroid and 100 meter sized asteroid hitting the Earth within this century as being around ten and two percent, respectively (Harris et al. 2015-references Boslough & Crawford 2008). For an asteroid over one kilometer in size, which would destroy most life on Earth, the odds are one in 5,000 of occurring within this same time frame (Schweickart et al. 2003). In 2000, an event with odds of occurring once a year happened when a meteor blew up over the Yukon; it was only two to three meters in diameter, but it still created "a force equivalent to four or five kilotons of TNT," (Schweickart et al. 2003). More recently, a potentially devastating meteorite exploded over Chelyabinsk in Russia, with a likely kinetic yield of 400-500 kt (Reddy et al. 2014-references Brown et al. 2013; Harris et al. 2015-references Brown et al. 2013; https://cneos.jpl.nasa.gov/). Harris et al. (2015) have the odds of Tunguska and Chelyabinsk events occurring as one in five hundred years and one in fifty years, respectively. In 2013, and beyond, we are still discovering new NEAs, some of which we haven't seen until they were too close, such as in Russia. Unlike in the movies, exploding an asteroid with a nuclear bomb will likely cause more problems. The bomb could break up the asteroid into several large pieces, or the asteroid itself could be a rubble pile that would absorb the effects from the bomb. In both of these scenarios, the asteroid keeps going towards the Earth (Holsapple 2002; Schweickart et al. 2003; Harris et al. 2015). Different ideas to deter asteroids have been presented, including some that can also work in combination with mining (Gertsch et al 1997; Schweickart et al. 2003). One of these ideas involves the use of a space tug to alter the asteroid's Earth-hitting orbit, while another has a gravitational tractor to

tow the asteroid away (Schweickart et al. 2003; Lu & Love 2005). Since asteroids have different compositions, knowing an effective mitigation technique requires knowledge of what the asteroid is made of through spectroscopy and rendezvous (Schweickart et al. 2003; Gaffey 2011; Harris et al. 2015).

The main importance of learning asteroid compositions, mineralogy, and petrology is because asteroids tell us about the history of the solar system and minor planet formation and evolution (Gaffey et al. 1993b; Gaffey 2011). Despite being called the "vermin of the skies" by astronomers for many decades, asteroids are useful (McSween 1999 p.79). They are some of the only remaining in situ pieces of evidence in our solar system (Gaffey et al. 2002; Gaffey 2011). Using the information we gather from asteroids creates a map of where things occurred, since asteroids, unlike meteorites, are not thought to have moved very far since formation. Meteorites that have landed on Earth give a timeline to add to this map, since most are pieces from asteroids. Both contribute data that can be used in the solar system formation models (McSween 1999; Gaffey et al. 2002; Sunshine et al. 2004; Gaffey 2011; Grady et al. 2015 p.1). For instance, the meteorites and asteroids give us clues about the heating of the solar nebula and how it was not as isotopically homogeneous as previously thought (Gaffey 1997; McSween 1999). This research can help us learn more about how the Earth formed as well, since Earth undergoes constant geologic processes that destroy and alter the older rocks (Gaffey et al. 1993b; McCoy et al. 2006).

Using these important fields of research for motivation, I looked at predominantly high-calcium pyroxenes in sample, mixture, and meteorite spectra. By studying the changes in spectra minima of the major pyroxene bands, I hoped to learn if there were any possible relationships when high-calcium pyroxenes were incorporated into mixture and meteorite spectra. By looking

at these possible changes, I hoped to contribute band minima data, as there are limited high-calcium pyroxene data in the literature. I also hoped these minima and information from mixtures could eventually aid in meteorite and asteroid classifications, as many types have high-calcium pyroxenes in their mineralogies.

## Pyroxene Spectroscopy

Spectroscopy uses the electromagnetic spectrum that ranges from cosmic rays to radio waves (Gaffey 2011). Specific minerals and elements within absorb light at certain wavelengths depending on their valence state, their coordination site, and the distortion of the crystal structure (Burns 1993; McSween 1999; Gaffey 2011-references Burns 1970, 1993). The main areas of the electromagnetic spectrum that are useful for determining asteroid compositions are the visible and near-infrared, typically from 0.4 to 2.5 microns (μm) as a minimum range (Gaffey 2011). Since asteroids do not emit their own light, scientists use the reflected light from the sun on the asteroid to obtain reflectance spectra in the visible and near-infrared wavelength range (Burns 1993; Gaffey et al. 1993b; McSween 1999; Gaffey 2011). "The measurable reflected flux depends on the incident sunlight (proportional to the inverse square of the asteroid's heliocentric distance), on the inverse square of the asteroid-Earth distance, on the illuminated and observed surface area of the asteroid, and on the surface albedo of the asteroid," (Gaffey et al. 1993b). Outside of the 0.3-2.6 µm range has Earth's atmospheric absorption problems when observing asteroids and other remote objects (Burns 1993; Gaffey 2011). Between this range, the solar flux is high (Cloutis & Gaffey 1991). The vast majority of asteroids have experienced many impacts and therefore are in pieces and/or have regoliths that can sample what the asteroids are made of, even if the remote sensing is just sensing the "surface" (Gaffey et al. 1993a; Pompilio et al. 2007; Gaffey 2011).

Using crystal field theory and knowledge of mineralogy, one can use spectroscopy to determine the mineralogy, compositions, and petrology of asteroids. Band positions are one of the most important determinants of composition, as these do not change with different albedos, grain sizes, or phase angles. The band positions only change with different compositions, such as differing amounts of iron (Gaffey 2011). Exceptions are made at high temperatures, as the two micron band shifts to slightly longer and shorter wavelengths in orthopyroxenes and clinopyroxenes, respectively (Singer & Roush 1985; Burns 1993). However, asteroids, at around 175 K, are not at temperatures up to 450 K as they were in Singer and Roush (1985) (Burns 1993; Moriarty & Pieters 2016). Also, the samples I am looking at are measured at room temperature, therefore this will likely not cause any issues. There are both band minima and band centers. Band minima are the lowest reflectances in a feature. They are the same as band centers if there is a level continuum, but move towards the "down slope" direction if the continuum has a slope (Gaffey 2011). Another measurement that is used to help identify the makeup of asteroids is the band area ratio (BAR). Like band positions, these are also mostly insensitive to particle size; however it can only be used with olivine-orthopyroxene mixtures (Cloutis et al. 1986). Band width, another parameter, varies with the amount of certain elements, grain sizes, viewing geometry, phase angle, body shape, crystallinity, and temperature (Burns 1993; Gaffey 2011-references Roush 1984, Roush & Singer 1986, Lucey et al. 1998, Moroz et al. 2000, Hinrichs & Lucey 2002, Gradie & Veverka 1981, 1982, 1986, Clark et al. 2002). It also can depend on "the composition of the sample, the absorption site, and the partitioning of ions in different sites," (Sunshine & Pieters 1993).

Some of the most important minerals on asteroids are pyroxenes. Not only are they extremely common on most types, they also have very strong spectral signatures. This is

6

important for distinguishing pyroxenes among the mixtures of different minerals that make up

asteroid rocks (Cloutis et al. 1986; Sunshine & Pieters 1993; McSween 1999; Klima et al. 2011;

Gaffey 2011). Pyroxenes are chain silicates that incorporate elements in their eight-fold, six-fold,

or tetrahedral coordination sites (Burns 1970; Nesse 2012, p.294-295). The general formula is

$XYZ_2O_6$, with Z in the tetrahedral site usually being silicon ($Si^{4+}$) or sometimes aluminum

($Al^{3+}$); X in the M2 site usually being either magnesium ($Mg^{2+}$), ferrous iron ($Fe^{2+}$), or calcium

($Ca^{2+}$); and Y in the M1 site usually being $Mg^{2+}$, $Fe^{2+}$, ferric iron ($Fe^{3+}$), or $Al^{3+}$, with other

possible substitutions for all three sites (Burns 1970; Cameron & Papike-Prewitt-1980; Nesse

2012, p.294-295). Pyroxenes are mafic silicates and are generally found in basaltic and gabbroic

rocks (Nesse 2012, p.215). With asteroidal surfaces and compositions, I am focused on its

origins from basalts, which are extrusive igneous rocks that cool more rapidly than intrusive

rocks like gabbros (Winter 2010, p.28-29). As such, pyroxenes are particularly important

because they can give information to the thermal history of an asteroid (Cloutis & Gaffey 1991).

Since most asteroids are believed to have experienced heating, as mentioned below, pyroxenes

are very useful (Gaffey 2011-references Keil 2000). Pyroxenes are usually graphed on a

triangular diagram with endmembers of wollastonite (Wo = $Ca_2Si_2O_6$), enstatite (En =

$Mg_2Si_2O_6$), and ferrosilite (Fs = $Fe_2Si_2O_6$) (Nesse 2012, p.295). However wollastonite is a

pyroxenoid, which has distorted silicate chains, so the diagram usually gets shortened to a

trapezoid, with the top line around $Wo_{50}$ (Cameron & Papike-Prewitt 1980; Nesse 2012, p.295).

There are some sodic pyroxenes as well, but I am not going to focus on those, as they are less

common (Nesse 2012, p.296). In addition, there are several types of pyroxenes, the two main

groups being orthopyroxenes and clinopyroxenes. The names come from their crystal systems,

being orthorhombic and monoclinic, respectively (Nesse 2012, p.295-300). Orthopyroxenes

usually contain iron and magnesium, with occasionally up to five percent calcium (Morimoto et al. 1988). Clinopyroxenes incorporate iron and magnesium as well, but can include up to 50 % calcium, along with the silicate tetrahedra (Morimoto et al. 1988). In addition, clinopyroxenes have two space groups, based on symmetry: $P2_1/c$ and $C2/c$. High-calcium pyroxenes are in the $C2/c$ group. Lower-calcium clinopyroxenes are usually in the $P2_1/c$ group, unlike orthopyroxenes which typically are restricted to Pbca (Klima et al. 2011). Figure 1 is from Klima et al. (2011) and shows the pyroxene quadrilateral and the different space groups.
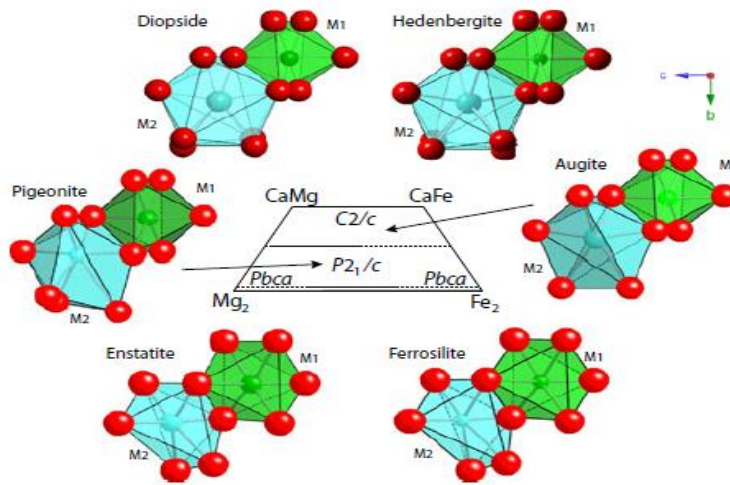


Figure 1. The pyroxene quadrilateral and different space groups from Klima et al. (2011).

Understanding of coordination sites and spectral features come from crystal field theory. "In the crystal field theory, which is an offshoot of the electrostatic theory, interactions between the transition metal ion and surrounding anions or dipolar molecules (ligands) are regarded as purely electrostatic forces, and ligand atoms are treated as point negative charges," (Burns 1970 p.2). Certain elements have partially filled degenerate d orbitals that split into different energy levels when a transition metal ion is in a crystal structure (Burns 1970; Burns 1993; Clark 1995). These transition metals are usually titanium (Ti), vanadium (V), chromium (Cr), manganese

(Mn), iron (Fe), cobalt (Co), nickel (Ni), and copper (Cu) (Burns 1970 p.1; Burns 1993; Nesse, 2012 p.126). These different energy levels form the features that tell us what mineral is in a spectrum and even what specific elements are in that mineral (Clark 1995; Nesse 2012 p.126). "The energy levels are determined by the valence state of the atom (e.g. $Fe^{2+}$, $Fe^{3+}$), its coordination number, and the symmetry of the site it occupies," along with ligand types, site distortion, and metal-ligand interatomic distance (Burns 1970; Burns 1993; Clark 1995). When the d-levels split into different energy levels in octahedral coordination, they split into two main groups of d electrons: one group that reaches towards the oxygen ligands and one group that reaches towards the spaces in between the oxygen ligands (Burns 1970; Burns 1993). The first group mentioned has a higher energy level and destabilizes the ion when electrons are present, while the second group is made of three orbitals that have less energy and stabilize the ion when electrons are there (Burns 1970; Burns 1993). The electron placement results in the crystal field stabilization energy (CFSE) (Burns 1970; Burns 1993). Iron (both ferric and ferrous) is one of the transition metals that can have both low- and high-spin states in octahedral sites, depending on the pairing energy of the electrons (Burns 1970). The excitation of electrons among the d orbitals causes some absorption features that are related to the energy of the change in energy levels (Burns 1970; Burns 1993). With pyroxenes, the predominant two features are from the ferrous iron transitions that are in centrosymmetric sites (Adams 1975; Cloutis 2002; Gaffey 2011-ref Burns 1970, 1993). Burns (1970, 1993) only has the M1 site being centrosymmetric, however. Elements like silicon, aluminum, magnesium, oxygen, and calcium do not have features between 0.3-2.6 µm, particularly because of the lack of d level electrons, although they can still contribute to the features and other spectral changes, as is talked about below (Hunt 1977).

Adams (1974-references Adams 1968, McCord 1968) was one of the first papers to attribute the crystal field theory of pyroxene spectra as a possible application to asteroids and other objects through remote sensing. Previous studies had mainly dealt with polarized transmission spectra; it was determined that diffuse reflectance spectra show the main two absorption features of pyroxenes as well (Adams 1974-references White & Keester 1966, Adams & Filice 1967, Adams & McCord 1972, Lewis & White 1974; Adams 1975-references White & Keester 1966, Adams & Filice 1967). The samples that I observed for this research were diffuse reflectance spectra from powdered pyroxene samples. Previous studies had mainly been looking at the Moon; not many attempts had yet been made with remote sensing to determine asteroid compositions (Adams 1974-references McCord et al. 1972, Adams & McCord 1970, 1972, 1973, McCord & Adams 1973, Pieters et al. 1973, Gaffey 1973, Chapman & Salisbury 1973, Charette et al. 1974, Adams et al. 1974). Adams' graphs (1974 Fig. 1, 1975 Fig. 11) of the different minerals and their features are the basis for my graphs further on in this paper. For these, he plotted each feature of a mineral's spectrum against all the other features in their individual spectra. In this way one can see the different groups that cluster around each other and compare the different types to one another.

Clinopyroxenes have two coordination sites in addition to their silicate tetrahedra. Generally in these the M1 site is in octahedral coordination, being more distorted than the M1 site in orthopyroxenes, while the M2 site is in very distorted eight-fold coordination (Burns 1970-references Warren & Bragg 1929; Burns 1993; Papike 1996; Klima et al. 2011; Nesse 2012 p.294-295). In other clinopyroxenes with smaller cations, this M2 site can be in six-fold coordination as well (Burns 1970; Papike 1996). This is in comparison to orthopyroxenes, where both the M1 and M2 sites are generally in (six-fold) octahedral coordination, with M2 being

distorted (Burns 1970; Cameron & Papike-Prewitt 1980; Papike 1996; Nesse 2012 p.294-295).

These different coordination sites help distinguish between these two general types and are critical for identifying pyroxenes in spectra. These sites contribute to the spin-allowed transition crystal field absorption features, with the ideal order of cation assignments for pyroxenes being tetrahedral sites, M1 sites, and then M2 sites. The archetypal cation ordering proceeds as Si, Al, $Fe^{3+}$, $Ti^{4+}$, $Cr^{3+}$, $Mg^{2+}$, $Fe^{2+}$, $Mn^{2+}$, $Ca^{2+}$, $Na^{2+}$ (Morimoto et al. 1988; Cloutis 2002- references Warren & Bragg 1929, Clark 1957, Ghose 1965, White & Keester 1966, Bancroft & Burns 1967, Bancroft et al. 1967a, Burns 1970, Burns et al. 1972a, 1972b; Schade et al 2004-references Deer et al. 1978, Cloutis 2002). The cation in a site "depends on the bulk composition of the pyroxene, temperature and pressure of formation, cooling rate, and subsequent metamorphism," (Klima et al. 2011-references Wang et al. 2005). These features from the M1 and M2 sites take place near 1 μm, 1.2 μm, and 2 μm in the near-infrared (Rossman-Prewitt 1980). More specifically, pyroxenes tend to have their bands around 0.90-1.05 μm and 1.8-2.3 μm, with a possible inflection around 1.2 μm and faint shorter wavelength features: orthopyroxenes have bands around 0.9 μm and 1.8 to 2 μm, pigeonites are around 0.93 and 2 μm, subcalcic augites are around 0.99 and 2.18 μm, and diopsides are near 1.04 and 2.3 μm (Adams 1974-references Adams 1974; Adams 1975; Rossman-Prewitt 1980). There is also likely a "strong absorption in the ultraviolet portion of the spectrum," that is likely from "charge-transfer absorptions" (Adams 1975). Usually the features from the M2 site are stronger than the features from the M1 site, because the M2 site is more distorted (Burns 1993; Cloutis 2002-references Warren & Bragg 1929, Clark 1957, Ghose 1965, White & Keester 1966, Bancroft & Burns 1967, Bancroft et al. 1967a, Burns 1970, Burns et al. 1972a, 1972b; Klima et al. 2011). The ferrous iron in the M2 site typically is responsible for the features around 1 μm and 2 μm, with Na, $Co^{2+}$, $Zn^{2+}$, $Cr^{2+}$, and

$Mn^{2+}$ ideally partitioning there in all types of pyroxenes; the M1 site has ferrous iron features near 1 μm and 1.2 μm, with partitioning preference also from trivalent cations, $Ti^{4+}$, and $Ni^{2+}$ (Rossman-Prewitt 1980; Cloutis 2002-references Warren & Bragg 1929, Clark 1957, Ghose 1965, White & Keester 1966, Bancroft & Burns 1967, Bancroft et al. 1967a, Burns 1970, Burns et al. 1972a, 1972b, Adams 1975, Hazen et al. 1978, Rossman 1980, Burns 1993). In high-calcium clinopyroxenes in particular, $Fe^{3+}$, $Ti^{3+}$, $Ti^{4+}$, and $Cr^{3+}$ prefer the M1 site (Cloutis 2002-references Cameron & Papike 1980, Rossman 1980, Burns 1993). Calcium and ferric iron do not have any CFSE in ideal octahedral sites, while trivalent chromium has a large CFSE, therefore it prefers those ideal octahedral coordination sites (Burns 1970; Burns 1993). However, there are other factors, such as distortion and pairing energies that affect absorption band positions. Orthopyroxenes and low-calcium clinopyroxenes usually have ferrous iron in the slightly larger M2 sites, while magnesium, being smaller, is predominantly located in the M1 sites (Burns 1970; Adams 1975; Rossman-Prewitt 1980; Burns 1993; Klima et al. 2011-references Burns 1993; Nesse 2012 p.295-296). The M2 site distortion in orthopyroxenes "results in complete resolution of the 3d orbitals of $Fe^{2+}$ ions in M2 positions," resulting in greater CFSE there for the ferrous iron ions (Burns 1970 p.91; Klima et al. 2008-references Burns 1993). Pigeonite, a low-calcium pyroxene, can have between 10 and 30 % calcium in its M2 sites, with Klima et al. (2011) putting it usually between 5-15 % calcium (Nesse 2012 p.297). High-calcium clinopyroxenes take in varying amounts of calcium, a larger ion, into the M2 sites, leaving little room for ferrous iron ions in the site (Burns 1970-references Bancroft, Burns, & Maddock 1967b; Burns 1993-references White & Keester 1966, Burns & Huggins 1973, Hazen et al. 1978; Cameron & Papike-Prewitt 1980; Cloutis 2002). Therefore, M1 sites in clinopyroxenes have more ferrous iron in them than in orthopyroxenes (Adams 1974-references Burns 1970, Adams 1974; Adams

1975; Burns 1993; Nesse 2012 p.295-296). Magnesium is also typically located in these M1 sites (Nesse 2012 p.295-296).

These two main absorption features generally move to longer wavelengths with increasing iron or calcium abundances, with calcium generating larger spectral shifts (Adams 1974; Sunshine et al. 2004-references Adams 1974, Cloutis & Gaffey 1991, Burns 1993). This has been found to depend on the type of pyroxene however. Burns (1965) looked into orthopyroxenes and how the bands near one micron "change linearly to longer wavelengths with increasing $Fe^{2+}$," (Adams 1974-quote; Burns 1993-references Goldman & Rossman 1979). With clinopyroxenes, an increase in $Ca^{2+}$ leads to both of the two major bands to move to longer wavelengths (Adams 1974). However, pyroxenes with calcium contents greater than $Wo_{30}$ don't have their 2 µm feature move much past 2.3 µm, suggesting that "the ligand field around the M2 sites do not change significantly even as more $Ca^{2+}$ is added to an augite," (Klima et al. 2011). With higher iron contents in high-calcium pyroxenes, the opposite of orthopyroxenes occurs and both of these same bands move to shorter wavelengths (Adams 1974). Higher amounts of calcium in clinopyroxenes ($Wo_{>30}$) cause non-linear changes, as calcium cations take over the M2 site in place of ferrous iron, until it reaches around $Wo_{50}$, which is the maximum amount of calcium a pyroxene can technically have before turning into a pyroxenoid (Klima et al. 2011). These changes are in part from the space groups changing from $P2_1/c$ to C2/c with the addition of more calcium (Klima et al. 2011). Pigeonites tend to behave more like orthopyroxenes and are more linear in these changes as long as the calcium content remains below 10 %; with higher amounts of calcium, band I moves towards longer wavelengths (Adams 1974-references Burns 1965; Cloutis & Gaffey 1991; Klima et al. 2011). However, calcium contents can be from $Wo_{0-15}$ in pigeonites (Huebner-Prewitt 1980). Huebner from Prewitt (1980) says that orthopyroxene

usually only has calcium contents below $Wo_5$ (Cloutis & Gaffey 1991-references Morimoto et al. 1988; Sunshine et al. 2004). Low-calcium pyroxenes that have iron contents of $Fs_{>50}$ are also different, as both coordination sites contain iron (Cloutis 2002-references Ross & Sowerby 1996). The main absorption features also tend to become stronger with increasing ferrous iron contents (Cloutis 2002). Pyroxenes that are rich in other cations such as titanium, aluminum, and ferric iron will not follow the linear changes as well, as they have been plotted against features of typical pyroxenes and are always off the general positive-correlation trend line that goes from orthopyroxenes to high calcium clinopyroxenes (Adams 1974 Fig. 2; Rossman-Prewitt 1980; Cloutis & Gaffey 1991 Fig. 13). More aluminum in orthopyroxenes contributes to a stronger UV edge from charge-transfers and to bands to be located at lower than expected wavelengths (Burns 1970; Cloutis & Gaffey 1991). The high-calcium pyroxene augite in particular tends to have more scatter in comparison to this trend line, as its structure allows these other cations to substitute in more frequently (Adams 1974; Adams 1975; Cloutis & Gaffey 1991; Papike 1996). More ferric iron in these will lead to a "masking" of the ferrous iron bands (Adams 1975). Titanaugites, which usually have greater than 2 wt. % $TiO_2$, have absorption features at longer wavelengths than high-calcium pyroxenes with similar iron amounts (Adams 1974; Hamilton 2003-references Deer et al. 1972).

To complicate spectra even more, many clinopyroxenes are part of mixtures or have exsolution lamellae (Cloutis 2002-references White & Keester 1966, Bell & Mao 1972a, Burns et al. 1972b). If the mixtures are made of similar types of pyroxenes they may still plot on the trend line that Adams (1974) made, and they form a type of "average" between the two. However, if they are not that similar, it causes different separate bands or a non-linear combination of the two. The features of these mixtures and of exsolved samples also tend to be

wider and weaker (Adams 1974; Singer 1981). "Even small-scale exsolutions (< 1 µm wide)

seem to be sufficient to significantly alter spectral properties," (Cloutis & Gaffey 1991). I tried to

use samples that had the least amount of impurities and exsolution in order to find clearer trends.

Exsolution happens during cooling, when pyroxenes can separate, or "unmix", into low-calcium

orthopyroxenes and high-calcium clinopyroxenes (Winter 2010 p.47; Nesse 2012 p.296-297).

Exsolution is found with equilibrium, which occurs with slower cooling, while zoning occurs in

faster cooling (Sunshine & Pieters 1993). Generally, equilibrium is defined as "any state that is

not undergoing some form of transition," and is considered as such in this case when there is a

grouping of minerals that have reached stability (Winter 2010 p. 518). Compositional zoning is

when the mineral changes composition as it cools in equilibrium, leading to a gradation (Winter

2010 p.38). In this paper I am mainly concerned with equilibrium as a result of the

homogenization of pyroxene compositions that occurs with increased metamorphism and

igneous activity (Binns 1970-refences Keil & Fredriksson 1964; Brearley & Jones-Papike 1998;

Grady et al. 2015 p.4-6 from references 1.33, 1.33 and table 1.1 with references 1.18, 1.24, 1.37).

In pyroxenes with even a small amount of calcium, there will be some exsolution, even if at very

small sizes (Sunshine et al. 2004-references Camera et al. 2000, Lorimer & Champness 1973).

Pigeonite can also alter to orthopyroxene upon cooling, with exsolved augite taking the excess

calcium (Buseck et al. –Prewitt 1980; Huebner-Prewitt 1980; Papike 1998; Sunshine et al. 2004;

Nesse 2012 p.297). These complications makes calibration difficult, as these different types and

mixtures contribute to the non-linearity of the relationship between cation contents and

wavelength (Singer 1981). In addition, both orthopyroxenes and clinopyroxenes have decreased

reflectance and increase in band depth with increasing particle size; however, once it reaches a

maximum depth with increasing particle size, the depth begins to decrease again (Cloutis &

Gaffey 1991-references Adams & Filice 1967, Hunt & Salisbury 1970, Pieters 1974; Clark 1995-references Clark et al. 1993b). Saturation of the bands (flat on the bottom) can be an indicator of this, although it is unlikely that this will happen with remote sensing of asteroids because of the large variety of grain sizes on their surfaces (Cloutis & Gaffey 1991).

Clinopyroxene spectra have an extra complexity, as there are two different main kinds: Type A and Type B (Cloutis & Gaffey 1991; Cloutis 2002). Type B spectra superficially appear to be similar to orthopyroxene spectra, with a main absorption feature near 1 μm, a possible faint feature near 1.2 μm, and a feature around 2 μm (Cloutis 2002; Klima et al. 2011-references Adams 1975, Cloutis & Gaffey 1991). Meanwhile, the type A spectra mainly have the features around 0.9 μm and 1.15 μm (Cloutis 2002; Klima et al. 2011-references Adams 1975, Cloutis & Gaffey 1991). Burns (1970) found that this separation of the features is from ferrous iron in the M1 site. Adams (1975) found that there were no obvious chemical differences between the two types of clinopyroxenes. Cloutis and Gaffey (1991) did not find a systematic relationship in type A clinopyroxenes with respect to iron and calcium contents, absorption feature wavelength positions, or band separation. They also found that there was little spectral detail for the feature minima which made positions hard to pinpoint, with some having best estimates within $\pm \sim 30$ nanometers (Cloutis & Gaffey 1991). Schade et al. (2004-from Reddy et al. 2008) noted that high-iron high-calcium pyroxenes tend to be type A, while other high-calcium pyroxenes that are low in iron are more often type B. These low-iron high-calcium pyroxenes have weak band II features and therefore spectrally act like olivine in mixtures (Reddy et al. 2008- references Adams 1974, Cloutis et al. 1991, Reddy et al. 2007). Klima et al. (2011) also confirm that type A pyroxenes are saturated with calcium, leading to generally only the ferrous iron in M1 sites providing features (Cloutis & Gaffey 1991). Type B clinopyroxenes typically have $\sim Wo_{<50}$, with

overlap around $Wo_{50}$ with the Type A clinopyroxenes (Cloutis & Gaffey 1991). Type A clinopyroxenes with $Wo_{>45}$ were also found to have manganese and ferric iron as cations in terrestrial samples (Klima et al. 2011-references Schade et al. 2004). For both the Type B clinopyroxenes and the orthopyroxenes, the 1 µm feature tends to be less wide and more intense than the 2 µm feature (Adams 1975). In type A clinopyroxene-orthopyroxene mixtures, the band centers proceed along the orthopyroxene trend line that was previously mentioned, but once the clinopyroxene amount is over seventy percent, the band centers leave the trend line; it is also noted that an inflection at 1.15 µm is present when there is $\geq$ 40 % of the type A clinopyroxene in the same said mixture (Reddy et al. 2008- references Adams 1974, Cloutis et al. 1991, Reddy et al. 2007).

There are other smaller spectral features in pyroxenes as well. These include spin-allowed transitions, intervalence charge transfers, spin-forbidden transitions, and oxygen-metal charge transfers (Burns 1970; Burns 1993). The charge transfers are usually the strongest of these smaller features, occurring when a "local misbalance of charge occurs accompanying isomorphous substitution," while spin-forbidden transitions, occurring when the transitioning electrons have different spins, are the weakest (Burns 1970-quote initially p.68; quote from Hunt 1977-references Burns 1970b; Burns 1993; Clark 1995). Therefore with charge transfers, electrons can go either between ions or between ions and ligands (Burns 1970; Clark 1995). These shorter wavelength features have several different possible origins. I will go through by element, keeping in mind that some of these features are inconclusive in the literature. Chemical analyses, if available, can help with determining the likely causes for these different bands. Iron can appear in the smaller features as either from $Fe^{2+}$-$Fe^{3+}$ charge transfers or as $Fe^{2+}$ spin-forbidden transitions. $Fe^{3+}$, along with $Mn^{2+}$, have only spin-forbidden electronic transitions in

octahedral sites (Burns 1993 p.59). A $Fe^{2+}$-$Fe^{3+}$ charge transfer is possibly located at 0.44 µm for orthopyroxenes and low-calcium pyroxenes (Burns 1972a from Adams 1975). However, Rossman from Prewitt (1980-from Adams 1975) also has this feature possibly being from a $Fe^{2+}$ spin-forbidden band, while Cloutis (2002-references Runciman et al. 1973, Abu-Eid 1976, Langer & Abu-Eid 1977, Hazen et al. 1978, Goldman & Rossman 1979, Zhao et al. 1986, Burns 1993) has 0.445 µm, along with 0.425, 0.480, 0.505, and 0.545 µm to be from $Fe^{2+}$ spin-forbidden transitions in all types of pyroxenes. However, these features are stronger in low-calcium pyroxenes, which can be seen in the spectra in Fig. 3-5 below (Cloutis 2002-references Runciman et al. 1973, Abu-Eid 1976, Langer & Abu-Eid 1977, Hazen et al. 1978, Goldman & Rossman 1979, Zhao et al. 1986, Burns 1993). As mentioned previously, features near 0.505 µm are likely to be $Fe^{2+}$ spin-forbidden bands, which may help determine pyroxene calcium amounts (Burns 1972a from Adams 1975; Rossman-Prewitt 1980; Cloutis 2002-references Hazen et al. 1978, Cochran & Vilas 1998). Features near 0.65 µm have also been noted as possible $Fe^{2+}$ spin-forbidden features (Runciman 1973a from Adams 1975). Other features around 0.75-0.8 µm in high-calcium pyroxenes typically are attributed to $Fe^{2+}$-$Fe^{3+}$ charge transfers, usually from a few percent of ferric iron resulting from oxidation processes (Burns 1970; Adams 1975; Rossman-Prewitt 1980; Sunshine & Pieters 1993; Cloutis 2002).  Ferric iron also can cause spectra to have more reddened slopes (Cloutis et al. 2006a-references Cloutis 2002, Schade et al. 2004). Adams (1975) writes "in combination with the other, spin-allowed $Fe^{2+}$ bands the 0.75-0.80 µm band appears to be a unique indicator of calcic pyroxene containing some $Fe^{3+}$." For high-calcium clinopyroxenes, features around 0.45 µm can be attributed to $Fe^{2+}$ spin-forbidden absorptions, or to $Cr^{3+}$ if there are also other chromium features present (Adams 1975; Rossman-Prewitt 1980; Cloutis 2002).

Chromium is fairly prevalent among pyroxenes. With a range from 0.442-0.460 µm, along with a feature around 0.6-0.68 µm for both high- and low-calcium pyroxenes, these bands can be attributed to $Cr^{3+}$, although they are usually stronger in high-calcium pyroxenes (Cloutis 2002-references Mao et al. 1972, Rossman 1980, Burns 1985, Burns 1993). The bands near 0.6-0.68 µm in low-calcium pyroxenes do not need a lot of chromium to be formed ($Cr_2O_3 \geq 0.38$ wt. %). Specific common bands are 0.62 µm and 0.645 µm, which are usually attributed to $Cr^{3+}$ in M1 sites (Adams 1975; Rossman-Prewitt 1980). Several chromium features in high-calcium pyroxenes, around 0.455 and 0.65 µm, usually mean that there is $Cr_2O_3 \geq 0.9$ wt. % (Cloutis 2002). Hazen et al. (1978) and Cloutis and Gaffey (1991) found that several Cr-rich diopsides had "their major absorption band centers at longer than expected wavelengths relative to their Ca contents and shorter than expected wavelengths relative to their Fe contents," (Cloutis 2002). With further studies, the 1 µm band was found to not have general differences but the 2 µm band occurred at longer wavelengths more often (Cloutis 2002-references Adams 1974, Hazen et al. 1978, Cloutis & Gaffey 1991). Cloutis (2002) noted that samples with $TiO_2$ and/or $Cr_2O_3$ at $\geq 1$ wt. % plotted off the trend line with respect to iron and calcium versus band positions.

Titanium is another source of shorter wavelength absorption features. Bands near 0.65 µm (0.600 µm from Rossman) are considered to be from $Fe^{2+}$-$Ti^{3+}$ charge transfers (Burns 1972a from Adams 1975; Rossman-Prewitt 1980). Cloutis (2002-references Burns et al. 1976, Burns 1981, Burns 1993) has $Ti^{3+}$-$Ti^{4+}$ charge transfers around 0.50 µm and 0.65 µm, and $Fe^{2+}$-$Ti^{4+}$ charge transfers around 0.43-0.485 µm. Features around 0.46 µm can be associated with $Fe^{2+}$-$Ti^{4+}$ charge transfers when $TiO_2 \geq 1$ wt. % (Cloutis 2002). Lewis and White (1975, from Adams 1975) showed that titanium in augites usually subdue the 0.77 µm $Fe^{2+}$-$Fe^{3+}$ charge transfer band. Titanium abundance can also cause the two major pyroxene features to move to longer

wavelengths (Cloutis 2002-references Adams 1974, 1975, Hazen et al. 1978, Cloutis & Gaffey 1991). The 0.645 µm band can also be from $Ti^{3+}$ (Hunt 1977-references Prewitt et al. 1972 at 0.64 µm; Adams 1975), as can features around 0.455-0.475 µm (Hunt 1977-references Manning & Nickel 1969, Clark et al. 1969, Burns & Huggins 1973, Dowty & Clark 1973; Cloutis 2002-references Burns 1970; Burns 1993). An absence of shorter wavelength features below one micron in high-calcium clinopyroxenes suggests that titanium is in the sample as well (Adams 1975). Hunt (1977) reported that $Ti^{4+}$ does not have features in the wavelength range of 0.3-2.6 µm. I have not included $Mn^{3+}$ or any of the V cations in these analyses, as they are typically faint and not as abundant in the samples (Cloutis 2002).

In addition to their important spectral characteristics that can give information on spectroscopy and mineralogy, high-calcium pyroxenes are also very useful for petrology, as its presence is a significant indication that melting occurred on a body (Sunshine et al. 2004). "During early Fe, Ni-FeS and silicate partial melting, troilite, high-calcium pyroxene, and plagioclase are all preferentially incorporated in early partial melts from a chondritic precursor," (Sunshine et al. 2004-quote; McCoy et al. 2006). Out of all these signatures, high-calcium pyroxene has the best and most substantial absorption features in its reflectance spectra (Sunshine et al. 2004-references Adams 1974, Burns 1993). This marker is seen in meteorites, as chondrites have high-calcium pyroxene quantities in between those of primitive achondrites and eucrites, which are partial melt residues and partial melt crystallizations, respectively (Sunshine et al. 2004). The 1.2 µm feature is also important for petrology, as can be seen in the studies by Klima et al. (2008). In that study, it was determined that it is at least partially related to cooling rate; the faster the pyroxene cooled, the larger the 1.2 µm feature may be, and therefore the more disorder. Cooling rates of the pyroxenes in that study are obviously faster than those on asteroids

and so the synthetic pyroxenes have more disorder (Klima et al. 2008). Even though they were

cooled in water for 1-2 minutes after being at 900-1500 degrees Celsius, "this is probably not

fast enough to quench their high-temperature $Fe^{2+}$/Mg equilibria," (Klima et al. 2008). As

mentioned previously, this 1.2 µm feature is from $Fe^{2+}$ in the M1 site (Burns 1970), so this

feature is not usually large except in some high-calcium clinopyroxenes and high-iron pyroxenes

(Klima et al. 2008-references Adams 1975, Cloutis & Gaffey 1991a). For their study they used

synthetic pyroxenes that had no ferric iron or exsolution (Klima et al. 2008). This study also

looked at some howardite, diogenite, and eucrite meteorites for comparison and found that

diogenites had weaker 1.2 µm bands than the eucrites, both in comparison to their 2 µm bands

(Klima et al. 2008). For all of the samples, they modeled the spectra using the modified Gaussian

model that is discussed in more detail below. In these results, two hedenbergites were examined

that had the same endmember composition of $Fs_{50}Wo_{50}$ but one was type A and one was type B

(Klima et al. 2008). The type A hedenbergite showed a band around 0.75 µm, despite the fact

that Mossbauer spectroscopy had not detected any $Fe^{3+}$; I had a similar problem with some

samples below (Klima et al. 2008). With the other samples, it was found that decreasing calcium

led to decreasing distance between the M1 bands in the spectra of "Ca-undersaturated"

pyroxenes (Klima et al. 2008). The samples in this study that had the M1 site with less than 10 %

total iron were either slowly cooled or underwent metamorphism, causing the iron to change

sites (Klima et al. 2008). Despite the fact that light scattering is different in bulk samples in

comparison to crystals, the amount of ferrous iron in the sites was still related to the strengths of

the 1.2 µm and 2 µm features; Burns et al. (1991-from Klima et al. 2008) also found using

reflectance spectroscopy that there was a relation between the "percent area of the 1.2 µm band

relative to the sum of the areas of the 1.2 and 2 µm bands to the area of the M1 Mossbauer

doublet," the first part being the area ratio. Some small corrections were needed for the

Mossbauer data, however the changes were expected to be small. The intensity of a feature

changes with particle size. They found the intensity ratios using the same formula as the area

ratios, just replacing the areas with the intensities. The intensity ratios were found to be better to

work with than the area ratios, as area ratios use band width that can have changes from non-

mineralogical and non-compositional factors. In contrast, intensity ratios use intensities that are

"directly controlled by the probability of a crystal field transition occurring," and therefore also

are related to the amount of iron in the site (Klima et al. 2008-references Burns 1993). Plotting

both the band positions of the two micron features of the meteorites and the M1 intensity ratios,

they grouped together into different meteorite types, which may come in handy for remote

sensing of asteroids when trying to learn about both their mineralogies and petrologies (Klima et

al. 2008). This research again points out the usefulness of pyroxenes, although type A

clinopyroxenes would not be able to be used in this ratios method.

## Asteroids & Meteorites

There are many different asteroid classes. While categorizing the different types of

asteroids is convenient, the categories themselves unfortunately do not tell the compositions of

the asteroids (Gaffey et al. 1993a; Gaffey et al. 1993b; Gaffey 2011). Some of the most

commonly referenced types are by David Tholen and these classifications use spectral slope and

albedo properties (Gaffey et al. 1993a-references Tholen 1984, 1989; Gaffey et al. 1993b;

McSween 1999). A significant asteroid class is the S class, which has seven different

mineralogical subtypes (I-VII). These range from olivine-rich to low-calcium pyroxene-rich,

with many in between; some have experienced melting while others are more primitive (Gaffey

et al. 1993a; Gaffey et al. 1993b). When using the S-type asteroid categories to try to match

spectra to the different types, the high-calcium clinopyroxene band II can cause several problems. If it is a Type A, there is no band II feature to compare with the mineralogical subtype charts, as they typically use BARs. For other high-calcium pyroxenes, the right side of band II goes beyond the usual 2.5-2.6 µm range, underestimating the amounts in the spectra when calculating the BARs for classification (Gaffey et al. 1993a). Therefore, it is important to note that using the BARs with high-calcium pyroxene can lead to erroneous results, so it is necessary to look at several factors with the spectra (Sunshine et al. 2004-references Cloutis et al. 1986, Gaffey 1993, 2003). There are several asteroid classes that don't appear to have meteorites in the collection; while type doesn't describe mineralogy, some type S(II)'s, for example, have what appear to be mostly olivine with a significant fraction of high-calcium pyroxene (< 20 %). Although they seemed to be similar to brachinites, other primitive achondrites, or calcium pyroxene-bearing ureilites, they could also be olivine-clinopyroxene cumulates, clinopyroxene-bearing pallasites, or highly metamorphosed C-types, the last three not being in the meteorite collections (Gaffey et al. 1993a-references Nehru et al. 1983, 1992, Takeda et al. 1992). S(V) also has some asteroids that possibly include primitive achondrite-like or high petrographic type H chondrites that have been intruded by calcium pyroxene basalts (Gaffey et al. 1993a). It has been noted that for S-type asteroids greater than 100 kilometers in size, mafic silicates on the surface, such as pyroxenes give a "relatively constant spectral contribution"; on smaller asteroids, the silicates contribute more with smaller asteroid size (Gaffey et al. 1993a).

It has been suggested that space weathering can affect spectral parameters, particularly the slopes and albedos (Gaffey 2010; Gaffey 2011-references Adams & McCord 1971). Space weathering occurs from micrometeorite impacts, solar wind particles, and cosmic rays hitting the surfaces of asteroids. This was suggested as a way to connect the S-type asteroids to ordinary

chondrites, as the spectra for S(IV)-types were similar to the ordinary chondrite spectra (Gaffey 2011). While space weathering does appear to exist, experiments have shown that strong lasers causing extensive weathering, even more than what would occur on an asteroid, do not change the band positions or BARs, which are the main compositional markers (Gaffey 2010-references Moroz et al. 1996, Yamada et al. 1999, Hiroi & Sasaki 1999, 2001, Sasaki et al. 2001, 2002, 2003, Kurahashi et al. 2002, Ueda et al. 2002, Strazzulla et al. 2005, Marchi et al. 2005; Brunetto et al. 2006b, Brunetto et al. 2007). Therefore, even with space weathering affecting the albedos of asteroids, the compositions can still be determined (Gaffey 2010). It was noted in Sasaki et al. (2001-from Sunshine et al. 2004) that it was easier to produce iron grains from the laser on olivine in comparison to pyroxene. Some other space weathering has been studied with several of the asteroids that were visited by flybys (Gaffey 2011). Space weathering affected their spectra differently; all also had different space weathering effects than the Moon (Gaffey 2011-references Chapman 2004, Gaffey 2010). However, band positions were still not affected (Gaffey 2011-references Gaffey 2010). Therefore, while space weathering can have an impact on the spectra, the most important information is still available from mafic materials.

Most meteorites are pieces of asteroids that have landed on the Earth; a select few have come from the Moon and Mars as well (McSween 1999; Gaffey 2011). From the meteorites that have fallen, we have determined that there are at least 135 parent bodies in our collection. Around 80 % of these have undergone igneous processes while the remaining have experienced some heating (Gaffey et al. 2002-references Keil 2000; McCoy et al. 2006; Gaffey 2011-Keil 2000; Lunning et al. 2015-from Burbine et al. 2002). Nonetheless, the collection is biased and there are many missing pieces that we do not have, possibly because the materials are too weak or are too far from a resonance (McSween 1999; Gaffey et al. 2002; Gaffey 2011). While

meteorites have the advantage of being studied directly here on Earth, Earth's weathering

processes can cause issues with meteorite compositions and organics (McSween 1999; Grady et

al. 2015 p.1). However, they can give times, such as the terrestrial, cosmic ray exposure, and

break up/impact ages (McSween 1999). Meteorites are a great way to ground truth laboratory

spectra samples and mixtures (Sunshine et al. 2004). The laboratory and meteorite spectra results

can be used as a way to calibrate band positions and changes in spectra with different types of

minerals. These then can then be used as a way to standardize more asteroid spectroscopy. The

eventual goal from these processes is to determine mineralogy, and therefore composition and

petrology as well, giving a better picture of the formation and evolution of asteroids and the solar

system (Gaffey 2011).

There are three main categories of meteorites: stones, stony-irons, and irons. The stony

meteorites consist of chondrites and achondrites and are predominantly silicates and oxides

(McSween 1999). Chondrites are more primitive bodies, consisting of conglomerates/breccias of

different minerals, including small, previously melted spheres called chondrules (Gaffey 1997;

Brearley & Jones-Papike 1998; McSween 1999; Winter 2010, p.12; Grady et al. 2015 p.1-2).

They have solar abundances of most of their elements, the major exceptions being the volatiles

of hydrogen, helium, carbon, nitrogen, and oxygen (Gaffey 1997; Brearley & Jones-Papike 1998;

McSween 1999; Grady et al. 2015 p.1). These primitive types can make interpreting the spectra

more difficult, as the minerals have not reached equilibrium, despite the fact that some have

experienced metamorphism, aqueous alteration, and shock events (Brearley & Jones-Papike

1998; Shearer-Papike 1998; McSween 1999; Grady et al. 2015 p.4-7). With increasing

metamorphism in chondrites, the petrographic grade goes from 3 to 6; olivine and low-calcium

pyroxenes become homogeneous in compositions, while the low-calcium pyroxenes also become

more orthorhombic (Brearley & Jones-Papike 1998; Grady et al. 2015 p.4-6 from references 1.33, table 1.1, 1.18, 1.24, 1.37). The ones that have experienced igneous activity, including partial melting and crystallization, are moved into the achondrite category (McSween 1999; Winter 2010, p.12; Grady et al. 2015 p.2, p.8). There is also a group called primitive achondrites, which are "residues from partial melting," (Shearer-Papike 1998; McSween 1999). Partial melting is when a solid is not fully melted; the partial melt can stay as the solid melts further or it can separate, leaving behind a solid residue (Winter 2010, p.202). Grady et al. (2015 p.2) describe primitive achondrites as "meteorites that have an unfractionated composition, but textures that indicate they have been strongly heated, if not melted." Iron meteorites are likely the cores of asteroids, mainly made of nickel-iron metals, although a few seem to have silicate pieces that match some primitive achondrite types (Shearer-Papike 1998; McSween 1999; Winter 2010 p.11; Grady et al. 2015 p.10). Stony-irons mainly consist of both nickel-iron metals and silicates (Shearer-Papike 1998; McSween 1999; Winter 2010 p.12; Grady et al. 2015 p.9). For pyroxenes, I am mainly concerned with chondrites and achondrites, as these are the vast majority of the types that have silicates (McSween 1999). In particular, I am concerned with basalts, as pyroxenes are a significant component of these (McSween 1999).

Some other common silicate minerals in asteroids are olivine and plagioclase (McSween 1999). Plagioclase, which is a type of feldspar, has weak features. There is one feature in particular near 1.2 μm (Sunshine et al. 2004-references Burns 1993). This can cause difficulties in discerning it from pyroxenes in spectra if there is a large amount of plagioclase, although the presence of plagioclase usually just increases the spectral reflectance. Olivine generally has three features near the 1 μm mark, which sometimes combine in a way to look like one large "v"-

shaped feature (Gaffey 2011). One is able to use the 2 μm feature of pyroxenes, if available, to help determine the basics of what are included in a mixture spectrum.

I decided to focus on meteorite types with greater than or equal to five volume percent clinopyroxene, as these minerals will only make a significant spectral contribution when there is a certain amount present. The $\geq$ 5 vol. % limit was chosen because while smaller amounts of high-calcium pyroxenes do not make as much of an impact on spectra, they do begin to muddle and complicate the spectral features. I mainly focused on four kinds of pyroxenes: pigeonites $(Mg,Fe^{2+},Ca)_2Si_2O_6$, diopsides $(CaMgSi_2O_6)$, hedenbergites $(CaFeSi_2O_6)$, and augites $(Ca,Mg,Fe^{2+},Fe^{3+},Al)_2Si_2O_6$ (Nesse 2012 p. 300-301). Pigeonites are low-calcium clinopyroxenes, while the rest are high-calcium pyroxenes. I researched the different types of meteorites for their endmember compositions and clinopyroxene abundances (Scott & Taylor 1985; Bischoff 2000; Zolensky et al. 2002; Lorenzetti et al. 2003; Keil 2010; Cloutis et al. 2011a; Cloutis et al. 2011b; Cloutis et al. 2011c; Cloutis et al. 2012a; Cloutis et al. 2012b; Cloutis et al. 2012c; Cloutis et al. 2012d; Cloutis et al. 2012e; Grady et al. 2015; King et al. 2015; Lunning et al. 2015). From this, I limited my original meteorite choices to eucrites, angrites, ureilites, brachinites, acapulcoites, winonaites, and ordinary chondrites. It is important to note that some of these types are breccias and therefore those modal mineralogies can have high variability because of the heterogeneity (Li & Milliken 2015). For example, ureilites and winonaites are heterogeneous, and acapulcoites are depleted in basaltic components (McSween 1999; Dunn 2012-references Warren & Kallemeyn 1992, Goodrich et al. 1987, 2001, 2002; Grady et al. 2015 p.201 references 6.5, 6.7, 6.9-6.12, p.225 references 8.8, 8.10-8.13; Hunt et al. 2017). After more research, I narrowed it down to angrites, as this is a small, less studied group with high amounts of clinopyroxene, including type A.

Angrites are unusual achondrites that formed from fairly oxidized basaltic magmas (Burbine et al. 2006). They are generally 6-46 vol. % fassaite, which is a type of diopside with high amounts of titanium and aluminum, although Angra dos Reis has around 90 % of this particular diopside-hedenbergite (McSween 1999; Floss et al. 2003-references McKay et al. 1988a; Grady et al. 2015 p.252 references 10.3). In addition to the clinopyroxenes, angrites usually consist of 13-55 vol. % olivine and 25-39 vol. % anorthitic plagioclase feldspar (Mittlefehldt-Papike 1998; McSween 1999; Cloutis et al. 2006a-references McKay et al. 1988, 1990, Jambon et al. 2005; Grady et al. 2015 p.252 references 10.3). They have very low $Na_2O$ and $K_2O$ weight percentages, and typically don't have ferric iron at all or in large quantities (Mittlefehldt-Papike 1998, table p.4-138; Cloutis et al. 2006a-references Mittlefehldt et al. 1998; Burbine et al. 2006-references Hoffman 2002). Cores of clinopyroxenes in angrites show aluminum contents of 7-9 wt. % (Floss et al. 2003-references McKay et al. 1990, Mikouchi et al. 1996, Bischoff et al. 2000, Mikouchi & McKay 2001, Mittlefehldt et al. 2002). The angrites typically do not have high amounts of manganese either, with most being only slightly above 0.06 wt. % MnO (Burbine et al. 2006-references Crozaz & McKay 1990, Mittlefehldt et al. 1998, Mikouchi, personal communication). Of three samples, with two having several analyses, the clinopyroxene endmember compositions ranged from $Wo_{49.5-56.6}En_{0.0-35.7}$ in Mittlefehldt et al. (1998 in Papike-table p.4-133). Grady et al. (2015 p.253 references 10.1, 10.3) have compositions of $En_{0-26}Fs_{16-55}Wo_{45-58}$. It should be noted that angrites seem to be richer in Type A clinopyroxenes than other meteorite types, although the spectrally bizarre Angra dos Reis angrite has type B high-calcium pyroxenes (Schade et al. 2004; Burbine et al. 2006). Angra dos Reis has a very reddened slope, while other angrites have less reddened slopes; it also has a feature around 0.5 µm which is likely from a $Fe^{2+}$-$Ti^{4+}$ intervalence charge transfer transition (Burbine et

al. 2006-references Gaffey 1976, Mao et al. 1977, Burns 1993a). Angra dos Reis probably

formed as a cumulate or by "crystallization from a fractionated melt," while five other angrites

have plagioclase, type A fassaite, olivine, similar calcium contents, and are likely "crystallized

melts with only limited amounts of crystal accumulations," (Schade et al. 2004-references Prinz

et al. 1977, Mittlefehldt et al. 1998, 2002, Mikouchi et al. 2000, Bischoff et al. 2000, Kurat et al.

2001, Floss et al. 2001). Angra dos Reis has a fassaite with $En_{30}Fs_{11}Wo_{44}Ti_3$ (Burns 1993-

references Hazen & Finger 1977), while Burbine et al. (2006-references Prinz et al. 1977) have

the average as being around $Fs_{12}Wo_{55}$ and homogeneous. Other angrite samples have pyroxenes

and zoned pyroxenes with similar calcium contents (Cloutis et al. 2006a; Burbine et al. 2006-

references Goodrich 1988, Prinz et al. 1988, Crozaz & McKay 1990, Mittlefehldt et al. 1998,

Mikouchi & McKay 2001, Mittlefehldt et al. 2002). The clinopyroxene of asteroid 3628

Božněmcová is type A and has around $Fs_{10-20}$ and over 90 % of ferrous iron in the M1 site

(Cloutis et al. 2006a). In total it includes around 55-75 % clinopyroxene, 20-33 % plagioclase

feldspar, and < 20 % olivine (Cloutis et al. 2006a). It is possibly from "melting and

differentiation of an oxidized chondritic precursor," (Cloutis et al. 2006a). In addition to this

information, it has been noted in Burbine et al. (2006) that "the pyroxene compositions in

angrites fall outside the pyroxene quadrilateral due to high abundances of $Al^{3+}$ and $Ti^{4+}$ so using

ferrosilite and wollastonite contents may not be the best way to characterize these pyroxene

compositions."

## Previous Work

So far, most of the research on asteroid spectroscopy calibration and mixtures has dealt

with orthopyroxene and olivine (Cloutis & Gaffey 1991). There have not been as many papers on

clinopyroxene and its mixtures, and even less done on high-calcium clinopyroxene. The lack of

research has been in part because it is typically more complicated to calibrate their spectral changes for several reasons (Schade et al. 2004). One reason, as mentioned above, is that there are two main types: type A and type B. Another reason is because of exsolution and zoning in most natural samples. Older papers used to only report prevalent orthopyroxene in meteorite spectra because it was harder to discern high-calcium pyroxene due to its "small grain size and/or its presence only as very fine exsolution lamellae in orthopyroxene," (Gaffey et al. 2002 quote; Sunshine et al. 2004).

The different reports on pyroxene calibrations include modeling, and graphs and equations using band centers. One type of model, originally by Hapke (1981), is the radiative transfer model. Hapke's model (1981-references in Sunshine et al. 1990-also references Johnson et al. 1983, Clark & Roush 1984, Clark 1987, Mustard & Pieters 1987, Nelson & Clark 1988) separated spectra of mixtures within ± 5 %. It required many inputs, but it could also be used with other models and methods of interpreting spectra when ground truths were not available. Li and Milliken (2015) used high-calcium pyroxenes as possible endmembers in their radiative transfer model. It is interesting that they found that even after including similar high-calcium pyroxene endmembers, "no Ca-rich pyroxene compositions similar to those found in augite lamellae in cumulate eucrites were selected by the models." Li and Milliken (2015) also noted that good spectral fits do not guarantee it is accurate or realistic with respect to mineral abundances, compositions, and particle sizes.

Another commonly used model is the Modified Gaussian Model (MGM) (Sunshine et al. 1990). It is derived from the Gaussian model, which is based off the assumption that visible and near-infrared absorption features are shaped like Gaussian curves; Gaussian bands are then modeled to try to find a fit for absorption features in spectra (Sunshine et al. 1990; Burns 1993

p.47). By instead considering the average bond lengths, and therefore the energies of absorptions, to be Gaussian, the MGM is formed with a power law, with more unique results (Sunshine et al. 1990). For modeling, Sunshine et al. (1990) worked with orthopyroxene (enstatite), clinopyroxene, and olivine to demonstrate the capabilities of the MGM. The parameters in the model included widths, strengths, centers, continuum slope, and intercepts (Sunshine et al. 1990). A good fit has a root mean square error of the model and actual spectral differences on the order of the uncertainty of the laboratory spectrum (Sunshine et al. 1990). The clinopyroxene used in this study was one I examine later: PP-CMP-021 (Sunshine et al. 1990). The Gaussian model was used on clinopyroxene-orthopyroxene mixtures in Sunshine et al. (1990), and it needed fourteen free parameters (Sunshine et al. 1990). The fit for these unconstrained parameters were good, but not physically accurate to features that we would normally see in pyroxenes (Sunshine et al. 1990). The spectra deconvolved with the MGM in comparison to the Gaussian model, even with unconstrained parameters, was more physically accurate to the orthopyroxene-clinopyroxene mixtures and had band centers at nearly the same wavelengths as their endmember compositions (Sunshine et al. 1990). However, with the MGM and other models, mixtures with high-calcium clinopyroxenes in particular occasionally need more bands for the 1 and 1.2 µm areas. With more free parameters, the model has more fits that can possibly match the spectra and can hinder the accuracy (Sunshine et al. 1990). Klima et al. (2011) used the fact that the M1 site around one micron of high-calcium clinopyroxenes is nearly at the same wavelength as the M2 site around one micron at that resolution to minimize the parameters needed for the model (Gaffey 2011). However, in cases where the calcium is saturating the M2 site, they used two bands, as the M1 and M2 features are separated more at those calcium amounts (Klima et al. 2011). These bands sometimes outnumbered the inputs that

the model can have, which can cause problems with getting a reasonable and/or realistic fit to the mineralogy mixture of a particular spectrum (Gaffey 2011-references Sunshine et al. 1990, 1993, 1998, 2004, Schade et al. 2004, de León et al. 2004). For example, in pyroxene mixtures, the 1.2 µm absorption feature from ferrous iron in the M1 sites have similar band positions for both high- and low-calcium pyroxenes. This causes problems with separating different types of pyroxenes in mixtures, as more constraints are needed in order to distinguish the two different M1 features for both pyroxenes (Klima et al. 2008). As a result, lower-calcium pyroxenes usually can be modeled well with three absorption bands, while high-calcium pyroxenes need four (Klima et al. 2008). "Having four overlapping features in the spectrum (i.e., twelve free variables of an olivine-pyroxene mixture 'will lead to nonunique solutions that have no direct physical link to either olivine or pyroxene absorptions'," (Gaffey 2011-references Sunshine et al. 1998). Therefore, it is still important to work on creating better calibrations for the high-calcium clinopyroxenes so that these can be incorporated into models better (Gaffey 2011).

Klima et al. (2011-references Adams 1974, Hazen et al. 1978, Cloutis & Gaffey 1991) noted that previous work with trend lines plotting band I versus band II were made without spectral deconvolution and did not take into account changing space group, exsolution, or zoning. With natural pyroxenes, there is the possibility that they have exsolution and zoning, are weathered, and/or are mixtures, so it is important to look at purer samples and to know the basic geology about where they are from, if available. This way, one can get the best possible relationships for comparison with other pyroxenes (Moriarty & Pieters 2016). With high-calcium clinopyroxenes in particular, the 0.3-2.6 µm range is not usually enough to get the full band II feature, so one has to be careful with the continua they are using for their model and/or interpreting spectra; MGM uses the model to describe the continua, while other graphs and

equations use tangents to the spectra. While the tangent lines may or may not be accurate, they do have the advantage of at least being more consistent among different research (Cloutis & Gaffey 1991). More on the trend line research will be talked about below.

These models and calibrations are important, as most planetary mapping today just try to distinguish between high- and low-calcium pyroxenes, although there are exceptions where some asteroids have "equations to estimate specific pyroxene mineralogies," (Klima et al. 2011- references Pieters 1993, Mustard & Sunshine 1995, Gaffey et al. 2002, Hardersen et al. 2004, 2006, Bibring et al. 2005, Mustard et al. 2005). Models are very important but they have their limitations, so improving the knowledge and availability of high-calcium pyroxene (and other mineral) spectra in a large spectral library would be valuable to work together and get a more complete picture (Cloutis et al. 1986; Sunshine & Pieters 1993; Pompilio et al. 2007). Having more samples would also help with the current limitations of curve-fitting (Gaffey 2010; Gaffey 2011). There still are the sample shortcomings that asteroidal surfaces are different than terrestrial surfaces, such as with different oxidizing and weathering conditions, but that is why I looked at purer samples in order to get the basics; from there, I hoped to be able to contribute to understanding these different and more complex situations on planetary surfaces (Sunshine & Pieters 1993).

To go further in depth in past research, some mixtures that were examined for calibration involved olivine, orthopyroxene, clinopyroxene, limonite, and magnetite with Singer (1981). He used several different samples: unaltered natural olivine that had a composition of $Fo_{85}$; hypersthene that had a composition of $En_{86}$; diopside of $Wo_{41}En_{51}Fs_8$ that had some aluminum, titanium, ferric iron, and possibly some olivine impurities; limonite that possibly had some clay impurities; and magnetite that was at a smaller grain size to match basalts (Singer 1981). The

first mixture was of olivine and clinopyroxene, with intervals of 25 weight percent for each. The clinopyroxene was more opaque and dominated the spectra overall; the one micron area did not change much because they were similar for both minerals, and the two micron feature from the clinopyroxene did not change. The only major changes were that the 1 µm feature got narrower as more pyroxene was added, the reflectance increased with more olivine at wavelengths beyond 1.5 µm, and the 1.3 µm olivine feature was present in all mixtures containing olivine. At the mixture of half of both, the spectrum resembled clinopyroxene, with the one micron feature being right near the clinopyroxene feature's band position (Singer 1981). It is noted that plagioclase also has a feature around 1.25 µm, but that it does not change the slope or pyroxene band depth (Singer 1981-references Adams 1974). The next mixture involved olivine and orthopyroxene. There were similar results to the previous mixture. However, since the one micron features for both were more different and the orthopyroxene was more opaque, the orthopyroxene dominated and only moved when there was more than 50 % olivine in the mixture (Singer 1981). Similar effects were for the orthopyroxene as the clinopyroxene, but they were more pronounced with the orthopyroxene (Singer 1981). There was also a mixture of clinopyroxene and orthopyroxene. The one micron feature broadened and was asymmetrical, especially at 25/75 orthopyroxene/clinopyroxene and 50/50, both of which it started to move towards shorter wavelengths (Singer 1981). "The wavelengths of the minimum reflectance points for these bands vary nonlinearly with compositions between the two end-member positions," (Singer 1981). The two micron region had resolved features for both (Singer 1981). The features are less intense overall than the individual samples and there is an increase in slope in the two micron spectral region, such as was seen with the mixtures of olivine and pyroxene (Singer 1981).

Cloutis and Gaffey previously did a paper with Jackowski and Reed to observe and try to quantify orthopyroxene and olivine mixtures (1986). For this paper, seventy-three mixtures were used for the olivine-orthopyroxene mixtures to try to quantify the changes in spectra, while twelve mixtures were used (olivine-orthopyroxene, olivine-clinopyroxene, and orthopyroxene-clinopyroxene) to qualitatively describe the changes in spectra (Cloutis et al. 1986-references Singer 1981). The olivine had a composition of $Fo_{89}$, the orthopyroxene was a hypersthene with a composition of $En_{86}$, and the clinopyroxene was a diopside from Singer (1981) with a composition of $Wo_{41}Fs_8$ (Cloutis et al. 1986). Since the ferrous iron molar extinction coefficient in pyroxene is larger than in olivine, the pyroxene features dominate olivine-pyroxene mixtures when they have "subequal molar iron abundances," until there is mostly olivine in the mixture (Cloutis et al. 1986). The olivine-orthopyroxene mixtures had 5 wt. % intervals and were in four particle sizes. They observed wavelengths and ratios using features at 0.55 µm, 0.65 µm, 0.70 µm, ~ 1.0 µm, ~ 1.4 µm, and ~ 1.9 µm, although the 1.0 µm feature seemed to be the most useful (Cloutis et al. 1986). These features were ratioed to one another in order to have dimensionless parameters for a wider variety of possible calibration uses. "All potential calibrations were investigated using end-member abundances as the primary variable," (Cloutis et al. 1986). Potential calibration groups used the ratios, "absolute spectral parameters", or wavelength position changes (Cloutis et al. 1986). For this first calibration set, most of the mixtures' band area ratios were on a line, with 0, 5, 95, and 100 % pyroxene deviating from it systematically (Cloutis et al. 1986). The ratios were good for determining abundances of mineral phases but were independent of particle sizes and textures. These ratios are also only applicable to olivine-orthopyroxene mixtures but are unaffected by space weathering continuum slope changes, shock effects, and changes in end-member compositions (Cloutis et al. 1986-references Adams &

35

McCord 1970, Farr et al. 1980). The mixtures were a "function of both mineral phase composition and mineral phase abundance," (Cloutis et al. 1986). Absolute reflectance values were good for finding grain sizes but not for mineral abundances or endmember compositions. For example, the absolute reflectance at 0.65 µm can give particle size information if the endmember compositions and mineral abundances are known (Cloutis et al. 1986). When comparing phase abundance with band I, particle size is not a large factor if they are similar and the "wavelength positions of the olivine and orthopyroxene band I minima vary approximately linearly as a function of iron content," (Cloutis et al. 1986). Wavelength positions, as mentioned previously, were good for detecting mineral phase abundances and chemistries (Cloutis et al. 1986). The main potential problems with using wavelength positions is that there are small wavelength shifts depending on pure endmembers and on the instruments used, although the latter is not usually a problem with technology anymore (Cloutis et al. 1986). When the calibrations were used on unknowns that had results published previously (Singer 1981), they were within the ± 5-10 % uncertainties for both actual mineral abundances and calibrated spectral abundances, although the pyroxene was consistently underestimated, possibly from amphibole impurities (Cloutis et al. 1986).

Cloutis and Gaffey (1991- references Adams 1974, 1975 (which needed some small corrections), Nash and Conel 1974, Gaffey 1976, Hazen et al. 1978) have an important paper that involved quantitative ways to determine pyroxene compositions using two-part linear continuum and quadratic fitting (Moriarty & Pieters 2016). In it, they used several samples that I looked at later: PYX112, PYX036, PYX009, PYX020, PYX040, and PYX150 (Cloutis & Gaffey 1991). They looked at orthopyroxene-clinopyroxene mixtures and found that they don't add linearly and include intermediate, asymmetric features in the spectra between both endmembers (Cloutis &

Gaffey 1991). They noted that for pyroxenes with calcium contents between $Wo_{11-30}$, the spectra can have both orthopyroxene-like and clinopyroxene-like features (Cloutis & Gaffey 1991). They confirmed that the data, albeit limited, showed that there was a trend for $Wo_{<11}$ on the basis of band minima and $Fe^{2+}$ content (Cloutis & Gaffey 1991). This trend was similar to what Burns (1972b-references in Cloutis & Gaffey 1991) and Adams (1974) found, with the latter noting that the pyroxenes were spectrally homogeneous in "the central portion of the tetralateral." Therefore, with low-calcium orthopyroxenes, it can be possible to determine the $Fe^{2+}$ content from this trend, although with caveats if other cations are present in large amounts. For example, a "1 wt. % $Al_2O_3$ is spectrally equivalent to a 5 wt. % decrease in ferrosilite content," (Cloutis & Gaffey 1991-references Adams & McCord 1972, Adams 1974, 1975, Gaffey 1976, Cloutis 1985, Aoyama et al. 1987, Cloutis et al. 1990a (quote)). In this study, band centers were found to be seven nanometers higher than band minima on average, noting that this can change the $Fe^{2+}$ amount by up to 20 mol. % (Cloutis & Gaffey 1991). There is not a consistent spectral calibration for aluminum in orthopyroxenes, so absorption band features provide lower limits of $Fe^{2+}$ contents in these types of pyroxenes (Cloutis & Gaffey 1991-references Cloutis et al. 1990a). It is interesting that they pointed out that two samples have similar chromium contents, but display it differently (Cloutis & Gaffey 1991). PYX018 is a type B clinopyroxene with four different chromium absorption bands at 0.45 µm, 0.63 µm, 0.66 µm, and 0.70 µm. PYX020 is a type A clinopyroxene that does not have any chromium bands besides a possibly weak feature near 0.45 µm; it is likely a ferrous iron spin-forbidden feature as there are not any other bands due to chromium (Cloutis & Gaffey 1991-references Mao et al. 1972, Burns et al. 1972a, b, 1973, 1975, Schreiber 1977, 1978, Ikeda & Yagi 1977, 1978, Vaughan & Burns 1977). Using an electron microprobe, PYX018 has "small (< 20 µm sized) dispersed regions of a high Fe-Cr, low

Mg silicate totaling ~ 5 % of the total sample," while PYX020 only has a few regions of ~ 1 %

that have "an iron-rich phase lining some fractures" that is not chromite (Cloutis & Gaffey

1991). This shows the importance of site preference with the different cations and how they can

make such different changes in spectra (Cloutis & Gaffey 1991). I've noticed this in several

samples below, where similar chemical and endmember compositions can still lead to puzzlingly

different spectra.

Cloutis and Gaffey (1991) looked at some heterogeneous orthopyroxene-clinopyroxene

mixtures in intervals of 25 wt. %. Orthopyroxene dominated the spectra when there were equal

amounts of both (Cloutis & Gaffey 1991). They noted that "curve-fitting routines are a better

solution to the problem of deconvolving pyroxene mixture spectra because the positions of the

component absorption bands are invariant," (Cloutis & Gaffey 1991-references Sunshine et al.

1990). In samples that are zoned or exsolved, there were no patterns with regards to wavelength

positions, further showing the complexity of such samples (Cloutis & Gaffey 1991). One sample,

PYX103, had calcium-poor lamellae of less than one micron wide and it still showed up in the

spectrum as orthopyroxene being in the sample. Therefore it does not take much exsolution to

impact spectra (Cloutis & Gaffey 1991). Lower abundances of clinopyroxenes in these mixtures

were also more difficult to see (Cloutis & Gaffey 1991). They tried to use the wavelength

positions as geotherms, but the uncertainties were too large. In comparison to this and other

qualitative analyses done on orthopyroxene-clinopyroxene mixtures (Adams 1974, 1975, Cloutis

& Gaffey 1991), where the two main features move to longer wavelengths with increasing

clinopyroxene in the mixture, Sunshine et al. (1990-references in 1993) found with their MGM

model that the band centers remained fixed for both. In this case only the band strength changed,

with the stronger features from the majority pyroxene type.

Gaffey et al. (2002) created equations for calibrating and calculating the band centers and endmember compositions of pyroxenes, using the data from Adams (1974, 1975), King and Ridley (1987), and Cloutis and Gaffey (1991). There are several different equations for the wollastonite and the ferrosilite contents. One has to use the equations together to find the two unknowns, by means of the two main features of band I and band II (Gaffey et al. 2002). In this work he also found that the assumption holds that "the Band II position is approximately a linear function of the abundances of the low-Ca and high-Ca pyroxene components in such assemblages (ordinary chondrites)." Burbine et al. (2007) used these equations and found that they worked within the error bars for determining iron and calcium amounts of some howardite-eucrite-diogenites. "The Gaffey et al. formulas primarily had problems with meteorites with molar contents of Fs greater than 50 and Wo greater than 11," (Burbine et al. 2007).

For modeling, Sunshine and Pieters (1993) did more work with the MGM to quantify modal abundances and grain size by using nine mass fraction mixtures of enstatite, PE-CMP-030, and clinopyroxene, PP-CMP-021. They found that individual pyroxenes' absorption band centers, widths, and relative strengths were generally not related to particle size, while there were changes in relative band strength depending on the modal abundances (Sunshine & Pieters 1993). They looked at samples with exsolution lamellae 25-50 µm wide as well and were able to find the modal abundances within 5-10 % using this model (Sunshine & Pieters 1993). Zoned samples pointed to one pyroxene that had broader than normal features, probably signifying an average composition (Sunshine & Pieters 1993). The model used in this study was improved by adding constraints that prevented nonunique fit results; these constraints allow the user to weight uncertainties at different ranges of a spectrum (Sunshine & Pieters 1993-references Tarantola & Valette 1982). Mixtures with larger grain sizes cause saturation which leads to more residual

error. However, saturation is easy to detect and does not appear to affect the band parameters that the model develops (Sunshine & Pieters 1993). They also found that the component band strength ratio (CBSR) seemed to be independent of particle size, further suggesting that particle size usually will not influence models (Sunshine & Pieters 1993). This is important when looking at unknown spectra. They also proposed that the CBSR can be used to help limit the inputs needed to model unknown pyroxenes and can help with approximating modal abundances, since the CBSR is similar in both of the two main feature regions (Sunshine & Pieters 1993). For a final check in this paper, they looked at lunar basalts to see if the MGM could detect the zoning in pyroxenes (Sunshine & Pieters 1993). The MGM resulted in one main pyroxene, likely an average, with the bands being wider (Sunshine & Pieters 1993-references Adams 1974). Overall, Sunshine & Pieters 1993 (from Sunshine et al. 2004) showed that there is a methodical ratio relationship between the amount of high-calcium pyroxene and low-calcium pyroxene and their absorption strengths as their modal abundances change; this "is independent of particle size and is consistent whether measured in the 1 or the 2 µm regions."

Sunshine et al. (2004) also looked at some S-type asteroids that had both low- and high-calcium pyroxenes (ratio of ~ 0.4), and minor olivine, in order to find a method using high-calcium pyroxene as a petrological marker of igneous differentiation. They found through these studies that three asteroids and their families, along with two previously studied asteroids, were differentiated, leading to at least five differentiated parent bodies (Sunshine et al. 2004). They also studied calculations using a melting model of chondritic materials that suggest high-calcium pyroxene ratios could be used as said igneous markers for these types of precursors, as the ratios were < 0.1 for residues and > 0.3 for partial melts (Sunshine et al. 2004-references Asimow & Ghiorso 1998, Ghiorso & Sack 2005). Higher ratios indicated earlier partial melting, and 0.3

"requires less than ~ 30 % partial melting of an ordinary chondrite precursor," (Sunshine et al. 2004).

Schade et al. (2004) studied natural terrestrial high-calcium clinopyroxenes of compositions $Wo_{~45-50}$, with variable iron contents and oxidation states. They used the MGM mentioned above with five parameters and no constraints (Schade et al. 2004-references Sunshine et al. 1990, Press et al. 1992, Schade & Wasch 1999). They tentatively determined that type A pyroxenes include iron-rich pyroxenes from $Fs_{29-46}$ that have most of both types of iron in the M1 sites and calcium or and/or manganese in the M2 sites. They found that the lower iron high-calcium pyroxenes were more diverse, most being type B, unless they had significant amounts of calcium or ferric iron (Schade et al. 2004). Continuing with those results, they found that the two samples with the lowest amount of calcium had the highest amount of calculated ferrous iron in the M2 sites and were type B, while most samples with the highest amounts of calcium were type A (Schade et al. 2004). An exception was a type A sample that had a lower calcium amount ($Wo_{~45}$), low $Fe^{2+}$ in the M2 sites, high ferric iron, and high amounts of divalent manganese in the M2 sites (Schade et al. 2004). Another puzzling sample with a high calcium content ($Wo_{>50}$) was a type B, but calculations showed no ferrous iron in the M2 sites (Schade et al. 2004). The Angra dos Reis spectrum was looked at and found to resemble a terrestrial diopside; it is 93 vol. % clinopyroxene and does not appear to have $Fe^{3+}$ from reflectance or Mossbauer spectroscopy (Schade et al. 2004-references Keil 1977, Mao et al. 1977, Prinz et al. 1977). The titanium in it causes the steep positive slope of the spectrum's continuum (Schade et al. 2004). Angra dos Reis is unusual with its type B spectrum, but plotted close to other type B clinopyroxenes on a graph of $Fe^{3+}/ (Fe^{2+} + Fe^{3+})$ ratio vs Fs; a type A angrite D'Orbigny plotted closer to the high-iron type A clinopyroxenes, confirming their previous results (Schade et al.

2004). It was noted as well that the spectra of two type A angrite pyroxenes did not have resolvable 1 µm absorption features (which will cause problems in MGM), unlike the samples studied, and also lacked the 0.8 µm $Fe^{2+}$-$Fe^{3+}$ transfer feature. The one micron feature issues were both due to olivine and zoned pyroxenes in the angrites (Schade et al. 2004-references Burbine et al. 2001).

More previous work on calibrations for modeling has been studied by Klima et al. (2011). In this work, they used high-calcium pyroxenes with constant magnesium numbers (nMg/ ($nFe^{2+}$ + nMg) x 100) and varying iron and calcium amounts. Many of the DL-CMP samples below are in this study. The magnesium numbers formed a transect across the pyroxene quadrilateral. They found that with the magnesium number of zero that the 1 and 2 µm features got stronger with increasing iron but did not move much, "suggesting that the geometry of the M1 coordination polyhedron remains relatively constant," (Klima et al. 2011). This is likely because the $Ca^{2+}$ is in the M2 site and the $Fe^{2+}$ is the only cation in the M1 site (Klima et al. 2011). For this same magnesium number of zero, they found that the one micron feature did go to shorter wavelengths with less $Ca^{2+}$, but only by a small amount (Klima et al. 2011). Only when there was less calcium and a different shape group ($P2_1/c$) did the two micron feature show more significant changes to shorter wavelengths (Klima et al. 2011). In the samples with a magnesium number of twenty-five, the one and two micron absorption features increased dramatically in strength with decreasing calcium until it reached pyroxene 055 ($Wo_{26}$), when the two features were thereafter equal. As previously mentioned, the 1.2 µm feature is most intense when $Fe^{2+}$ is filling the M1 sites, and therefore also usually when $Ca^{2+}$ is saturating the M2 sites (Klima et al. 2011). Similar results for the magnesium number twenty-five samples occurred as for the one and two micron sites for magnesium number zero results, with the 2 µm feature staying around 2.3 µm until it

reached below $Wo_{20}$ and changed shape group (Klima et al. 2011). For magnesium number fifty, "the first evidence of the midquadrilateral miscibility gap becomes apparent," (Klima et al. 2011). The same is with magnesium number eighty, as samples with $Wo_{<25}$ had zoning and exsolution (Klima et al. 2011). Similar results of previous magnesium number groups occurred with the one and two micron regions (Klima et al. 2011). This study also performed experiments with constant calcium samples, although only one of the seven highest-calcium pyroxenes with $Wo_{\sim49}$ were type A (083), illustrating a need for more type A high-calcium clinopyroxene samples; the rest were type AB (Klima et al. 2011). With constant high-calcium in the pyroxenes, the M1 sites were strong in the spectra, with the model predicting the 1.2 µm feature to be stronger than the M1 1 µm feature (Klima et al. 2011-references Klima et al. 2008). With constant calcium around $Wo_{45}$, the one and two micron bands did not change much, as "there are few structural changes across the diopside-hedenbergite solid solution," (Klima et al. 2011-references Rustein & Yund 1969-quote). When calcium is in pigeonite amounts, such as around $Wo_{10}$, the one and two micron features did change, moving towards longer wavelengths with increasing iron. This was because they were now also in a different shape group (Klima et al. 2011). Using Gaffey et al. (2002-references Klima et al. 2011) equations, they found that the ferrosilite amounts were only $\pm 5$ % twenty percent of the time, while for similar wollastonite amounts it was thirty percent accurate. This was because most samples in this study had high calcium amounts and $Fs_{>30}$. This further shows the need for more spectral information and calibrations.

Work was also done with a parabola and two-part linear continuum algorithm-type (PLC) in order to be used to identify pyroxenes when there were high amounts of hyperspectral data to read from asteroids and the Moon (Moriarty & Pieters 2016). This was studied because the

MGM model is best used with individual spectra, not noisy spectra of an entire planet or solar system body (Moriarty & Pieters 2016). In comparison to other models, the PLC is fully automated and selects "continuum tiepoints and the wavelength range over which absorption bands are fit," in comparison to Cloutis and Gaffey (1991), who used a priori user input (Moriarty & Pieters 2016). When compared with previous MGM-derived band centers for synthetic pyroxenes, the results were similar for both, only differing by several nanometers. However, results were better for the two micron feature in comparison to the one micron feature that had a slight offset of three nanometers (Moriarty & Pieters 2016-references Klima et al. 2007, 2011). This offset is at least partially from the 1.2 µm band that was not taken into account with this algorithm, further showing the necessity for high-calcium clinopyroxene calibration research. Conversely, with rock mixtures this feature could also be from plagioclase feldspar, olivine, ilmenite, or glass (Moriarty & Pieters 2016-references Nash & Conel 1974, Singer 1981, Crown & Pieters 1987, Cheek & Pieters 2014, Horgan et al. 2014). For mixtures in rocks, the PLC can only determine a bulk rock pyroxene composition. Nevertheless, that can be used to determine the mixtures' types and amounts of pyroxenes (Moriarty & Pieters 2016). When there is high ilmenite or other dark materials, the pyroxene features can be masked and not understood well in the PLC algorithm (Moriarty & Pieters 2016-references Isaacson et al. 2011a, 2011b). This was a contributing factor to natural samples having rougher results, but overall they fit on the trend of pyroxenes, leading to future potential analyses of bulk pyroxenes (Moriarty & Pieters 2016).

## Sample Spectra & Data

The samples I have been looking at are either natural (handpicked and sorted usually) or synthetic pyroxenes, which are idealized spectra. The ideal spectra are not what one would find

on asteroids, as asteroids are made up of many minerals. However, it is a good comparison since pyroxenes have such strong spectral features; these sample spectra can also show how the different pyroxenes interact spectrally, both alone and with each other (Hunt 1977). With these samples I also typically do not have to worry about Earth's atmosphere causing problems like with asteroid remote sensing, where water features can interfere with the spectra. Still, water features from impurities in the sample or setup can sometimes cause spectral issues (Hunt 1977). These problematic features in the visible and near infrared wavelengths are around 1.4, 1.9, and 2.85-3 µm (Hunt 1977; Cloutis et al. 1986; Burns 1993; Clark 1995). To determine the changes in the band positions for clinopyroxenes, I first had to determine the endmembers in different meteorite types. This is important because I needed these to compare meteorites to the samples that I would be using, as I wanted them to be similar to what would be observed on asteroids.

Once I found meteorite compositional end members, I then went through several sample catalogs to see what was available. I focused on the Planetary Spectroscopy Laboratory (HOSERLab) at the University of Winnipeg in Winnipeg, Manitoba for my first group. They have an extensive pyroxene collection and provide many details on their compositions. I also used data from the Reflectance Experiment Laboratory (RELAB) from Brown University in Providence, Rhode Island and the USGS Denver Spectroscopy Laboratory and Spectral Library in Denver, Colorado. These last two databases also contain pyroxene samples, but there is less information on their compositions. The HOSERLab used some samples that were measured at RELAB as well. HOSERLab samples start with a PYX, RELAB samples start with predominantly DL-CMP or PP-CMP, and USGS samples generally start with NMNH. Samples for pure clinopyroxenes can be limited. Hamilton (2000) mentions that certain types ($Mg_{<50}$ and $Mg_{<10}$) are not common or are rare in nature, so that can provide some difficulties in obtaining

pure samples. Also, natural pigeonite tends to have exsolution and inverted properties that can cause complications with obtaining pigeonite (Hamilton 2000). I was unable to find many hedenbergite samples. In addition to the high-calcium pyroxenes and pigeonites, several of my samples were orthopyroxenes, which helped to establish a link between orthopyroxenes, low-calcium clinopyroxenes, and high-calcium clinopyroxenes.

The HOSERLab spectra I used that were done at this facility used the Analytical Spectral Devices FieldSpec Pro FR Hi-Resolution Spectrometer (ASD) (Cloutis et al. 2006a; Cloutis et al. 2006b; HOSERLab website). "The spectral resolution of this instrument varies from 3 nm at 0.7 μm, 6 nm at 1.4 μm, and 7 nm at 2.15 μm. The spectral sampling interval is 1 nm for the entire 0.35–2.5 μm interval," (Cloutis et al. 2006a; HOSERLab website-manual 2015). The light source bulb type was a 50 W Quartz Tungsten Halogen and had a Spectralon disk as the reflectance standard; the spectral wavelength calibration used different rare earth standards (HOSERLab website; Cloutis et al. 2006a). Most measurements were taken at i=30˚ and e=0˚, while a few had 0˚ for both. They also averaged a thousand spectra for most, although some type A clinopyroxene samples averaged more. Most spectra had breaks removed at 1000 and 1830 nm. There were a variety of different grain sizes for the powdered samples, but most were < 45 μm and 45-90 μm. For reference, I tried to use spectra with the same grain sizes when comparing them to the literature for added accuracy. Cloutis et al. (2006a) mentions that the powdered samples there are placed "into circular sample holders 10 mm in diameter and 4 mm in depth and then lightly tamped," and then were smoothed on top. The plagioclase sample I am interested in was measured at i=0˚ and e=0˚.

For the NASA RELAB facility at Brown University, the spectra were predominantly measured at i=30˚ and e=0˚, were measured relative to halon, and had a resolution of 5 nm, while

a couple of samples had 10 nm resolution (RELAB website). The sampling intervals were 5 or 10 nm. The source, detection, azimuth, and phase angles were usually 30˚, 0˚, 0˚, and 30˚, respectively. They were also usually measured at room temperature and in an ambient atmosphere (RELAB website). I usually used samples from the Bidirectional Visible-NIR spectrometer (BD-VNIR). Most spectra ranged from 0.3-2.6 µm, although the minimal range is from 0.32-2.55 µm (RELAB website). The light source was a quartz halogen lamp. There were bidirectional reflectance and spectral goniometry and the spectra were calibrated to NBS halon calibration (RELAB website-2006 manual, HOSERLab website). The grain sizes were typically < 45 and 45-90 µm, although there were some larger grain sizes as well. Most were powdered samples (RELAB website). The samples that start with DL-CMP, PE-CMP, and PP-CMP have been acquired by Carlé Pieters, the samples with CP-JJG are from Jeffrey J. Gillis-Davis, the samples with ER-TGS are from Thomas G. Sharp, the samples with FB-JFM and SR-JFM are from Jack Mustard, the samples with PA-RGB and SB-RGB is from Roger G. Burns, the samples from PP-ALS are from Ann L. Sprague, the sample from PX-DWS is from Derek W. G. Sears, and the sample from PX-RGM is from Rhiannon G. Mayne. For the angrite meteorite spectra used, MR-MJG spectra are from Michael J. Gaffey, the MT-TJM is from Tim McCoy, and the TB-TJM spectra are from Tim McCoy and Thomas H. Burbine.

For USGS, they used an integrating sphere (USGS website). The samples used the Beckman™ 5270 spectrometer and "standard, high resolution (hi-res), and high-resolution Next Generation (hi-resNG) models of ASD field portable spectrometers covering the range from 0.35 to 2.5 µm," (Kokaly et al. 2017). The Beckman spectrometer has a spectral range of 0.2-3.0 µm and the ASD has 0.35-2.5 µm. The Beckman spectrometer spectra were "corrected to absolute reflectance" using directional-conical light (Clark et al. 2007). The ASD used a "directional light

source and fiber-optic probe to collect light," and had incidence angles from 20 to 40 degrees (Clark et al. 2007). The spectral purity for all got worse with longer wavelengths (Clark et al. 2007).

The next step was to separate out the most useful samples. The ideal samples lacked impurities, such as from olivine and plagioclase feldspar, had similar amounts of minor or trace elements to specific meteorite types, and had detailed compositions. Figures 2-6 below include the samples portrayed on a pyroxene triangle and the spectra for all the samples, including more that I added later on below. For a complete list of samples with their band minima and endmember compositions, see Table 1 in the Appendices. For the available sample compositional analyses, see Table 5.
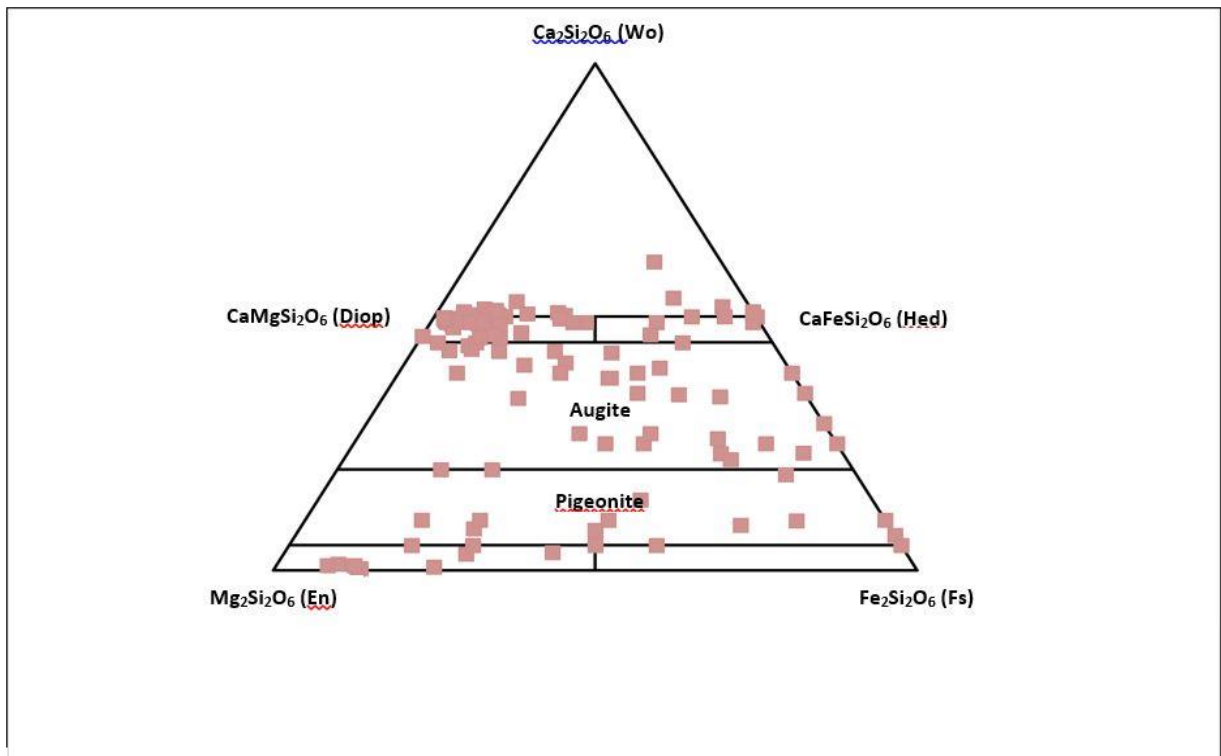


Figure 2. Graph of the pyroxene samples used in this study with respect to the pyroxene triangle (Morimoto 1988; Marshall 1996). Wo=wollastonite, Hed=hedenbergite, Fs=ferrosilite, En=enstatite, Diop=diopside. Sources: HOSERLab, RELAB, USGS Spectral Library.
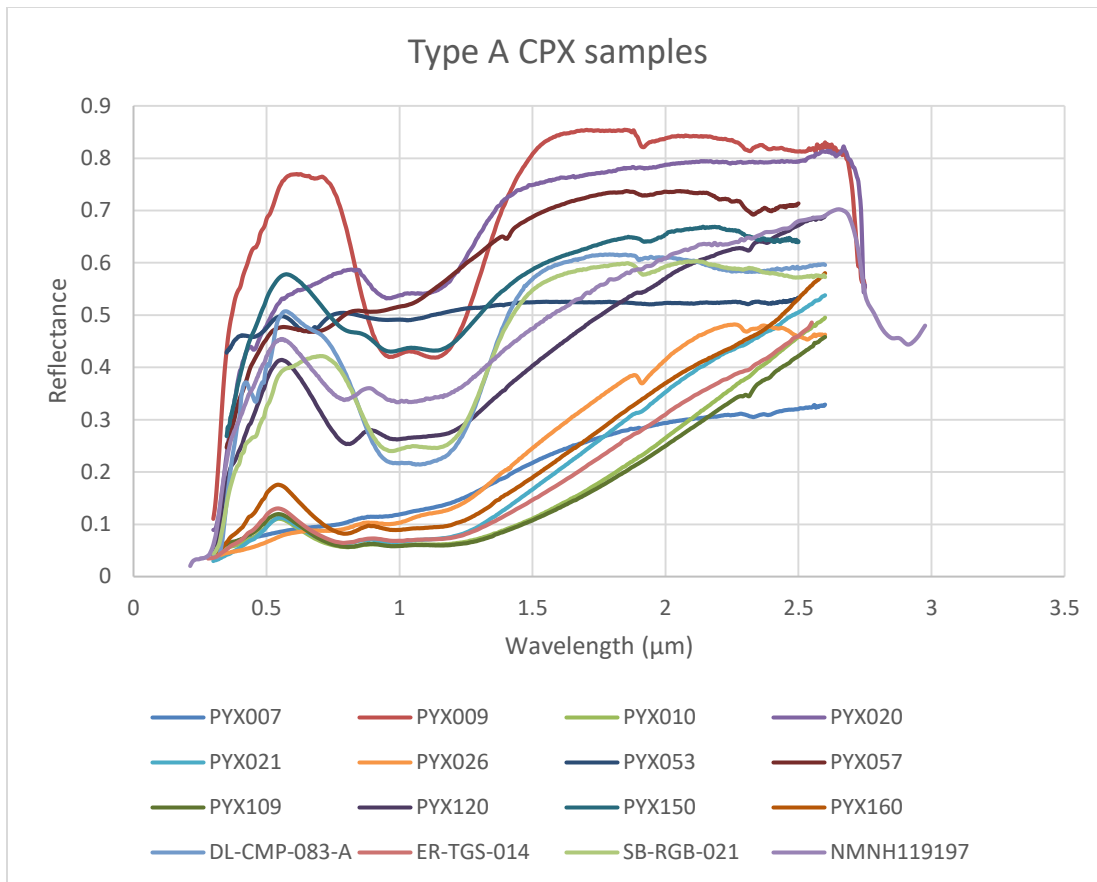
Figure 3. Type A clinopyroxene spectra of the samples used in this paper. Since there were so many samples, I did not separate them and just plotted them as is. Sources: HOSERLab, RELAB, USGS Spectral Library.
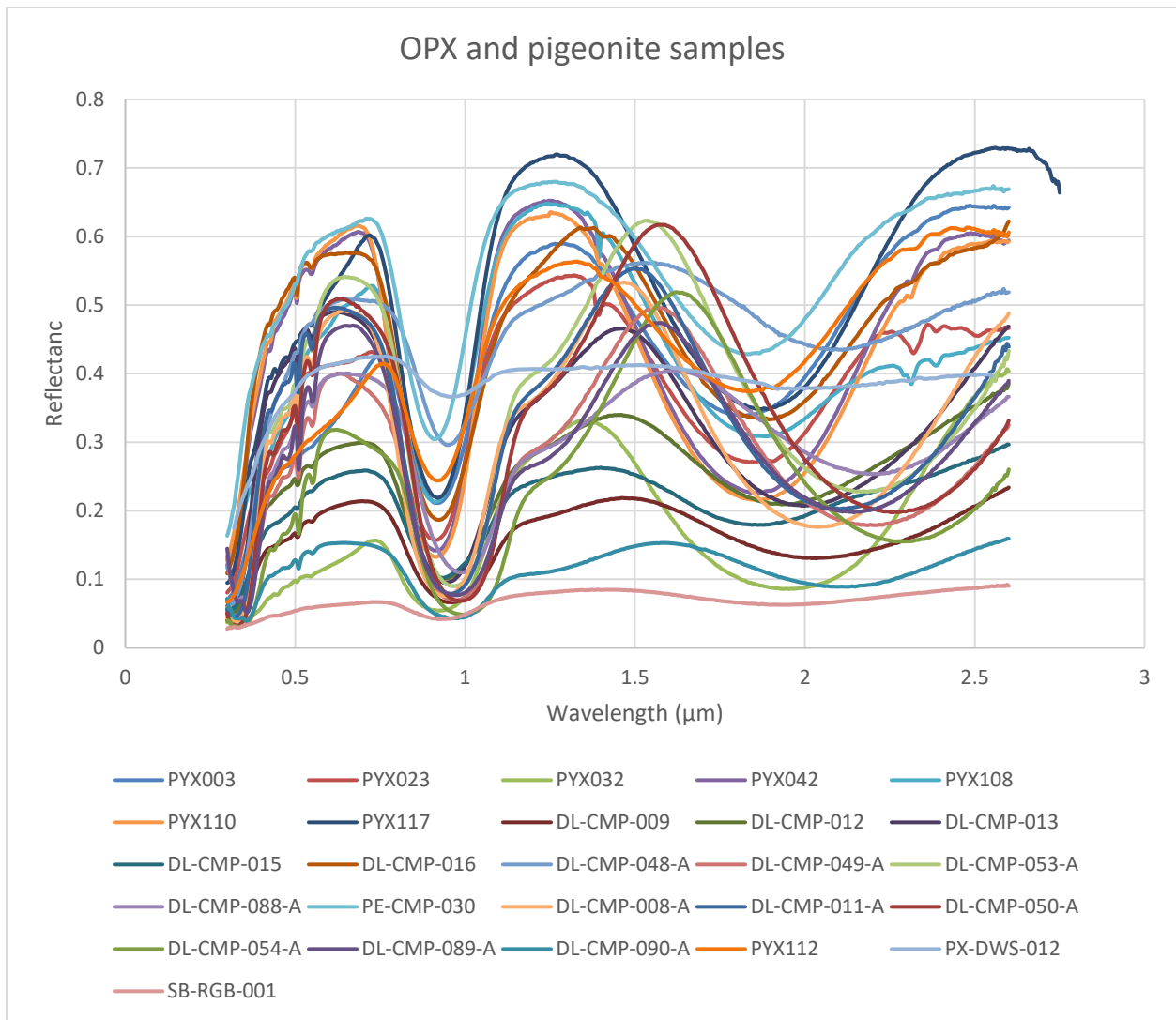
Figure 4. Orthopyroxene and pigeonite samples' spectra. Sources: HOSERLab, RELAB, USGS Spectral Library.
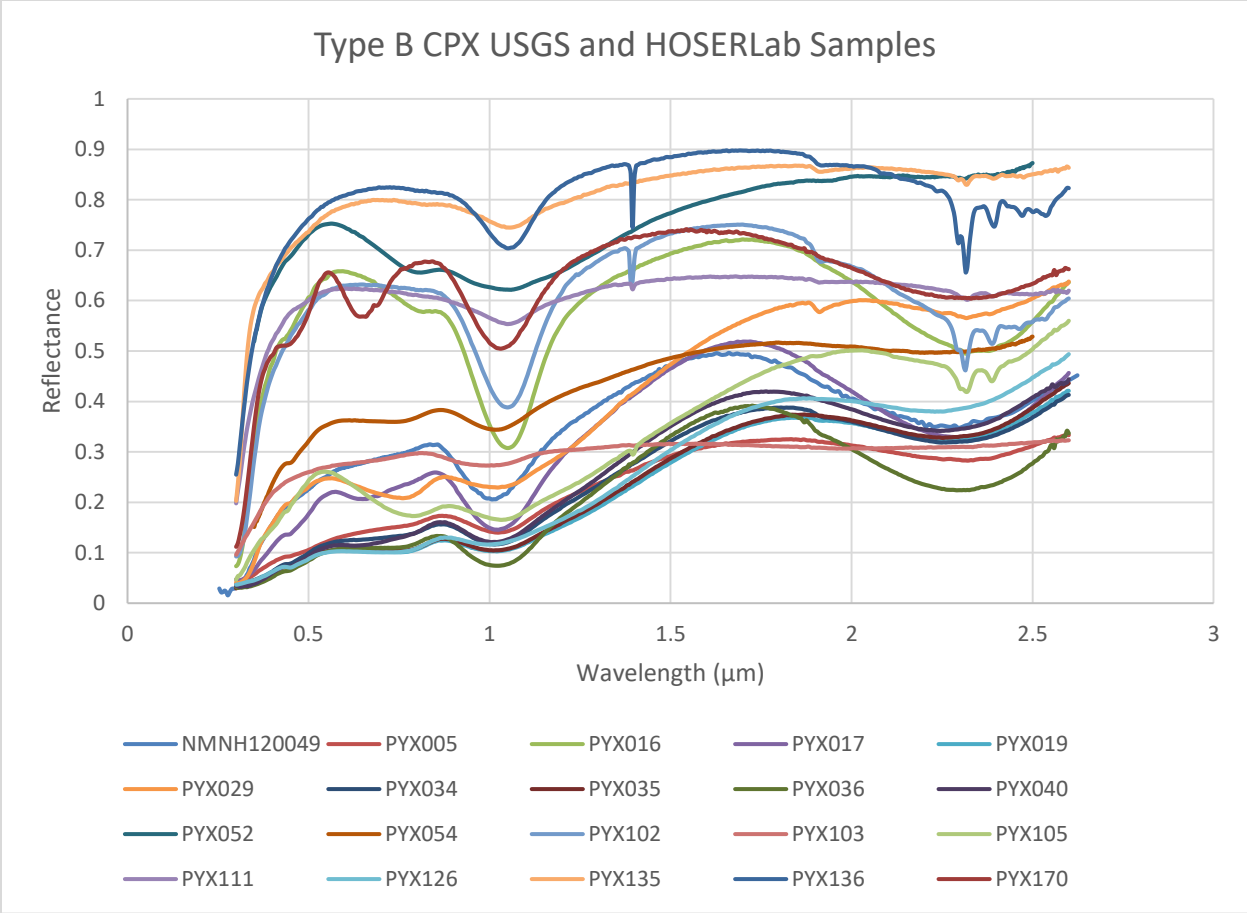
Figure 5. Type B clinopyroxene samples' spectra used in this paper from the HOSERLab and USGS Spectral Library.
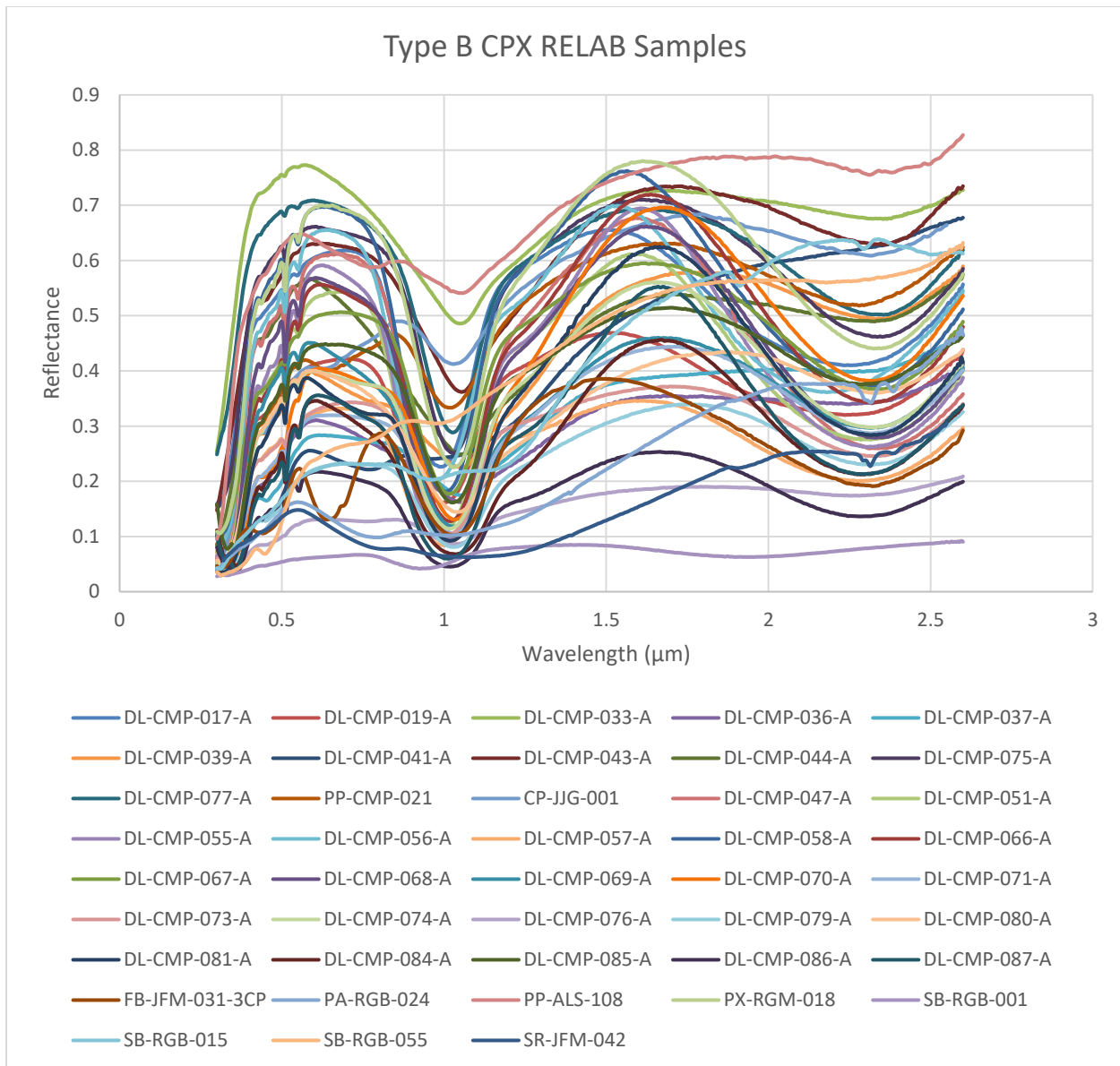
Figure 6. Type B clinopyroxene samples' spectra used in this paper from RELAB.

For this process, I printed out all of the spectra from the chosen samples so that I could visually see the different features and group them more easily. I reviewed the wavelength features of other typical cations that can be present in these pyroxenes, mainly titanium, ferric iron, and chromium (Burns 1970; Adams 1974; Adams 1975; Cloutis 2002). I marked down possible spectral features in each sample's spectrum. This was easier with the samples that had

the complete chemical analyses. Some spectra were cleaner than others, therefore not all of the spectral features I originally noted may be accurate, or even exist. I went through the samples' spectra three times: one time each for grouping similar spectral features, endmember compositions, and possible meteorite types. After this first review, I divided the spectra into the different approximate wavelength categories: 0.3-2.45/3.6 µm, which had 93 spectra; 2-14 µm, which had 2 spectra of one sample; 0-150 µm, which had 1 spectrum; 0.3-26/31 µm, which had spectra for nine samples; and 0-50 µm, which had 50 spectra. I further divided these into No iron/little iron/featureless, Type A/likely/possibly Type A, and Type B/likely/possibly Type B. There were also a few orthopyroxenes and a pigeonite, while some samples were difficult to categorize.

For the spectral feature groupings, I went through spectra in the visible and near-infrared wavelengths. These spectra were by far the most abundant, and they also have the main discernible features for pyroxenes. In order to see possible relationships between similar samples, I categorized them into groups if they had most or all of the spectral features in common. The features I were paying attention to the most were the main features at approximately 1 and 2 µm for type B clinoproxenes, pigeonites, and orthopyroxenes, and the features around 0.9 and 1.15 µm for type A clinopyroxenes. I tried to take slope into consideration as well.

The original spectral groupings that I made included a group that was all Type A, since there were limited samples for this type, although I had PYX120, PYX150, and PYX160 in particular stand out with each other. The group in total had PYX007, PYX009, PYX020, PYX053, PYX057, PYX120, PYX150, and PYX160. There was also a no iron/featureless group that consisted of DL-CMP-038-A, DL-CMP-052-A, DL-CMP-060-A, DL-CMP-072-A, and DL-

CMP-078-A. I did not end up using these as it was impossible to gather features from them. The other main group was mostly type B clinopyroxenes, although there were a couple unique ones, as well as a couple of orthopyroxenes and a pigeonite. The different groups were: PYX112; DL-CMP-035-A and DL-CMP-040-A; DL-CMP-048-A, DL-CMP-049-A, DL-CMP-053-A, and DL-CMP-088-A; DL-CMP-009 and DL-CMP-013; DL-CMP-010 and DL-CMP-018-A; PYX016, PYX102, and NMNHR18685; PYX101; PYX052, PYX105, PYX170, and DL-CMP-041-A; DL-CMP-033-A, DL-CMP-036-A, DL-CMP-037-A, DL-CMP-039-A, DL-CMP-043-A, and DL-CMP-044-A; DL-CMP-075-A and DL-CMP-077-A; PYX017, PYX019, PYX034, PYX035, PYX036, and PYX040; PYX054; DL-CMP-017-A and DL-CMP-019-A; PYX111, PYX135, PYX136, and DL-CMP-032-A; and the PP-CMP-021 group and NMNH120049.

I next grouped the visible and near infrared spectra that had similar endmember compositions of magnesium/enstatite, iron/ferrosalite, and calcium/wollastonite. I tried to use less than 5 wt. % difference as the limit for deciding similar endmembers. I wrote down if I knew they had notable amounts of other cations, such as chromium, titanium, or aluminum. However, I mostly relied on the spectral features for the samples, as I did not have chemical analyses for all of them.

After researching average and typical pyroxene endmember compositions for meteorites, I searched through the samples and information I had to group tentative samples that possibly corresponded to certain meteorite types. As can be seen above, several different meteorite types have a "large" amount of clinopyroxene, especially high-calcium pyroxene, which show the need to better understand what pyroxene compositions are making up the spectra from asteroids and meteorites. The group of meteorites I ended up focusing on, the angrites, is tricky because while

some of the endmember compositions might match, the samples might not have the usual amounts of aluminum or titanium like angritic pyroxenes.

Using these groupings, I made a tentative list of samples that had matching spectral features, possible meteorite types, and endmember compositions. I went over all of these potential groups and put them into categories of probable, possible, and least likely to be related. From these results, I found that there were five probable groups, with three out of the five having matches in all three categories. For possible groups, I found twenty groups, with eight having matches in all three categories. For the not likely groups, I found around thirty seven groups.

My probable groups consisted of nine samples. The groups were PYX135 and PYX136; DL-CMP-035-A and DL-CMP-040-A; PYX019 and PYX035; PYX016 and NMNHR18685; and PYX111 and PYX135. Going through these samples' spectra several times and observing their features, endmember compositions, chemical analyses if available, and possible meteorite matches have contributed to these tentative categorizations. I had more possible groups since my matching criteria was reduced. I had a total of twenty-eight samples and twenty-one groups. The groups were PYX120 and PYX150; PYX017 and PYX034; PYX035 and PYX054; DL-CMP-009 and DL-CMP-013; PYX016 and PYX102; DL-CMP-036-A with DL-CMP-037-A, DL-CMP-039-A; DL-CMP-033-A and DL-CMP-043-A; PYX111, PYX135, and PYX136; DL-CMP-075-A and DL-CMP-077-A; PYX034 and PYX035; DL-CMP-010 and DL-CMP-018-A; DL-CMP-049-A and DL-CMP-053-A; DL-CMP-017-A and DL-CMP-019-A; DL-CMP-036-A and DL-CMP-044-A; DL-CMP-039-A and DL-CMP-044-A; DL-CMP-037-A and DL-CMP-039-A; PYX102 and NMNHR18685; PYX102 and PYX135; and PYX102 and PYX136. However, some of these groupings have potentially problematic samples, which will be reviewed below. Therefore, these groups are tentative and the graphs later on are likely more useful

because they use all of the samples. All of the probable and possible original spectral groups are in table 4 in the appendices.

While reviewing the samples, I came across several that appeared to be impure or mixtures, despite what the databases had said. Some of the samples appeared to have olivine. Olivine is an orthorhombic orthosilicate, meaning it is made up of separate silicon and oxygen tetrahedra that are linked with cations, usually $Fe^{2+}$ and $Mg^{2+}$ (Burns 1970; Burns 1993; Nesse 2012 p.212). Olivine has three features around one micron (0.8 µm, 1.04 µm, and 1.3 µm) and the most common endmembers include forsterite, a magnesian olivine, and fayalite, an iron-rich olivine (McSween 1999; Gaffey 2011). This can change the shape of the one micron feature of a typical pure pyroxene, making it have more of the three featured "v" shape of a typical olivine. However, because olivine only has a one micron feature, the two micron feature of the pyroxene in an olivine-pyroxene mixture stays the same (Singer 1981). For olivine, with an increase of $Fe^{2+}$, the one micron features move to longer wavelengths with an increase in band depth, the wavelength position movement being similar to orthopyroxene (Burns 1970; Adams 1975; King & Ridley 1987). The 1.3 µm inflection of an olivine typically enlarges with this iron increase as well (Adams 1975). Ferrous iron and magnesium usually reside in six-fold coordination sites, both being distorted from octahedral coordination, although M1 is centrosymmetric and M2 is not (Burns 1970; Burns 1993). Iron in the M2 sites creates the really large feature around 1 µm, while iron in the M1 sites create the two shoulder features to each side of it (Burns 1970). Singer (1981) writes that even when there are other phases in a mixture, olivine's signature one micron features still appear, although they are much less intense.

Other possible impurities can be caused by plagioclase, which induces a faint inflection in pyroxenes around 1.25 µm and increases spectral reflectance (Adams 1975). Plagioclase is a

type of feldspar, which is a framework silicate (Nesse 2012 p.212). Its main cations include sodium and calcium (McSween 1999; Nesse 2012 p.212). It did not appear that my samples had this, but it is something to keep an eye out for. It takes a large amount of plagioclase to make a significant impact in the spectra, however.

There is a possibility that several of the samples were contaminated with amphiboles. Amphiboles are double chain silicates, in contrast with pyroxenes which are single chain silicates (Nesse 2012 p.212, p.294). Amphiboles have smaller absorptions from ferrous iron from 0.93-1 µm and around 2.3 µm, although this feature is typically much narrower than pyroxenes; like orthopyroxenes, more iron causes all bands to move to longer wavelengths (Burns 1970; Adams 1975; Burns 1993). Amphiboles that have a high amount of ferric iron have fainter 1 and 2.3 µm features (Adams 1975). The 2.3 µm feature is also thought to be from a combination of two bands, one from ferrous iron and the other from hydroxyl (Adams 1975). Clark (1995-references Clark et al. 1993b) notes a pyroxene sample that has a faint amphibole contributor at around 2.3 µm. Amphiboles can often cause hydroxyl and water bands to appear around 1.4 µm and 1.9 µm, because these silicates often contain hydroxyl (Adams 1975; McSween 1999; Gaffey 2011). Amphiboles often display a feature around 0.65 µm, which can be attributed to a $Fe^{2+}$-$Fe^{3+}$ charge transfer (Adams 1975-references Burns 1970b). Note that this is a common $Cr^{3+}$ band in pyroxenes, although other features usually need to be present in order to consider it to be from chromium. The cummingtonite (iron-magnesium) subgroup of amphiboles have stronger one micron bands than two micron bands. This would cause more changes in the one micron region if there were these impurities in pyroxenes, possibly resembling olivine (Cloutis et al. 1986; Nesse 2012 p.311-references Leake et al. 2003).

There are a few samples that appeared to have silica glasses and cristobalite. Usually, this will not make much of a difference since the amount of glasses is typically small. Iron-bearing silicate glasses do however show a weak feature from ferrous iron around 2 µm (Adams 1975; Klima et al. 2011-referencesBell et al. 1976; Horgan et al. 2014). With the model Klima et al. (2011) used, they needed to add a band around 1.8 µm so that the glass could be properly accounted for in order to make the 2 µm feature accurate. There can also be a band from glass around one micron, but the other features can obscure it somewhat, making it not necessary to model (Klima et al. 2011; Horgan et al. 2014-references Adams 1974, Minitti et al. 2002). Klima et al. (2011), while studying high-calcium clinopyroxenes from Turnock et al. (1973), found that glass has a small effect on those samples because they have higher albedos, weaker features, and less ferrous iron than the others. Horgan et al. (2014) looked at pyroxene and glass mixtures and found that less than 80 wt. % glass in mixtures only subtly widens and moves the one micron feature to longer wavelengths.

The samples that appeared to have impurities or are mixtures are NMNHR18685, PYX101, DL-CMP-010, DL-CMP-018-A, DL-CMP-032-A, DL-CMP-033-A, DL-CMP-035-A, DL-CMP-036-A, DL-CMP-037-A, DL-CMP-039-A, DL-CMP-040-A, DL-CMP-041-A, DL-CMP-043-A, and DL-CMP-044-A. The main issue with NMNHR18685 is rather strong weathering. PYX101 has an asymmetrical one micron feature. DL-CMP-010 and DL-CMP-018-A appear to be two-pyroxene mixtures, as each has two features around two microns. DL-CMP-035-A and DL-CMP-040-A also are bizarre and have two micron features at much shorter wavelengths than expected. Several of these samples were studied by Klima et al. (2011), although most on the RELAB site were the "–A" versions: DL-CMP-033-A, DL-CMP-036-A, DL-CMP-037-A, DL-CMP-039-A, DL-CMP-043-A, DL-CMP-075-A, and DL-CMP-077-A.

That paper also studied DL-CMP-009 and DL-CMP-088, but those ones did not appear to have issues with them, despite possible exsolution in the former (Klima et al. 2011). DL-CMP-032-A appears to have weak and noisy features around 1 and 2 µm but there is no iron in the endmember composition, so I did not include it. DL-CMP-041-A had a slope that made it hard to get the 2 µm feature, so there could be some error in that. I kept it as a sample, however. There were few impurities with the remaining samples, and their up-to-date endmember compositions and MGM-derived band centers are in table 2 in the appendices. DL-CMP-033-A had 1 % cristobalite, while DL-CMP-036-A was said to have 5 % bustamite. DL-CMP-039-A had 1 % impurities. The one micron features of DL-CMP-033-A, -036-A, -037-A, -039-A, and -043-A appear to possibly have olivine in them. Klima et al. (2011) found that DL-CMP-033-A, -036-A, -037-A, -039-A, and -043-A were transitional types between type A and type B high-calcium clinopyroxenes. I ended up still using those samples because there weren't any problems found by Klima et al. (2011). DL-CMP-075-A and DL-CMP-077-A do in fact have more similar endmember compositions, so it is more likely that they are more related than when categorized in the original spectral groups. The final group of possible problem samples have their spectra graphed in Figure 7.
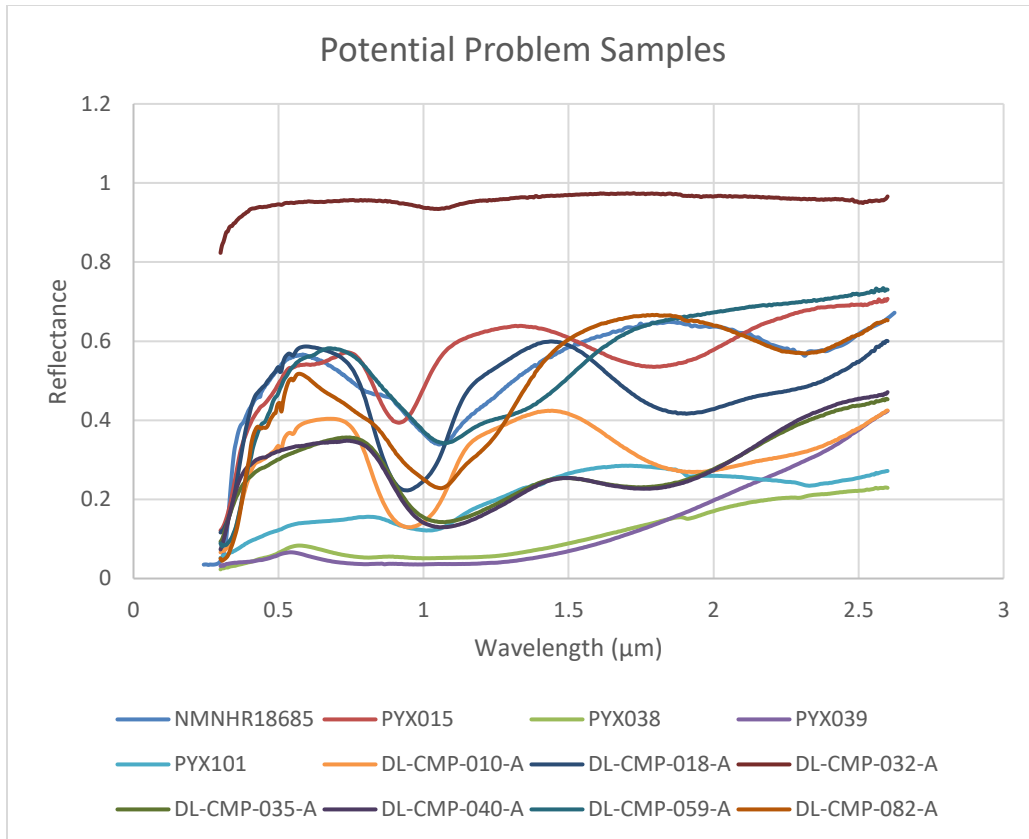
Figure 7. Potential problem samples from the USGS Spectral Library, HOSERLab, RELAB.

I went through the catalogs again and found other possible samples, including ones that are in some mixtures that I will talk about later. A few samples were not as pure but were still looked at because they were in mixtures. I also went through these catalogs in order to try to fill in any gaps that I could for my band minima graphs, particularly with hedenbergites and pigeonites. I also included some more orthopyroxenes in the pyroxene feature graphs, as they were present in some mixtures. In addition to finding those band minima, I also found some for several olivine and plagioclase feldspar samples, as again they were in the mixtures. For both of these types, it was harder to graph, especially when I graphed only the main features, since they only had one predominate feature each. In those cases, I graphed their one main band minimum

against one micron. The non-pyroxene and some mixture pyroxene information are in tables 9 and 10 in the appendices.

In addition to the previously mentioned "problem samples," I added PYX015, PYX038, PYX039, DL-CMP-059-A, and DL-CMP-082-A. These are also in figure 7 above. I included them in the graphs that I made, but I also made some graphs without them. PYX015 I took out because it had some olivine in it, but also because its minima were a bit bizarre for a clinopyroxene, as they were both at shorter wavelengths. It also had $Na_2O$ and $Cr_2O_3$ around 1.3 wt. %. PYX038 and PYX039 were type A clinopyroxenes but they had very weak features that made it hard to find the minima. I did manage to find some minima in the literature for these two at least, which will be mentioned below. DL-CMP-059-A I took out because its spectrum resembled olivine. DL-CMP-082-A also looked like it may have had some olivine in it; it had a similar possible issue to some of the DL-CMP-033-A types mentioned above.

I did not group these additional samples as I had with the previous group of samples, but I did graph them all together by the main two features, type of pyroxene, calcium amounts, iron amounts, and magnesium amounts, the latter three being from their endmember formulas. The endmember compositions may not be completely accurate for pyroxenes with higher amounts of other cations, but with all the samples I have it hopefully should not make too much of a difference. In addition to these graphs, I also graphed features from all the samples' spectra, as well as average band minima for the samples that had more than one spectrum. From all of these different graphs I hoped to see the big picture among all the various samples that are available. These graphs are in the next section.

As mentioned in a section above, Schade et al. (2004) tentatively stated that the samples with high iron and calcium were more likely to be type A, whereas lower iron and high calcium pyroxenes could be either, depending on the calcium amounts. Seven of the twelve type A samples I looked at that had endmembers were above $Wo_{50}$, while nine of those samples had above $Wo_{49}$. These samples included PYX007, PXY009, PYX010, PYX021, PYX026, PYX109, PYX120, PYX150, and PYX160. The remaining three samples were PYX020 at $Wo_{48.7}$, PYX053 at $Wo_{47.9}$, and PYX057 at $Wo_{41}$. The only really questionable sample that went against the high calcium amounts is PYX057, which had much higher amounts of aluminum, sodium, titanium, and potassium than most samples. This sample being a possible type A may be explained by different site occupancies, although there is a decent amount of iron still. There is a possibility that PYX057 might be an AB type, as its spectra weren't the cleanest and there was a dip after two microns. However that dip was at slightly longer wavelengths than the usual type B clinopyroxenes in this paper. The type B clinopyroxenes were more varied, like Schade et al. (2004) stated and this can be seen below in figure 16.

As will also be mentioned in the sections below, I performed some $3^{rd}$ order polynomial fittings to find the minima of all type A clinopyroxenes, some type B clinopyroxenes, all mixtures, and all meteorites in this study. I used the spreadsheets and equations from McCraig et al. (2017), which had comprehensive appendices on finding minima and other spectral features. Polynomial fittings are calculated for specific wavelength ranges that one chooses around absorption features in order to find minima that are not as affected by noise. The fitted minima are the closest actual measured values to the ideal minima values found from the polynomial equations. I chose the third order polynomial because it appears to be the most useful fitting in that it can find curves for minima with low-resolution, noisy remote sensing spectra, as well as

high-resolution laboratory spectra. Higher orders can start to curve around even noisy "features," which can make the minima less accurate (McCraig et al. 2017). In the samples I looked at, some minima I found using lowest reflectance were affected by noise, usually from water features around the two micron minima. Therefore, using the polynomial fitting provided more input into the accuracy of the previously found lowest reflectance minima. For each of the sections below, I have tables in the appendices that state the range of x values I used for fitting to help make the steps repeatable for future studies. If needed, there are supplementary spreadsheets as well.

The appendices and Excel spreadsheets in McCraig et al. (2017) were specifically made to both help standardize analyzing spectral features and to help newer students, such as myself, navigate curve fitting. The spreadsheets were created so that one could use the available equations and sheets by simply inputting one's own variables and changing the ranges in the name manager to get their relevant results. Once that was done, one usually needed to tweak the axes and labels on the graphs as well. Since I am new to the field and I am looking at many spectra, it was a useful way to both learn about polynomial fittings and apply the data.

## Discussion of sample band minima and centers

For the next part in my research, I created many graphs. The first major groups of graphs were visually comparing spectra. I stacked the grouped spectra so that they could be viewed more easily in one graph. I plotted them all as they were and, if necessary, added constants so that the features could be separated since sometimes the spectra were on top of one another. I did this for my probable groups, my possible groups, and the original spectral groupings. By graphing the spectra, I could see more pronounced differences and similarities between the samples. Their spectra can again be seen in Fig. 2-7 above.

These graphs were used in the next step, which was to find the two main feature band minima from each sample. With the initial research I did, I found the band minima using the lowest reflectance among specific wavelength ranges around absorption features. Luckily these were laboratory spectra, so for many samples the minima were close to the centers. It is important though because "currently, there are no calibrations which can be routinely used to correct a band minimum determination for this shift," (Gaffey 2011). It was sometimes difficult as several samples, particularly Type A clinopyroxenes, had steep slopes and faint minima, which interfered with the results. Finding the lowest reflectance point could also be influenced by noise in the data (Cloutis et al. 1986). This was the case with some Type B clinopyroxenes that had water features seemingly interfering in the two micron region. For certain samples I used polynomial fitting later on to compare, which was useful for the noisier samples. It was also important for future work when looking to compare with noisy, low-resolution asteroid spectral data (McCraig et al. 2017).

The continuum slopes of the samples were mostly even and not reddened, but there were some that had steeper slopes. I tried to identify all features using lines from rulers and Excel's tools. To tentatively group the spectra initially, I had used a ruler and printed out spectra to compare them. From the lines, I narrowed down ranges of the wavelength positions. For the features themselves, I needed more accuracy, so I used Excel, since curve fitting can be subjective (Gaffey et al. 2002; Gaffey 2011-references Nedelcu et al. 2007). For this, I took the data from around that position and sorted it to find the smallest reflection value. I did this for both of the two main features, which were around 0.9 and 1.15 µm for the Type A clinopyroxenes and around 1 and 2 µm for the Type B clinopyroxenes, orthopyroxenes, and pigeonites. There were several difficulties and patterns with finding the minima. The easiest

samples to find the minima for were the orthopyroxenes, as they typically were very clean and had stronger features. The pyroxenes I was most interested in, type A clinopyroxenes, were typically the hardest samples for which to find the minima. This was because many of these samples are extremely red-sloped, which made it difficult to impossible to find one of the two pyroxene features around one micron. This can sometimes be attributed to ferric iron in the sample (Cloutis et al. 2006a). I did my best to find the minima for these, but due to those difficulties, the vast majority of the type A samples will have some error with the second one micron feature. With the type B clinopyroxenes and type AB clinopyroxenes, the one micron feature was usually easy to find, but the two micron feature was sometimes noisy from water features. I noticed that this noise was usually visually around the same position as the minima, but it is still another source of error to keep in mind. Type AB samples were sometimes red-sloped, causing complications with the two micron feature. Pigeonites were not difficult for the most part with finding the minima, however there were very limited samples for this kind and they were noisier than your average orthopyroxene samples. With the olivine samples, I only found the main one micron feature and not the shoulders because they were harder to get due to the slopes. Plagioclase feldspar samples had minima that were pretty easy to obtain for the most part since there was only one main feature.

After finding two main features for all samples, I graphed them against each other in the probable groups, possible groups, and original spectral groups. After making all of these smaller graphs, I finally graphed them all against each other in a large final graph, which can be seen in Fig. 8 and 9 here. From these, I could see a potential sample trend of which I wanted to go into more depth. As expected, there were distinct regions of the graph that defined the Type A clinopyroxenes, the orthopyroxenes and low-calcium pyroxenes, and the type B clinopyroxenes.

As a reference, I generally considered the sample a type B clinopyroxene if the calcium content was above $Wo_{25}$, as that is around the change in shape group. The curve between the orthopyroxenes and type B clinopyroxenes was a mixture of the two. This makes it appear to be at least somewhat of a smooth transition between the two types, which was also found in Cloutis and Gaffey (1991). I looked more in depth into that region later on when I went into more detail with the calcium and iron amounts of the samples. There were some random features that stuck out in Fig. 8 that were some of the "problem samples," particularly DL-CMP-035-A and DL-CMP-040-A, which as mentioned before were possibly mixtures of two pyroxenes. There were a couple of other samples that stuck out from the rest but that still fit the trends, namely PYX057, DL-CMP-059-A, and PYX103. PYX057 may be off the trend for likely type A clinopyroxenes for several reasons, including that it had high aluminum, at 14.02 wt. % $Al_2O_3$; it also appears to have a faint 2 µm feature, making it possibly a type AB. Cloutis and Gaffey (1991) mention that samples high in aluminum end up below the trend, which was happening with this sample. However, they found that for the orthopyroxene trend so it may not apply here. Also in the type A group, I ended up considering DL-CMP-059-A a problem sample because it resembled olivine so I took it out of the graphs that did not have the problem samples. Some possible reasons for PYX103 sticking out in the orthopyroxene-type B section were that it had 0.35 wt. % $TiO_2$, which isn't negligible, or that there was some error because the two micron feature was rather weak in this sample. It also had some orthopyroxene exsolution which might have been causing some of the difficulties with the 2 µm feature (Cloutis et al. 1991). Again, Cloutis and Gaffey (1991) found that titanium, and chromium, in diopsides and augites go off the general trend, which was something to consider here. The bottom of the second curve that had orthopyroxenes and type B clinopyroxenes was, as expected, predominantly orthopyroxene samples. There were

also some pigeonite samples among the orthopyroxenes, but not at the very bottom of the curve. The one lone type B clinopyroxene at the very bottom of the curve was PYX015, which I considered an unusual sample, as mentioned in the previous section. There were also DL-CMP-010 and DL-CMP-018-A in the bottom half of that curve, although they were likely pyroxene mixtures, as they had two 2 µm features. The type B clinopyroxenes covered a wider area than the bottom of the curve, but that was probably because there were vastly more samples in this study of clinopyroxenes than orthopyroxenes. This area was somewhat noisy but I did not have the chemical analyses for many of the samples off the curve to see if they were high in aluminum or titanium. This second curve of the orthopyroxenes and the type B clinopyroxenes resembled the curves from papers mentioned previously, such as Cloutis and Gaffey (1991). Type A trends did not appear to be in the literature. The type A trend that I found was a steeper and straighter slope than for the orthopyroxene to type B clinopyroxene trend, which went fairly straight through the orthopyroxenes and then deviated slightly to form a curve of the type B clinopyroxenes.

When I removed the problem samples, the trends were even straighter and more apparent for all the different pyroxene types. A graph that more easily shows these distinctions is in Fig. 10. From this it is easier to see the different sections. Type A clinopyroxenes were again on the left hand side near the shorter wavelengths. Orthopyroxenes and pigeonites started to appear around 1.8 µm and gradually went in a near straight line towards the type B clinopyroxenes. There were a couple interlopers of both types but there was a pretty clear boundary between the two groups, which was also distinguished by the change in curve and slope.

I have tried to cover as much of the pyroxene tetrahedral as I could in order to look at these possible trends. I then made the same graph but grouped the different samples with

different shapes and colors so as to differentiate between them. I also graphed only averages to make it easier to read. It should be noted that when I went through samples in more detail, a few samples with multiple spectra had features with varying wavelength positions.
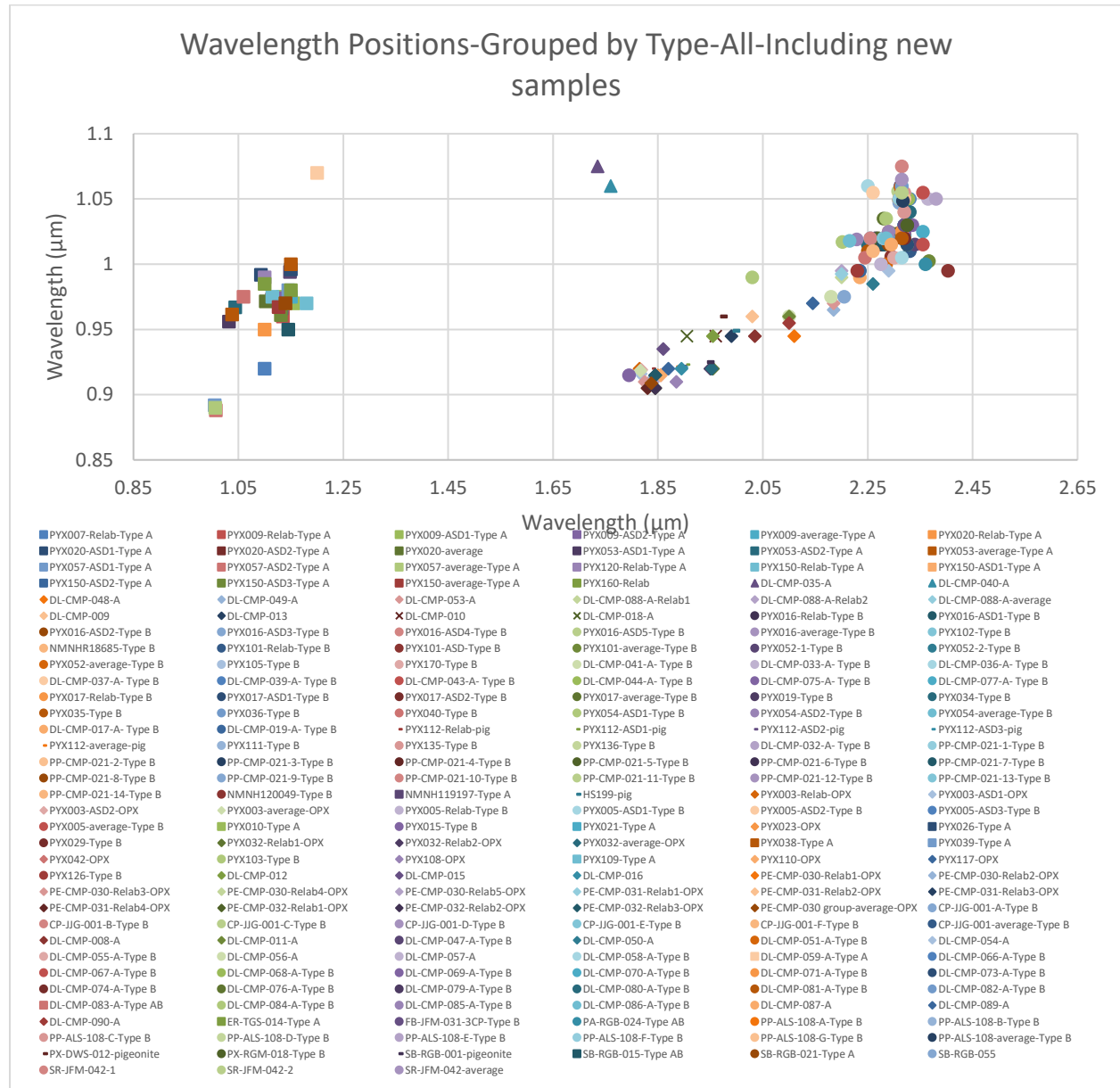


Figure 8. All samples' two main wavelength position features graphed against one another. Squares=type A/AB clinopyroxenes, circles=type B clinopyroxenes, diamonds=orthopyroxenes, and dashes=pigeonites. The triangles and X's represent two groups that were unknown and likely mixtures of pyroxenes. Sources: HOSERLab, RELAB, USGS Spectral Library.
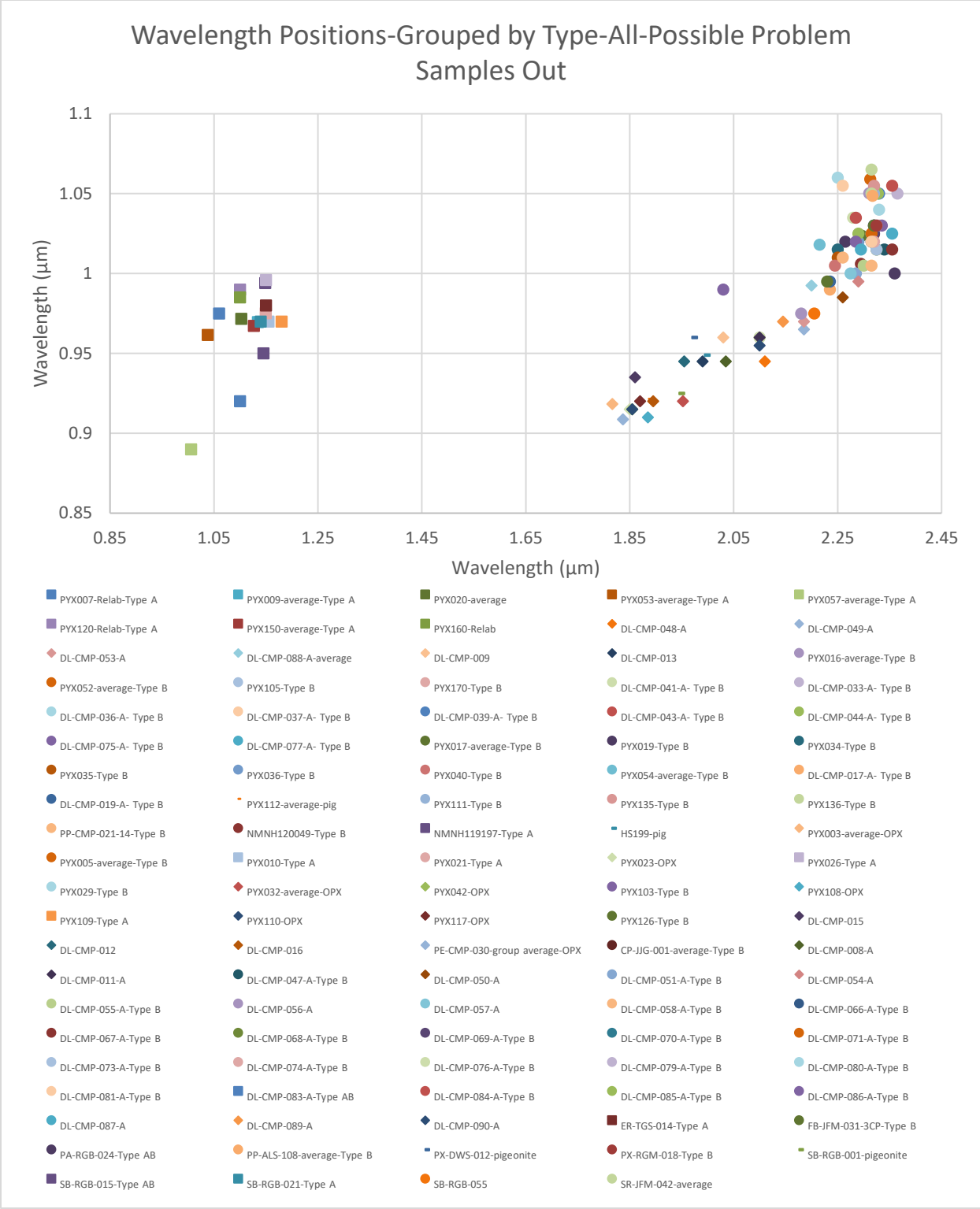
Figure 9. Main two pyroxene wavelength positions graphed against each other for all samples excluding the problem samples which were discussed above. Squares=type A/AB clinopyroxenes, circles=type B clinopyroxenes, diamonds=orthopyroxenes, and dashes=pigeonites. Sources: HOSERLab, RELAB, USGS Spectral Library.
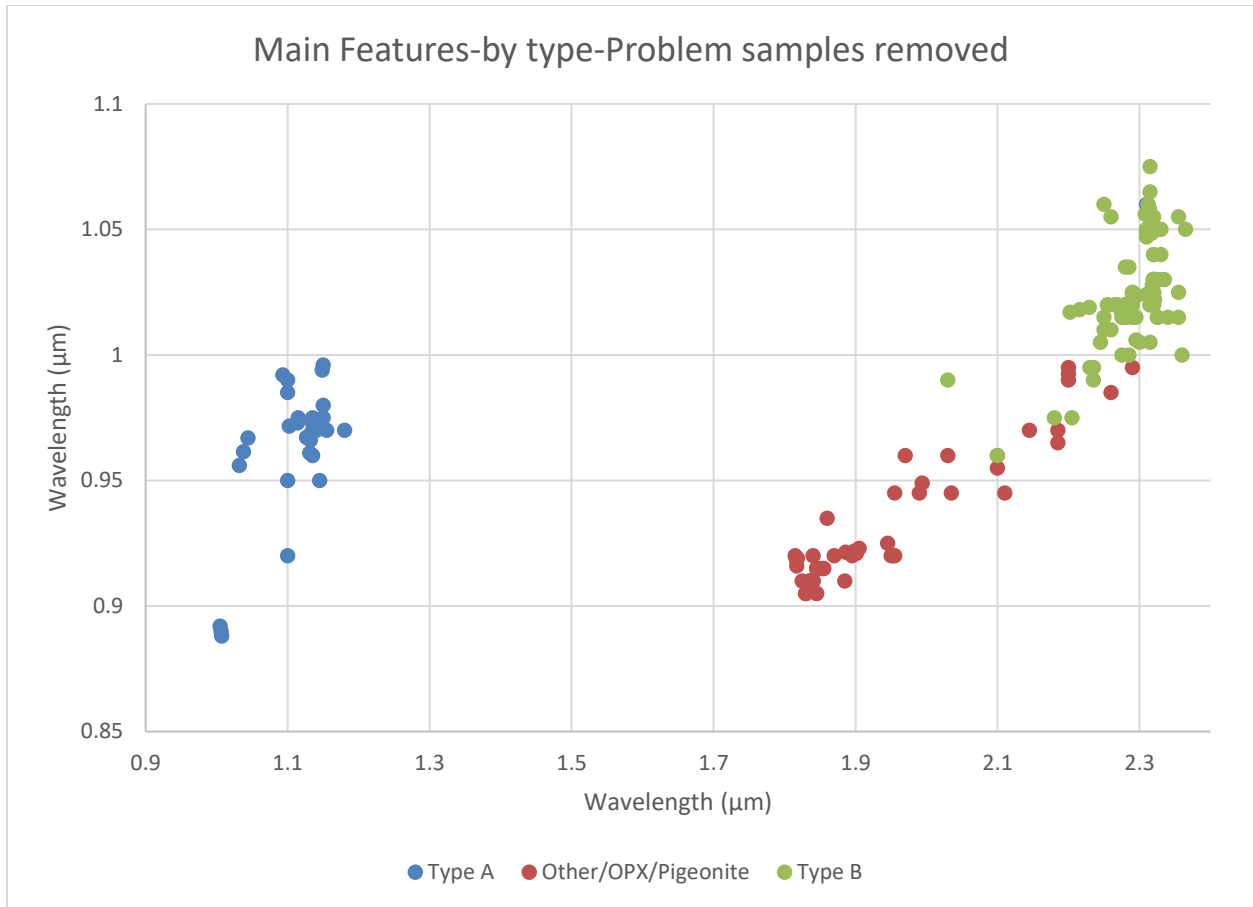
Figure 10. Main two pyroxene features by type. Sources: HOSERLab, RELAB, USGS Spectral Library.

I also took the graph of all of the samples and grouped them according to their original spectral groups, as seen in figures 11 and 12. This was another comparison and can aid with interpretation of a possible trend. With the original groups, there were few orthopyroxene samples. The original spectral groupings and information are in table 4 in the appendices. In figure 11 there were some samples that stuck out, such as DL-CMP-035-A and DL-CMP-040-A. These two were previously talked about being possible problem samples, so I took them out for some of the graphs. The two separated curves represented the type A clinopyroxene and orthopyroxene-pigeonite-type B clinopyroxene curves. The type A curve was noisier, but that could be because some of the features' wavelengths were harder to get from type A

clinopyroxene samples. The other curve actually started at the bottom with DL-CMP-010 and

DL-CMP-018-A, which were likely mixtures of two pyroxenes and were therefore problem

samples as well. Around the bottom of the curve was also the lone confirmed pigeonite,

PYX112, which was followed by some orthopyroxenes as one went up the curve. When all the

samples, not just the averages, were used for these original groups, the curves were noisier,

which was to be expected as there was some slight variability between each sample. However,

the vast majority of these samples also had other features, so I next created those graphs to try to

get the whole picture.
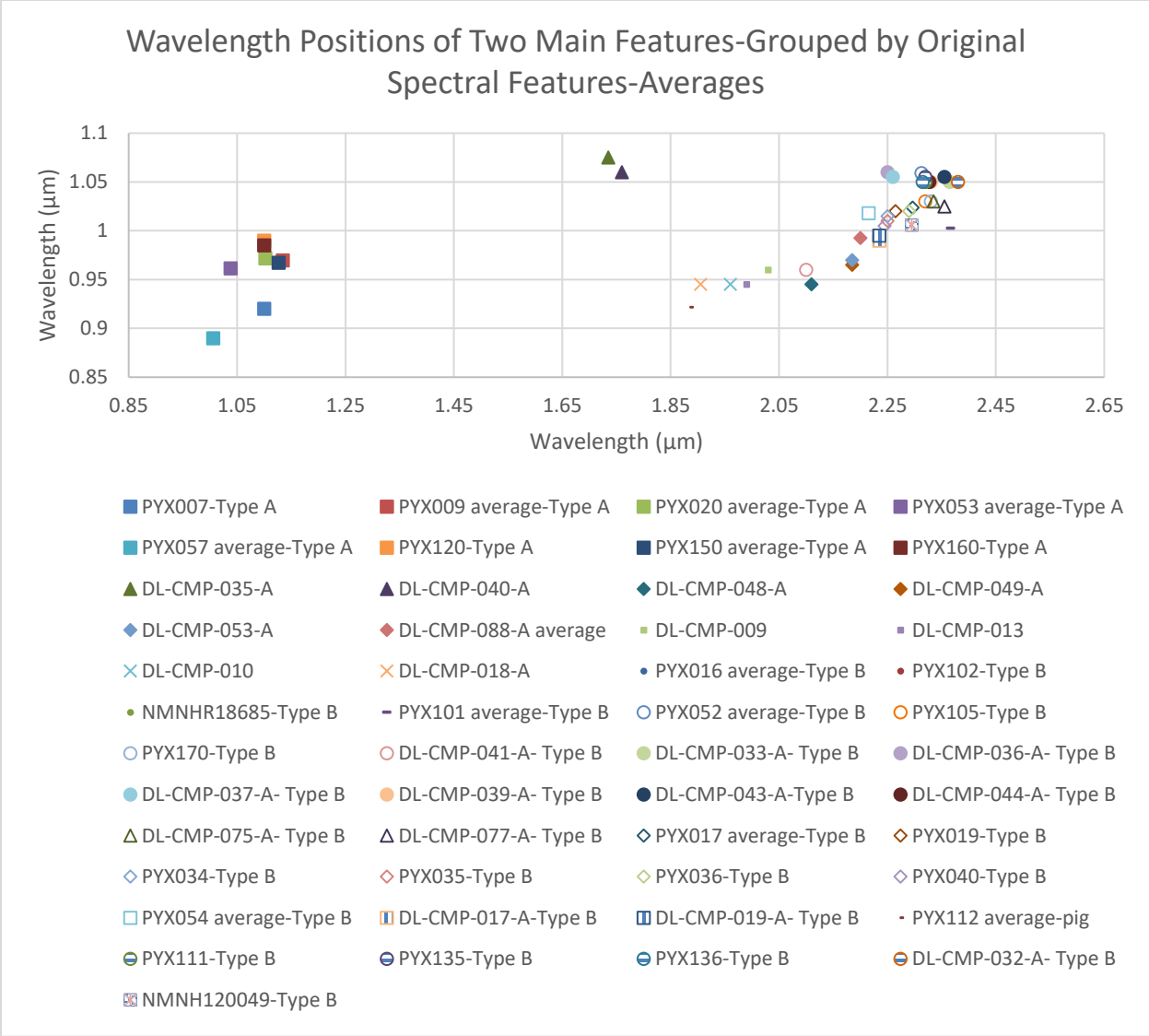
Figure 11. Graph of the two main features for the original spectral groups, including possible problem samples. The different symbols represent the different groupings. Sources: HOSERLab, RELAB, USGS Spectral Library.
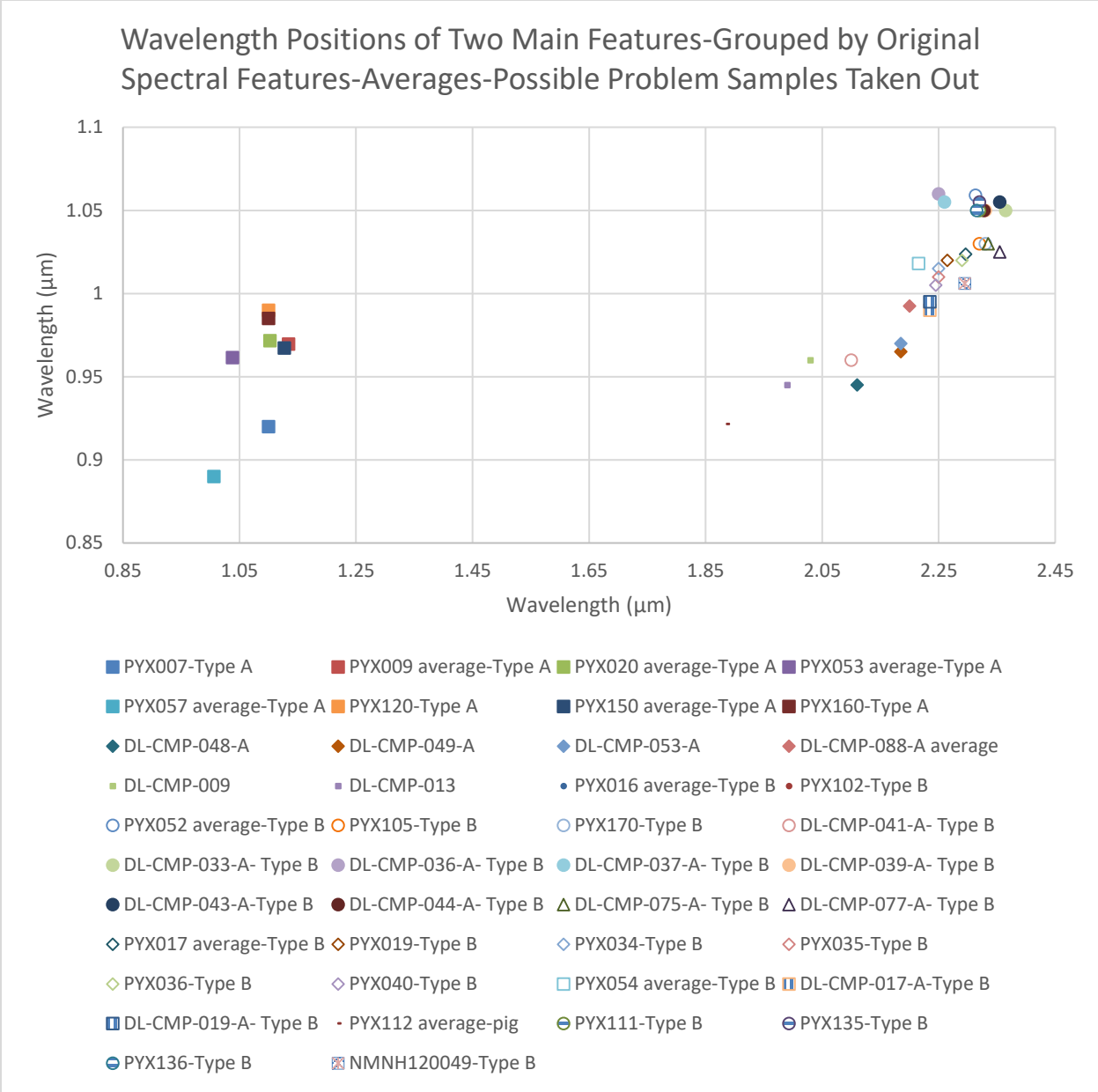
Figure 12. Graph of the two main pyroxene features sorted by the original spectral groupings. The different symbols represent the different groupings. Source: HOSERLab, RELAB, USGS Spectral Library.

I had a similar process for finding the other spectral features. As per Adams' graphs

mentioned previously (1974; 1975), I graphed all the features of a particular sample against the

other features, always putting the longer wavelength feature on the x-axis. In this way, similar

samples would be grouped in similar areas on the graphs. These smaller features were sometimes

harder to find because of the typical steep slope around the 0.4 µm region. The features that I

picked to investigate were ones that appeared to not just be noise in the spectra, although it could be hard to differentiate. Taking that into account, I went through all the spectra again to find the regions with features. I had to be stricter with my wavelength ranges for these because of the slopes. So while some of the ranges did not change when I sorted them, there was still a feature in that region. Therefore, I am hoping that the slope did not cause too many problems. To be more accurate with these harder to find features, I changed the x-axis if possible in order to more definitively narrow down the wavelength position ranges. Like with the other features, I made graphs to compare them with each other in the probable, possible, and original spectral features groups. The original spectral features groups graph is in Fig. 13. The different spectra ranged from having zero to four other features in addition to the main two features. I then graphed them all together as before to make it easier to compare with each other, which is in Fig. 14. Since there were so many samples, it was hard to discern the different groupings and types, which is why I made some graphs below and separated them by pyroxene types, calcium amounts, iron amounts, and magnesium amounts. I graphed the data by type in Fig. 15, so there were three groups: Type A, Other/OPX/Pigeonite, and Type B. In this way it was easier to see possible distinct areas such as was seen in Fig. 10 above. The graph is still pretty crowded but it did appear to be that orthopyroxene band minima were consistently at shorter wavelengths. Type A clinopyroxenes also appeared to have fewer shorter wavelength features, which could possibly be because of the reddened slopes and additional cations usually present. However, in general, the different types had different shorter wavelength features, so it can be harder to compare. I did notice that samples, both orthopyroxenes and type B clinopyroxenes, had similar sharp shorter wavelength features around 0.5 µm and 0.54 µm when they were high in iron. The type B clinopyroxenes dominated the 0.7 µm features area over the other groups. The vast majority of

type A clinopyroxene samples plotted between 0.9-1.2 µm on the graph's x-axis, which makes sense considering their features.
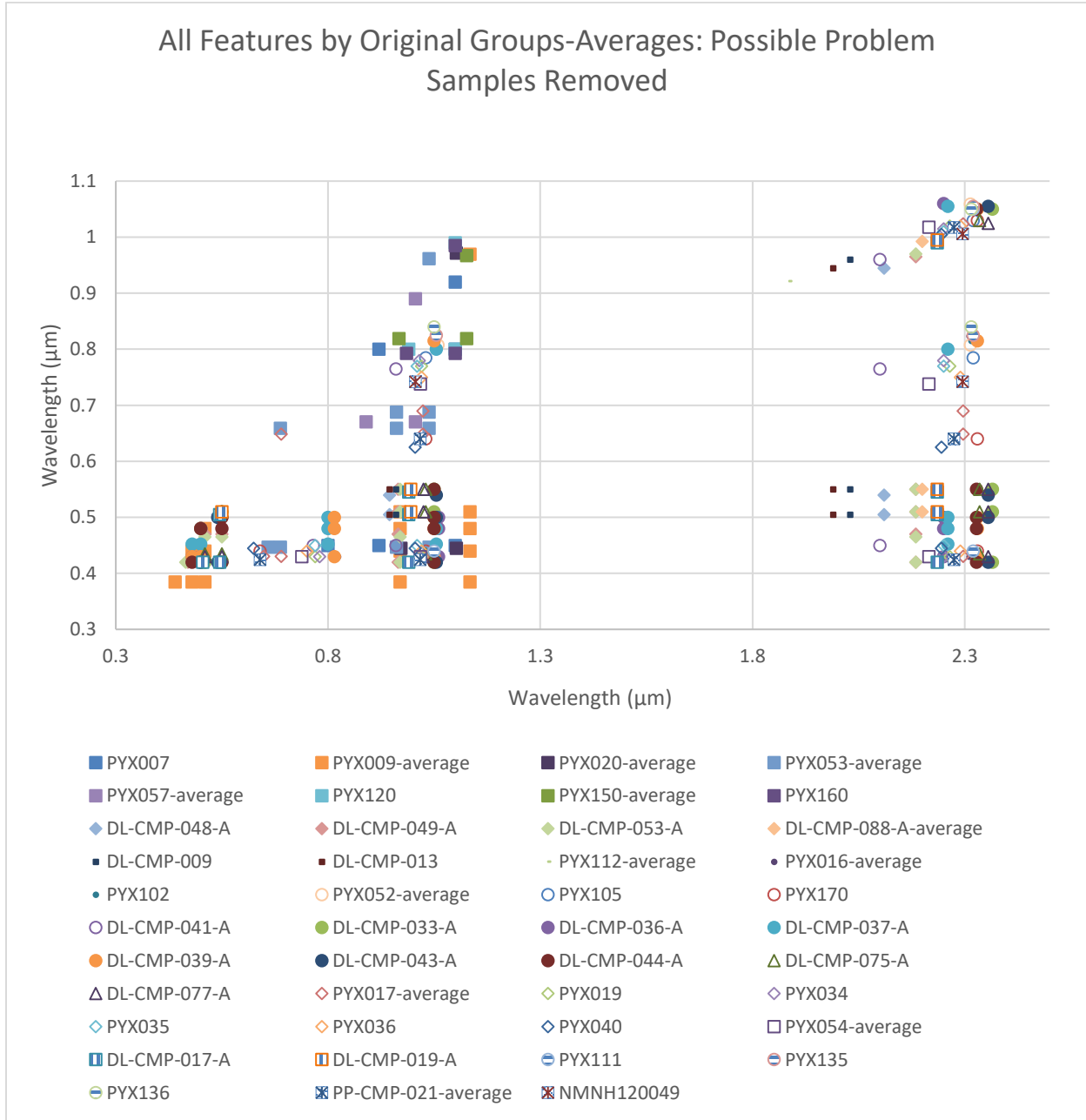


Figure 13. Graph of all features by original spectral groups. The different symbols represent the different groupings. Sources: HOSERLab, RELAB, USGS Spectral Library.
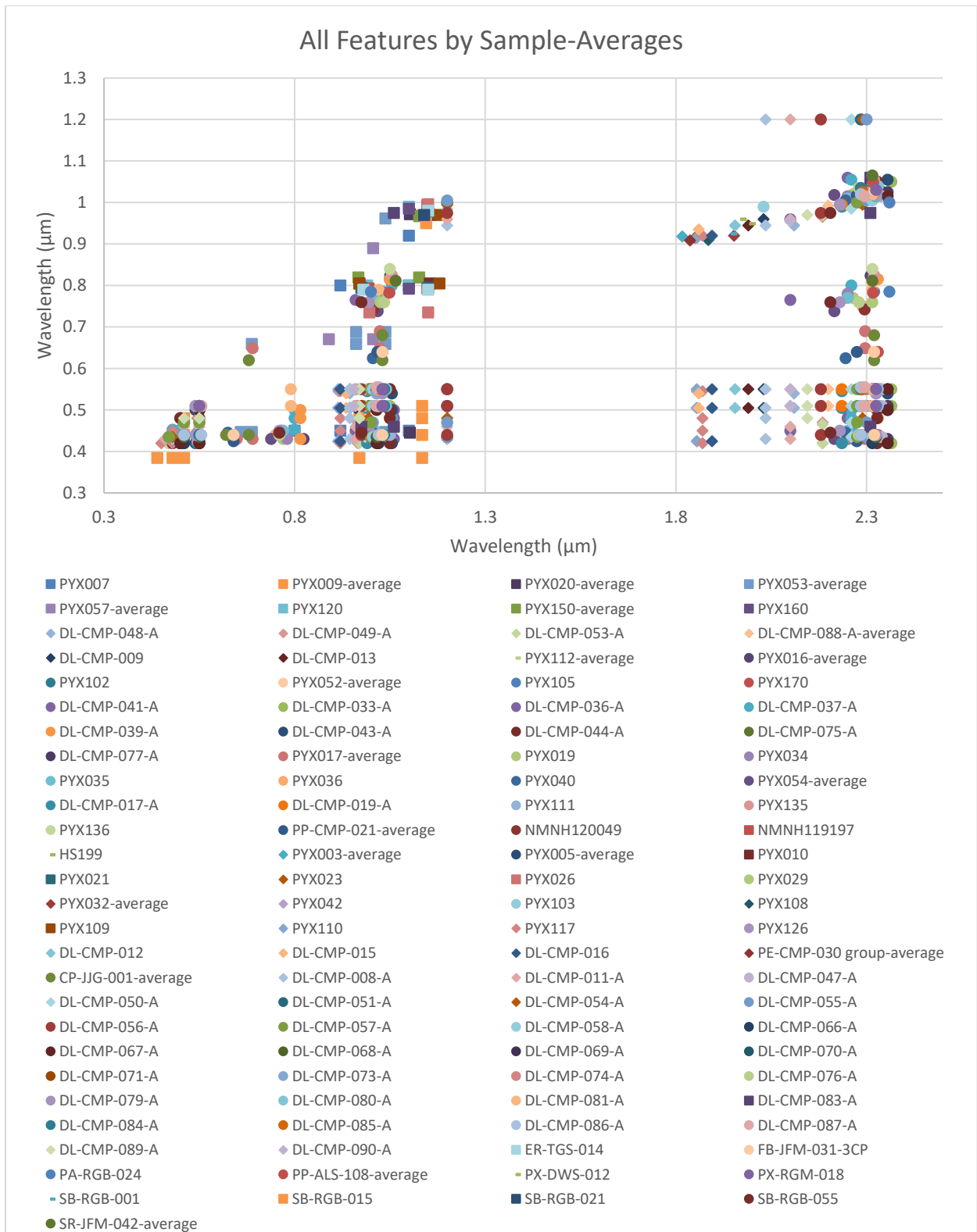
Figure 14. Graph of all features for all samples except the problem samples discussed below. Squares=type A clinopyroxenes, circles=type B clinopyroxenes, dashes=pigeonites, diamonds=orthopyroxenes. Sources: HOSERLab, RELAB, USGS Spectral Library.

Figure 15. Graph of all the features by type with the problem samples removed. Sources: HOSERLab, RELAB, USGS Spectral Library.

In addition, I grouped the two main pyroxene features graphs and the all features graphs by calcium, iron, and magnesium endmember composition amounts to try to see a possible trend. I have graphed these in figures 16 through 21 below. I was particularly interested in the calcium amounts to see if there were samples that were possible bridges between the different calcium pyroxene types and between the orthopyroxene and clinopyroxene types. As a further note, I did

not choose to do band centers because there are many different ways and models to measure band centers and I wanted to keep it as consistent and reproducible as possible.

Starting with the main cation of concern, calcium, there was an obvious separation of the different symbols in Fig. 16. The type A area of the graph had high-calcium pyroxenes. One sample was between $Wo_{40}$ to $Wo_{44}$, while the rest were over $Wo_{45}$ and $Wo_{50}$. I am not sure if it means a very slight possible trend, but the type A clinopyroxene section had predominantly $Wo_{\geq50}$ samples at slightly longer wavelengths. However, they had a fair amount of noise, especially in comparison to the orthopyroxene-type B clinopyroxene section. This is in part because their spectra were more red-sloped and noisier, which made it harder to get the features. There were also limited samples, which needs to be taken into consideration. It seemed to be consistent however with Schade et al. (2004) who thought that most type A clinopyroxenes were around $Wo_{50}$. Later on in this section I looked into this with more detail. For the orthopyroxene-type B clinopyroxene section, it started with $Wo_{<30}$, which may be a high amount but since nearly all of the high-calcium clinopyroxenes I looked at had over $Wo_{30}$, I considered it a reasonable categorization. Among the samples, not including the problem ones, only one deviated from this trend, PYX103. It had a calcium endmember composition categorization of $Wo_{40-44}$, and I've mentioned it has stuck out before. Only at around 2.1 µm on the x-axis did other amounts of calcium start to appear, although all in a bunch, ranging from $Wo_{<30}$ to $Wo_{>50}$. There did not appear to be any sort of trend among that area except for the fact that most samples with $Wo_{\geq50}$ are at the end of the curve, which made sense because the main features of clinopyroxenes are typically at longer wavelengths with increasing calcium. Also, most of the $Wo_{<30}$ samples that went up the trend were below the curve in that area, meaning they were at slightly lower Band I wavelengths than the samples with higher calcium above them.  Finally,

78

there were much fewer samples with $Wo_{30}$ to $Wo_{39}$ than the other amounts, as I did not have as many samples of those.

Figure 17 shows the calcium endmember amounts again but with all the possible pyroxene features. It is therefore a much messier graph and it is harder to note any possible implications. The graph again had noticeable areas, such as in the fact that the samples with $Wo_{<30}$ were at shorter wavelengths. They also tended to have more shorter wavelength features, particularly around 0.5 µm, which makes sense with what was written above for orthopyroxene features. These could be seen in the minor features' slightly distinct groups that were separated throughout the graph. The higher calcium pyroxenes, from $Wo_{35}$ to $Wo_{>-50}$, with most being $Wo_{\geq 45}$ were all at the longest wavelengths typically. This may or may not mean anything, but the higher-calcium pyroxenes did seem to have more transition features involving ferric iron around 0.75 µm, so that is possibly why they were grouped in that area.
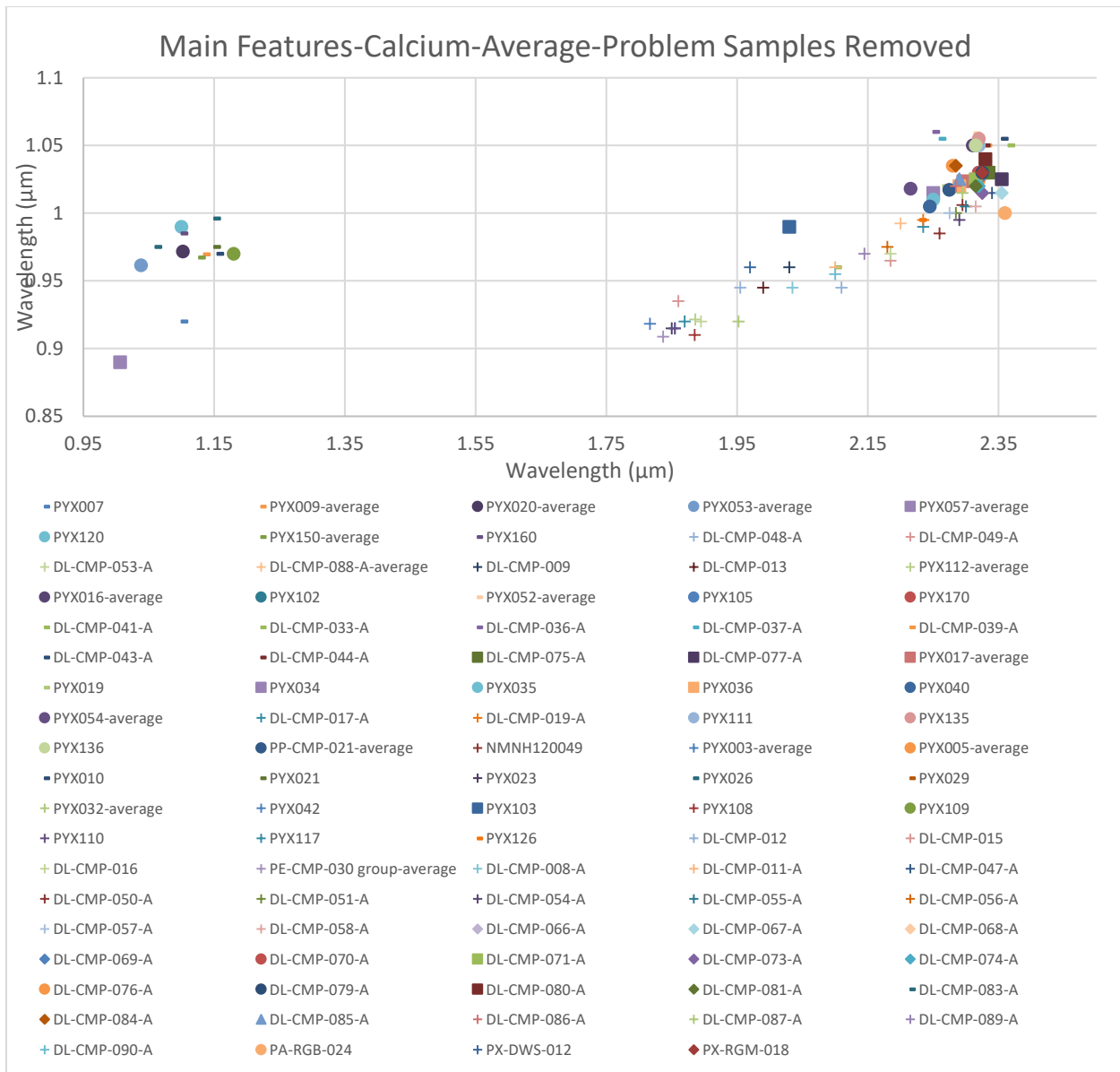
Figure 16. Main features of pyroxene graphed against each other and labeled by calcium endmember amounts. Dash=Wo$_{\geq 50}$, Circle=Wo$_{45\text{-}49}$, Square=Wo$_{40\text{-}44}$, Diamond=Wo$_{35\text{-}39}$, Triangle=Wo$_{30\text{-}34}$, +=Wo$_{<30}$. Sources: HOSERLab, RELAB, USGS Spectral Library.

Figure 17. Same as Fig. 16 but with all the possible pyroxene features. Dash=Wo$_{\geq 50}$, Circle=Wo$_{45-49}$, Square=Wo$_{40-44}$, Diamond=Wo$_{35-39}$, Triangle=Wo$_{30-34}$, +=Wo$_{<30}$. Sources: HOSERLab, RELAB, USGS Spectral Library.

The iron and magnesium graphs were much more jumbled than the calcium graphs. Since there isn't much to take away from these graphs, I will just note a few things. For both iron graphs, Fig. 18 and 19, the middle of the orthopyroxene-type B pyroxene trend had nearly all samples with $Fs_{\geq 50}$. It is interesting because they did not appear much anywhere else. I also noticed with the iron graph that the majority of the smaller amounts of iron occurred in areas that typically had higher amounts of calcium. This makes sense, as a higher amount of calcium would lead to a smaller amount of iron. Again, the magnesium graphs of Fig. 20 and 21 were also more varied. The main thing I noticed here was that the $En_{\geq 50}$ samples were nearly all in the orthopyroxene section at the very beginning of that curve.
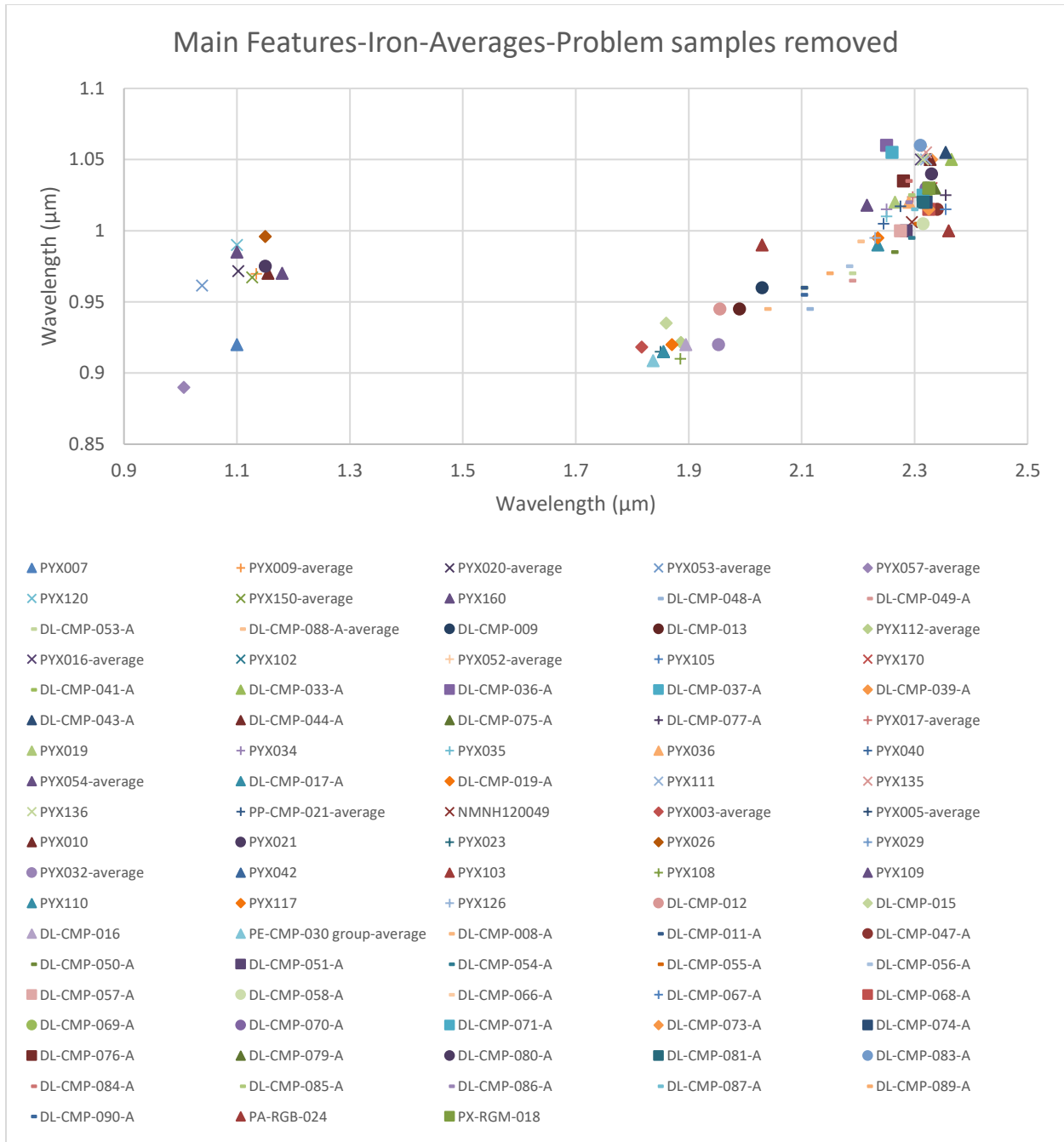
Figure 18. Main features of pyroxene graphed against each other and labeled by iron endmember amounts. Dash=Fs$_{\geq 50}$, Circle=Fs$_{40-49}$, Square=Fs$_{30-39}$, Diamond=Fs$_{20-29}$, Triangle=Fs$_{10-19}$, +=Fs$_{5-9}$, X=Fs$_{<5}$. Sources: HOSERLab, RELAB, USGS Spectral Library.
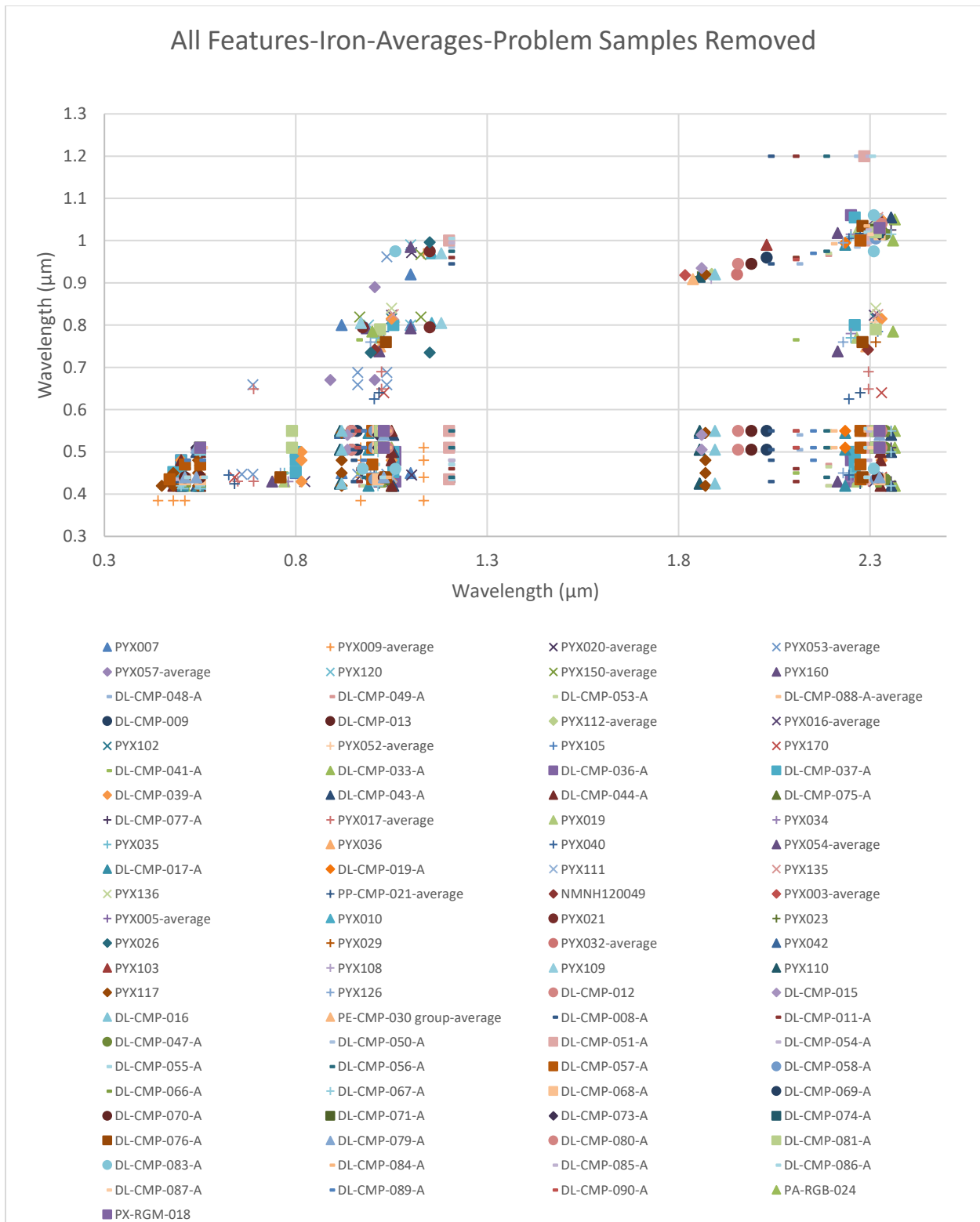
Figure 19. Same as Fig. 18 but with all the possible pyroxene features. Dash=$Fs_{\geq 50}$, Circle=$Fs_{40-49}$, Square=$Fs_{30-39}$, Diamond=$Fs_{20-29}$, Triangle=$Fs_{10-19}$, +=$Fs_{5-9}$, X=$Fs_{<5}$. Sources: HOSERLab, RELAB, USGS Spectral Library.
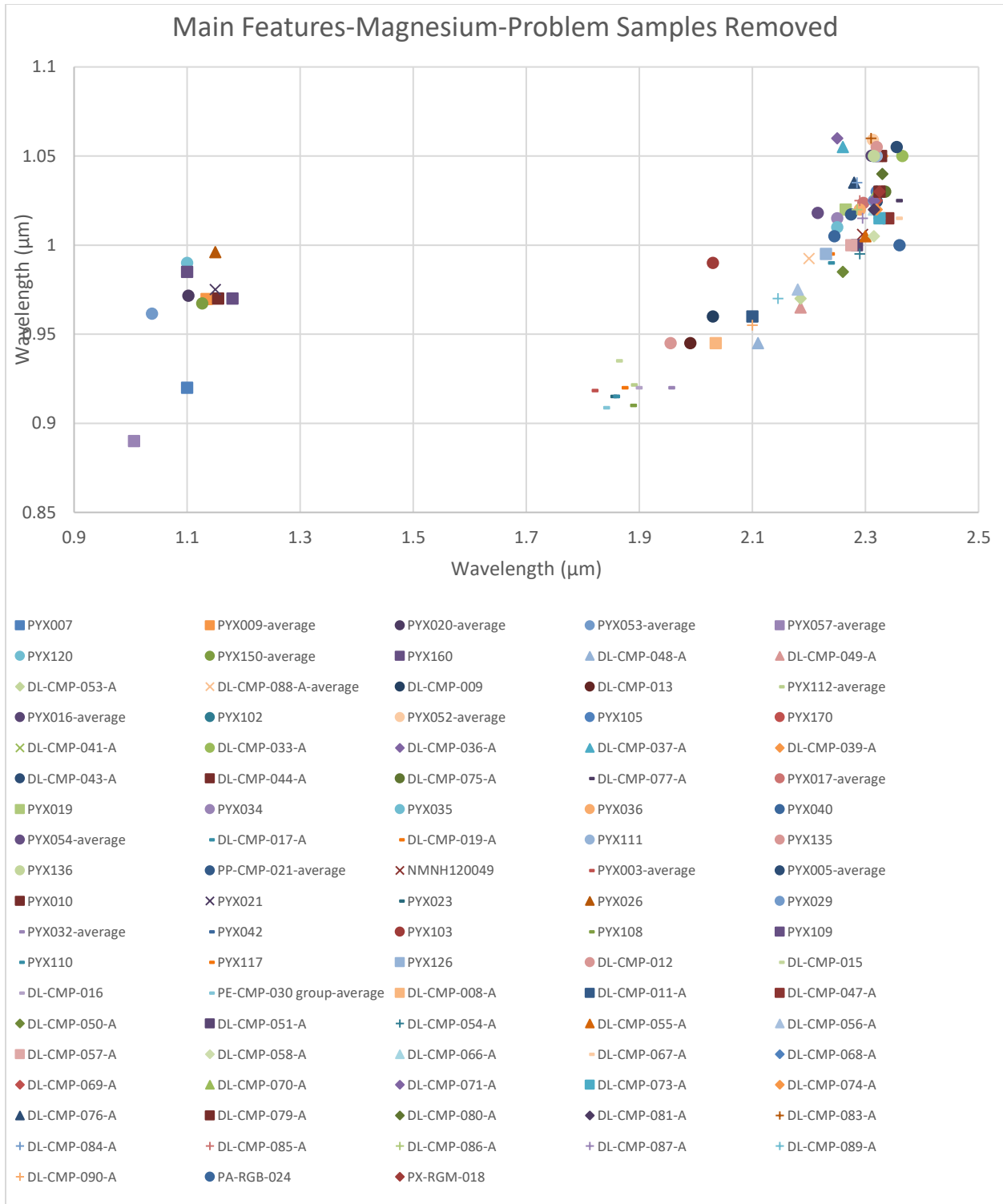
Figure 20. Main features of pyroxene graphed against each other and labeled by magnesium endmember amounts. Dash=En$_{\geq 50}$, Circle=En$_{40-49}$, Square=En$_{30-39}$, Diamond=En$_{20-29}$, Triangle=En$_{10-19}$, +=En$_{5-9}$, X=En$_{<5}$. Sources: HOSERLab, RELAB, USGS Spectral Library.
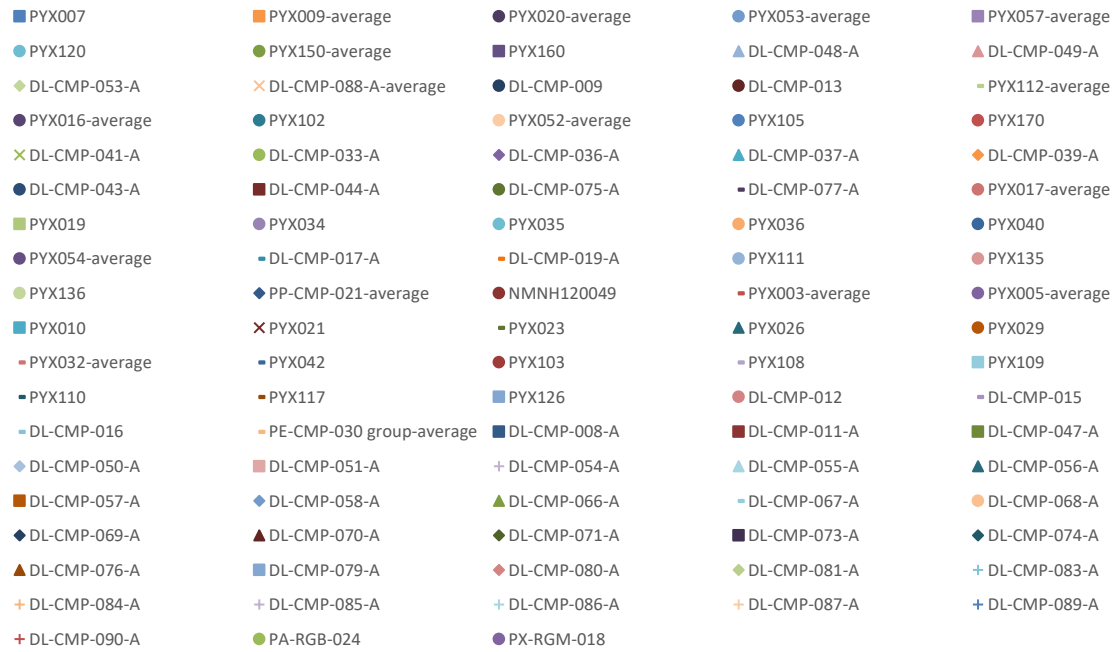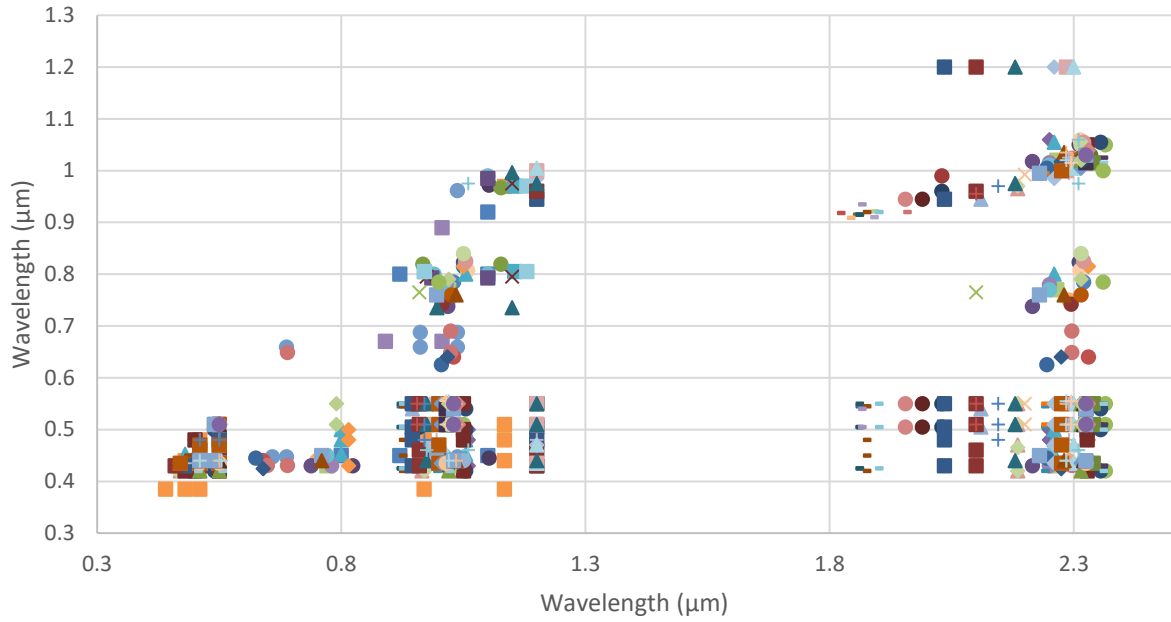
Figure 21. Same as Fig. 20 but with all the possible pyroxene features. Dash=En$_{\geq 50}$, Circle=En$_{40-49}$, Square=En$_{30-39}$, Diamond=En$_{20-29}$, Triangle=En$_{10-19}$, +=En$_{5-9}$, X=En$_{<5}$. Sources: HOSERLab, RELAB, USGS Spectral Library.

Klima et al. (2011) stated that the 2 µm feature in clinopyroxenes tended to not really change much with increases in calcium greater than $Wo_{30}$ because there was no change in shape group after that point. While my samples did not have constant magnesium or calcium like in that study, I did graph the band minima against the calcium content such as in that paper and found this to possibly be true with the samples here. This can be seen in Fig. 22, where I have included orthopyroxenes. One can see that there was an increase from $Wo_0$ to $Wo_{\sim25}$, which was to be expected, and then it leveled off at higher calcium levels. I found a $R^2$ value for this to be 0.6637 to see if it was close to a linear relationship. With just the type B clinopyroxenes, the R value was nearly nonexistent because the data was so scattered, which can be seen in Fig. 23. So there appeared to be no relationship after samples with $Wo_{30}$ and higher and with band minima after 2.3 µm, overall agreeing with Klima et al. (2011). However, the two micron features were noisier, so that needs to be taken into consideration. The band I features for type B clinopyroxenes were also scattered and had a weak relationship. It had a stronger relationship than the band II features, with an $R^2$ value of 0.476, when two extreme outliers of PYX103 and DL-CMP-041-A were removed, which can be seen in Fig. 24. When I only included samples with $Wo_{30}$ or higher the results were more scattered and less of a relationship was apparent. Cloutis and Gaffey (1991) noted that it is likely that there is this positive relationship between wavelength positions and calcium content for type B clinopyroxenes, no matter the amount of iron in the sample. They also mentioned a possible slight negative correlation for samples with $Wo_{>50}$, which could potentially be seen in Fig. 24 as well, but there was too much scatter (Cloutis & Gaffey 1991). I have also graphed both band positions for type A clinopyroxenes in figures 25 and 26. There was scatter but a weak possible positive relationship between the samples. Again, however, there was noise in these samples, which can cause error. The noise and non-constant

endmember compositions leads these to be interesting graphs, but not necessarily that meaningful. I also graphed the band I polynomial fitted minima for type A clinopyroxenes and selected type B clinopyroxenes below in figures 51 to 55.
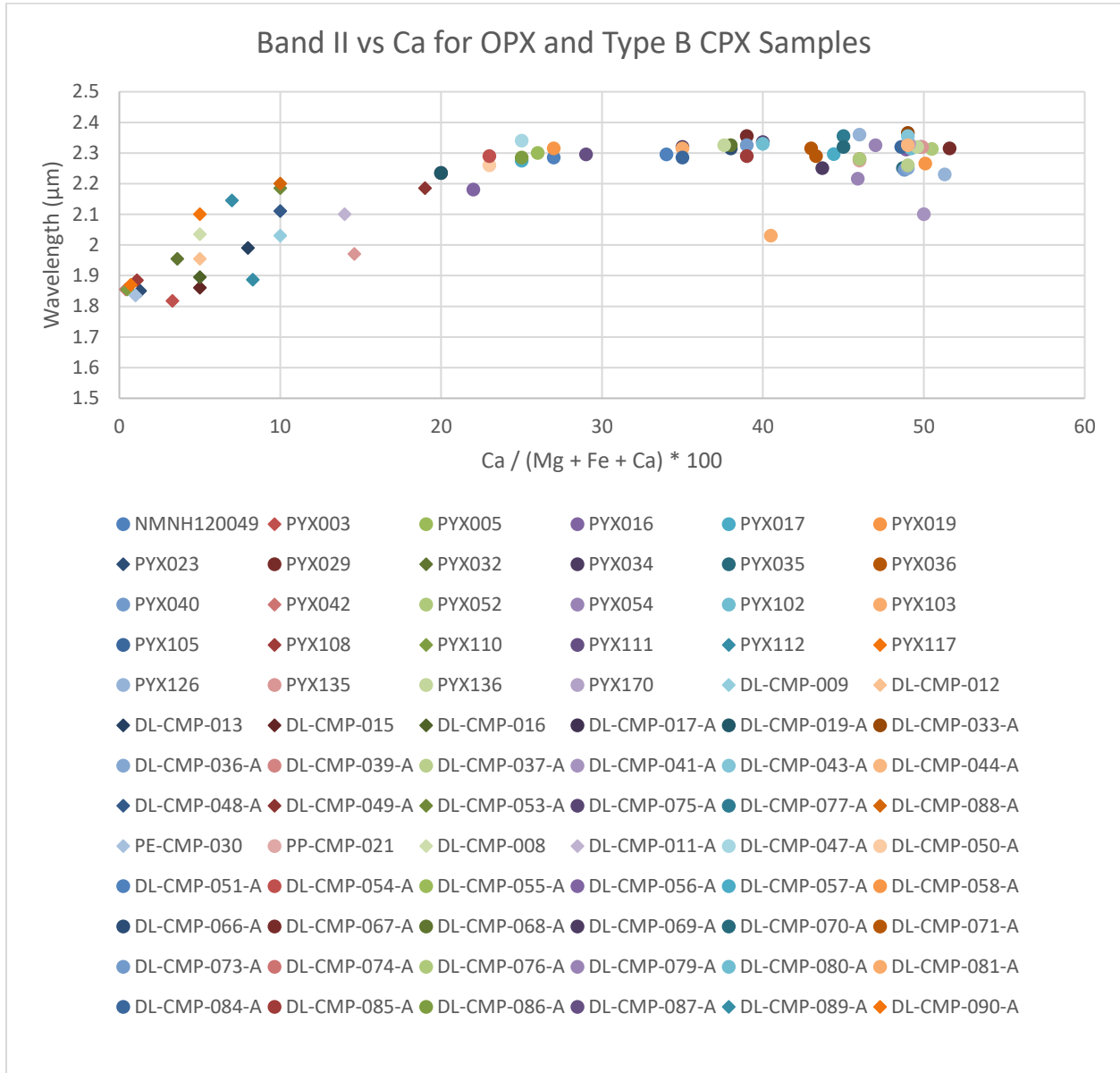


Figure 22. Orthopyroxene and Type B clinopyroxene samples used in this study to compare band minima for the two micron feature and calcium content. The two extreme outliers are PYX103 and DL-CMP-041-A. Sources: HOSERLab, RELAB, USGS Spectral Library, Klima et al.2011.
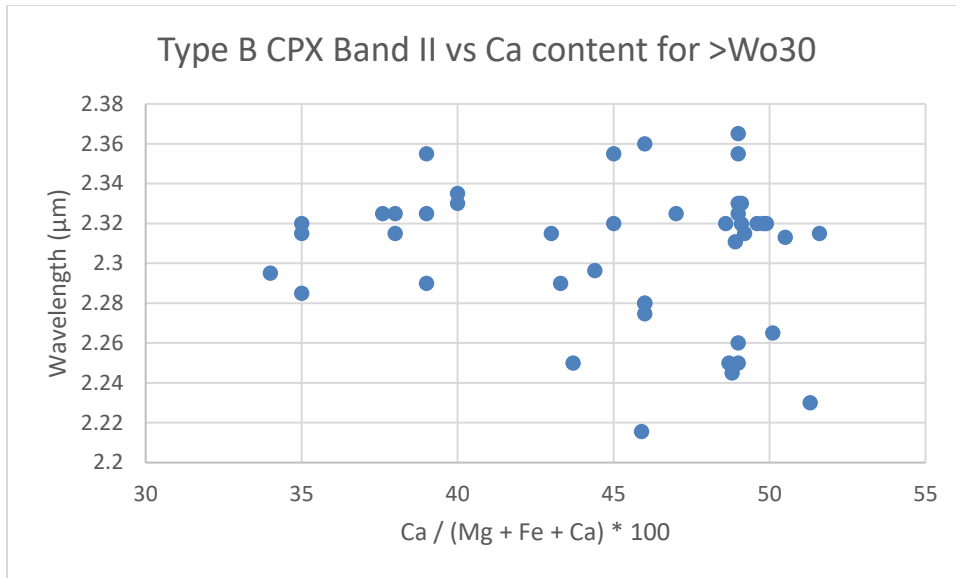
Figure 23. Type B clinopyroxene samples' Band II versus calcium content for samples with Wo>30. Sources: HOSERLab, RELAB, USGS Spectral Library, Klima et al. 2011.
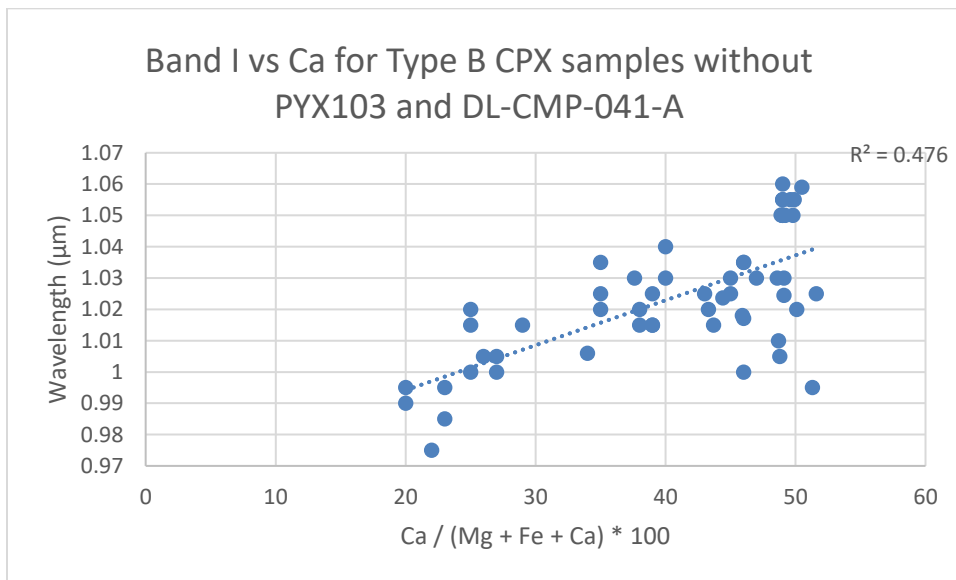


Figure 24. Type B clinopyroxene samples' Band I minima versus calcium content after excluding two extreme outliers of PYX103 and DL-CMP-041-A. Sources: HOSERLab, RELAB, USGS Spectral Library, Klima et al. 2011.
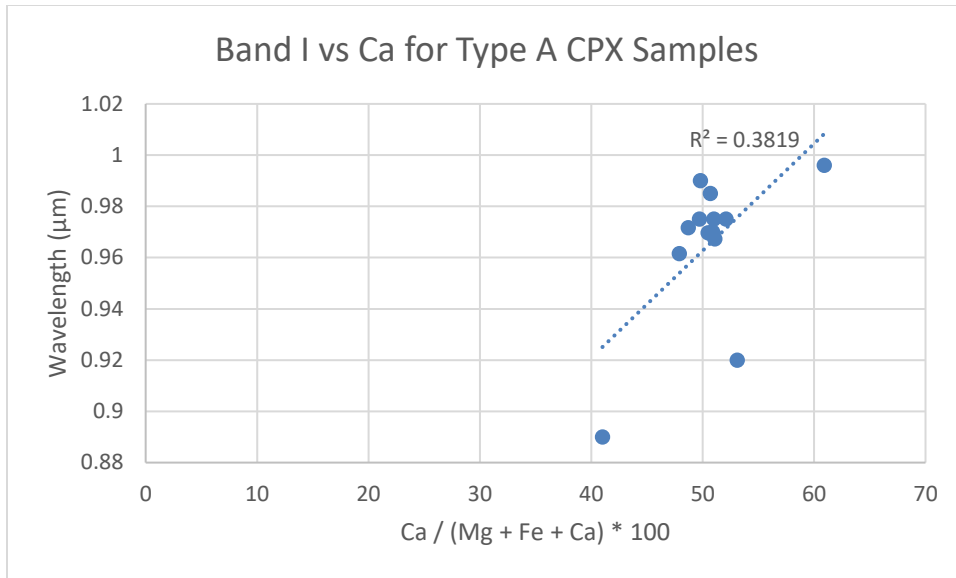
Figure 25. Band I minima versus calcium content for Type A CPX Samples. Sources: HOSERLab, RELAB, USGS Spectral Library, Klima et al. 2011.
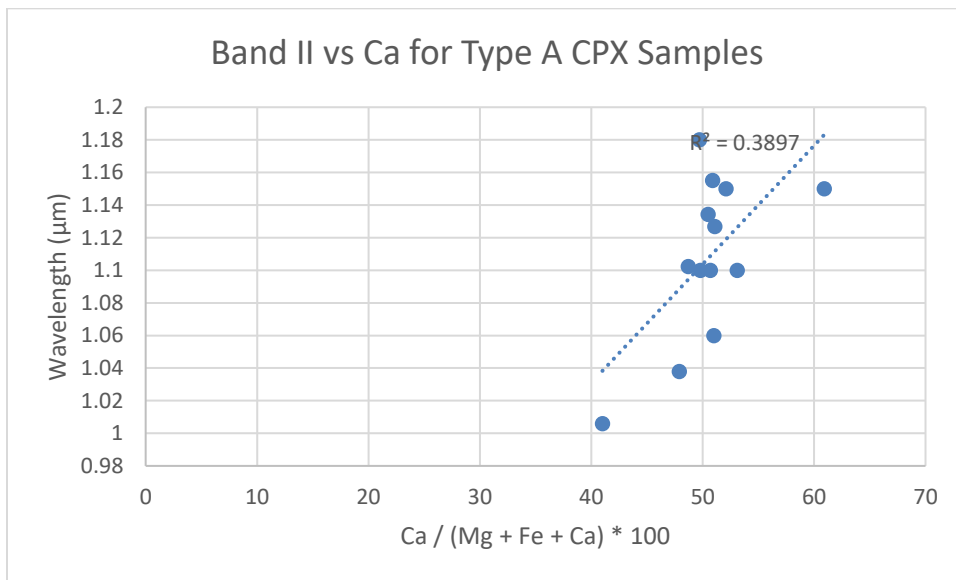


Figure 26. Band II minima versus calcium content for Type A CPX Samples. Sources: HOSERLab, RELAB, USGS Spectral Library, Klima et al. 2011.

Klima et al. (2011) also reiterated with graphs that with respect to increasing iron contents, orthopyroxenes and clinopyroxenes increased and decreased in wavelength positions, respectively. I did the same with the samples here in this paper and found similar results. While there was scatter, orthopyroxenes versus increasing iron content generally increased in

wavelength position. Type B clinopyroxenes had very low $R^2$ values. These can be seen in Fig. 27, 28, 29, and 30. There were two extreme outliers in Fig. 30, which happened to again be PYX103 and DL-CMP-041-A but it only negligibly affected the $R^2$ value. Type A clinopyroxene samples did not appear to show much of a trend, which can be seen below in Fig. 31 and 32.
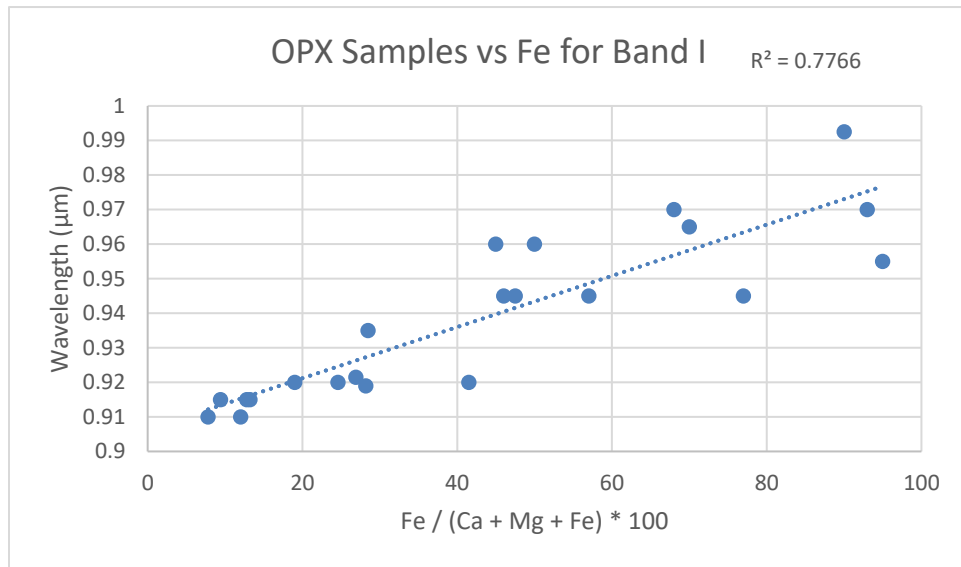


Figure 27. Orthopyroxene band I minima vs Fe content. Sources: HOSERLab, RELAB, USGS Spectral Library, Klima et al. 2011.
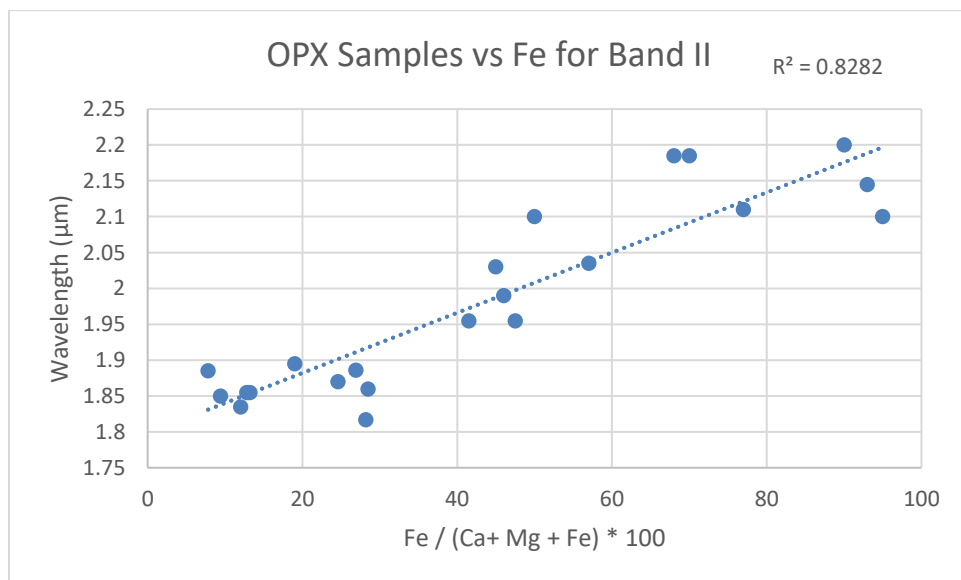


Figure 28. Orthopyroxene band II minima vs Fe content. Sources: HOSERLab, RELAB, USGS Spectral Library, Klima et al. 2011.

91
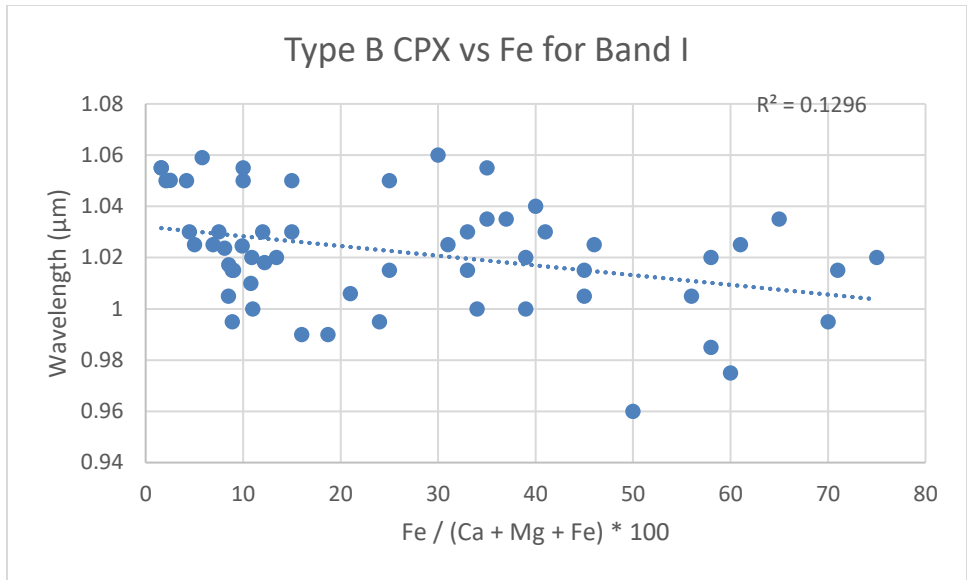
Figure 29. Type B clinopyroxene band II minima vs Fe content. Sources: HOSERLab, RELAB, USGS Spectral Library, Klima et al. 2011.
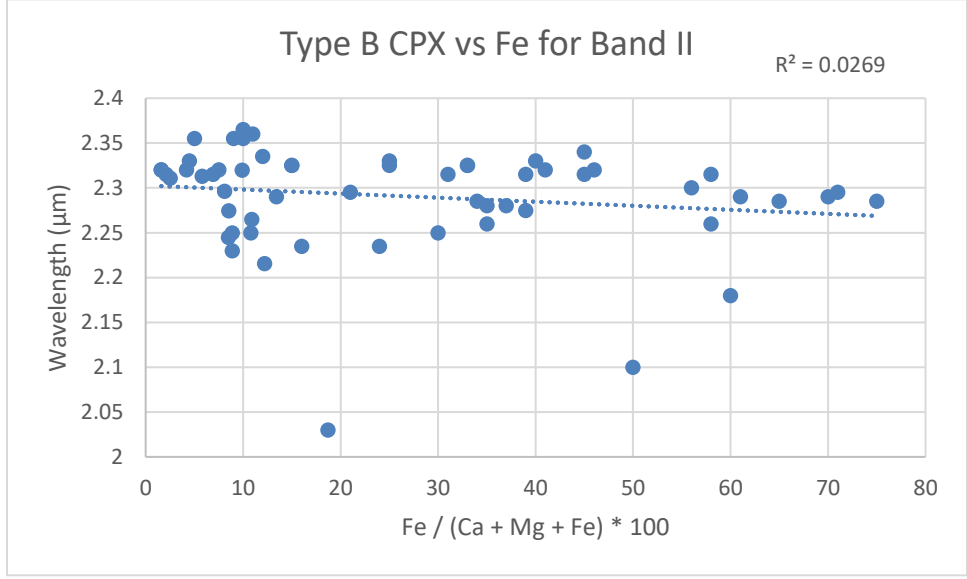


Figure 30. Type B clinopyroxene band II minima vs Fe content. Sources: HOSERLab, RELAB, USGS Spectral Library, Klima et al. 2011.
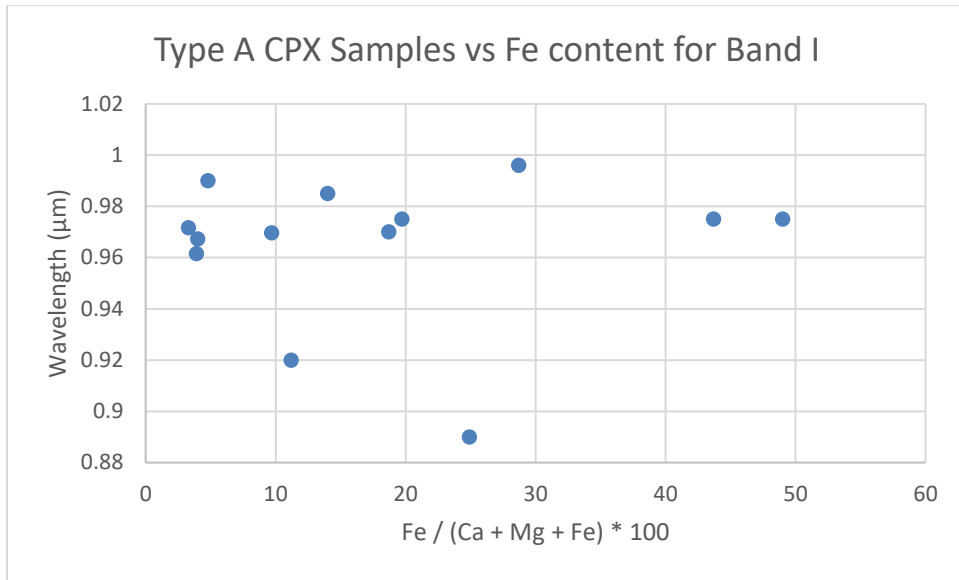
Figure 31. Type A clinopyroxene band I minima vs Fe content. Sources: HOSERLab, RELAB, USGS Spectral Library, Klima et al. 2011.
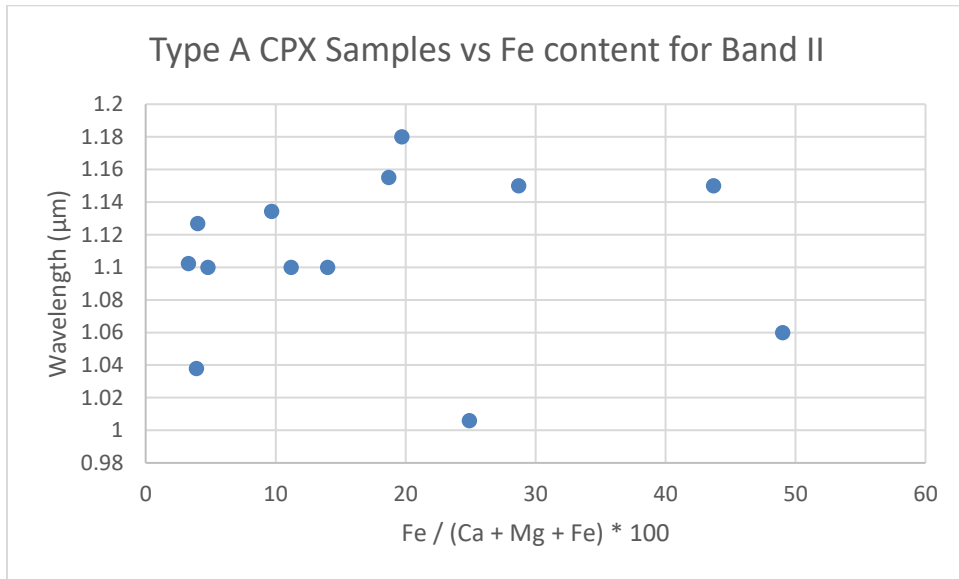


Figure 32. Type A clinopyroxene band II minima vs Fe content. Sources: HOSERLab, RELAB, USGS Spectral Library, Klima et al. 2011.

These graphs additionally built on findings by Cloutis et al. (1991), who, as stated above in a previous section, did not find any relationship between type A clinopyroxenes, iron, and calcium.  With the previous figures, I unfortunately did not find much of any relationships either. I decided to make some of the graphs seen in the figures above with respect to magnesium just to

check and see if there could be anything possibly related, but I found similar scattered results, which can be seen in Fig. 33 and 34. It is important to note from all of these graphs that I only compared one variable each and since there were three variables, it could be hard to make generalizations. Orthopyroxenes, since they predominantly have only two main variables of magnesium and iron, had noticeable relationships to spot, such as the one with wavelength position and iron content mentioned above. However, it was still useful to see in an easier way how the wavelength positions could change with an increase or decrease in calcium, iron, and magnesium contents, which was why I included them here. There was too much scatter to discern much meaning for the Type B clinopyroxenes as well.
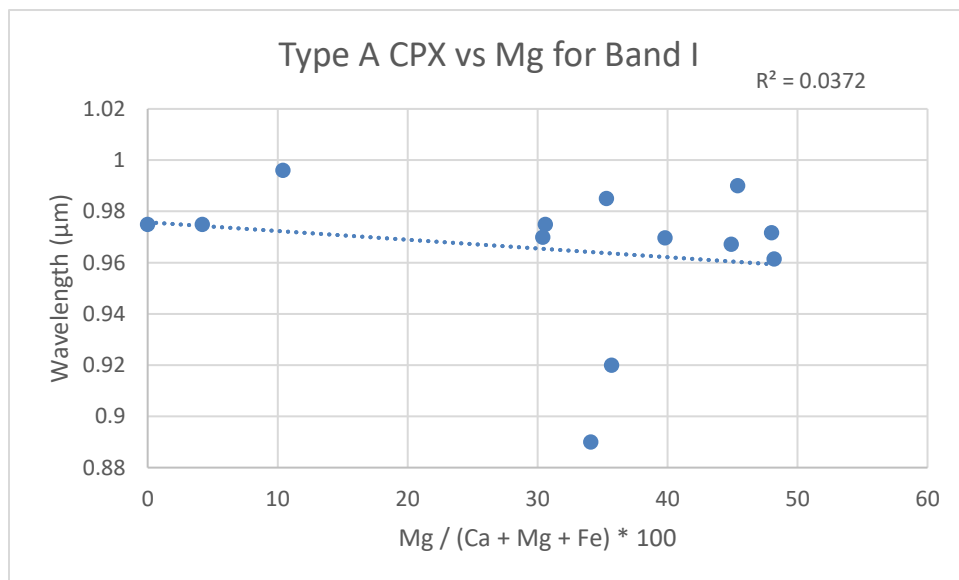


Figure 33. Type A clinopyroxene band I minima vs Mg content. Sources: HOSERLab, RELAB, USGS Spectral Library, Cloutis & Gaffey 1991, Klima et al. 2011.

94
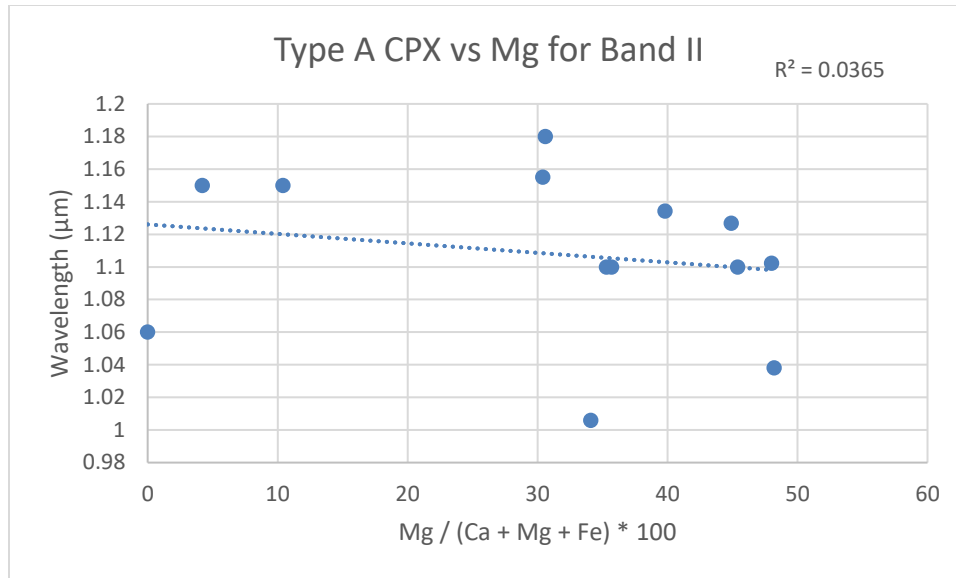
Figure 34. Type A clinopyroxene band II minima vs Mg content. Sources: HOSERLab, RELAB, USGS Spectral Library, Cloutis & Gaffey 1991, Klima et al. 2011.

As mentioned before, Hazen et al. (1978, Cloutis and Gaffey (1991), and Lewis and White (1975, from Adams 1975) mentioned how high amounts of chromium and titanium can affect the band wavelength positions in high-calcium pyroxenes. To look into this I found several samples that had high amounts of either, or both, and compared them to samples that had similar iron and calcium amounts. A type A clinopyroxene PYX007 had almost 4 wt. % $TiO_2$, with an iron amount of $Fs_{\sim10}$. PYX009, another type A clinopyroxene, had similar calcium and iron amounts to PYX007 but without heavy additions of other cations. To see a comparison between their two spectra, see Fig. 35. Right away it was noticeable that PYX007 had a reddened slope and weaker features, which made it difficult to find its band minima. This was likely due to the titanium but also in part to high amounts of ferric iron, which PYX009 lacked.

There were three different type B clinopyroxenes that had similar calcium, iron, and titanium amounts, although one also had high chromium. I thought it would therefore be interesting to compare PYX017, PYX034, and PYX035, with the first sample having chromium.

95

Their spectra are shown in Fig. 36. All three had some ferric iron, which could be seen in a likely $Fe^{2+}$-$Fe^{3+}$ charge transfer around 0.75 µm. They had similar band positions and all three had a strong reddened slope to create the hump from 1.5 µm to 2 µm, although PYX017 had the greatest. PYX017 also had an added feature near the iron intervalence charge transfer, which was likely due to the chromium.

PYX053 was a type A clinopyroxene that had a high amounts of chromium. PYX120 had similar iron and calcium amounts to PYX053 and was also a type A clinopyroxene, so I compared them below in Fig. 37. PYX053 had weaker features, and it seemed that PYX120 had a strong ferric iron feature around 0.75 µm. The slope of PYX120 also drastically became reddened after ~ 1.25 µm, possibly due to the ferric iron, whereas PYX053 had a mainly flat slope. However, PYX053 had similar amounts of ferric iron and no feature around 0.75 µm, so that was puzzling. PYX120 also had more discernible features around 0.9 and 1.15 µm than PYX053. The feature around 0.65 µm in PYX053 was likely due to chromium and was absent in PYX120, which made sense due to PYX120 having very little chromium.
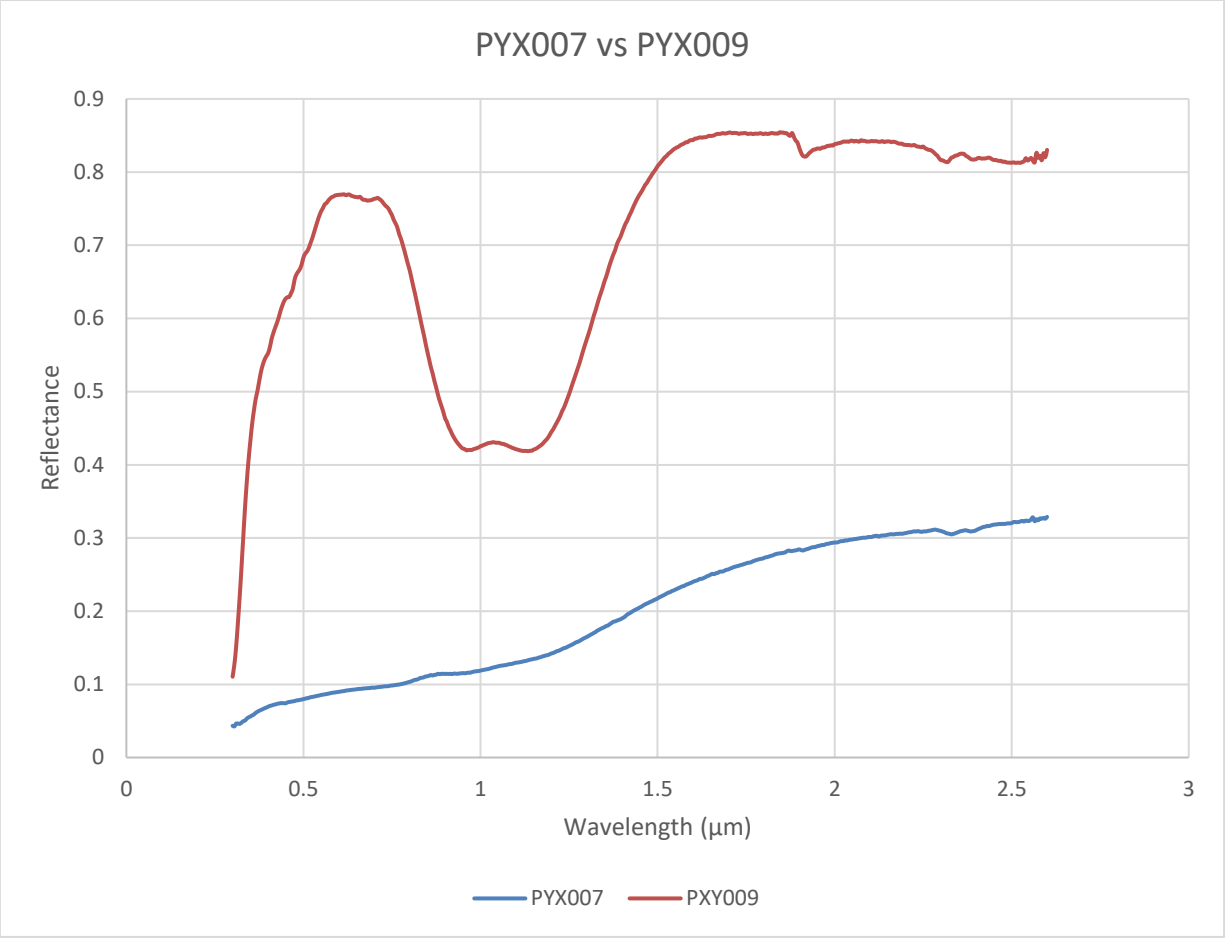
Figure 35. PYX007 versus PYX009 spectra. Sources: HOSERLab, RELAB.
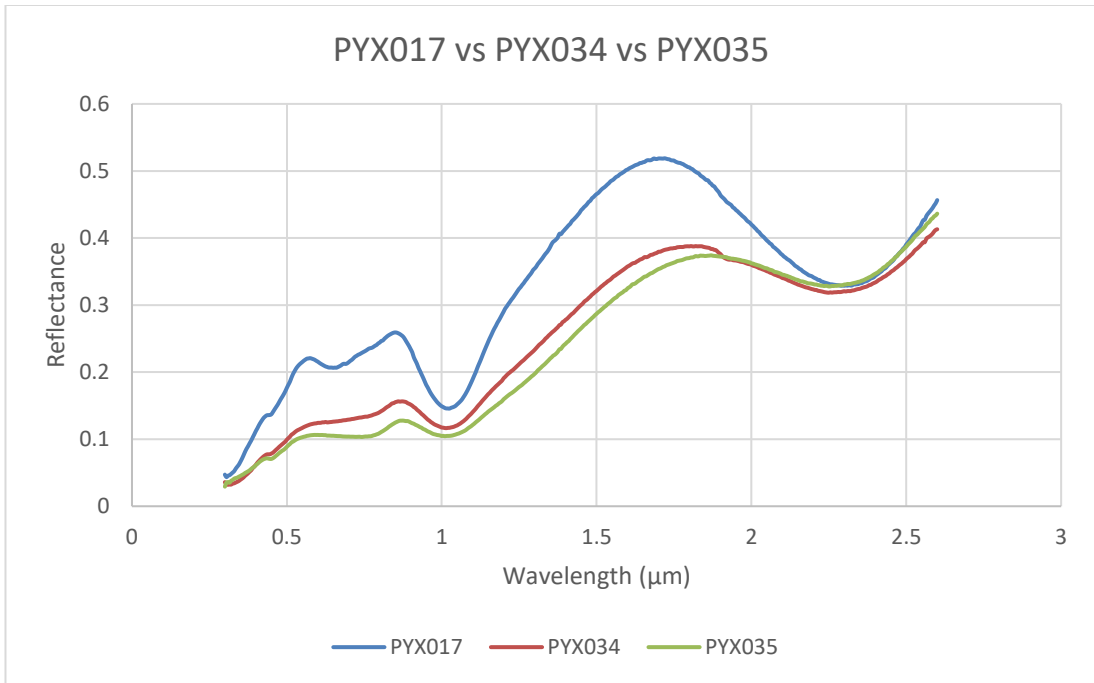
Figure 36. Comparison of PYX017, PYX034, and PYX035. Sources: HOSERLab, RELAB.
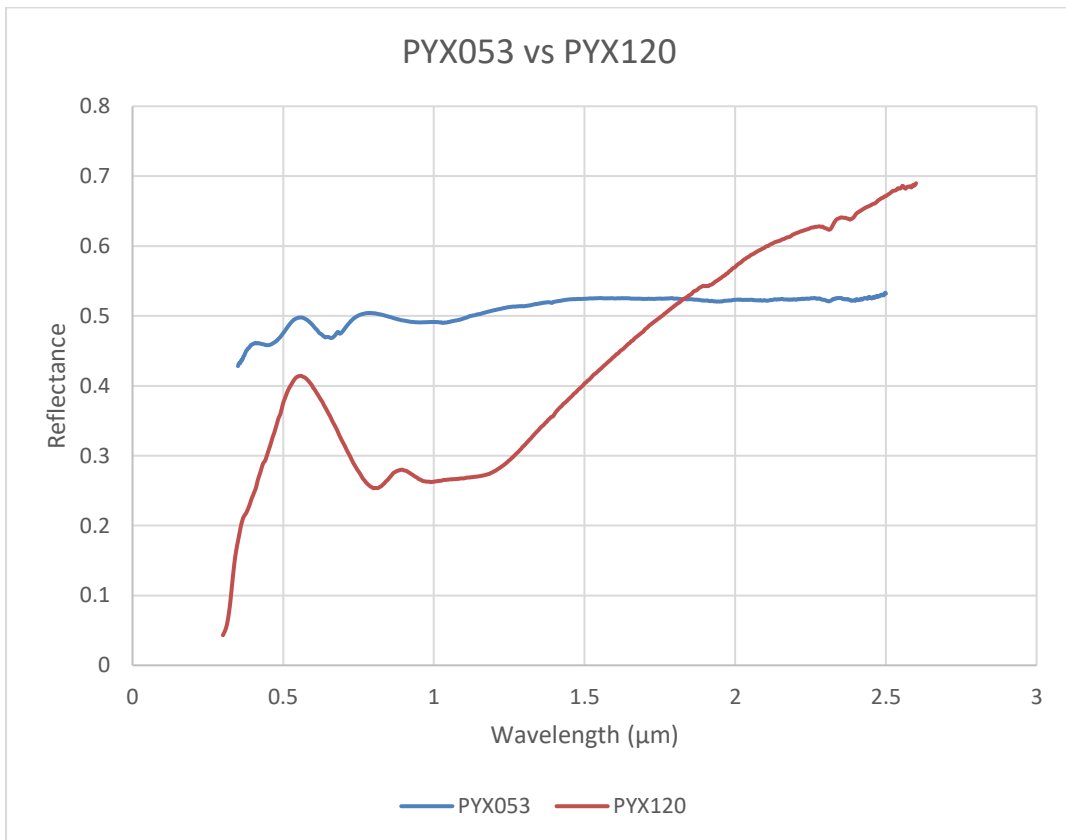


Figure 37. PYX053 vs PYX120. Sources: HOSERLab, RELAB.

After finding my own band minima for the samples I then went back to the literature and searched for their available band minima and centers. Unfortunately I did not find as many samples' information as I would have liked, but there was still a sizable number. I found minima from the HOSERLab Mineral and Rock Sample Database, and band centers from Sunshine & Pieters 1993, Duffard et al. (2005), Cloutis et al. (2006a), Klima et al. (2011), and Gietzen et al. (2012). The HOSERLab Mineral Database's band minima were found using mainly polynomial fits, while several were found both using and dividing by straight line continua. Sunshine & Pieters 1993 used the MGM, which is mentioned above. Duffard et al. (2005-pyroxene samples used reference Carlé Pieters) used the methods in Cloutis et al. (1986) and Gaffey et al. (1993) for determining its band centers; they divided straight-line continua out over each of the two main features and then used a second order polynomial around the minima. Cloutis et al. (2006a) referenced its methods for finding the band centers from Cloutis and Gaffey (1991) and Cloutis (2002). These methods also used straight line continua over the main features and then used quadratic and polynomial fitting for the features themselves (Cloutis & Gaffey 1991; Cloutis 2002). However, they specified that they used a horizontal tangent continua for the two micron features, as it can be incomplete, especially with clinopyroxenes (Cloutis & Gaffey 1991). Klima et al. (2011) also used the MGM to find the band centers, which used a straight line continuum as well. Gietzen et al. (2012) used the MGM too. These centers and minima from the literature are in table 2 in the appendices. It was hard to fully compare the band centers and minima from the literature and the minima I found from the lowest reflectance, as they were found in different ways. As expected, the orthopyroxenes were the closest matches generally, while the type A clinopyroxenes were the worst; the 1.1 and 2 µm features also had the most differences, likely due to the reddened slopes in type A clinopyroxenes and the water features and noise in the

99

orthopyroxenes and type B clinopyroxenes. Possible exceptions were when there was asymmetry in one micron features. There is a large table available as supplementary material in Excel that compares the lowest reflectance minima, literature centers and minima, and polynomial fitted minima.

As was mentioned above, I decided to go over some of the samples that were in mixtures again and find their minima using a $3^{rd}$ order polynomial fit. This is a method of empirical curve fitting, based on the idea that absorption features are Gaussian in shape (McCraig et al. 2017). Since these are laboratory spectra, I decided to use this method because for the most part the continuum is not a problem. I chose to fit all type A clinopyroxene samples, type B clinopyroxene samples that had noisy two micron features, and samples that were in mixtures. I chose the type A clinopyroxene and noisy type B clinopyroxene samples because I wanted to compare the results and see if they were similar to the minima I found previously. I also wanted to go over the type A clinopyroxene and mixture samples because they were pertinent to the focus of this study to see possible relationships in spectral mixtures. I did not go over all the type B clinopyroxene and orthopyroxene samples because most were not noisy and sloped. The table of the samples' polynomial fits is in the appendices as table 3. To make it easier to see visually, I have included some graphs here in the following figures, most of which have been separated into groups by type in order to make it easier to view, since there were so many samples. As a note, a few samples, particularly some type A clinopyroxenes, had at least one feature that had $\sim \leq 2$ % depth in reflectance. Therefore that should be taken into consideration when looking at the polynomial fitting results, as that can increase the error of the fitting (McCraig et al. 2017). Graphs in figures 38-41 show comparisons for the type A clinopyroxene samples, including

when comparing calcium, iron, and magnesium endmember composition amounts. Graphs in figures 42-45 show the same but for orthopyroxenes, pigeonites, and type B clinopyroxenes.

Like with the original minima I found, many samples of the type A clinopyroxenes unfortunately had some faint and/or sloped features that made some minima impossible to fit. The original minima had some estimates for those samples. I did not estimate problem feature minima after several attempts of getting lines instead of curves as fits. This only happened with some type A clinopyroxene samples, which has been talked about above. Despite some issues, I still tried to get the results that I could, all of which can be seen in the appendix table 3 and some of which can be seen in the graphs below. The first feature refers to either the ~ 0.9 or 1 µm features of type A or type B clinopyroxene/orthopyroxene/pigeonite samples, respectively. The second feature refers to either the ~ 1.1 or 2 µm features of type A or type B clinopyroxene/orthopyroxene/pigeonite samples, respectively.

For the polynomial fittings, most of the type A clinopyroxene samples had minor zero-crossing issues, where the roots in the fittings did not cross exactly at zero. I double checked all of these to make sure nothing was amiss with the formulas or equations. Despite the minor zero-crossing issues, everything else generally seemed fine with the inflection points and $R^2$ values. Good $R^2$ values were considered as above 0.9 and were seen in most of the fittings. I considered an inflection point satisfactory as long as there was a lone visible spike on an inflection graph. These and the zero-crossings were mainly used as checks to make sure that there were no major mistakes being made (McCraig et al. 2017). These graphs and calculations are available as supplementary materials.

PYX007 had a faint ~ 0.9 µm feature that was below the < 2 % reflectance standard and the zero-crossing for it was further off the x-axis than most samples. The second feature could not be identified with the polynomial fitting because the fit produced a sloped line. Therefore, while the first feature's polynomial fitted minimum is in table 3, it is not graphed below. All polynomial fitted samples that only had one available minimum were not graphed below. I was also not able to get the second main feature for PYX020 because it was weak and had a sloped line fit. The first feature did not cross the x-axis at zero either, but had no issues with the inflection point or $R^2$ value. PYX021 had weak features for both minima and a slight spectral slope. I was able to find a minimum for the first feature, although at < 2 % reflectance depth and slightly off the zero-crossing x-axis, but was not able to get the second feature. PYX026 had the same issues as PYX021. PYX053 had a weak 0.9 micron feature and the range fitted had part of an extra inflection point; this was likely due to the feature being so weak and the other feature being very close by. PYX057 was a bizarre, possible A/AB type sample. I was able to find the feature around 0.9 µm, but not the one around 1.05 µm because of the faintness and slope. The possible feature around 2.35 µm was impossible fit because the spectrum appeared to cut it off at 2.5 µm and it was very noisy, even giving two inflection points for the results. PYX109 had very weak features that were below 2 % depth in reflectance, but otherwise had no issues except for being slightly off the zero-crossing x-axes for both features. PYX120 had the second feature below the 2 % depth in reflectance. The first feature I was able to get, although the zero-crossing was a little off the x-axis. The $R^2$ value was still high though. I was unable to get the second feature due to the faintness and slope. PYX150's features for the < 45 µm grain size spectrum were slightly off the x-axes for the zero-crossings but were fine in $R^2$ values. The second feature was noisier as well, which can be seen in the inflection point graph, as another inflection point

started to form in the fitting range before the one at the observed minimum. PYX160 had a faint feature around 0.9 µm and the zero-crossing was a little above the x-axis; however, the $R^2$ value was high and it had a lone inflection point. I was unable to get the second feature due to faintness and slope. DL-CMP-083-A was possibly a combination of type A and type B clinopyroxenes, so it had three features. The first two were weak by themselves and below the 2 % reflectance depth; they almost looked like one large flattened feature. The second of those two was fainter and was below the x-axis for the zero-crossing graph. There were no issues with the third feature. ER-TGS-014's two main features were both around 2 % reflectance depth, were off the x-axes for the zero-crossing graphs, and had mediocre $R^2$ values. SB-RGB-015 had both features off the x-axes for the zero-crossing graphs, but had strong reflectance values. The $R^2$ value for the first feature was good, while the one for the second feature was lesser but still decent. Finally, SB-RGB-021 had similar results as SB-RGB-015, except that the $R^2$ value was good for the second feature as well.

For the minima themselves, the results were generally better than when compared to the literature. Most features around 0.9 µm were within these samples' usual spectral resolution of five nanometers difference from the minima I had originally found. The exceptions were one of the PYX009 45-90 µm samples at -14 nm, PYX020 45-90 µm samples at -10 and 13 nm, PYX026 at 41 nm, one PYX053 sample at 9 nm, one PYX057 sample at -9 nm, DL-CMP-083-A at -15 nm, ER-TGS-014 at -30 nm, and SB-RGB-015 at -10 nm. For the features around 1.1 µm, there were more differences, which makes sense since those features tended to be more sloped and fainter. As a reminder, I was unable to get these second features for PYX007, PYX021, PYX026, PYX057, PYX120, and PYX160. The samples and spectra that had greater than 5 nm differences for these second features were PYX010 at 25 nm, PYX020 45-90 µm samples at 15

and 29 nm, one PYX053 sample at 7 nm, PYX109 at 25 nm, two PYX150 < 45 µm samples at -15 and -21 nm, DL-CMP-083-A at -10 nm, SB-RGB-015 at 40 nm, and SB-RGB-021 at 10 nm. In addition, the third feature around 2 µm for DL-CMP-083-A was 5 nm off the original minimum found.

The orthopyroxenes, pigeonites, and type B clinopyroxenes had less possible problems with their polynomial fittings. Several samples had some issues with the zero-crossings not being at zero, such as the first feature in the PYX016 45-90 µm grain size spectrum, the first feature in the PYX023 45-90 µm grain size spectrum, the first feature in PYX135, the first features in the PE-CMP-030 < 45 and 45-75 µm grain size spectra, the first features in the PP-CMP-021 <45, 45-75, and 75-125 µm grain size spectra, the first feature in FB-JFM-031-3CP, and both features in PX-DWS-012. Only the first of that list had a zero-crossing that was very noticeably off the x-axis. However, PYX016 also had several spectra with similar results, so I don't think it is of much concern. Also, all of these fittings in the list had strong, lone inflection points and good $R^2$ values. PYX102 had its first feature's zero-crossing fairly far off the x-axis, but had a strong $R^2$ value and lone inflection point. Its second feature was noisier and had a slightly off zero-crossing as well, but also had a strong inflection point and decent $R^2$ value. PYX105 and PYX136 had similar results as PYX102, with the exception that the $R^2$ value for the second feature of PYX136 was poorer. PYX111 was the only type B clinopyroxene that had a feature I was unable to get, as the second feature was too noisy to accurately get a fitting. Its first feature had a zero-crossing that was a bit off the x-axis but had a strong inflection point and a good $R^2$ value. PA-RGB-024 had a slightly off zero-crossing point for its first feature, but also a strong inflection point and a good $R^2$ value. Its second feature was noisier, had a slightly off zero-crossing point, a lone inflection point, and a poor $R^2$ value. PP-ALS-108 had strong inflection points for both

features. Its first feature had a zero-crossing point that was far off, however the $R^2$ value was good. The second feature had a zero-crossing point that was slightly off with a fairly good $R^2$ value as well. Both features for SR-JFM-042 had zero-crossing points that were slightly off but strong inflection points. The $R^2$ value was good for the first feature and poor for the noisier second feature.

The results for the type B clinopyroxenes, orthopyroxenes, and pigeonites were generally positive with the one micron features when comparing the minima I originally found with the ones I found from polynomial fitting. This was helped in part because their features were generally stronger, less sloped, and less noisy. The one micron features that were not within five nanometers of the minima I found previously were the PYX032 < 45 µm spectrum at -14 nm and PA-RGB-024 at -15 nm. The spectra with two micron features that were not within five nanometers were PYX005 < 45 µm at -26 nm, PYX005 45-90 µm at 10 nm, PYX005 90-180 µm at -19 nm, PYX016 < 45 µm at -38 and -36 nm, PYX016 45-90 µm at -30 and -37 nm, PYX017 45-90 µm at -10 nm, PYX023 < 45 µm at -23 nm, PYX032 < 45 µm at -58 nm, PYX102 at -30 nm, two PYX112 < 45 µm samples at 65 and 59 nm, PYX135 at -25 nm, PYX136 < 45 µm at -45 and -40 nm, one PE-CMP-030 < 45 µm sample at -10 nm, one PE-CMP-030 45-75 µm sample at 15 nm, all three PE-CMP-030 75-125 µm samples at 15 nm, three PP-CMP-021 < 45 µm samples at 10 nm, all three PP-CMP-021 45-75 µm samples at 10, 10, and 20 nm, all three PP-CMP-021 75-125 µm samples at -10, -10, and 15 nm, FB-JFM-031-3CP at 10 nm, PA-RGB-024 at 40 nm, three PP-ALS-108 samples at -10 nm, and PX-DWS-012 at -30 nm. With the comparison graphs in figures 38 and 42 including both the literature minima and centers as well as the polynomial fitted minima, the differences just mentioned can be seen visually, although it is difficult with figure 42.

The calcium, iron, and magnesium endmember amounts graphed with the polynomial features were similar to the lowest reflectance minima graphs above in figures 15, 17, and 19. For type A clinopyroxenes in figure 39, the calcium amounts appeared to also be scattered and all but one were $Wo_{\geq 45}$. For the type B clinopyroxenes, orthopyroxenes, and pigeonites in figure 43, there were also similar trends in that there was predominantly $Wo_{<30}$ until ~ 2.2 µm. The main exception was once again PYX103, which did have some exsolved orthopyroxene in it. PYX111 also stuck out with a long wavelength position, but that was a minimum from the Sample Database at the University of Winnipeg. The rest of the curve was type B clinopyroxenes that were a scattered bunch of samples with mainly $Wo_{>40}$, which was also similar to before.

In figure 40, the graph for type A clinopyroxene samples by iron content was similar to the previous graph as well, as most samples had $Fs_{<5}$ and were scattered. There were also not many obvious trends in figure 44 with the orthopyroxenes, pigeonites, and type B clinopyroxenes with respect to iron. The same area as previously noted, around 1.9 to 2.2 µm, did have high amounts of iron, $Fs_{\geq 50}$. Also, the type B clinopyroxenes had the most samples in comparison to the orthopyroxenes and pigeonites with respect to $Fs_{<10}$. Finally, there are the magnesium graphs in figures 41 and 45. These were also similar for all of the samples, with much scatter except for the zone of $En_{\geq 50}$ in orthopyroxenes and pigeonites around 1.8-1.95 µm.
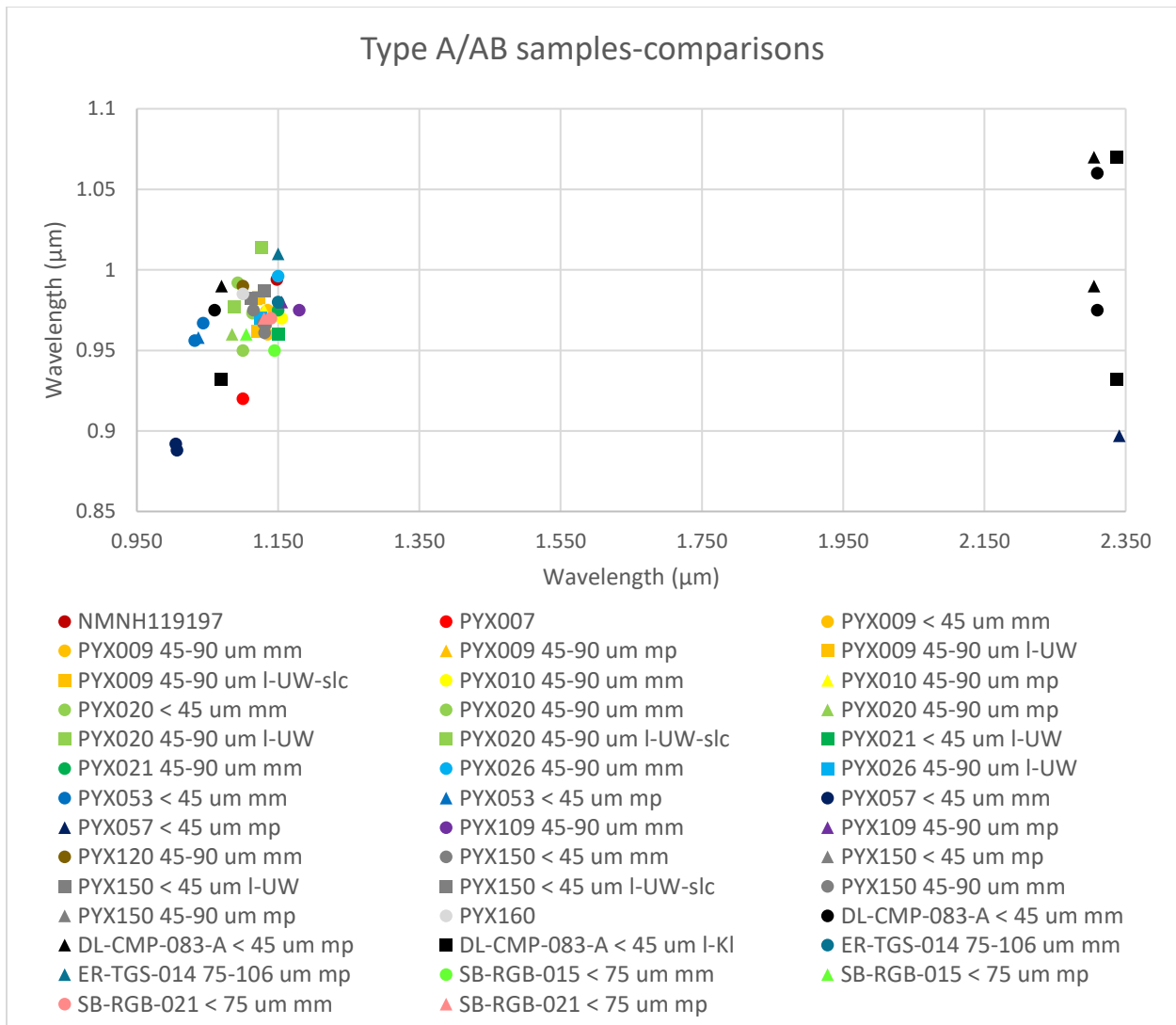
Figure 38. Comparisons of minima from type A clinopyroxene samples used. Circles=minima I originally found (mm), Squares=literature minima (l; UW= minima from the University of Winnipeg Samples Directory; slc=minima from spectra with straight line continua; Kl=centers from Klima et al. 2011), and Triangles=polynomial fitted minima (mp). Colors are different for each sample. Sources: HOSERLab, RELAB, Klima et al. 2011, McCraig et al. 2017.
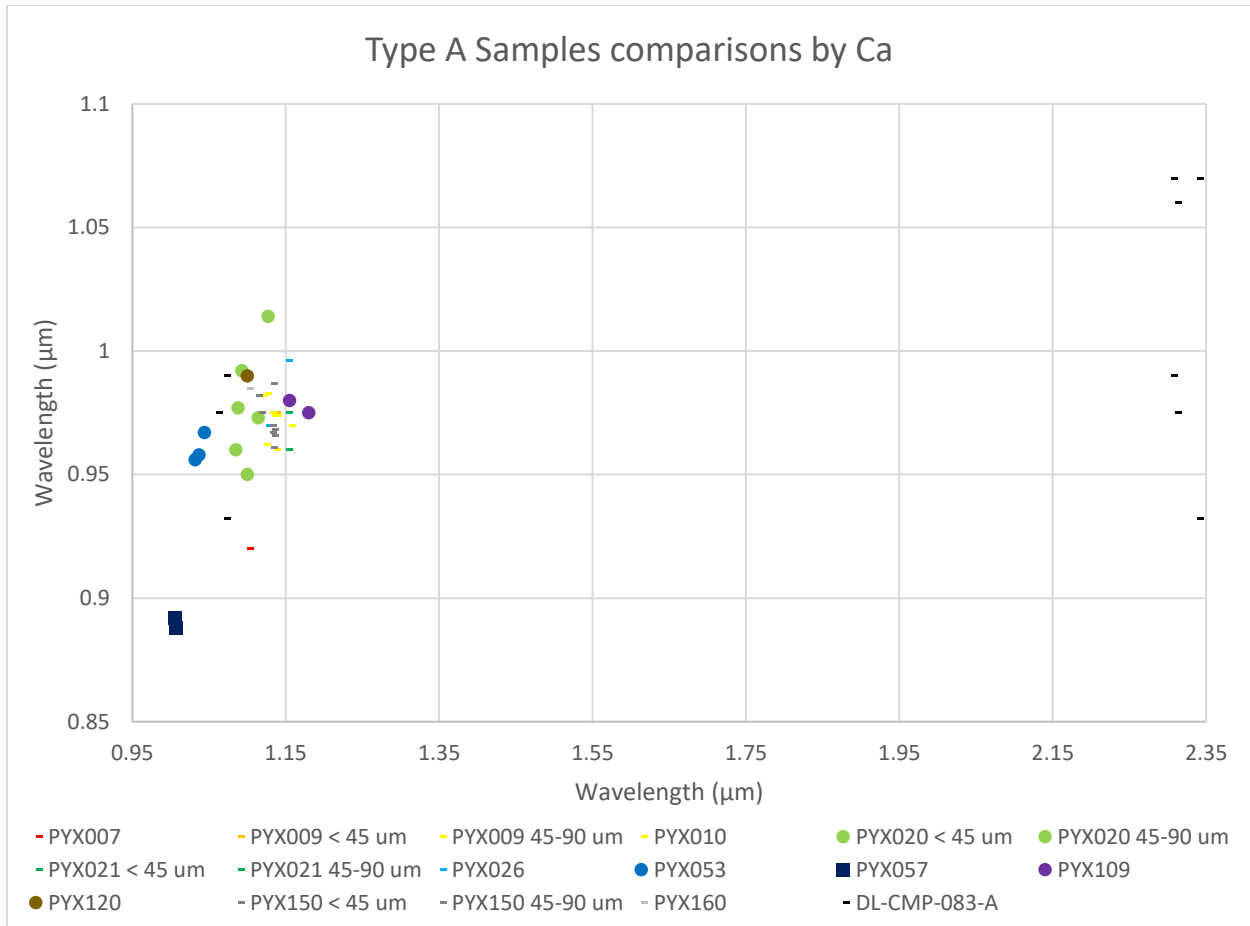
Figure 39. Type A clinopyroxene minima from all methods shown in Fig. 38 in comparison to calcium endmember amounts. Dash=Wo$_{\geq 50}$, Circle=Wo$_{45-49}$, Square=Wo$_{40-44}$. Colors are different for each sample. Sources: HOSERLab, RELAB, Klima et al. 2011, McCraig et al. 2017.
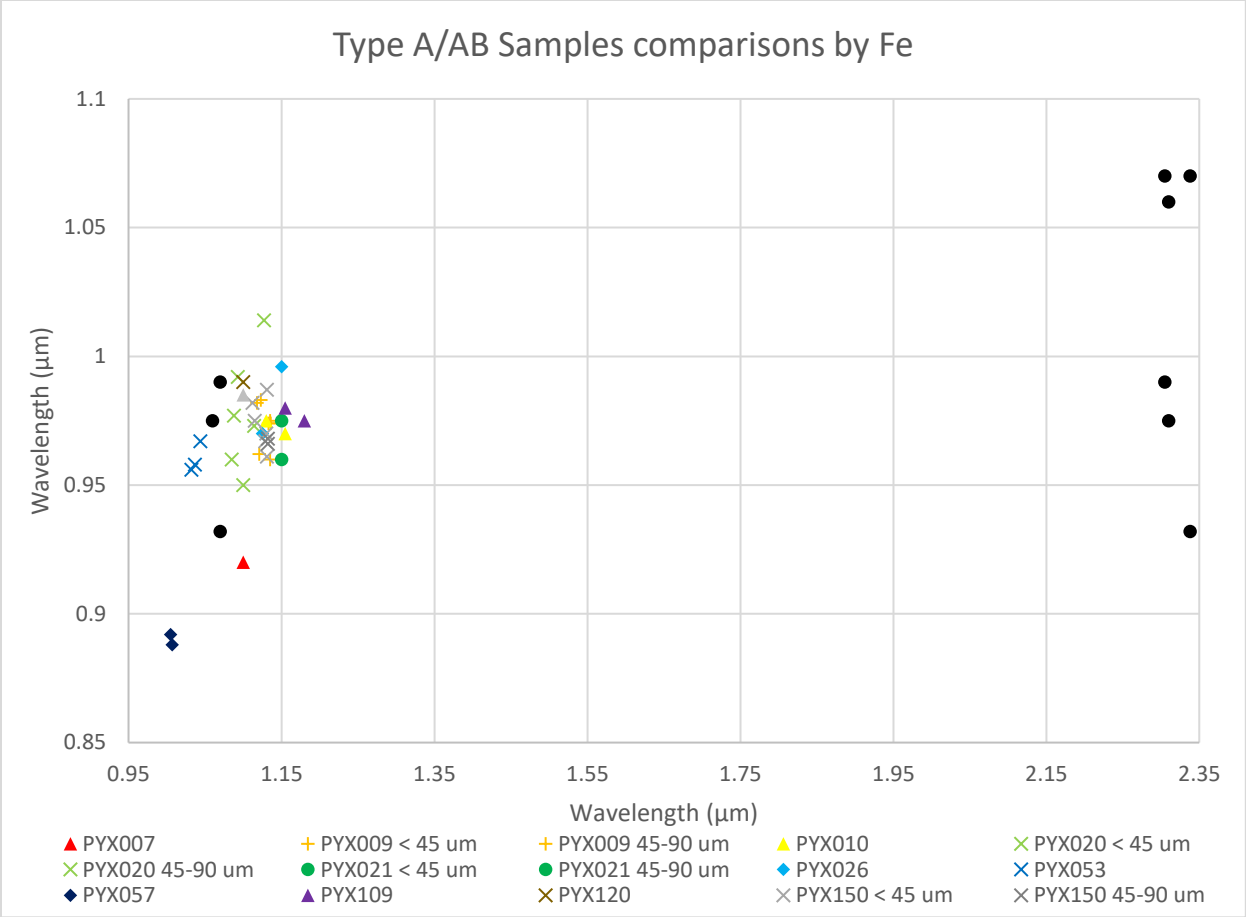
Figure 40. Type A clinopyroxene minima from all methods shown in Fig. 38 in comparison to iron endmember amounts. Circle=$Fs_{40-49}$, Diamond=$Fs_{20-29}$, Triangle=$Fs_{10-19}$, +=$Fs_{5-9}$, X=$Fs_{<5}$. Colors are different for each sample. Sources: HOSERLab, RELAB, Klima et al. 2011, McCraig et al. 2017.
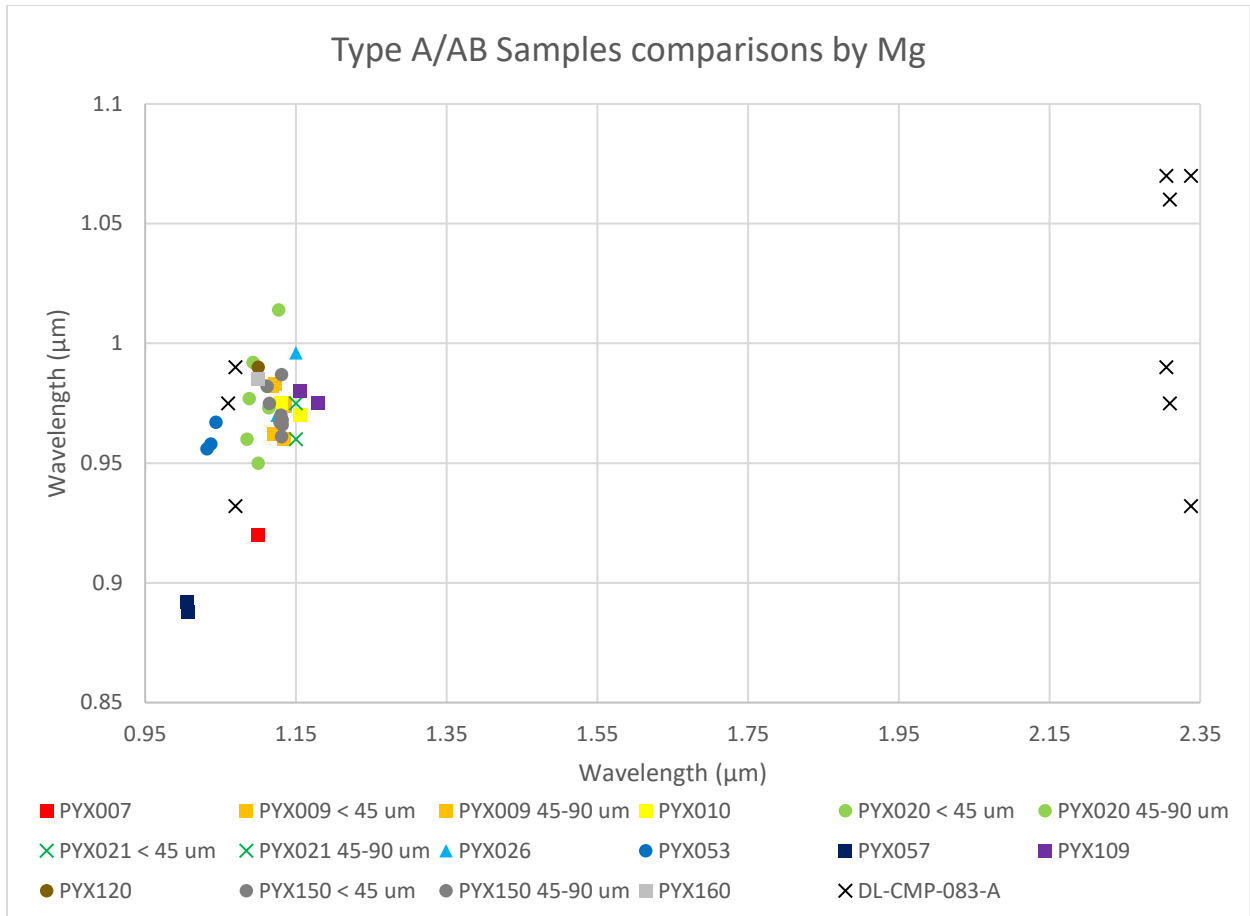
Figure 41. Type A clinopyroxene minima from all methods shown in Fig. 38 in comparison to magnesium endmember amounts. Circle=$En_{40-49}$, Square=$En_{30-39}$, Triangle=$En_{10-19}$, X=$En_{<5}$. Colors are different for each sample. Sources: HOSERLab, RELAB, Klima et al. 2011, McCraig et al. 2017.
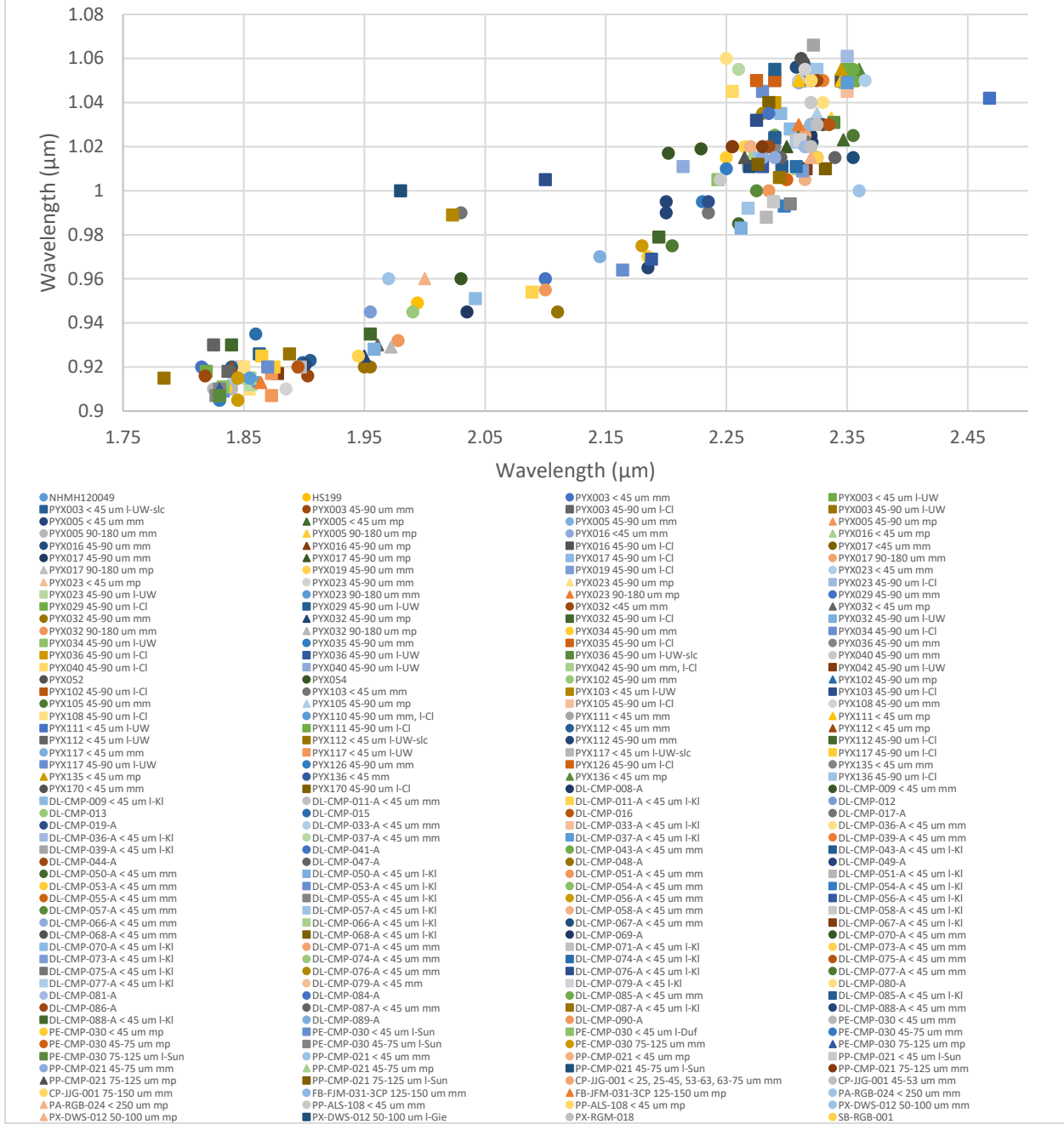
Figure 42. Comparisons of minima from orthopyroxenes, pigeonites, and type B clinopyroxene samples used. Circles=minima I originally found (mm), Squares=literature minima and centers (l; UW= minima from the University of Winnipeg Samples Directory; slc=minima from spectra with straight line continua; Sun=centers from Sunshine et al. 1990, 1993; Duf=centers from Duffard et al. 2005; Cl=centers from Cloutis et al. 2006a; Kl=centers from Klima et al. 2011, Gie=centers from Gietzen et al. 2012), and Triangles=polynomial fitted minima (mp). Colors are different for each sample. Sources: HOSERLab, RELAB, USGS Spectral Library, Sunshine et al. 1990, Sunshine & Pieters 1993, Duffard et al. 2005, Cloutis et al. 2006a, Klima et al. 2011, Gietzen et al. 2012, McCraig et al. 2017.
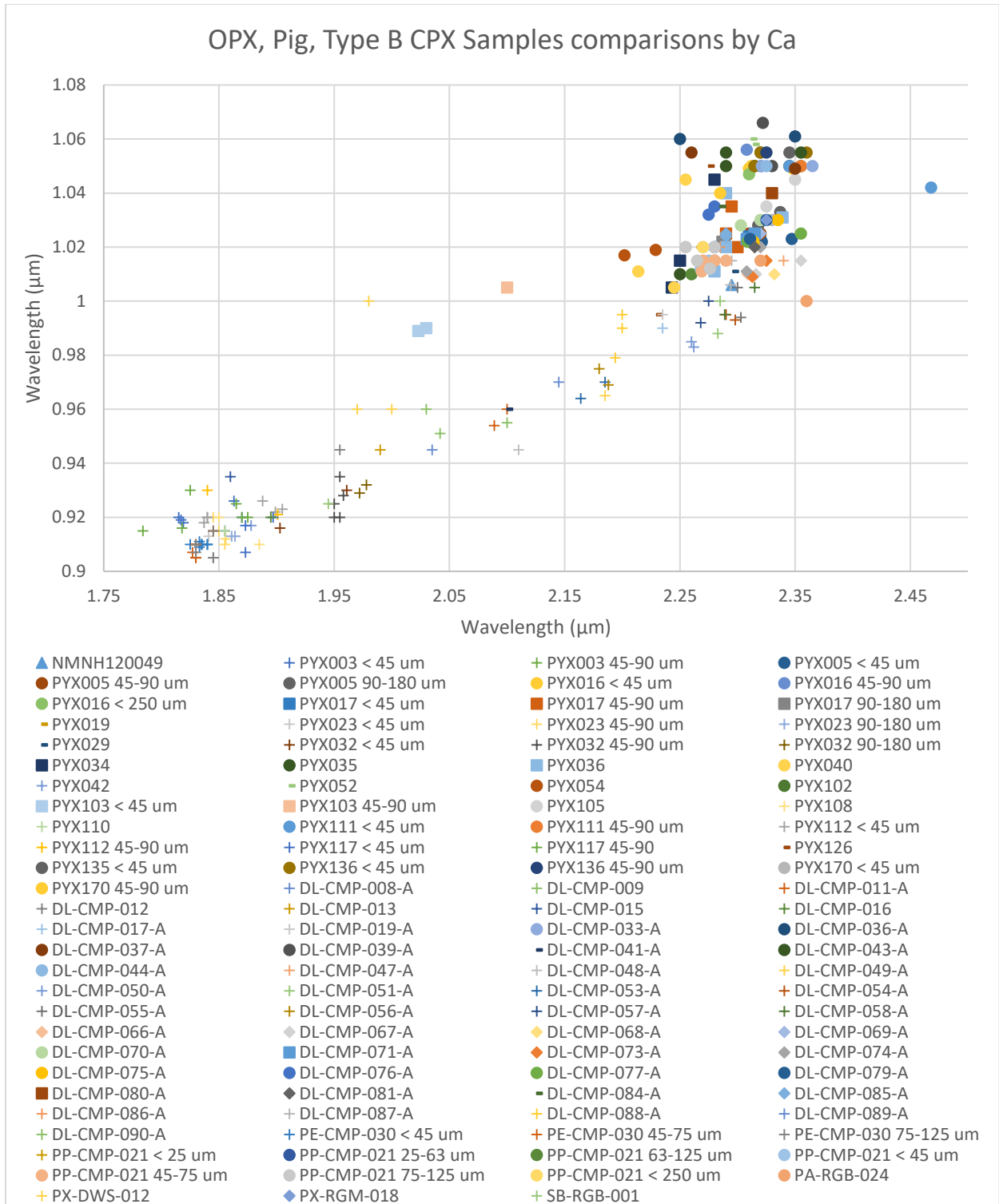
Figure 43. Orthopyroxene, pigeonite, and type B clinopyroxene minima from all methods shown in Fig. 42 in comparison to calcium endmember amounts. Dash=$Wo_{\geq 50}$, Circle=$Wo_{45-49}$, Square=$Wo_{40-44}$, Diamond=$Wo_{35-39}$, Triangle=$Wo_{30-34}$, +=$Wo_{<30}$. Colors are different for each sample. Sources: HOSERLab, RELAB, USGS Spectral Library, Sunshine et al. 1990, Sunshine & Pieters 1993, Duffard et al. 2005, Cloutis et al. 2006, Klima et al. 2011, Gietzen et al. 2012, McCraig et al. 2017.
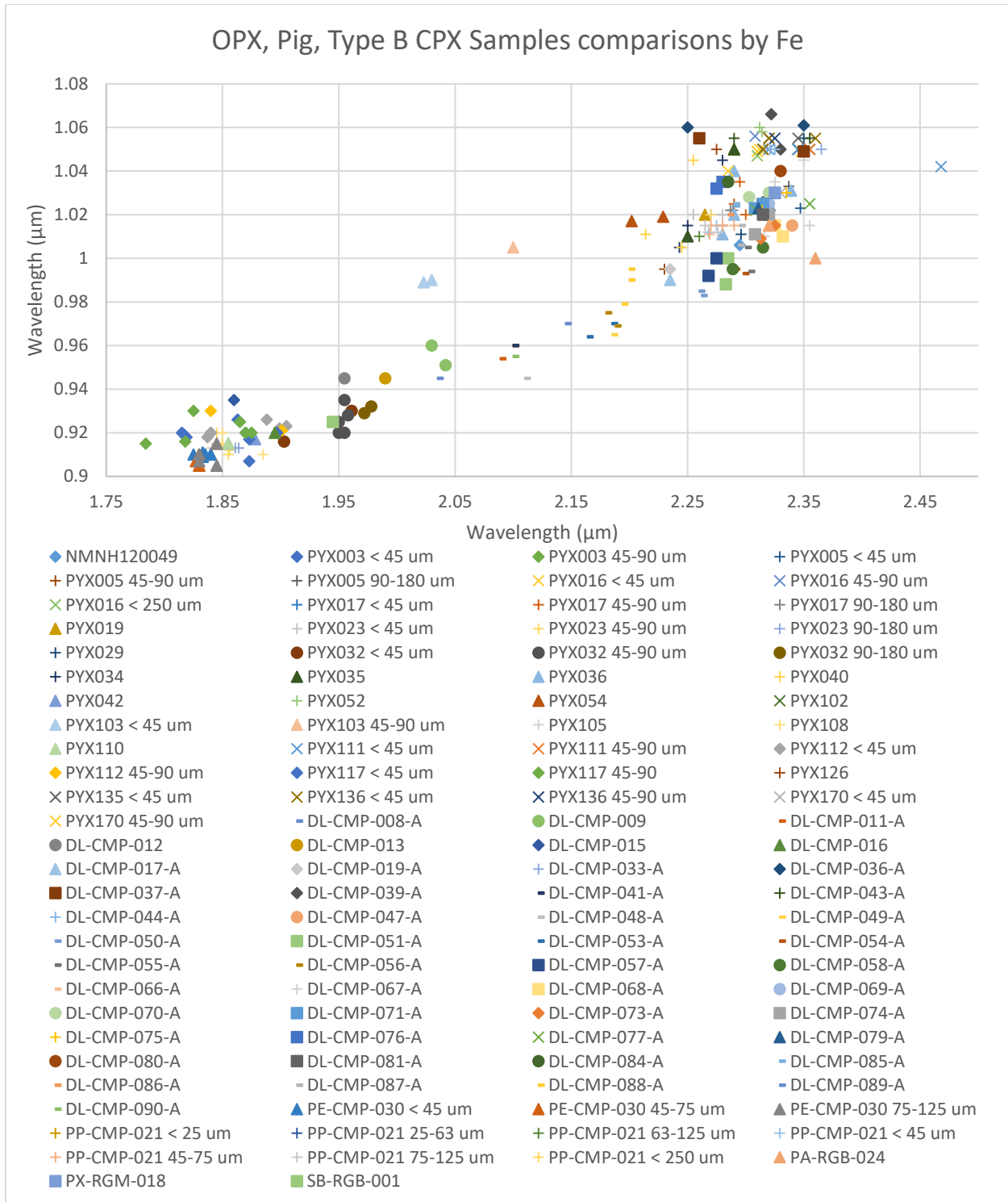
Figure 44. Orthopyroxene, pigeonite, and type B clinopyroxene minima from all methods shown in Fig. 42 in comparison to iron endmember amounts. Dash=$Fs_{\geq50}$, Circle=$Fs_{40-49}$, Square=$Fs_{30-39}$, Diamond=$Fs_{20-29}$, Triangle=$Fs_{10-19}$, +=$Fs_{5-9}$, X=$Fs_{<5}$. Colors are different for each sample. Sources: HOSERLab, RELAB, USGS Spectral Library, Sunshine et al. 1990, Sunshine & Pieters 1993, Duffard et al. 2005, Cloutis et al. 2006, Klima et al. 2011, Gietzen et al. 2012, McCraig et al. 2017.
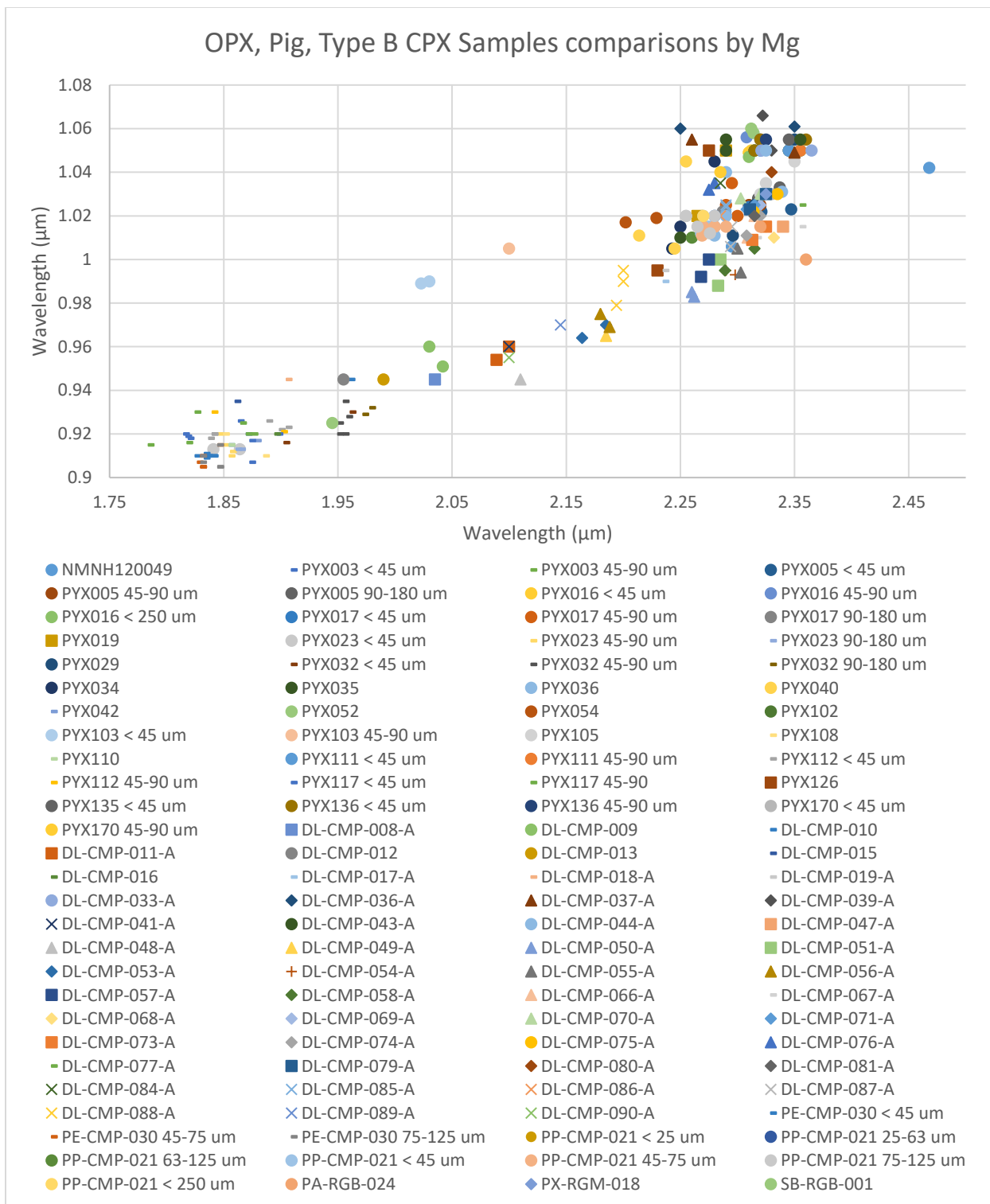
Figure 45. Orthopyroxene, pigeonite, and type B clinopyroxene minima from all methods shown in Fig. 42 in comparison to magnesium endmember amounts. Dash=En$_{\geq 50}$, Circle=En$_{40-49}$, Square=En$_{30-39}$, Diamond=En$_{20-29}$, Triangle=En$_{10-19}$, X=En$_{<5}$. Colors are different for each sample. Sources: HOSERLab, RELAB, USGS Spectral Library, Sunshine et al. 1990, Sunshine & Pieters 1993, Duffard et al. 2005, Cloutis et al. 2006, Klima et al. 2011, Gietzen et al. 2012, McCraig et al. 2017.

Because the largest differences between the lowest reflectance and polynomial fitted

minima were with the ~ 1.1 and ~ 2 µm features in type A and type B clinopyroxenes,

respectively, I graphed the ~ 0.9 and ~ 1 µm features of said samples in comparison to their

calcium, iron, and magnesium endmember abundances. I wanted to see if there were any

possible relationships using just the first features, as they were similar using both methods,

primarily because of less noise and slope than the second features. Firstly, I graphed just the

polynomial fitted minima and compared among all three elements, which are in figures 46

through 49. With the small number of samples, it is impossible to really come to any more

conclusions. I then graphed the type A 0.9 µm features versus the same three elements in figures

50-52, followed by the type B 1 µm features in figures 53-55. The same graphs for the type A

clinopyroxenes band I comparisons from the lowest reflectance minima are above in figures 24,

30, and 32, for calcium, iron, and magnesium, respectively. The same graphs for type B

clinopyroxenes are above with lowest reflectance minima in figures 23 and 28, for calcium and

iron, respectively. I did not find an $R^2$ value for the polynomial fitted minima graphs, so this is

just a comparison based on visuals and what was previously found. I included the lowest

reflectance and literature band minima and centers as well for comparison. The type A

clinopyroxenes were scattered for all three, which was also what was previously found. For the

type A clinopyroxene iron and magnesium graphs, most of the samples seem to hover around the

same wavelength area despite varying contents. However, the iron and magnesium amounts for

these samples also vary for the clinopyroxenes much more than the calcium amounts. The type B

clinopyroxenes however, had possible slight increases in wavelength position with increasing

calcium and magnesium, and a decrease in wavelength position with increasing iron. This is

perhaps similar to what was found previously, although there were weak $R^2$ values in figures 23 and 28.
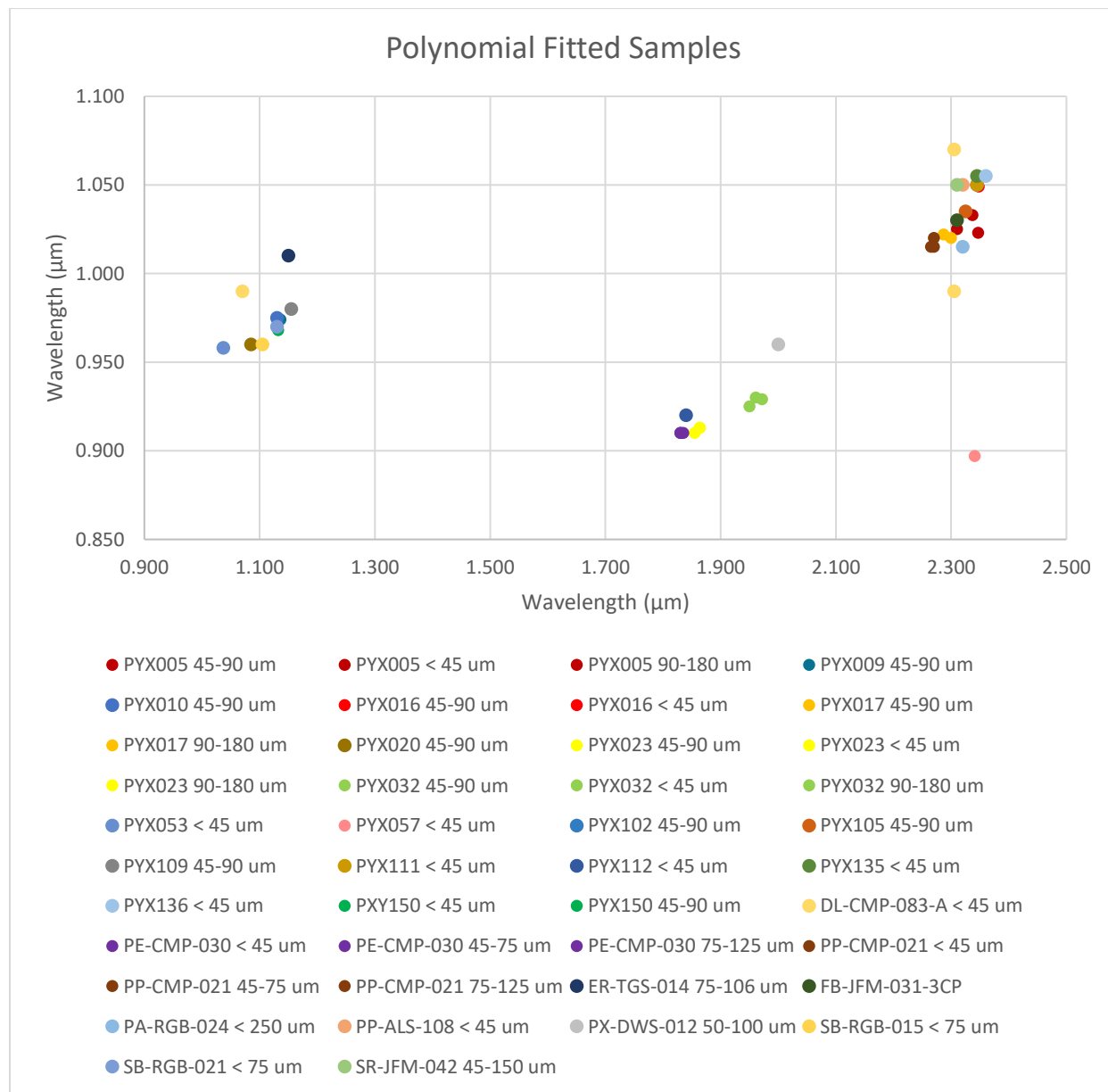


Figure 46. Selected samples with polynomial fitted minima graphed against each other. Sources: HOSERLab, RELAB, McCraig et al. 2017.
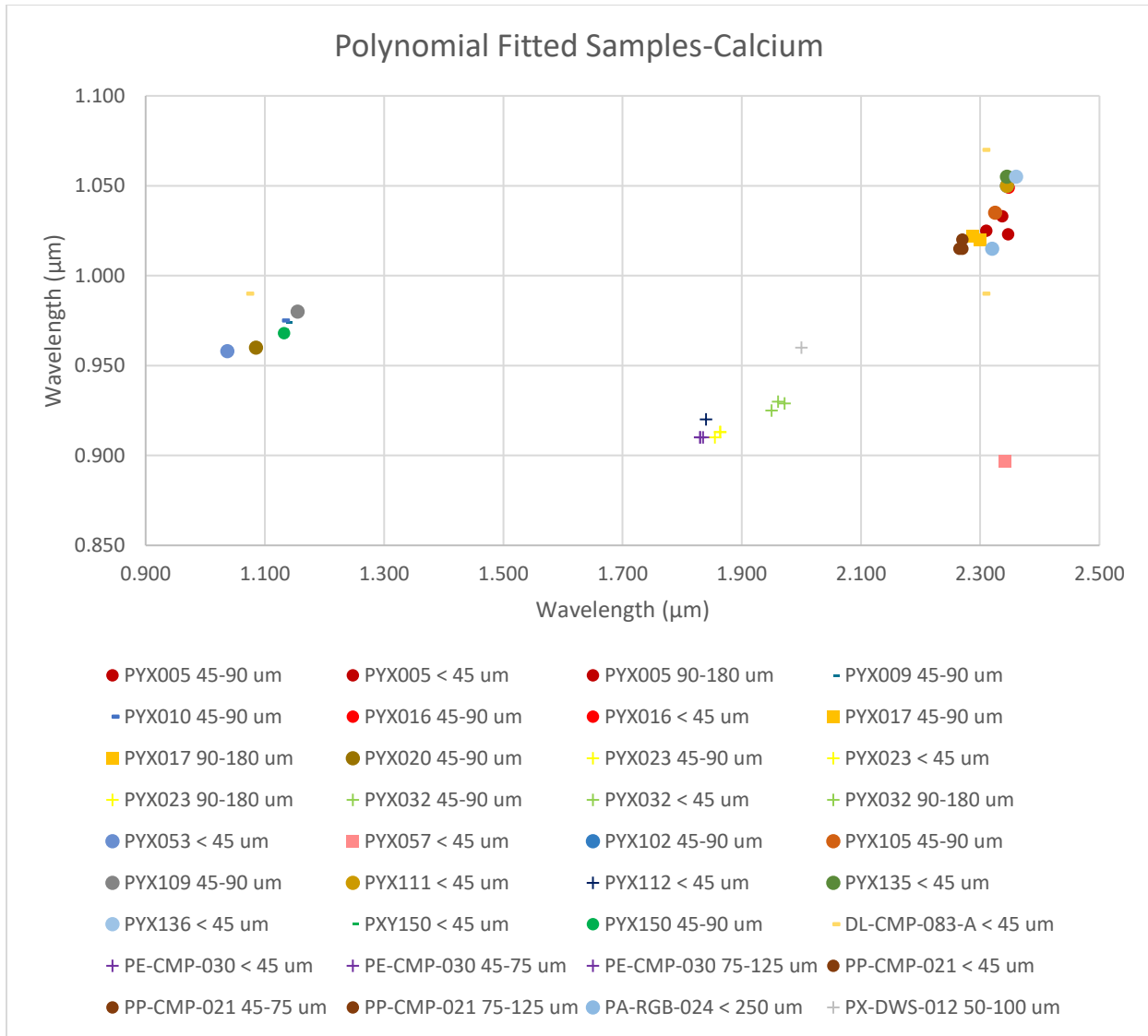
Figure 47. Selected samples with polynomial fitted minima graphed against each other versus calcium endmember amounts. Dash=Wo$_{\geq 50}$, Circle=Wo$_{45-49}$, Square=Wo$_{40-44}$, +=Wo$_{<30}$. Sources: HOSERLab, RELAB, McCraig et al. 2017.
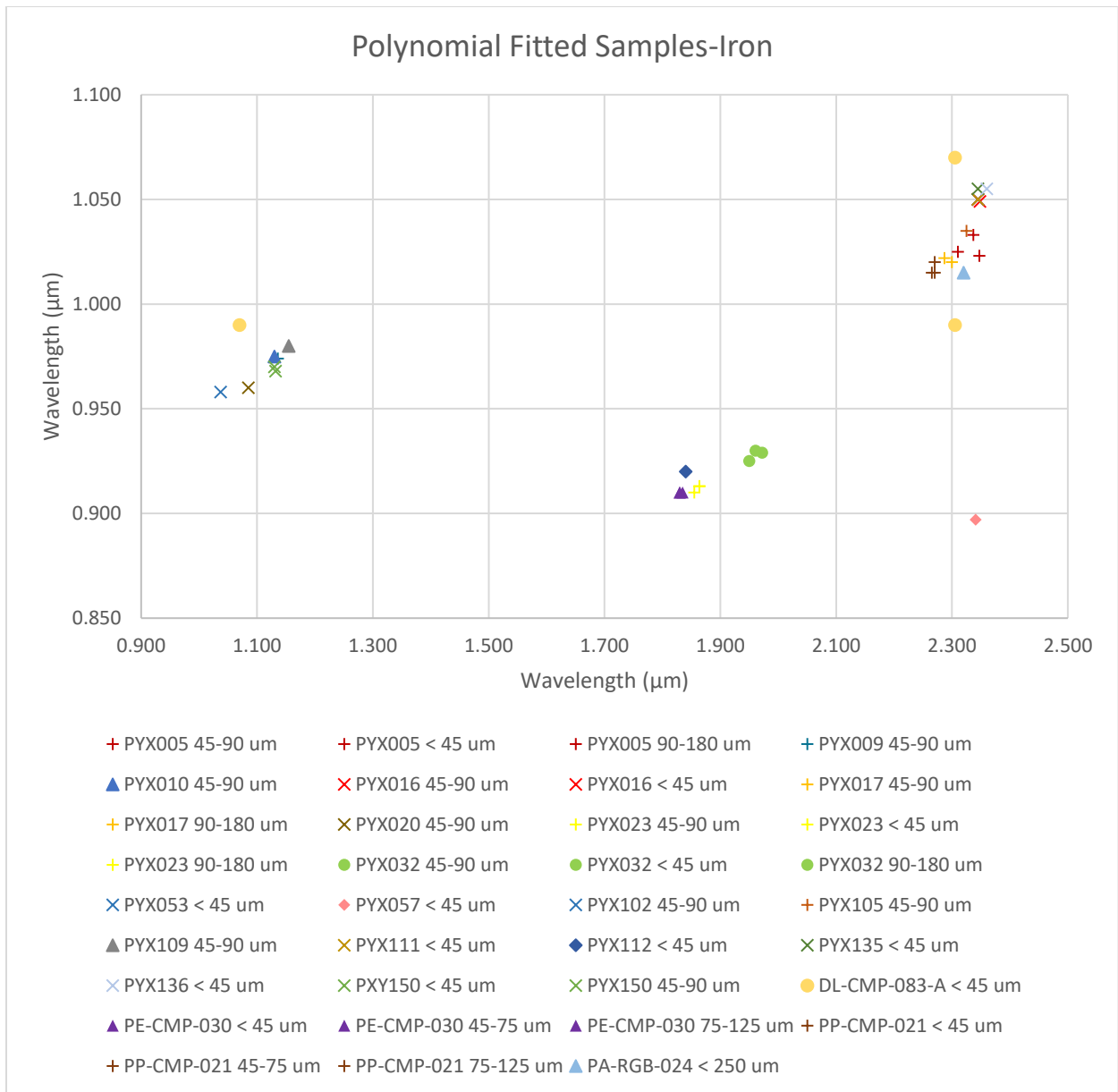
Figure 48. Selected samples with polynomial fitted minima graphed against each other versus iron endmember amounts. Circle=$Fs_{40-49}$, Diamond=$Fs_{20-29}$, Triangle=$Fs_{10-19}$, +=$Fs_{5-9}$, X=$Fs_{<5}$. Sources: HOSERLab, RELAB, McCraig et al. 2017.
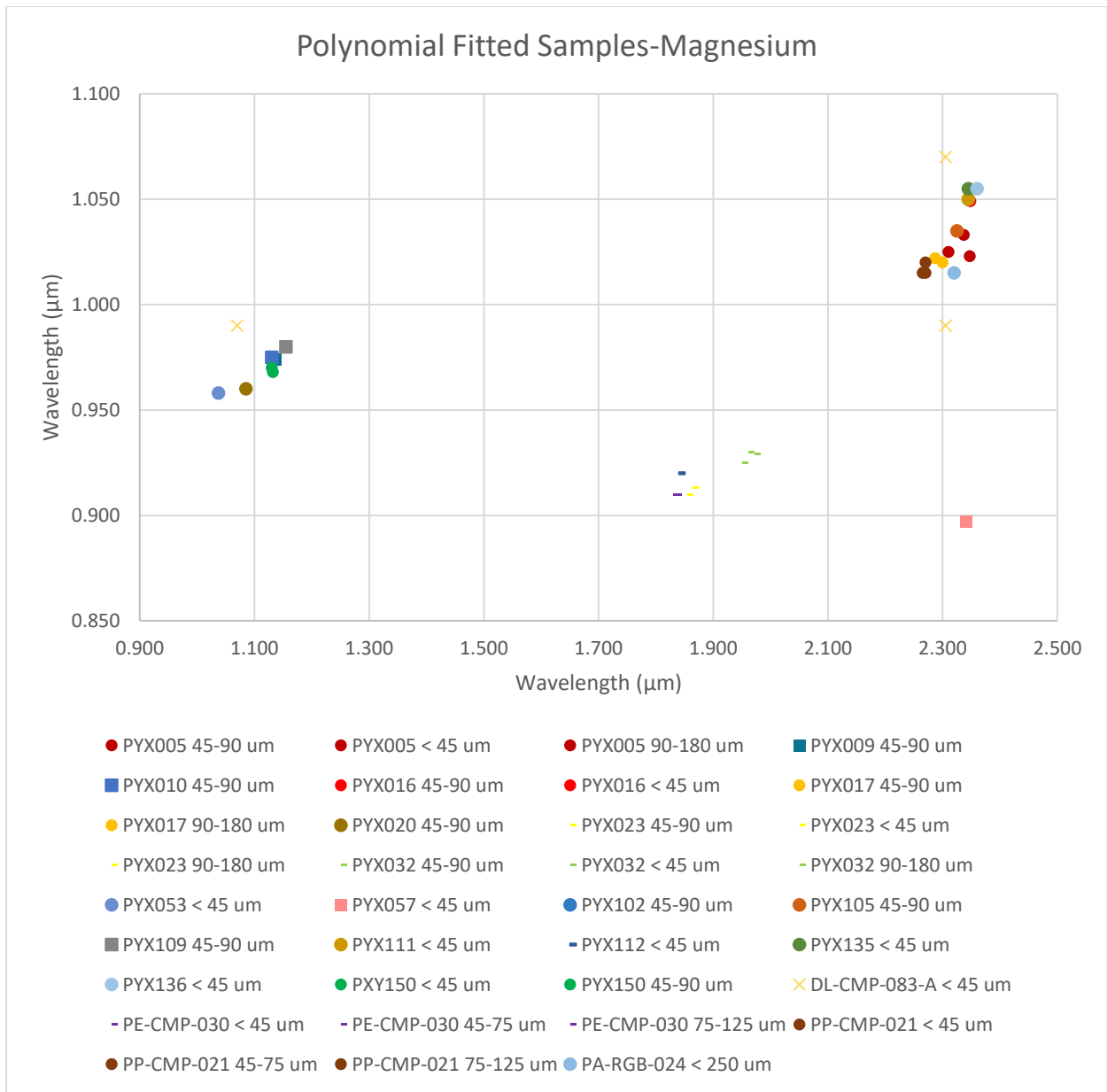
Figure 49. Selected samples with polynomial fitted minima graphed against each other versus magnesium endmember amounts. Dash=En$_{\geq 50}$, Circle=En$_{40-49}$, Square=En$_{30-39}$, X=En$_{<5}$. Sources: HOSERLab, RELAB, McCraig et al. 2017.
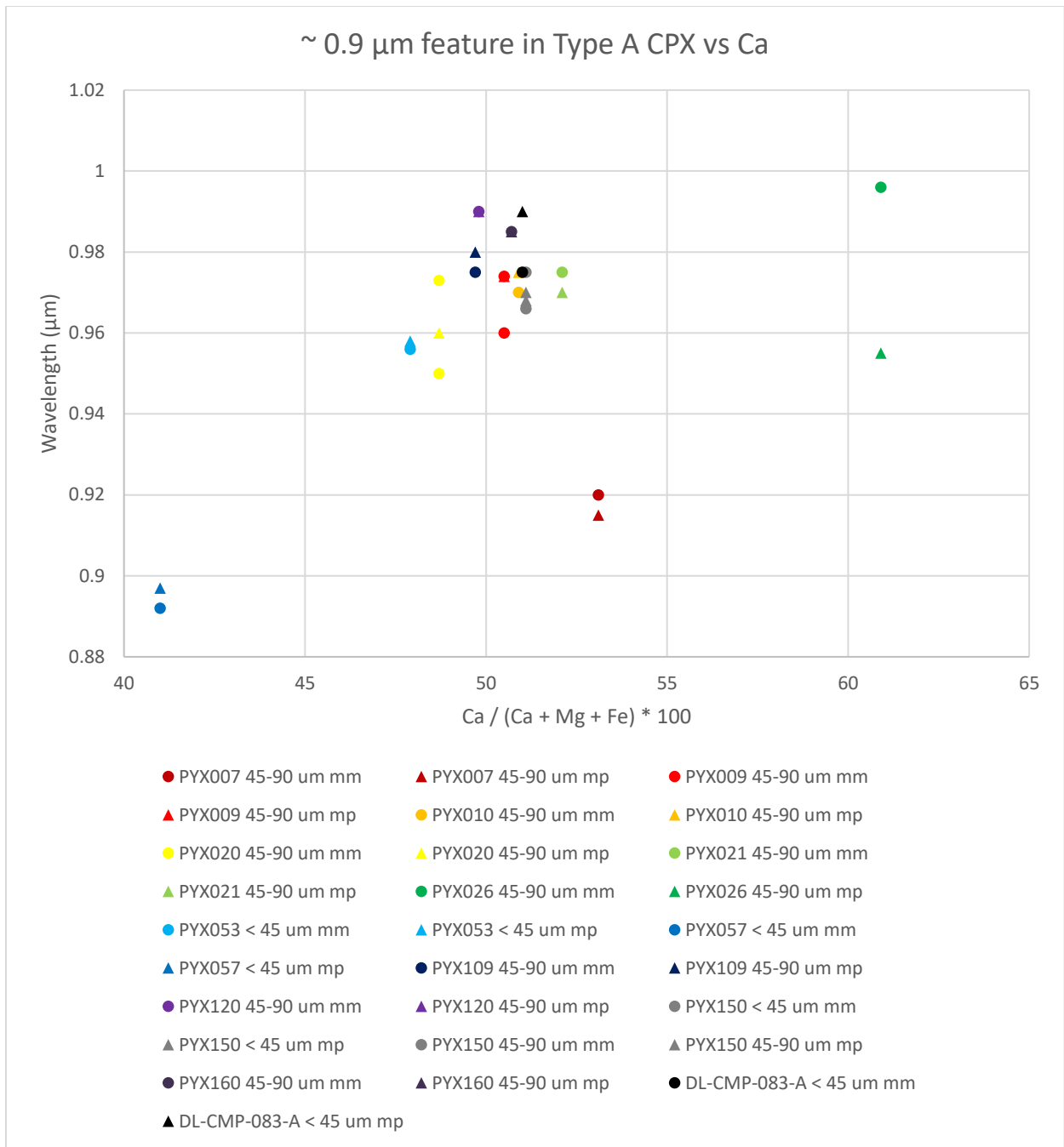
Figure 50. Selected type A clinopyroxene sample 0.9 μm minima versus calcium endmember amounts. Circles=minima found by lowest reflectance, Triangles=minima found by polynomial fitting. Each sample has a different color. Sources: HOSERLab, RELAB, McCraig et al. 2017.
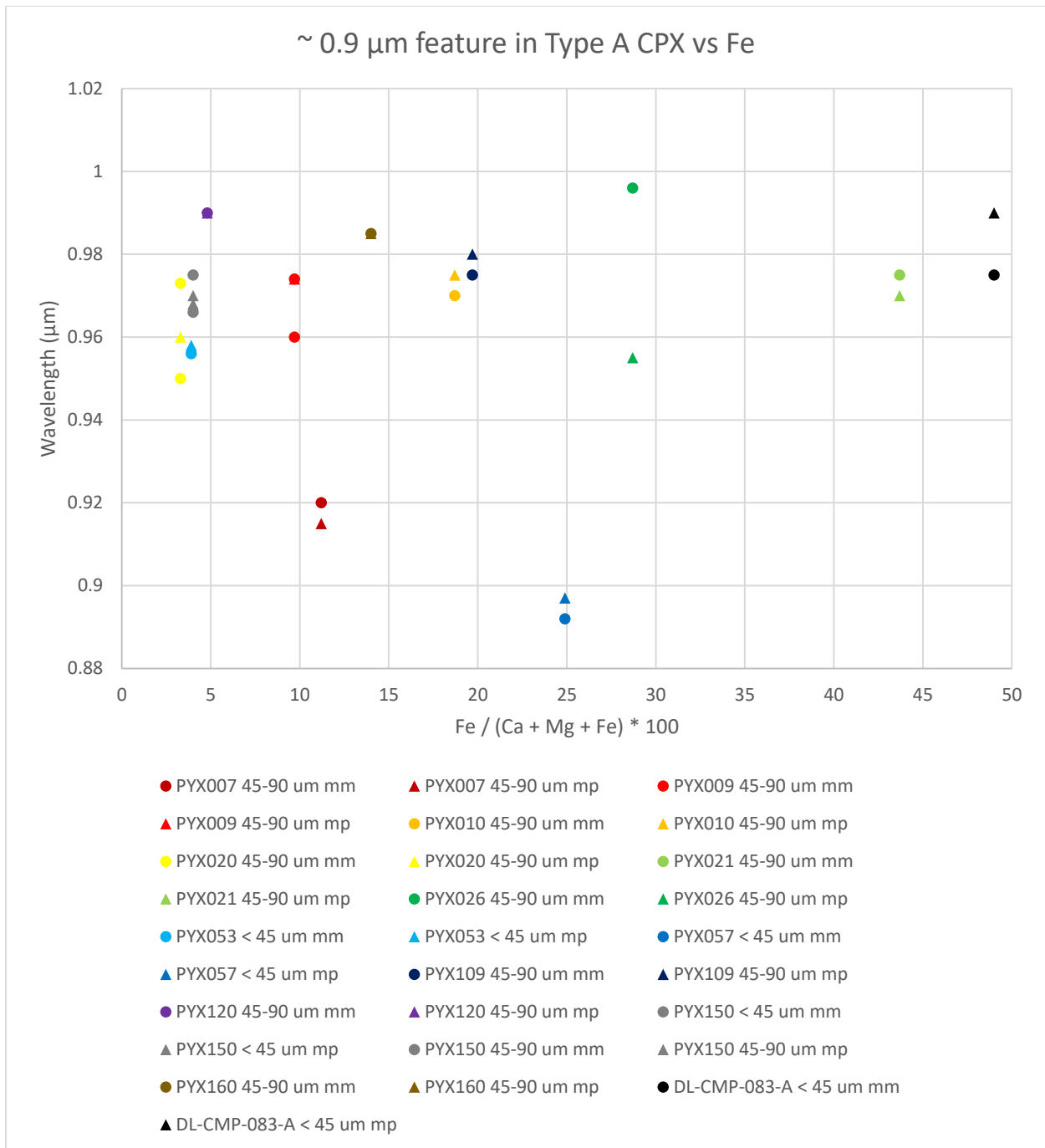
Figure 51. Selected type A clinopyroxene sample 0.9 µm minima versus iron endmember amounts. Circles=minima found by lowest reflectance, Triangles=minima found by polynomial fitting. Each sample has a different color. Sources: HOSERLab, RELAB, McCraig et al. 2017.
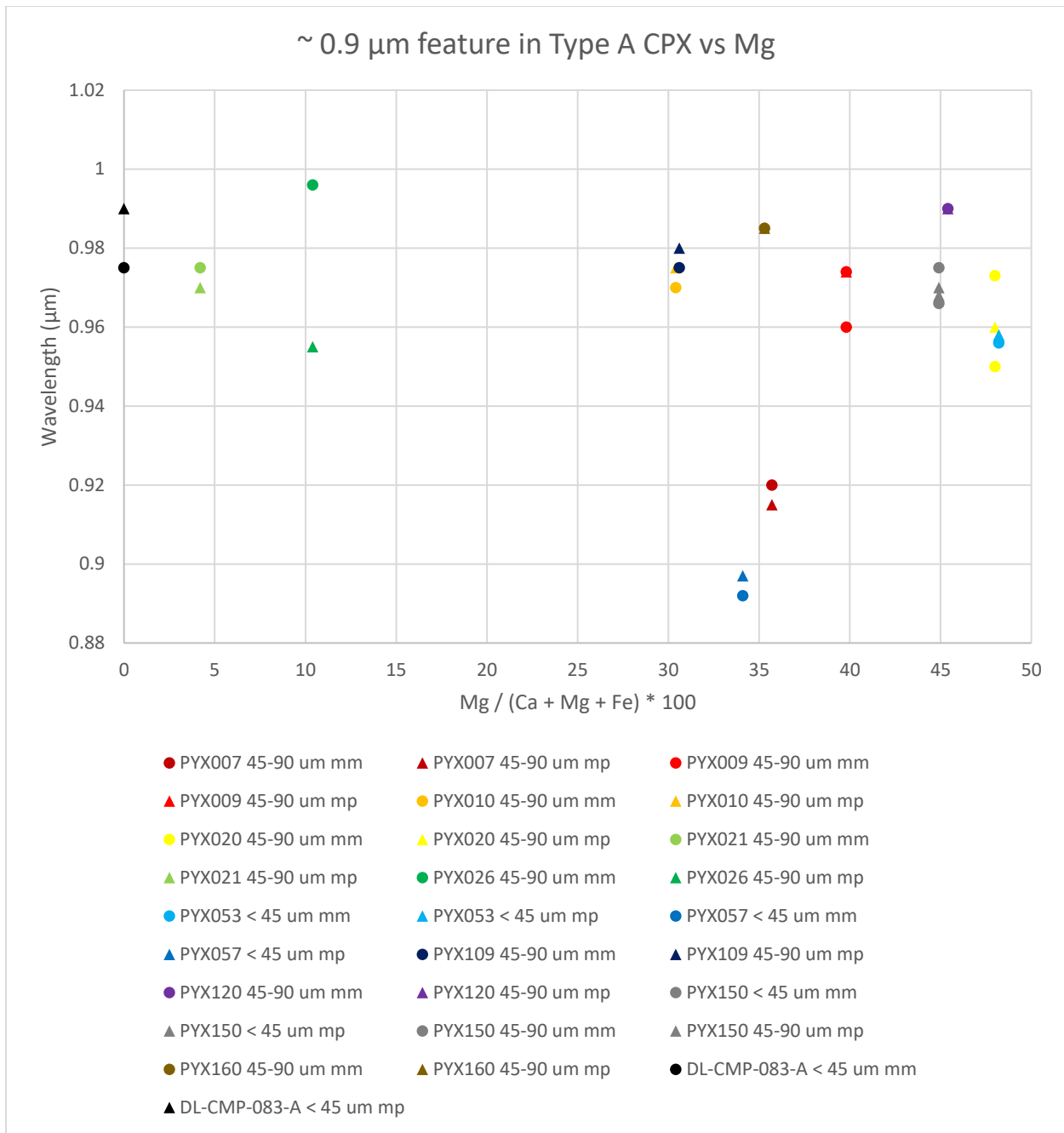
Figure 52. Selected type A clinopyroxene sample 0.9 µm minima versus magnesium endmember amounts. Circles=minima found by lowest reflectance, Triangles=minima found by polynomial fitting. Each sample has a different color. Sources: HOSERLab, RELAB, McCraig et al. 2017.
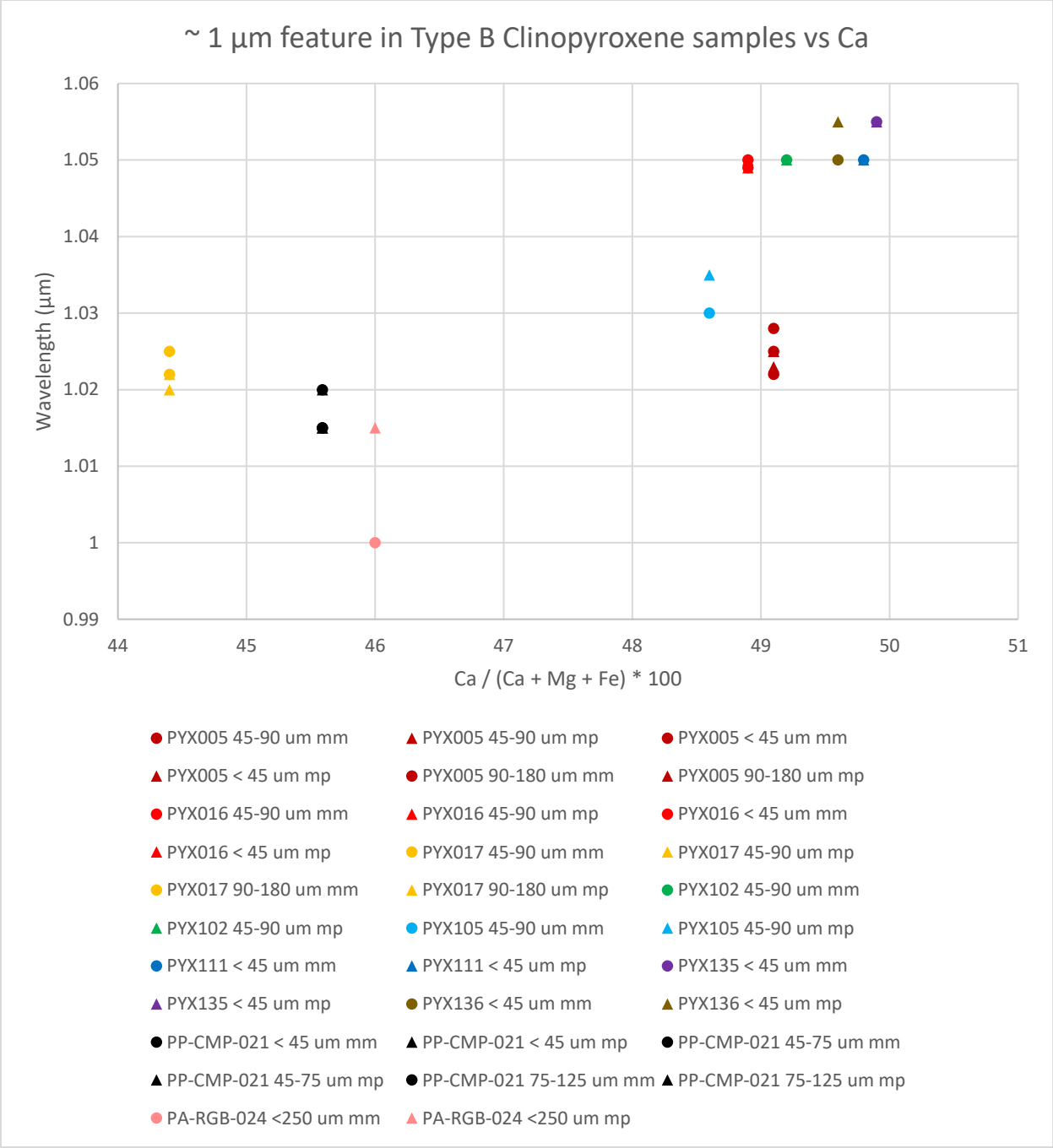
Figure 53. Selected type B clinopyroxene sample 1 µm minima versus calcium endmember amounts. Circles=minima found by lowest reflectance, Triangles=minima found by polynomial fitting. Each sample has a different color. Sources: HOSERLab, RELAB, McCraig et al. 2017.
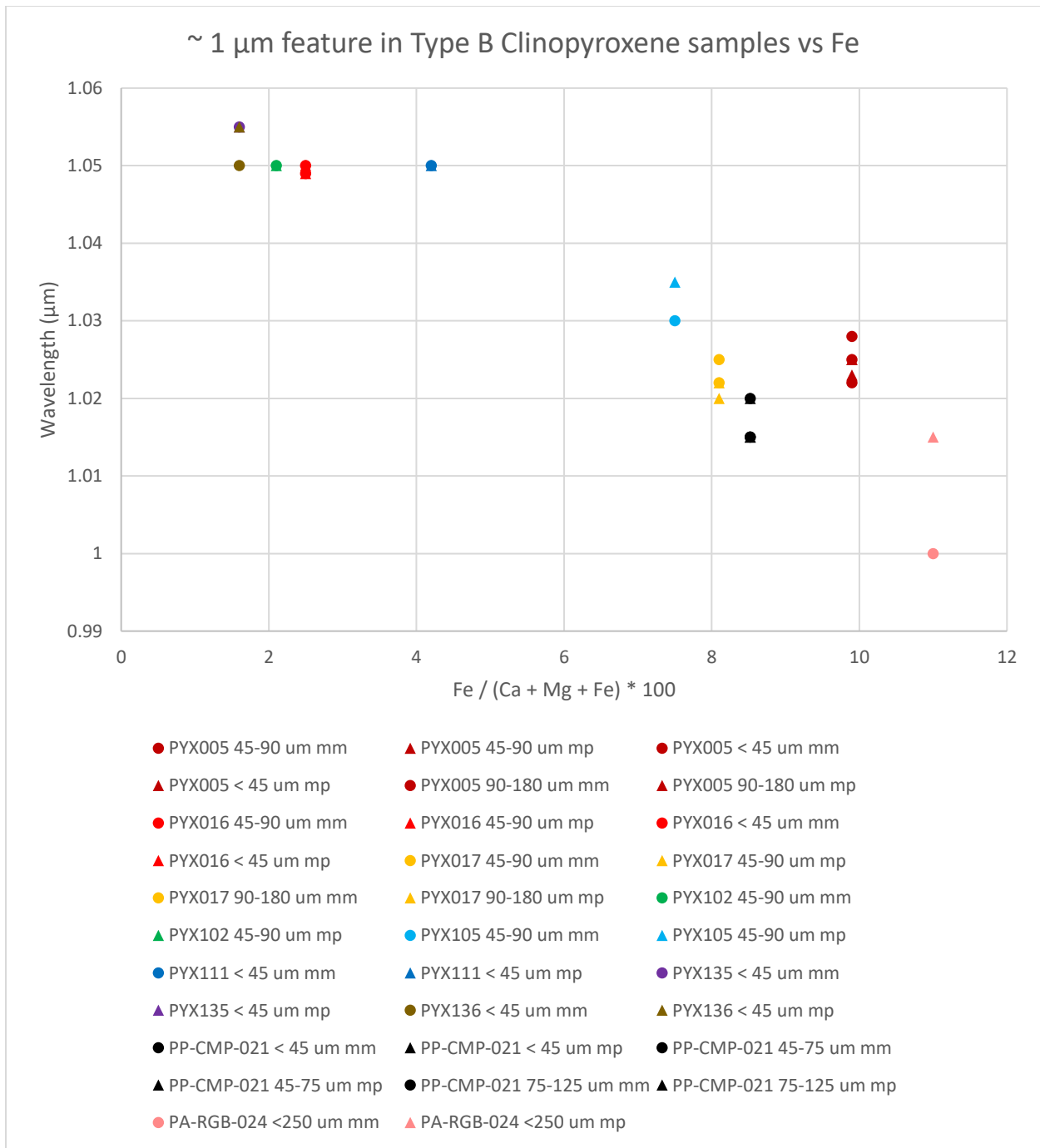
Figure 54. Selected type B clinopyroxene sample 1 µm minima versus iron endmember amounts. Circles=minima found by lowest reflectance, Triangles=minima found by polynomial fitting. Each sample has a different color. Sources: HOSERLab, RELAB, McCraig et al. 2017.
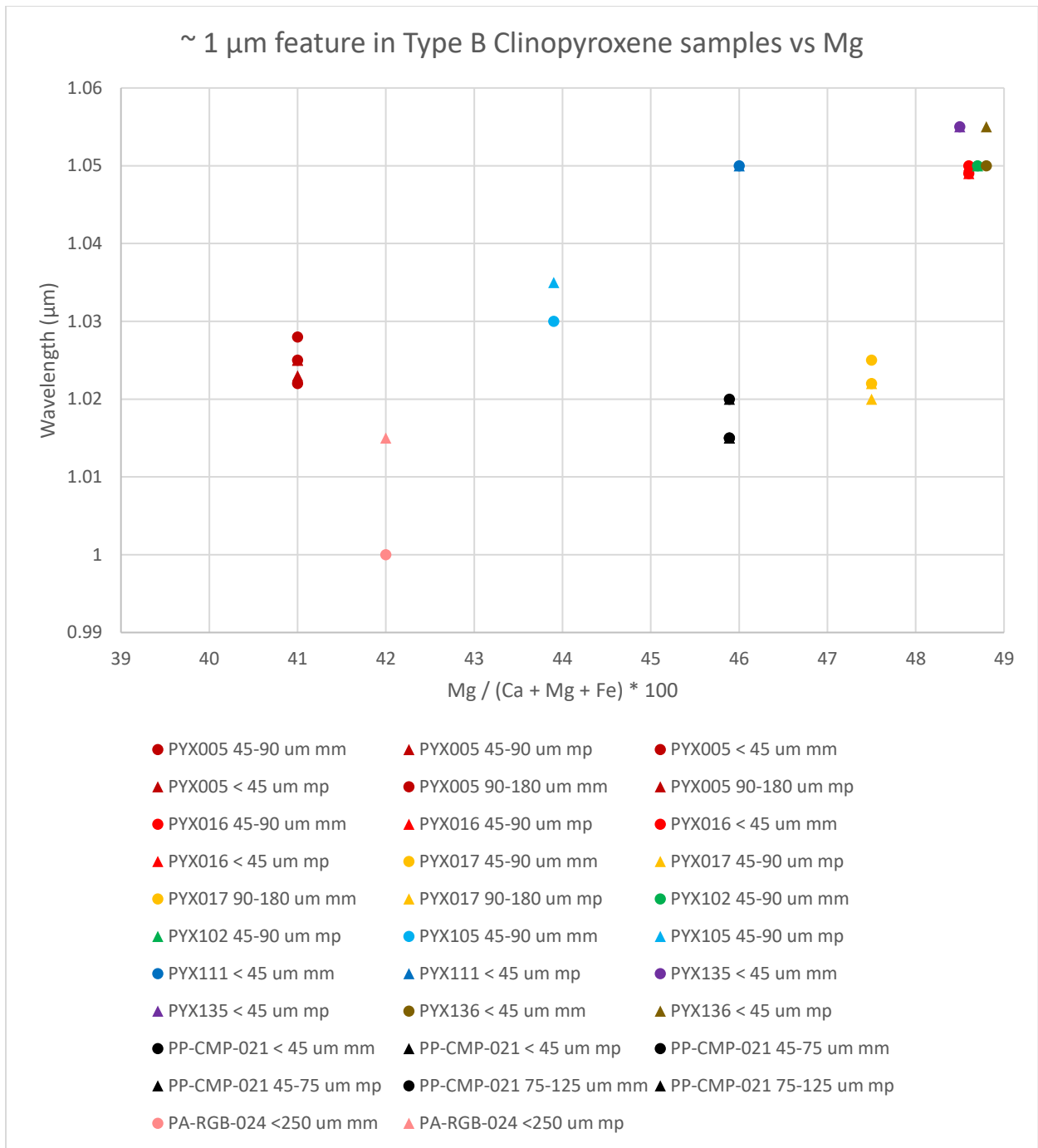
Figure 55. Selected type B clinopyroxene sample 1 μm minima versus magnesium endmember amounts. Circles=minima found by lowest reflectance, Triangles=minima found by polynomial fitting. Each sample has a different color. Sources: HOSERLab, RELAB, McCraig et al. 2017.

# Discussion of mixture band minima and centers

In addition to looking at samples themselves, I also looked at mixtures of pyroxenes, olivines, and plagioclases in the literature. I focused on the mixtures that included samples I looked at, but I also looked at other mixtures as well. I categorized them into type A two pyroxene mixtures, type A pyroxene-olivine mixtures, type B two pyroxene mixtures, type B pyroxene-olivine mixtures, and random pyroxene mixtures that usually involved different pyroxenes, olivines, and plagioclases. The different mixtures that I am focusing on and the wavelength positions of minima found from lowest reflectance are located in the Appendices in table 6.

As expected, there were many clinopyroxene mixtures, but most were of type B clinopyroxenes. HOSERLab had some type A clinopyroxene mixtures so I am going to start with them. PYX150, a type A clinopyroxene was mixed with the orthopyroxene PYX032, both of which have been mentioned above and are also located in the Appendices tables 1 and 3. Most were at 10 % intervals, with the exception of the 70 % to 100 % clinopyroxene mixtures which were measured in 5 % intervals. There were two sets of these mixtures, one of < 45 µm grain sizes and the other of 45-90 µm grain sizes. The spectra from these different mixtures are located in figures 56 and 57. I have color-coded them to make it easier to see the transitions, with the colors of the rainbow. Starting from red and going to black, they represent low to high clinopyroxene percentages.
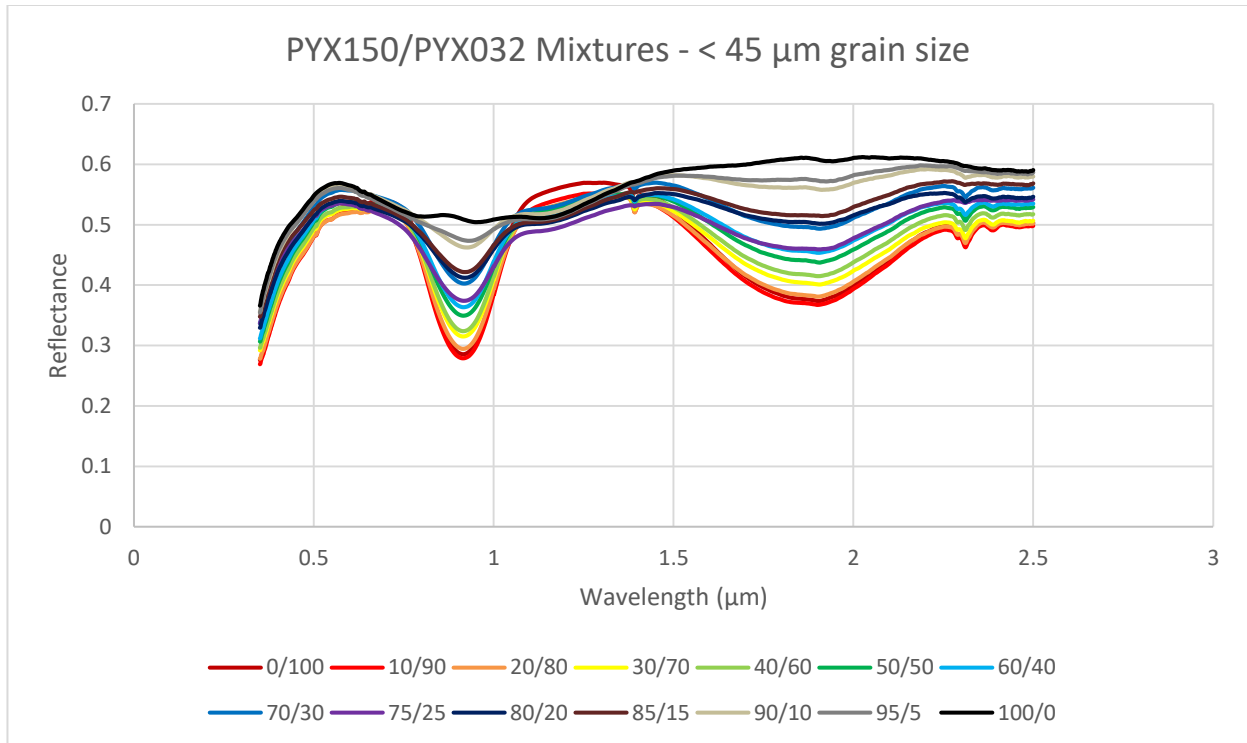
Figure 56. Type A clinopyroxene (PYX150) and orthopyroxene (PYX032) mixtures at < 45 µm grain size. Source: HOSERLab.
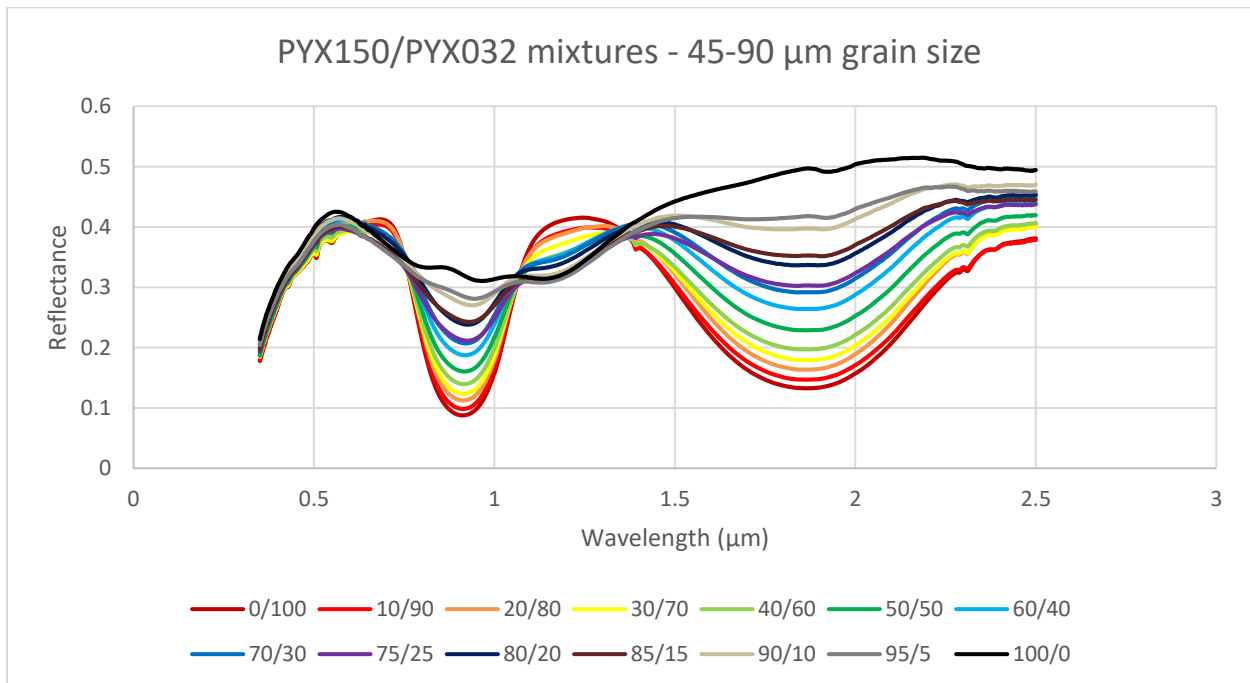


Figure 57. Type A clinopyroxene (PYX150) and orthopyroxene (PYX032) mixtures at 45-90 µm grain size. Source: HOSERLab.

Overall these two mixtures had similar results. It was noticeable right away that there was a large change around the 80/20 of type A clinopyroxene to orthopyroxene for < 45 µm grain sizes and 75/25 for 45-90 µm grain sizes. This was when a 1.2 µm feature started appearing, although I was not necessary able to find the minima for that feature. At around 85/15 for both the 1.2 µm feature appeared to reach its final strength as it did not change much when going to 100/0. Schade et al. (2004) stated that the 1.15 µm starts to be present at ≥ 40 % type A clinopyroxene which did appear to be the case here too, albeit the features were faint until the ratios mentioned above. With regards to the 0.9 µm features, it did not change much from its original position in the 0/100 ratio up until around 75/25 when it finally started moving to longer wavelengths. This also seemed to agree with Schade et al. (2004) as that was when the mixture started leaving the orthopyroxene general trendline and started to behave like a type A clinopyroxene. As the mixture progressively got more clinopyroxene-rich it also increased in reflectance typically, with the < 45 µm grain size mixtures at higher reflectances. The 2 µm feature only started to get faint at 90/10 ratios after slowly getting shallower when more clinopyroxene was added. Several of the wavelength amounts for the 2 µm features had an interfering water feature that may have affected the results for the lowest reflectance minima. This occurred in most spectra in the < 45 µm grain sizes and from 75/25 to 100/0 for the 45-90 µm grain sizes. In the 45-90 µm spectra in particular, the orthopyroxene dominated spectra had many shorter wavelength features, likely from the much larger amounts of iron in PYX032 than PYX150. These went away once the mixture was around 60/40 clinopyroxene/orthopyroxene. I polynomial fitted minima from the spectra to see how that would change the results, which can be seen below and in table 8 in the appendices.

The next group was the type A clinopyroxene and olivine mixtures. There was only one group of this and it involved PYX150 again with OLV003, a forsterite of $Fo_{90.4}$. The chemical analyses of OLV003 is in table 10 in the appendices and once again the mixture's band minima from lowest reflectance are in table 6 in the same section. These mixtures were measured at < 45 µm grain sizes and were in 10 % intervals. Once more I color-coded the graph in rainbow-like order with red being olivine and brown being clinopyroxene. A compilation of the mixtures are in Fig. 58. Again, right away there was a distinction between the different spectra in that mixtures with 70 % and more clinopyroxene resembled the clinopyroxene while mixtures with less than 70 % resembled olivine, although the 70/30 clinopyroxene/olivine mixture had one broadened 1 µm feature from both the olivine and clinopyroxene, such as what can be seen in angrites. As olivine decreased, the spectra also increased in reflectance until 70/30 and the side lobe features became less pronounced. The 80/20 mixture was when the 0.9-1 µm feature started moving to shorter wavelengths and the 1.1 µm feature appeared, both to align with the clinopyroxene features.
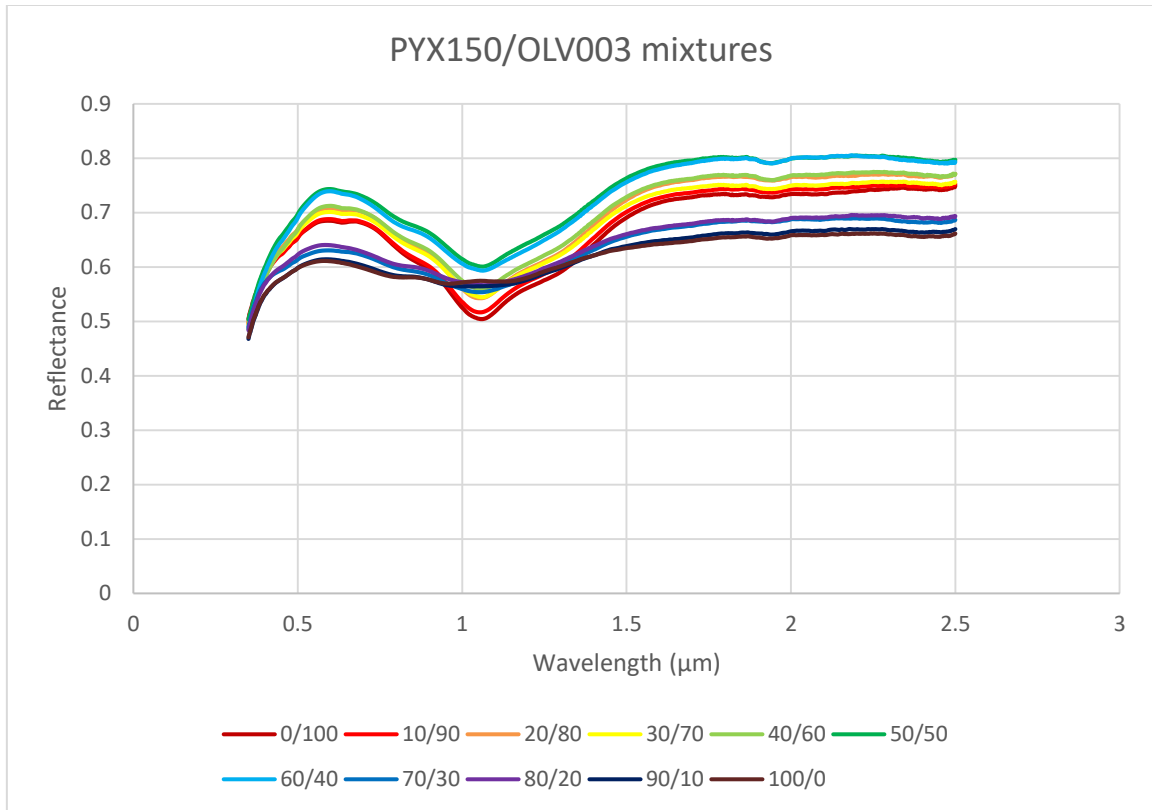
Figure 58. Type A clinopyroxene (PYX150) and olivine (OLV003) mixtures at 45-90 µm grain sizes. Source: HOSERLab.

As mentioned above, since there were some differences, I decided to go over some of the mixtures with polynomial fits to find the minima again; I did this for all the mixtures, but particularly the mixtures that had wavelength positions in the literature and for type A mixtures. Even though there were not band positions for these latter mixtures in the literature, I think it will provide a better picture of what was happening with the addition of clinopyroxene. In general, I tried to graph the mixture minima in the same color scheme as the spectra graphs.

Starting with the COMIX < 45 µm grain size mixtures with PYX150 and PYX032, a Type A clinopyroxene and orthopyroxene mixture, there were not many issues with getting the polynomial fitted minima. A good reason to use the polynomial fitting for these mixtures was to get a more accurate ~ 1.8 µm feature for mixtures with PYX032, as there was a water feature around 1.9 µm that may have caused issues with the original minima found. As with the lowest

130

reflectance minima, I was not able to get the forming 1.1 µm feature from PYX150 until the mixture was 90/10 PYX150/PYX032, as the slope was too steep to get a fitting of it. Even at 90/10, it was a weak feature. 90/10 and 95/5 are also the two mixture spectra that had the worst $R^2$ values for the ~ 1.8 µm feature from PYX032. This was likely because it was getting shallower and weaker and the noise from the water feature was stronger, causing the fit to appear a little more twisted than the other curves. The results were similar to the lowest reflectance minima, as there were few changes in the 0.9 µm feature until ~ 90/10 CPX/OPX, when it started to increase in wavelength much more. The ~ 1.8 µm feature also hovered around the same area until 95/5, while the 1.1 µm feature kept increasing in wavelength starting at 90/10. As another minor note, the 100/0 PYX150/PYX032 ~ 0.9 µm feature fitting had a zero-crossing that was very slightly above the x-axis, but had a lone inflection point and a good $R^2$ value. For the differences between the lowest reflectance and polynomial fitted minima, all of the one micron features were within 4 nm. The spectra that had two micron feature minima had much greater differences. The ones with greater than 5 nm differences were COMIX1101 at 17 nm, COMIX1102 at 24 nm, COMIX1103 at 17 nm, COMIX1104 at 20 nm, COMIX1105 at 15 nm, COMIX1106 at 14 nm, COMIX1107 at 18 nm, COMIX1108 at 21 nm, COMIX1109 at 22 nm, and COMIX1109.5 at 41 nm. The mixtures that had other features all had large differences of COMIX1108.5 at 31 nm, COMIX1110 at 31 nm, and COMIX1110.5 at 114 nm. These differences in the second and other features is likely because of the fainter features around 1.1 µm and noisy features near 1.8 µm, both of which were hard to obtain with the lowest reflectances.

There were similar results with the COMIX 45-90 µm grain size mixtures with PYX150 and PYX032, with the ~ 1.1 µm feature from PYX150 not being able to be fitted until the

mixture was 90/10 PYX150/PYX032. The $R^2$ values for the 1.8 µm features started to really

decrease by 85/15 PYX150/PYX032, although there were no other issues with them. The results

were similar to the lowest reflectance minima, as there were few changes in the 0.9 µm feature

until ~ 85/15 CPX/OPX, when it started to increase in wavelength much more. Interestingly,

both sets of minima had the 0.9 µm feature slightly increasing in wavelength position with each

mixture's addition of clinopyroxene until the larger changes started around 85/15 and 90/10. The

~ 1.8 µm feature also hovered around the same area until 95/5, although for the lowest

reflectance minima, it started to increase in wavelength a bit starting at 50/50 and had much

more varying minima. The 1.1 µm feature kept increasing in wavelength position starting at

85/15 for the lowest reflectance minima and 90/10 for the polynomial fitted minima. The

polynomial fittings could not get the 1.1 µm feature around 85/15, however. These results are in

figure 59 below, where the circles are the original minima I found and the triangles are the

polynomial fitted minima I found after. Similar to the previous set of mixtures, in COMIX2

spectra there were no 0.9-1 µm features that had differences in minima position greater than 2

nm. The second features had smaller minima differences than above; the ones that had greater

than 5 nm differences are COMIX2105 at 9 nm, COMIX2107 at -20 nm, COMIX2108 at -23

nm, COMIX2108.5 at -26 nm, and COMIX2109 at -22 nm. The mixtures with third features that

were able to be fitted all had differences in minima greater than 5 nm: COMIX2109.5 at -27 nm,

COMIX2110 at 15 nm, and COMIX2110.5 at 52 nm. The differences were possibly from the

mixed features of the two pyroxenes, which were hard to find accurately using lowest

reflectances. These minima comparisons are in figure 60.

There were no issues with fitting PYX150 and OLV003 in the OCMIX mixtures, with the

note that the 1.1 µm feature was rather weak for the 100/0 PYX150/OLV003 mixture spectrum.

The only two spectra that had minima differences above 5 nm in any of the features were OCMIX1009 at -7 nm and OCMIX1101 at 12 nm. For both sets of minima, there were no real changes in wavelength position until 90/10 clinopyroxene/olivine, when the combined 1 µm feature decreased in wavelength and then split into the two clinopyroxene features. These minima comparisons are in figure 61, where the spectra with only one feature are graphed against one micron.
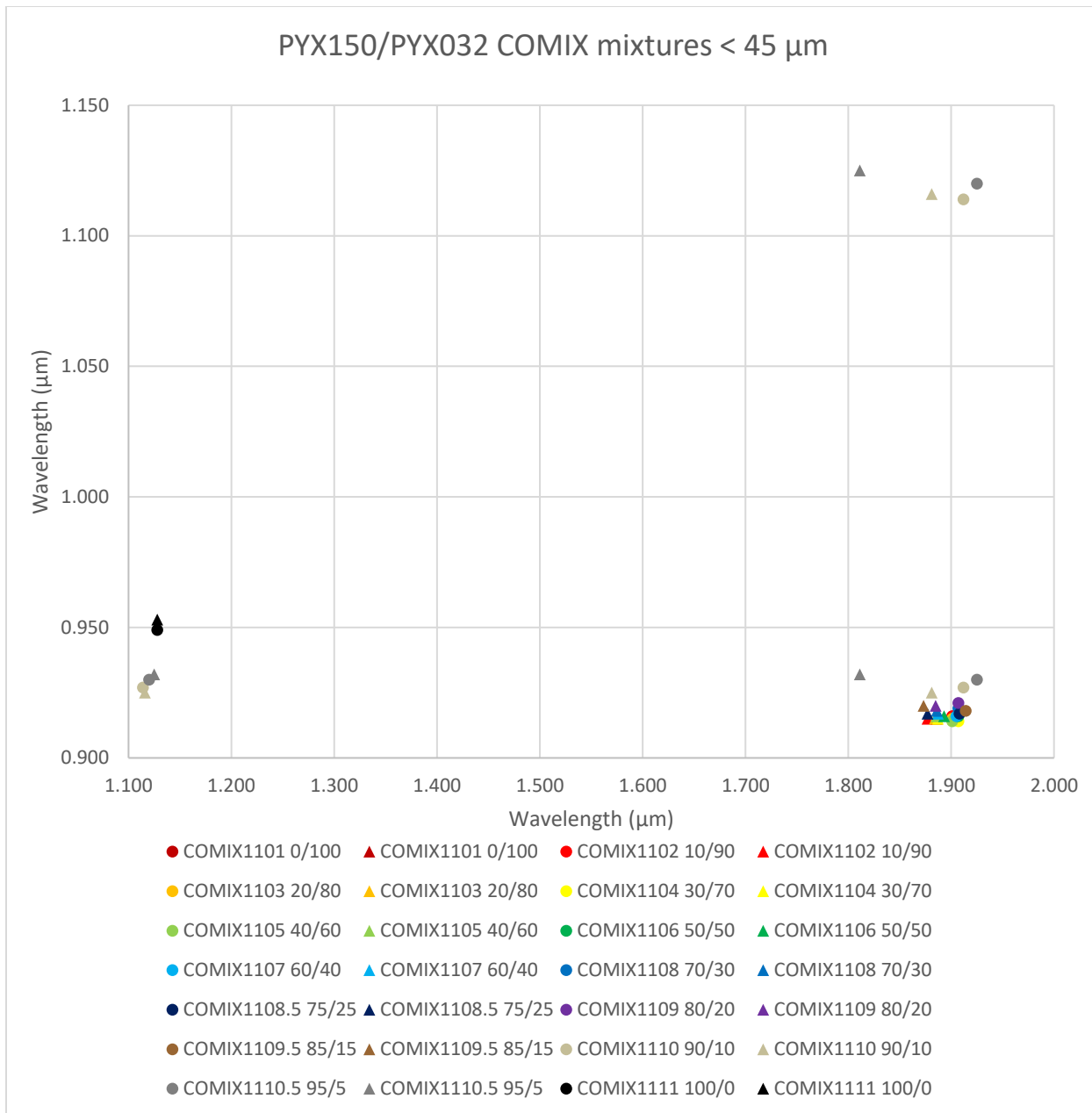
Figure 59. Minima comparisons for the COMIX mixture spectra of PYX150 and PYX032. The circles are the minima I originally found while the triangles are the minima I found using polynomial fitting. Sources: HOSERLab, McCraig et al. 2017.
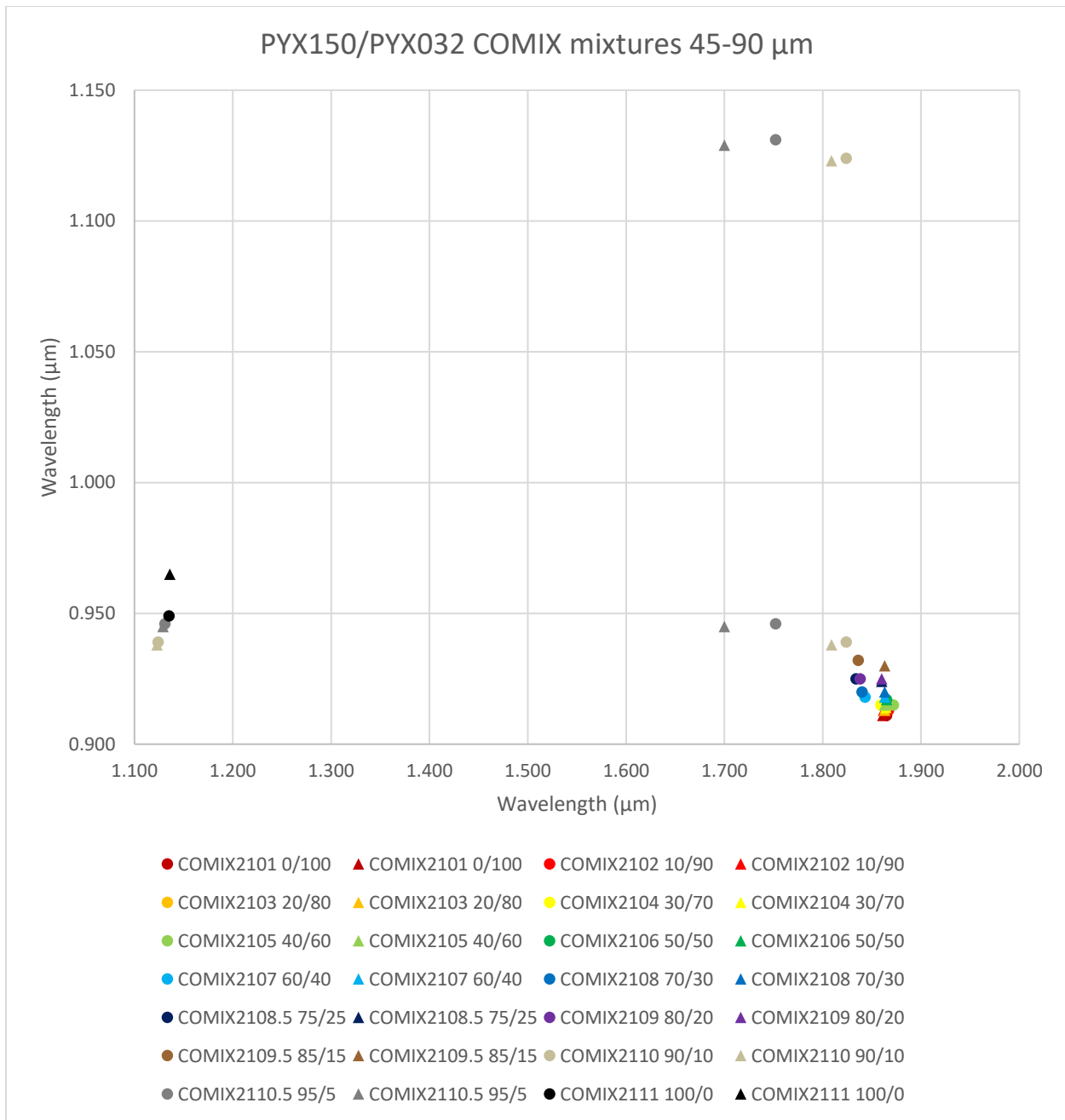
Figure 60. Minima comparisons for the COMIX mixture spectra of PYX150 and PYX032. The circles are the minima I originally found while the triangles are the minima I found using polynomial fitting. Sources: HOSERLab, McCraig et al. 2017.
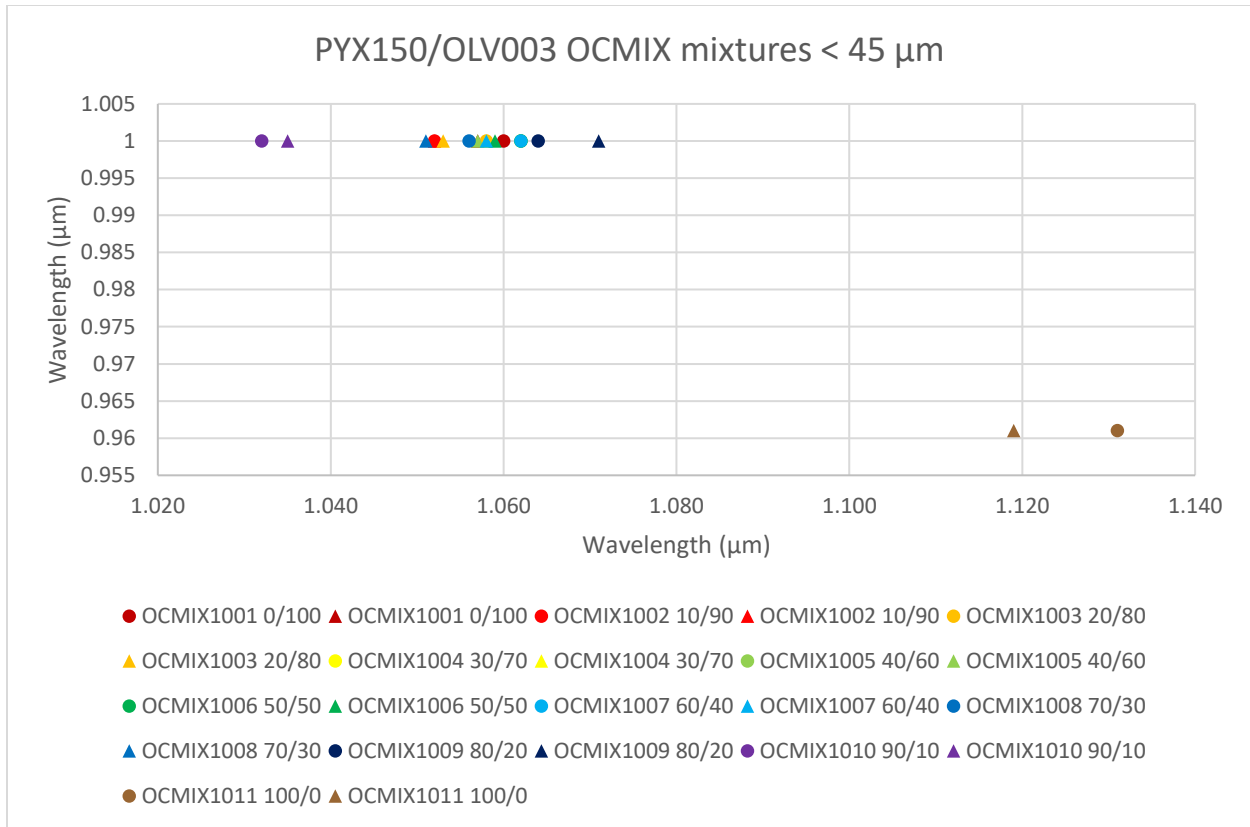
Figure 61. Minima comparisons for the OCMIX mixture spectra of PYX150 and OLV003. The circles are the minima I originally found while the triangles are the minima I found using polynomial fitting. The spectra with only one main feature are graphed against 1 µm. Sources: HOSERLab, McCraig et al. 2017.

There were many more mixtures of type B clinopyroxenes and orthopyroxenes. Two groups of mixtures, again from HOSERLab, used PYX005 and PYX023, which were a type B clinopyroxene and an orthopyroxene, respectively. The mixtures included sets of both < 45 and 90-180 µm grain sizes, with the first group measured in intervals of ten and the second group in intervals of twenty weight percent. The graphs of the spectra of these two groups are in figures 62 and 63. For figure 62, there was a steadier transition around the one micron feature than with the type A clinopyroxene-orthopyroxene mixtures, which was to be expected because these samples had more similar features. The spectra decreased in reflectance with increasing clinopyroxene, with more drastic decreases with the one micron feature since it was stronger; the two micron feature transitions were more complicated because their wavelength positions were

more spread apart. Once the mixture reached around 70/30 clinopyroxene/orthopyroxene, the

one micron feature became wider and appeared to be a mixture of the two different one micron

features. At 90/10 the one micron feature was asymmetrical but much closer to the minimum for

the clinopyroxene feature. The two micron feature area for these mixtures was more

complicated, in part because of a water feature around 1.9 µm. Still, the two micron feature

decreased in strength when getting more clinopyroxene-rich. Around 40/60, the two micron

feature did appear to start moving to longer wavelengths, although it varied, likely due to the

issue with the water features.  Around 60/40 and 70/30 there started to be the appearance of two

2 µm features. At around 80/20, there was only the clinopyroxene two micron feature that was

truly discernible and it did not move much in position after that. There were faint dips around

0.51 and 0.75 µm in the orthopyroxene that appeared to get fainter and then disappear with

increasing clinopyroxene, mainly disappearing by 30/70. The water features at 1.4, 1.9, and 2.3

µm in the orthopyroxene also got fainter with increasing clinopyroxene, but that was likely due

to the specific samples. A faint dip around 0.49 µm in the clinopyroxene got even fainter with an

increase in orthopyroxene as well. Most of these results were similar to the larger grain size

mixtures in figure 63, although the water features were stronger. There were faint double two

micron features in the 60/40 and 80/20 spectra and the one micron feature in the 80/20 spectrum

was not as wide. These spectra also generally decreased in reflectance with increasing

clinopyroxene, although the 80/20 spectrum had a shallower two micron feature than in 60/40. It

was harder to discern these and other changes due to the larger intervals of 20 % instead of 10 %.

The 90-180 µm spectra mixtures were all at lower reflectances than the < 45 µm mixtures.
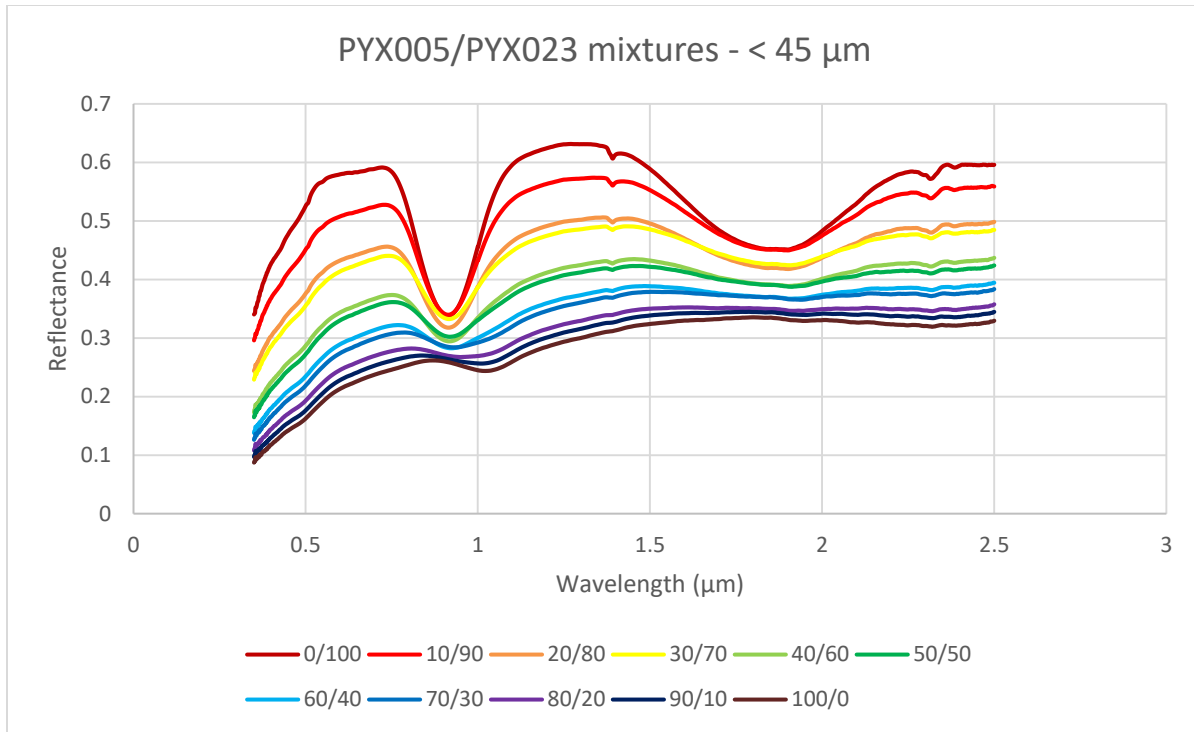
Figure 62. Type B clinopyroxene (PYX005) and orthopyroxene (PYX023) mixtures at < 45 µm grain size. Source: HOSERLab.
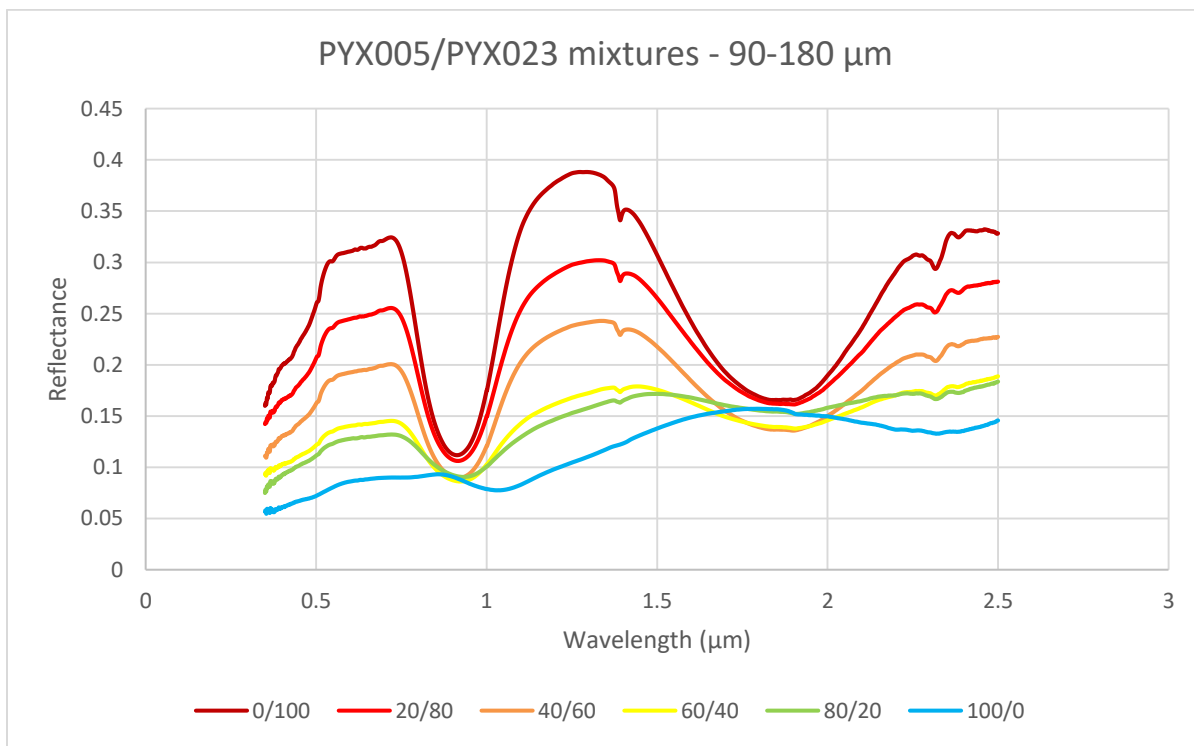


Figure 63. Type B clinopyroxene (PYX005) and orthopyroxene (PYX023) mixtures at 90-180 µm grain size. Source: HOSERLab.

138
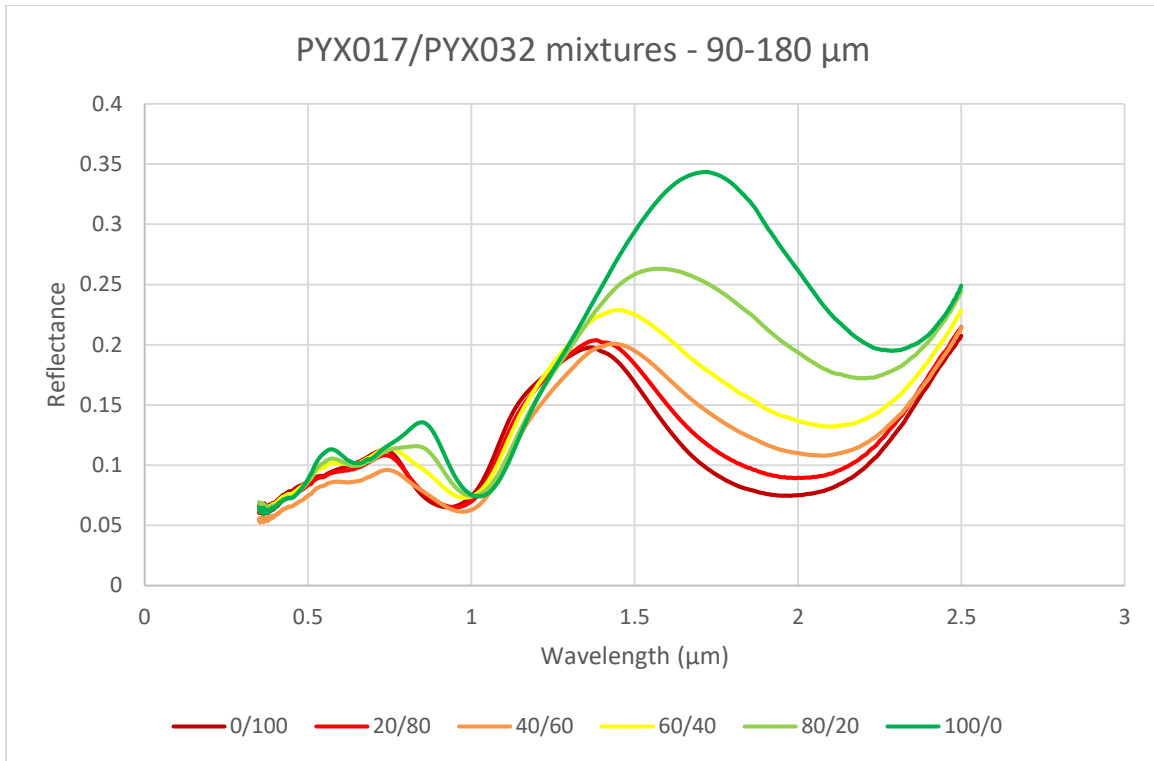
Figure 64. Type B clinopyroxene (PYX017) and orthopyroxene (PYX032) mixtures at 90-180 µm grain size. Source: HOSERLab.

Another type B clinopyroxene-orthopyroxene mixture from HOSERLab included PYX017 and PYX032. These spectra were measured in 20 % intervals at 90-180 µm grain sizes. The spectra are shown in figure 64. From 0/100 to 20/80 clinopyroxene/orthopyroxene there was almost no difference in the spectra until ~ 1.4 µm where the band positions moved to slightly longer wavelengths and higher reflectances. From then on the one and two micron features progressively moved to longer wavelengths. The hump around 1.4 µm went to slightly longer wavelengths and barely moved in reflectance from 0/100 to 40/60 but then after it started to drastically rise in reflectance until it was at 100/0. When it reached 80/20 it also jumped to around 1.6 µm and moved further still after that. For the shorter wavelength features around 0.6 µm in PYX017, these started to appear around 40/60. In PYX017 this may be predominantly

from chromium as it had more chromium than PYX032. The slope around 1.2 to 1.4 µm also increased as more clinopyroxene was added.

The PYX005 and PYX023 mixtures above had endmember compositions of $Wo_{49.1}En_{41}Fs_{9.9}$ and $Wo_{1.3}En_{89.3}Fs_{9.4}$, respectively, while PYX017 and PYX032 had $Wo_{44.4}En_{47.5}Fs_{8.1}$ and $Wo_{3.6}En_{54.9}Fs_{41.5}$. PYX017 had more ferric iron (1.25 vs 0.77 wt. %) and chromium (0.78 vs 0.17 wt. %) and less titanium (1.04 vs 1.48 wt. %) than PYX005. PYX023 had less aluminum (0.76 vs 1.24 wt. %), ferric iron (0.83 vs 5.11 wt. %), and manganese (0.17 vs 0.53 wt. %) and more chromium (0.45 vs 0.04 wt. %) than PYX032, in addition to the huge iron and magnesium disparities shown above. So from this, PYX005 and PYX023 had similar iron contents, while PYX017 and PYX032 did not.

For the polynomial fitted minima for the PYX005 and PYX023 < 45 µm mixtures, there were similar minima to the lowest reflectance minima. Both had the one micron features steadily decreasing with increasing orthopyroxene. The largest decreases went until 50/50 and from then on there were smaller decreases. The ~ 2.3 µm features in the polynomial fitted minima hovered around the same from 100/0 clinopyroxene/orthopyroxene to 80/20 when they started to generally decrease from 80/20 to 70/30. After that they could not be fitted and were too weak. For the lowest reflectance minima, the same feature stayed around the same point until 60/40, possibly because of the water features interfering. For both sets, the ~ 1.9 µm features mostly decreased from 70/30 to 30/70, after which they hovered around the same position. At PMIX1103, when the mixture was 80/20, the 2 µm feature was very weak and noisy, which caused two inflection points to show up and a low $R^2$ value. This was likely because of the two faint ~ 2 µm features from the different pyroxenes that were slightly separated, as well as some possible water interference. The combination of the two gave a polynomial fitted minimum of

2.043, but I was able to separate them with polynomial fitting with decent $R^2$ values for both features. The ~ 2.3 µm feature got even weaker from there and had poor $R^2$ values as PYX023 was added until 60/40, when I was unable to fit that feature anymore. There were no other issues with fitting this group of mixture spectra. There were no differences in the original minima and polynomial fitted minima that were greater than 5 nm for the one micron features. For the two micron features, all but one had differences greater than 5 nm: PMIX1101 at -14 nm, PMIX1102 at -9 nm, PMIX1104 at 14 nm, PMIX1106 at 10 nm, PMIX1107 at 9 nm, PMIX1108 at -35 nm, PMIX1109 at -45 nm, PMIX1110 at -22 nm, and PMIX1111 at -29 nm. The two samples that had other features were both under 2 nm in differences. The comparisons of the minima are in figure 65.

The PMIX spectra of these same samples at 90-180 µm grain sizes were in 20 weight percent intervals so I was unable to distinguish between the two 2 µm features. Therefore, the 2 µm features for both the lowest reflectance and the polynomial fitted minima decreased until around 60/40 clinopyroxene/orthopyroxene, stayed around the same for the next two mixtures, and then decreased again for the 0/100 mixture spectrum. The one micron feature for both sets decreased with increasing orthopyroxene, which was similar to the < 45 µm mixtures. As before, none of the one micron features had minima differences greater than 5 nm. All but one of the two micron minima had differences greater than 5 nm: PMIX2101 at -12 nm, PMIX2102 at 10 nm, PMIX2103 at 12 nm, PMIX2104 at 27 nm, and PMIX2105 at 27 nm. These minima comparisons are graphed in figure 66.

The PYX017 and PYX032 mixture group had no problems with the polynomial fitted minima. Despite the somewhat varying 2 µm minima because of the combination of the two features and the water features, both sets steadily decreased in wavelength with increasing

orthopyroxene. The one micron minima were more similar and both sets of minima steadily

decreased as well. None of the one micron feature minima differences were greater than 5 nm.

The spectra with two micron feature minima differences of greater than 5 nm were PMIX2002 at

6 nm, PMIX2004 at 14 nm, PMIX2005 at -9 nm, and PMIX2006 at 6 nm. The results are in

figure 67.
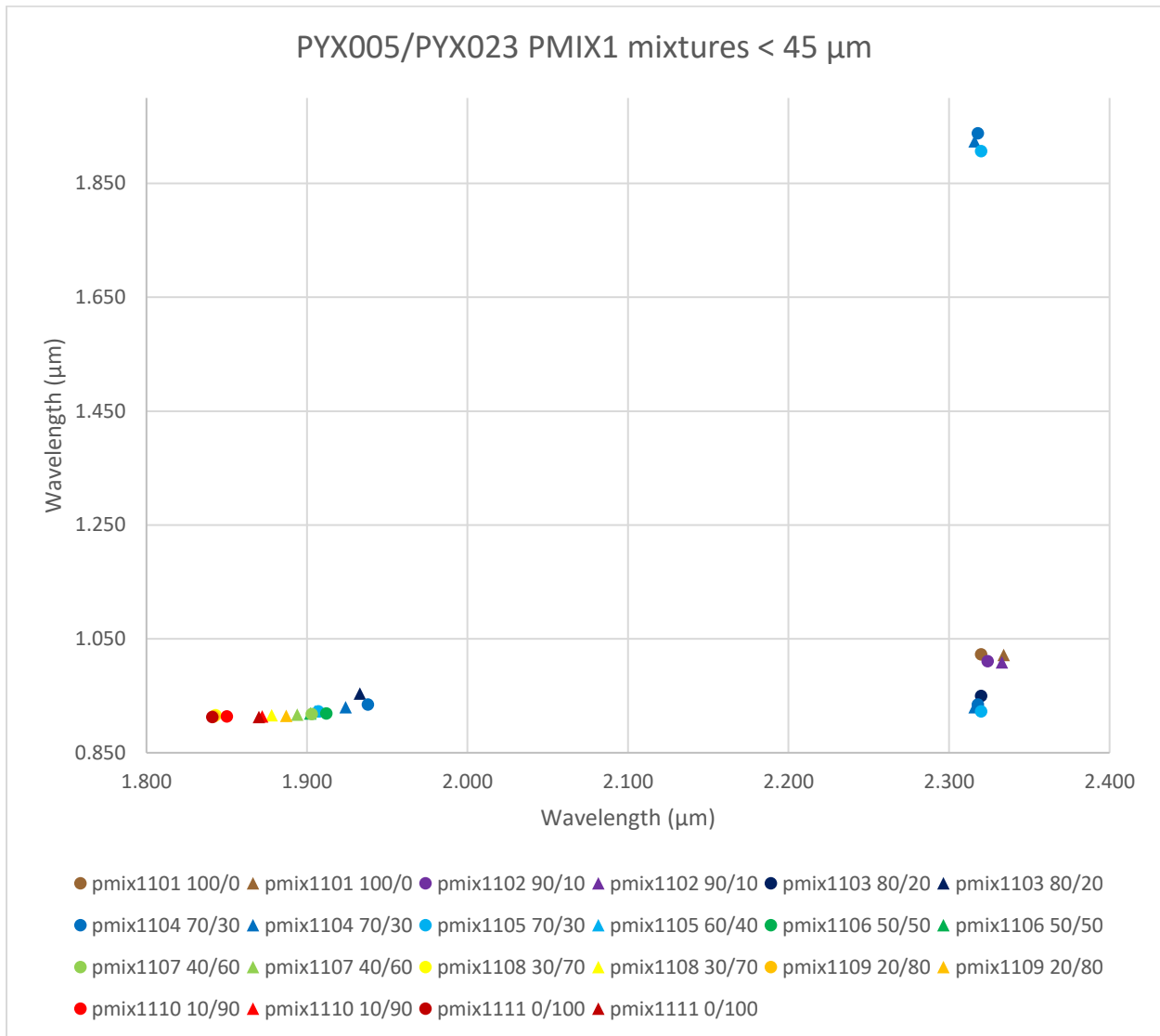


Figure 65. Minima comparisons for the PMIX1 mixture spectra of PYX005 and PYX023. The circles are the minima I originally
found while the triangles are the minima I found using polynomial fitting. Sources: HOSERLab, McCraig et al. 2017.
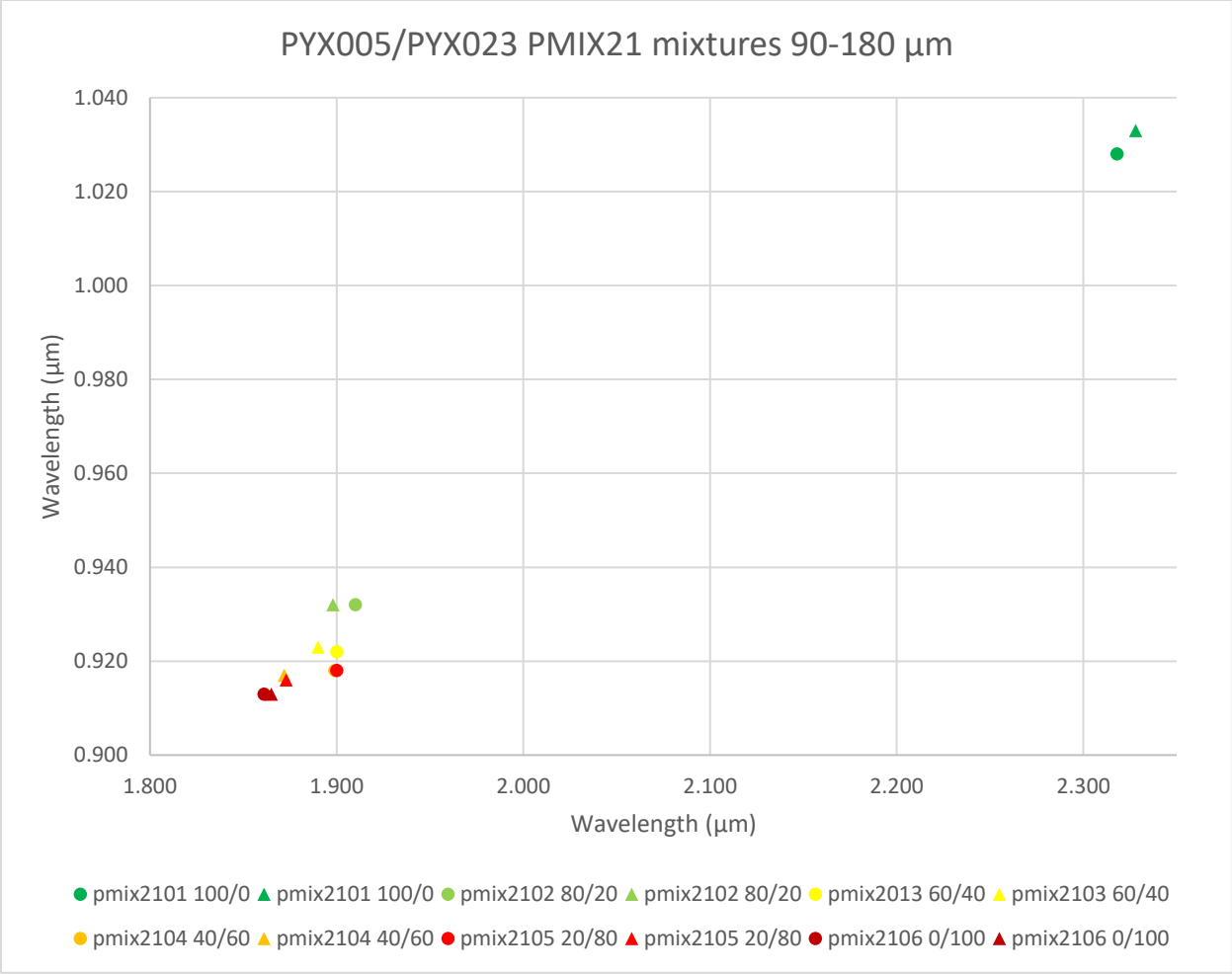
Figure 66. Minima comparisons for the PMIX21 mixture spectra of PYX005 and PYX023. The circles are the minima I originally found while the triangles are the minima I found using polynomial fitting. Sources: HOSERLab, McCraig et al. 2017.

143
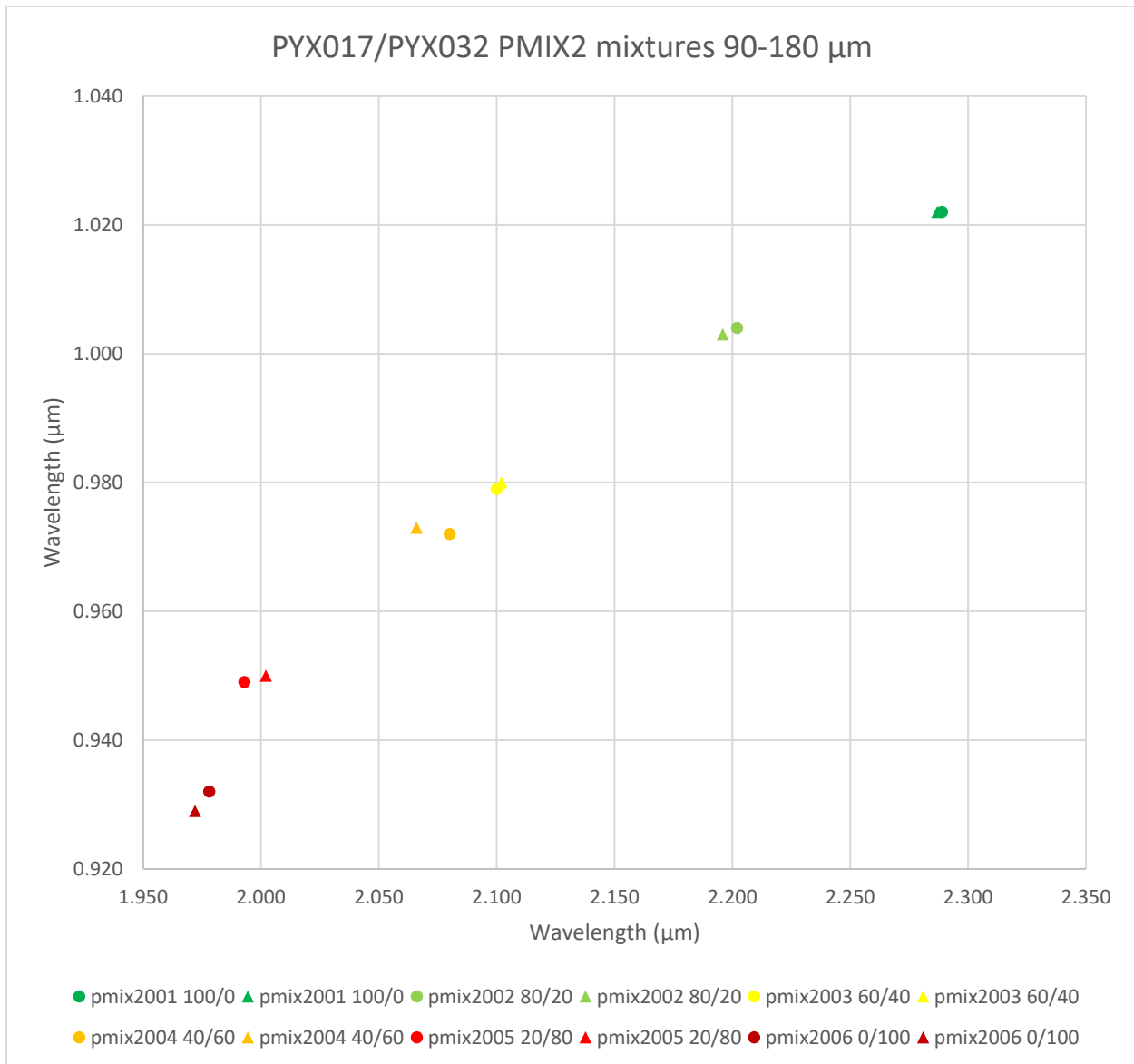
Figure 67. Minima comparisons for the PMIX2 mixture spectra of PYX017 and PYX032. The circles are the minima I originally found while the triangles are the minima I found using polynomial fitting. Sources: HOSERLab, McCraig et al. 2017.

There was a group of type B clinopyroxene and orthopyroxene mixtures from Sunshine & Pieters 1993, RELAB, and HOSERLab. These groups used the type B clinopyroxene PP-CMP-021 and the orthopyroxene PE-CMP-030. These had two spectra each for < 45, 45-75, and 75-125 µm grain sizes and 75/25 and 60/40 ratios of type B clinopyroxene to orthopyroxene. Their info and band positions are in the appendices below, in table 6. The 1 µm feature from c1xp14, which had 75/25 at < 45 µm grain sizes, had a zero-crossing that was slightly below the

x-axis, although the $R^2$ value and inflection point graph were fine. There was an attempt to get the first ~ 2 µm feature that was from the orthopyroxene, but it was weak, had multiple inflection points on the graph, had a poor $R^2$ value, and the zero-crossing point was far above the x-axis. I was unable to get this same feature in c1xp24, which was the same mixture as c1xp14 but at 45-75 µm grain sizes. The 1 µm feature for this spectrum had a zero-crossing point that was a little above the x-axis, but no other issues. I was unable to get the first 2 µm feature from c1xp05 as well, which was the 75/25 mixtures at 75-125 µm grain sizes. The 1 µm feature also had a zero-crossing point that was a little off the x-axis but had no other concerns. The other three mixtures were 60/40 clinopyroxene/orthopyroxene. The 1 µm feature for c1xp12, which included < 45 µm grain sizes, had a zero-point crossing that was slightly off the x-axis but no other problems. The feature around 2.3 µm had the same issue but with a lower yet still decent $R^2$ value. The c1xp22 spectrum, which had 45-75 µm grain sizes, did not have a strong enough feature at ~ 2.3 µm to fit. The spectrum of c1xp03 at 75-125 µm grain sizes had both the 1 and 2 µm features slightly off the x-axis in their zero-crossing graphs but everything else was fine. For all of these groups, none had any one micron feature minima differences greater than 5 nm. For the two micron features, the spectra with greater than 5 nm differences were c1xp14 at 20 nm, c1xp12 at 15 nm, and c1xp03 at 10 nm. The one that had an extra feature, c1xp12, had a difference of -15 nm. These minima are compared in figure 68.
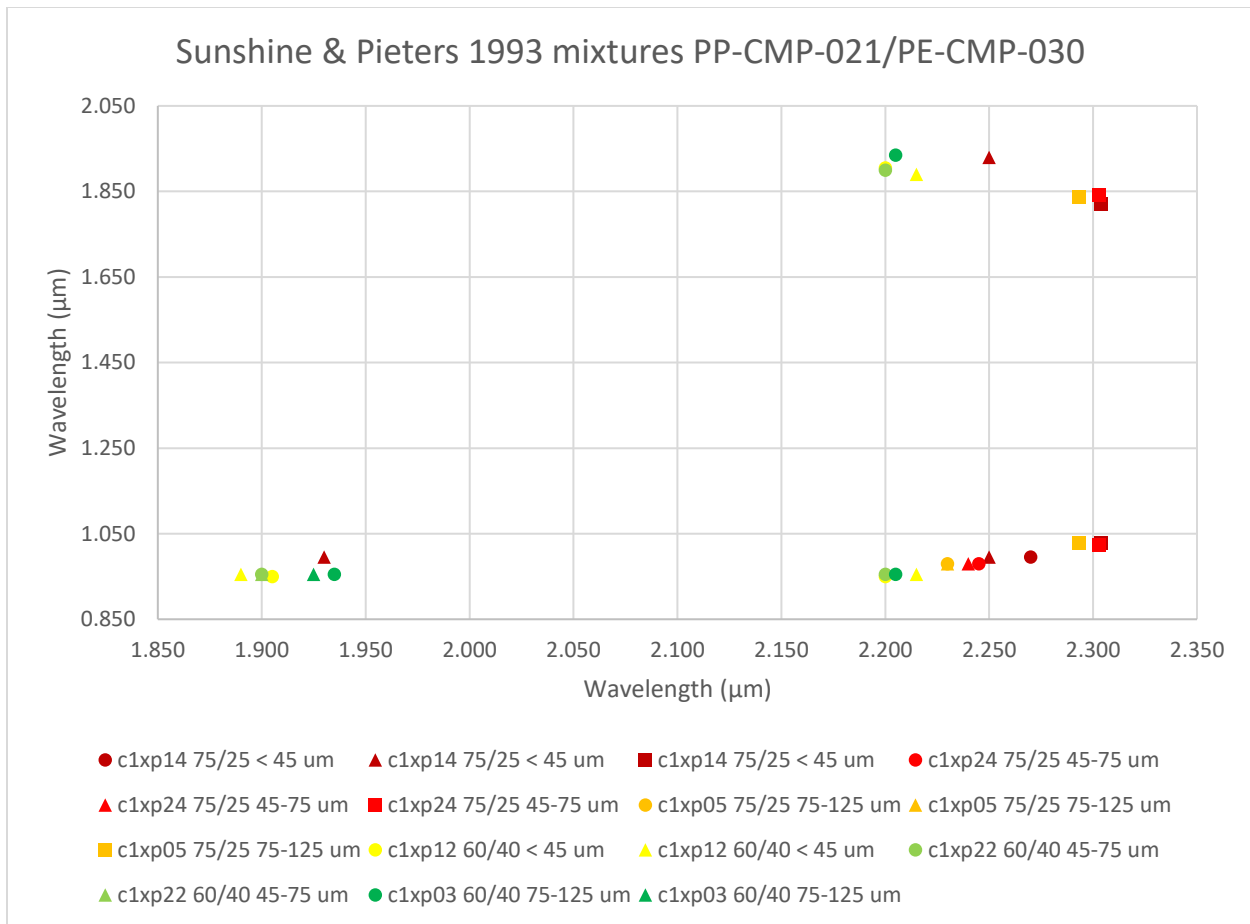
Figure 68. Minima comparisons for the c1xp mixture spectra of PE-CMP-030 and PP-CMP-021. The circles are the minima I originally found, the triangles are the minima I found using polynomial fitting, and the squares are centers found in the literature (Sunshine & Pieters 1993). Sources: HOSERLab, RELAB, Sunshine & Pieters 1993, McCraig et al. 2017.

There was one mixture in HOSERLab that used a type B clinopyroxene and an olivine, PYX016 and OLV003. OLV003 was used in a mixture with a type A clinopyroxene above as well. These were measured at < 45 µm grain sizes and the spectra were in 20 weight percent intervals. The graph of the spectra are in figure 69. Right away the olivine features were noticeable in most of the spectra, having the typical olivine shape until 80/20 of type B clinopyroxene to olivine. The features around one micron got fainter and increased in reflectance with increasing clinopyroxene. It was interesting that the one micron feature did not appear to actually move, as they were both around the same position. This could be in part because both samples had low amounts of iron, $Fs_{2.5}$ and $Fa_{9.6}$. The one micron feature did however also get

narrower with increasing clinopyroxene, which corresponded to results from Singer (1981). The feature around 0.75 µm in the clinopyroxene sample only really started to appear around 80/20 as well. The olivine did not have any similar shorter wavelength features in that region. The 2 µm feature in the clinopyroxene started to appear at 20/80 and continued to deepen as more clinopyroxene was added, although the biggest jump to lower reflectances was from 0/100 to 20/80. There were decreases in reflectance at the two micron feature with increasing clinopyroxene, unlike the one micron feature area mentioned above.

The comparisons of the minima are graphed in figure 70. Both the lowest reflectance and polynomial fitted one micron feature minima stayed around the same position, as did the two micron feature lowest reflectance minima. However, the polynomial fitted two micron minima decreased with increasing clinopyroxene until it was 100 % clinopyroxene, where it increased again. The < 45 µm MIX mixtures of the type B clinopyroxene PYX016 and the olivine OLV003 had no fitting concerns even with the noisier 2 µm features from PYX016. None of the one micron features had minima differences greater than 1 nm, while the two micron features all did: PYX016 at -31 nm, MIX031 at -51 nm, MIX032 at -42 nm, MIX033 at -33 nm, and MIX034 at -19 nm.
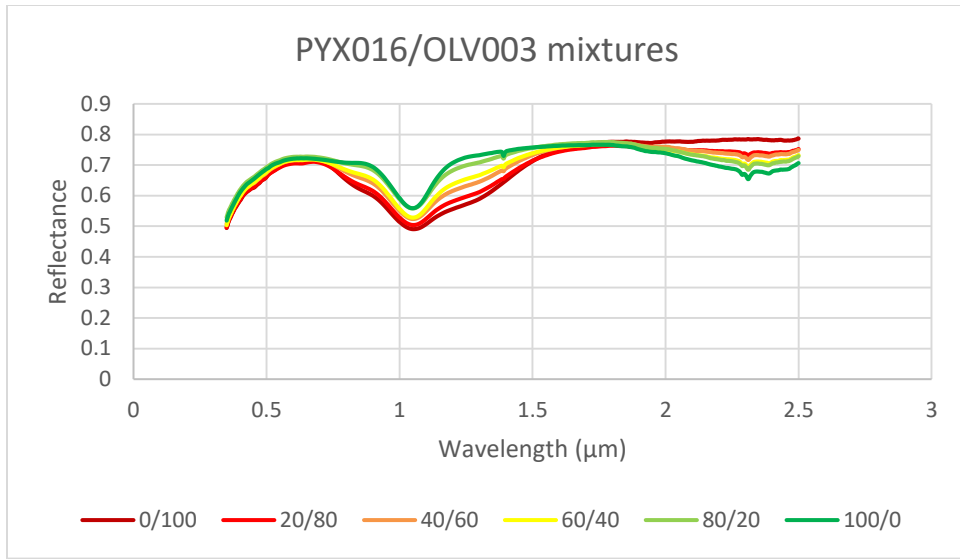
Figure 69. Type B clinopyroxene PYX016 and olivine OLV003 mixture spectra. Source: HOSERLab.
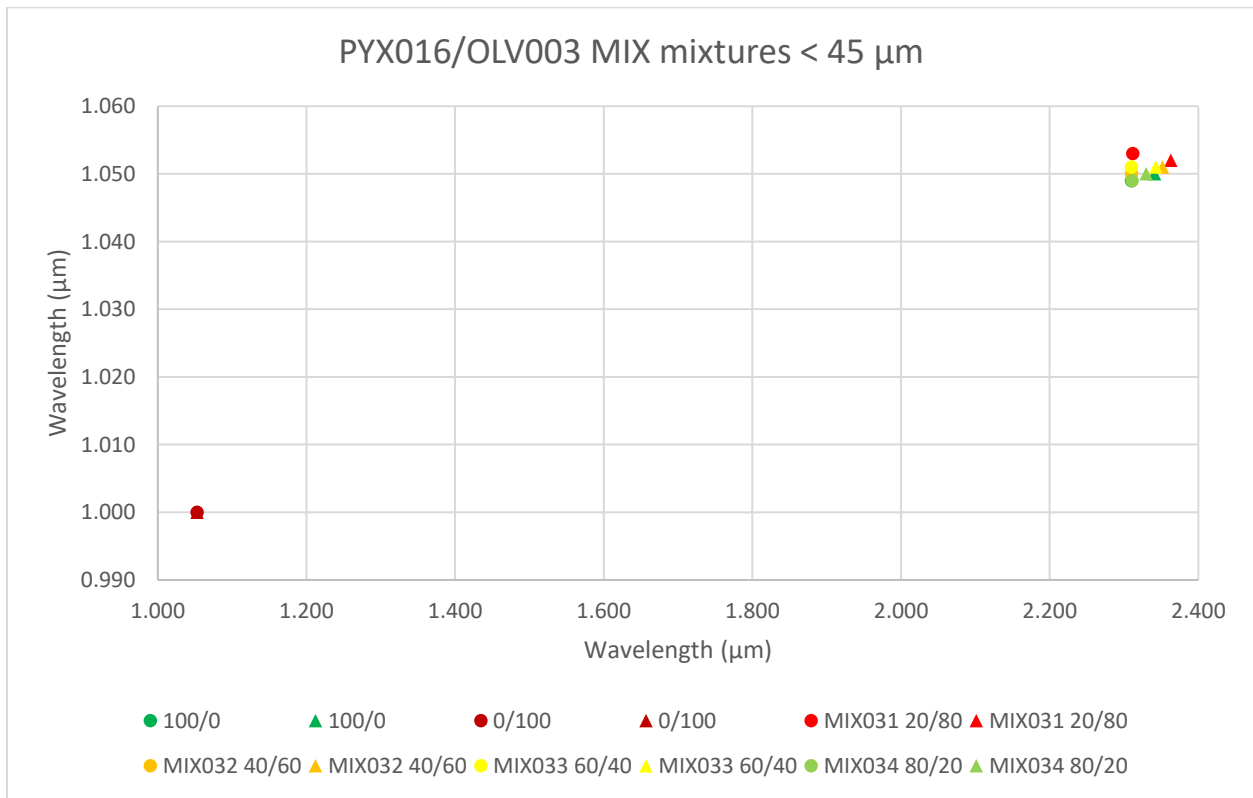


Figure 70. Minima comparisons for the PMIX mixture spectra of PYX016 and OLV003. The circles are the minima I originally found while the triangles are the minima I found using polynomial fitting. The spectra that only had one feature are graphed against 1 µm. Sources: HOSERLab, McCraig et al. 2017.

148

There was a large group of mixtures from AG-TJM in RELAB that included orthopyroxene, type B clinopyroxene, plagioclase, and olivine. The olivine was $Fo_{90}$, the orthopyroxene was a hypersthene, the clinopyroxene was an augite, and the plagioclase was a labradorite, a calcic-sodic feldspar. Their chemical analyses are in table 10 in the appendices. The individual samples were measured at < 45 µm while the mixtures are measured at < 38 µm grain sizes and at various intervals. Since there were so many mixtures, I have broken them down into several groups: orthopyroxene-clinopyroxene, orthopyroxene-olivine, olivine-orthopyroxene-clinopyroxene, plagioclase-orthopyroxene-clinopyroxene, and all four mixtures. I started with the olivine-orthopyroxenes since they were not the main focus of this paper. The spectra for these mixtures are in figure 71. In these mixtures, the orthopyroxene sample dominated the mixtures starting at 70/30 olivine/orthopyroxene. The one micron features for the individual spectra were vastly different, as there was a large jump from 90/10 to 70/30, where once at 70/30 the one micron feature did not move much with increasing orthopyroxene. Even at 90/10 the one micron feature has moved to shorter wavelengths than the 100/0 and the shorter wavelength side lobe of olivine and the center feature have been distorted. At 70/30 the 1 µm feature was also distorted but with the 1.3 µm olivine feature still visible. The shorter wavelength side lobe of olivine has basically disappeared. From thereon, the spectra did not change much besides decreasing in reflectance. The biggest decreases in reflectance for both main pyroxene features were from 90/10 to 70/30.
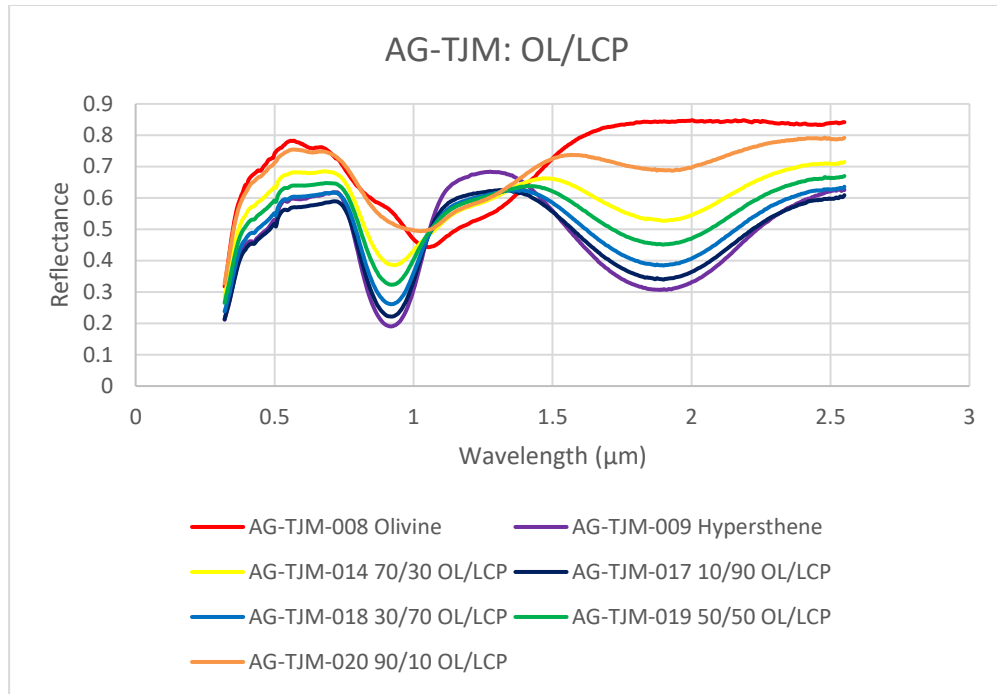
Figure 71. Olivine and orthopyroxene mixtures from AG-TJM. Source: RELAB.

The next group was the orthopyroxene-clinopyroxene mixtures, which are in figure 72. There were very few mixtures of just these two so the only main observations were that the two micron feature drastically moved to longer wavelengths with increasing clinopyroxene after 50/50 orthopyroxene to clinopyroxene. It moved only slightly towards longer wavelengths from 85/15 to 50/50. The one micron feature got less deep with increasing clinopyroxene and also only really moved to longer wavelengths after 50/50.
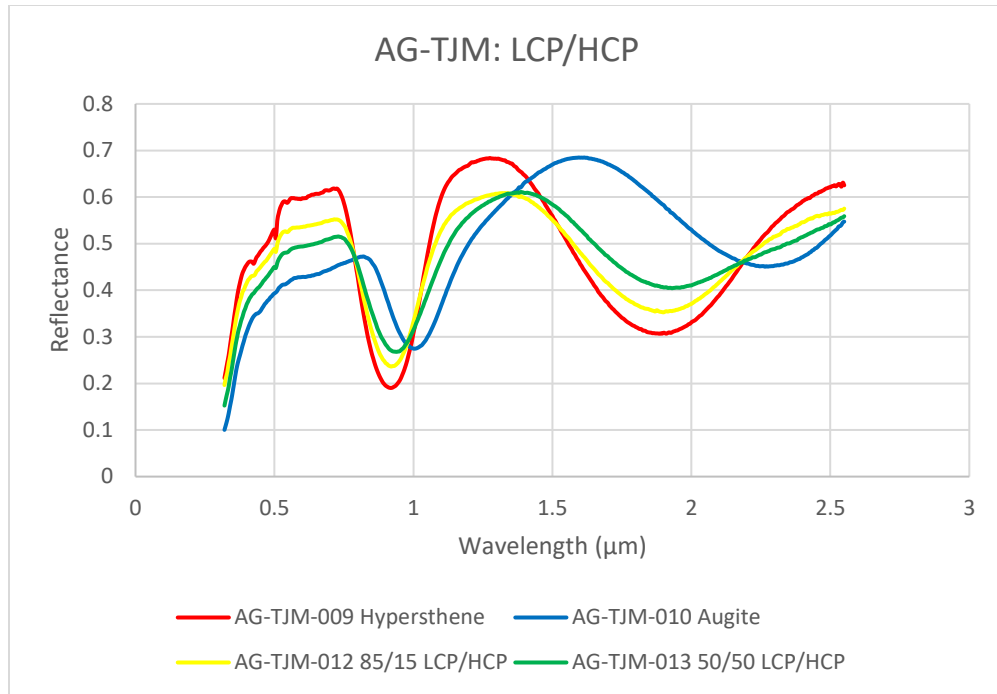
Figure 72. Orthopyroxene-type B clinopyroxene mixtures from AG-TJM. Source: RELAB.

The third group was of olivine-orthopyroxene-clinopyroxene mixtures that are in figure 73. Since that graph was fairly messy, I broke it down into two groups, with lower and higher amounts of clinopyroxene, in figures 74 and 75. Again, to try to make it easier to view, especially with three changing variables now, I have colored the spectra in order of rainbow colors, starting with olivine as red to clinopyroxene as black. In figure 74 the pure augite sample stood out, since these mixtures only used small amounts of clinopyroxene. In comparison, the pure orthopyroxene sample fit in with the other mixtures, even though the amount of orthopyroxene goes only up to 68 %. From 100/0/0 to 80/17/3 the main one micron feature for olivine went to shorter wavelengths and became distorted with the pyroxene features, mainly from the orthopyroxene. The shorter wavelength sidelobe of olivine was gone but the longer wavelength sidelobe was still there and only started to fade at 50/42.5/7.5. The pyroxene two micron feature was predominantly from the orthopyroxene sample, as there was much more of it.

151

At 80/17/3, the two micron feature was almost at the position for the orthopyroxene sample; with increasing orthopyroxene and decreasing olivine the two micron feature moved to shorter wavelengths and got deeper, going to lower reflectances. The one micron feature also went to lower reflectances with decreasing olivine and increasing orthopyroxene. The clinopyroxene, being at such low amounts, did not appear to affect the spectra as much, although past 2.3 µm the slope started to flatten out more, unlike the more concave shape with the pure orthopyroxene. In figure 75 this was more apparent, as there was more clinopyroxene in the mixtures. The addition of a faint second 2 µm feature from the clinopyroxene was likely the cause of this. This could be seen the most in 20/40/40, which was also the mixture with the most amount of clinopyroxene and least amount of olivine. This was also the mixture spectrum with the most orthopyroxene, which may explain why the feature was so weak still, along with the decent amount of olivine. The two micron feature for the mixtures was shallower in figure 75 than in figure 74 as well. In addition, the 80/10/10 mixture was less asymmetrical than in figure 74, being rounder. The 1.3 µm olivine sidelobe feature also seemed to get fainter sooner than in figure 74, as it seemed to be get much fainter by 60/20/20 and 50/25/25. Other than these details, the results seemed similar for figure 74 and figure 75.
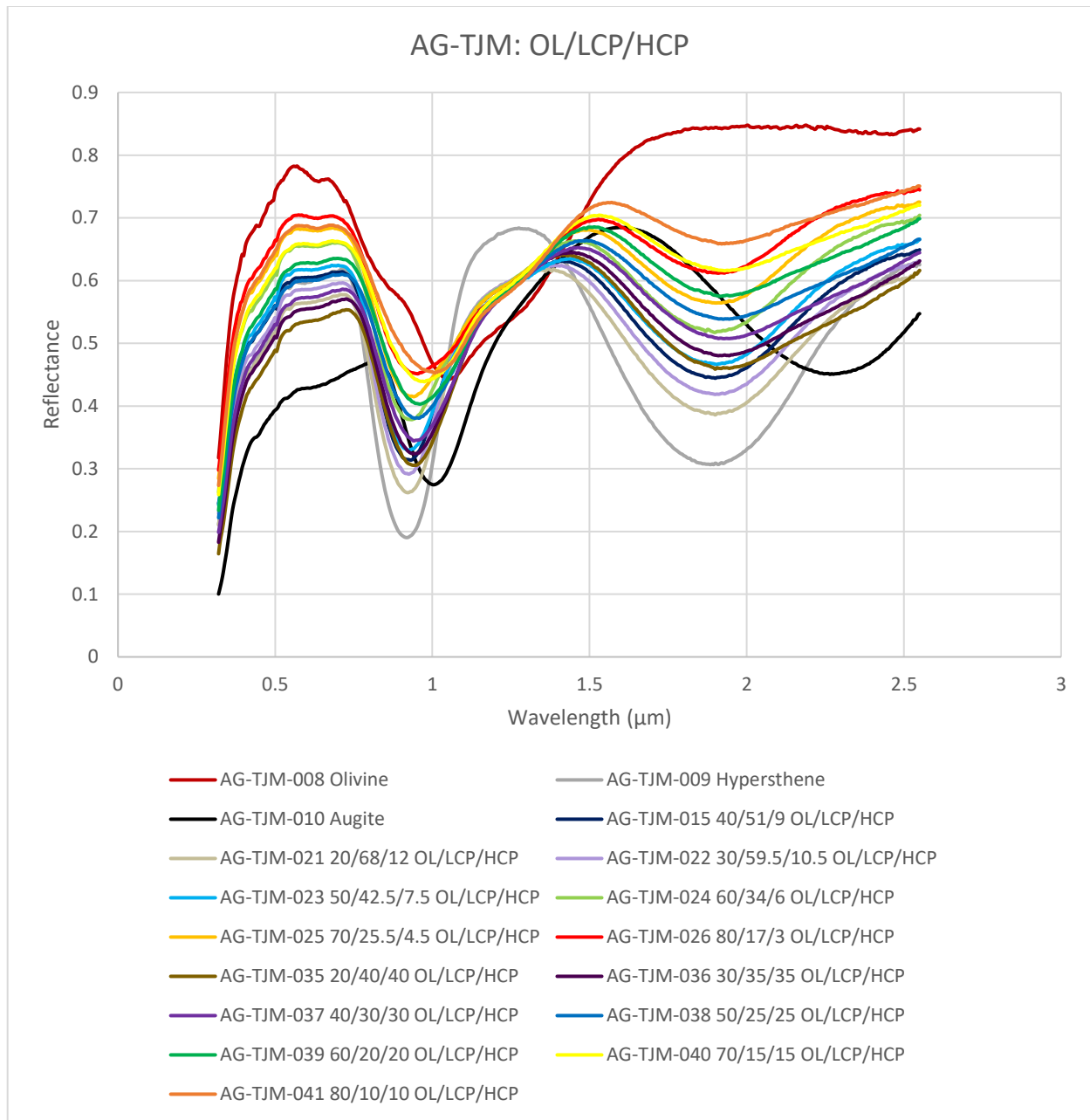
Figure 73. Olivine-orthopyroxene-clinopyroxene mixtures from AG-TJM. Source: RELAB.
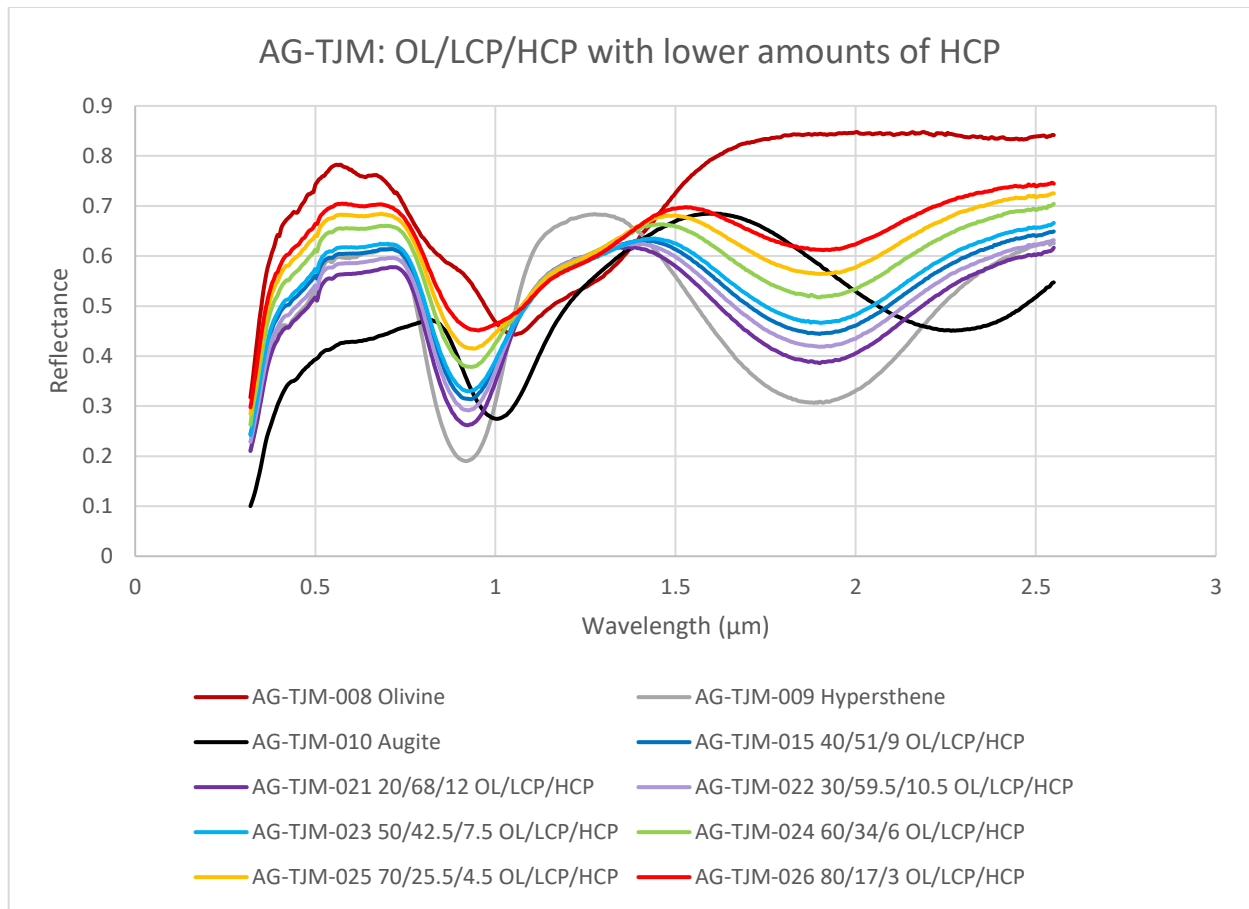
Figure 74. Same as figure 73 but mixtures with lower amounts of clinopyroxene only. Source: RELAB.
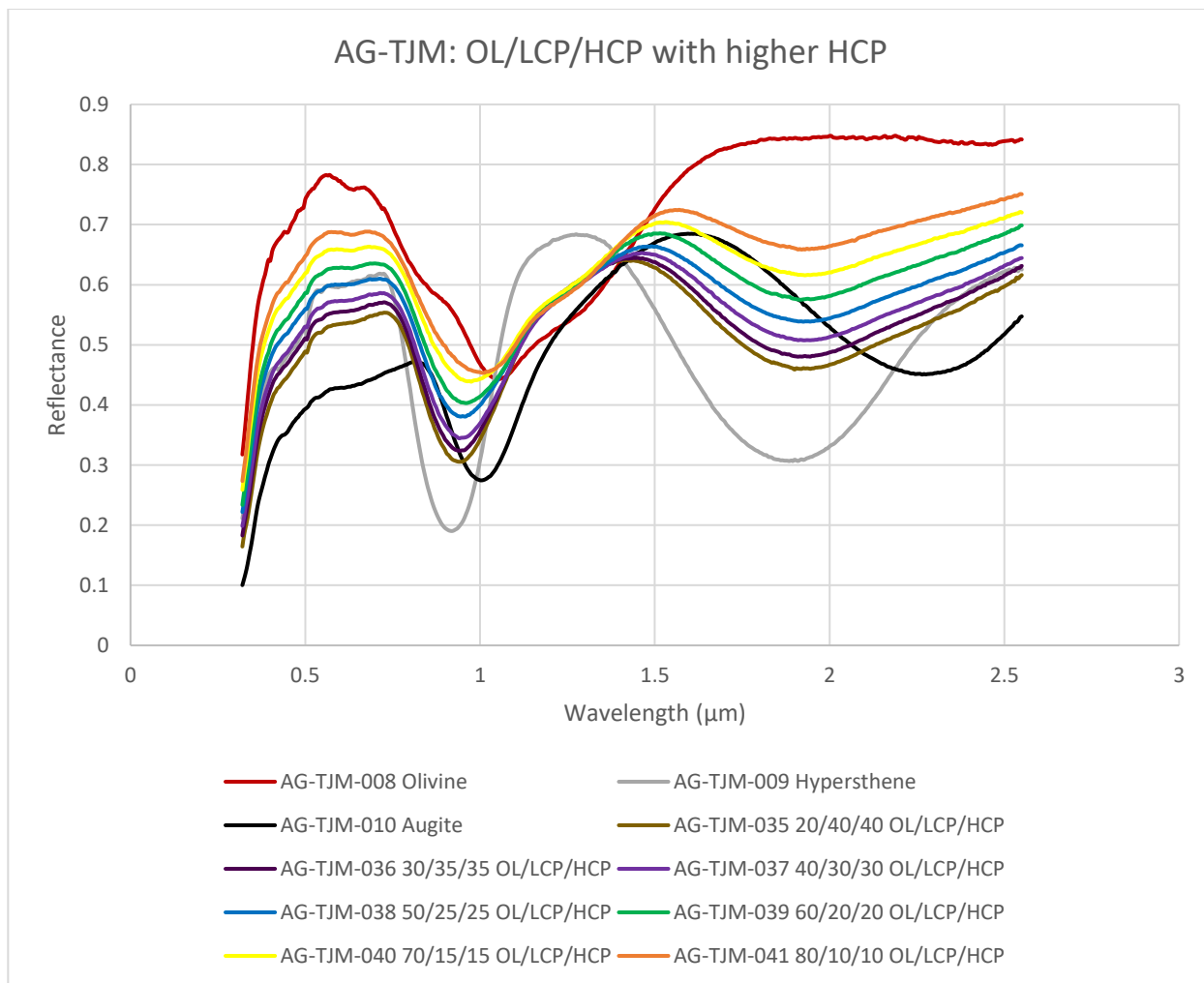
Figure 75. Same as figure 73 but with higher amounts of clinopyroxene only. Source: RELAB.

The next mixtures in this group used plagioclase, orthopyroxene, and type B clinopyroxene. As with the last group, there were many mixtures so I again broke it into lower and higher amounts of clinopyroxene. These graphs are in figures 76, 77, and 78 below. These appeared to be similar to the orthopyroxene-clinopyroxene mixtures because plagioclase only affects spectra weakly, as talked about in previous sections. With an increase in plagioclase in both, the spectra increased in reflectance, which was to be expected. The spectra resembled mainly orthopyroxene with the exception of the pure endmembers in figure 77, likely in part because of the lack of appreciable clinopyroxene in these spectra. The two main pyroxene

features also became shallower with an increase in plagioclase. The area from around 1.2-1.4 µm in figure 77 appeared to be flatter and similar to the pure orthopyroxene sample while the same region in figure 78 was more curved in the spectra with the higher amounts of clinopyroxene. The mixtures with higher amounts of clinopyroxene had the same faint straight slope after 2.3 µm as the olivine mixtures in figure 75, with no individual 2.3 µm clinopyroxene feature able to be resolved. There was also slight asymmetry in the one micron feature with higher amounts of plagioclase starting at 50/25/25 plagioclase/orthopyroxene/clinopyroxene.
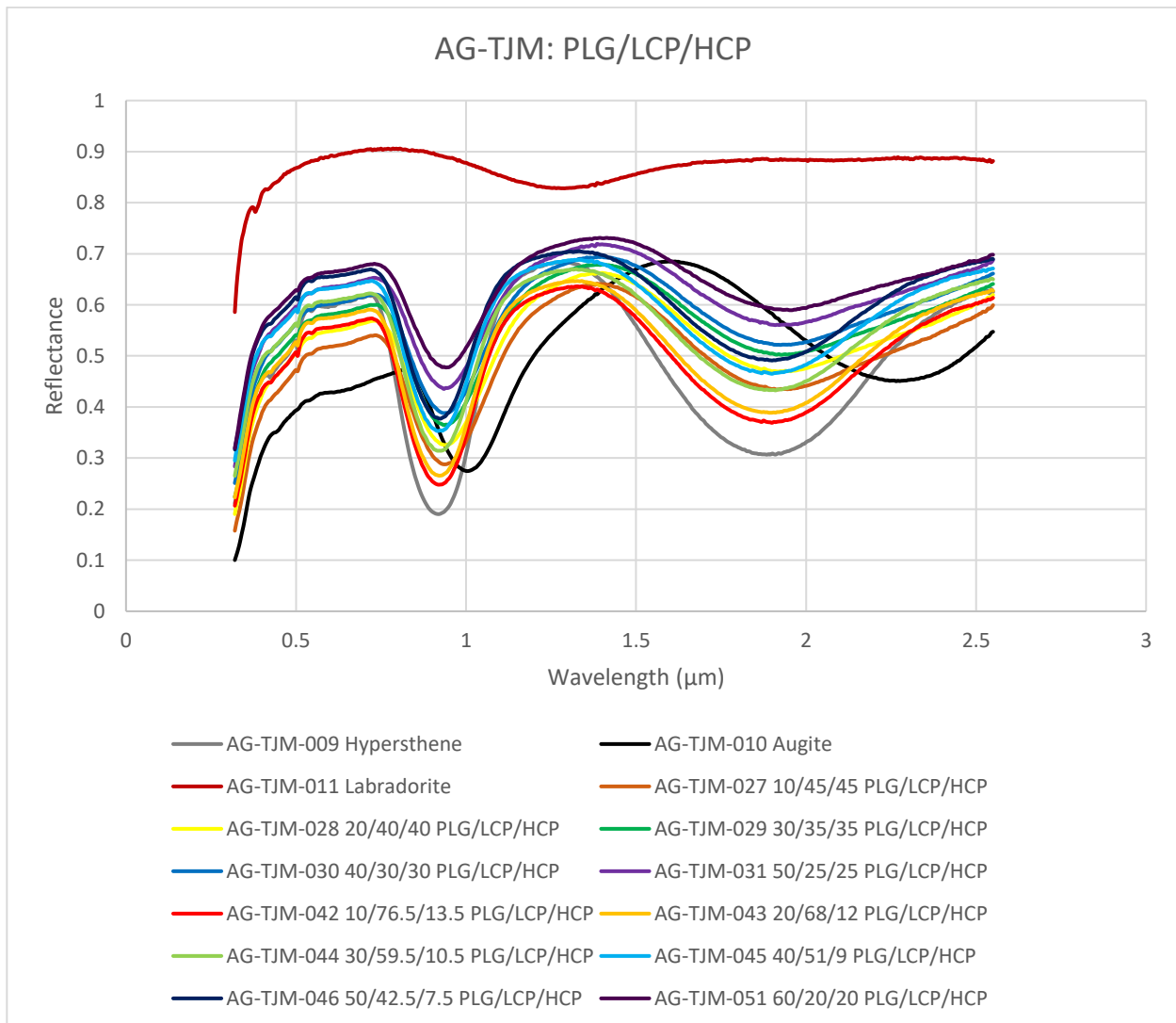


Figure 76. Plagioclase-orthopyroxene-clinopyroxene mixtures from AG-TJM. Source: RELAB.

156
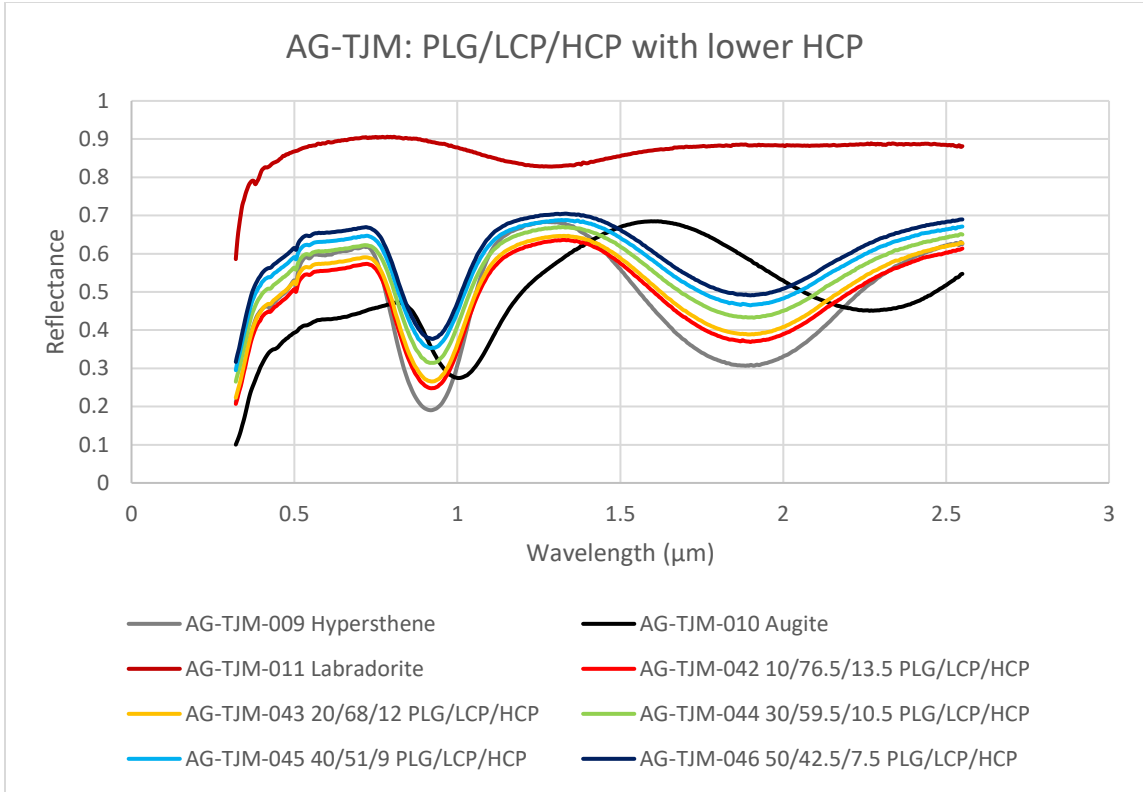
Figure 77. Same as figure 76 but with lower amounts of clinopyroxene only. Source: RELAB.
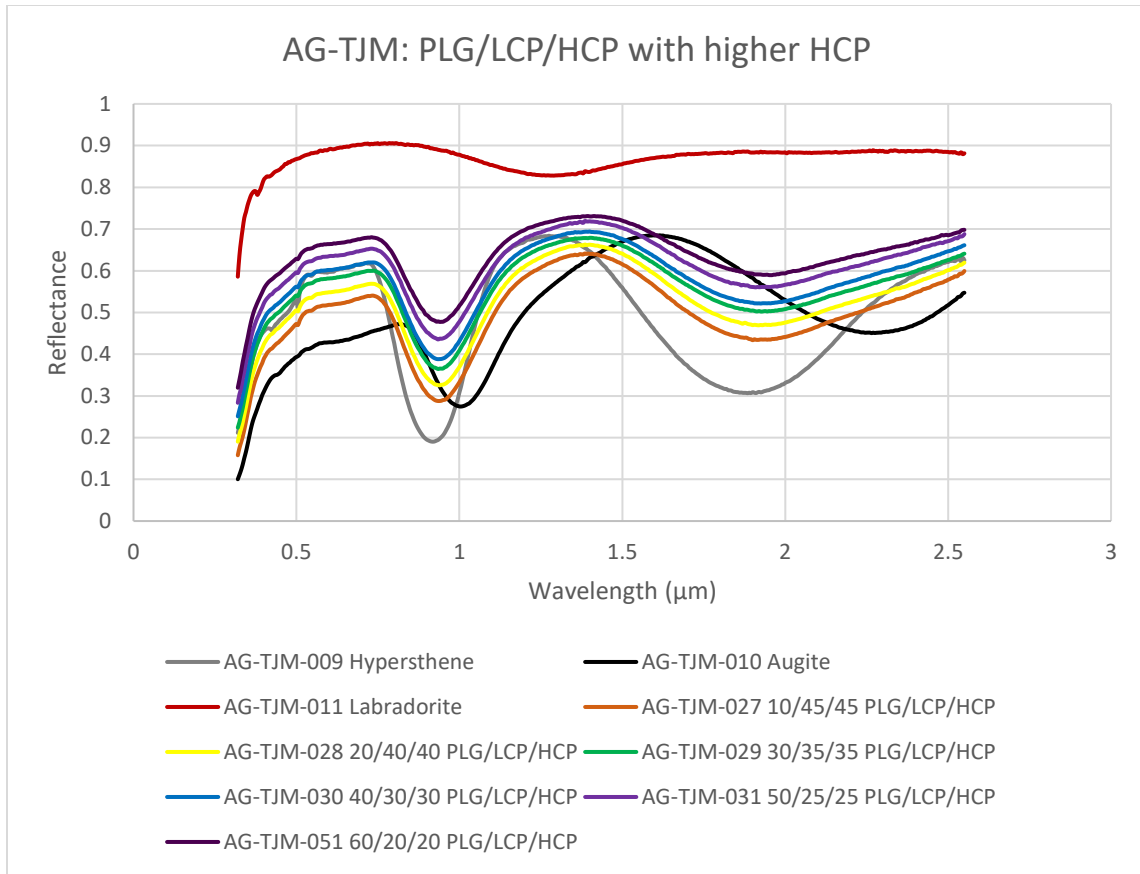
Figure 78. Same as figure 76 but with higher amounts of clinopyroxene only. Source: RELAB.

Finally, there were mixtures of all four minerals. Since there were four variables, I have

three graphs again to help distinguish the changes in figures 79, 80, and 81. One graph displays

them all, one has lower amounts of high-calcium clinopyroxene, and one has higher amounts of

clinopyroxene. The latter two were also graphed by increasing plagioclase, orthopyroxene, and

clinopyroxene for easier viewing, with again using rainbow colors starting with the most olivine.

None of these mixtures had high amounts of clinopyroxene, with the most being 10 %. In figure

80 the first spectra of pure olivine and then 90/5/4.25/0.75

olivine/plagioclase/orthopyroxene/clinopyroxene resembled olivine, with the latter having a two

micron pyroxene feature around 1.9 µm. After this mixture, the shorter wavelength olivine

sidelobe got too faint. The 1.3 µm sidelobe however was present in all of the mixtures because

the lowest amount of olivine was 60 %. The one micron feature was widened around

80/10/8.5/1.5 and after that became distorted, likely due to the larger amounts of orthopyroxene.

Even though plagioclase was increasing in the mixtures as olivine was decreasing, the mixture

spectra decreased in reflectance a little bit around the one micron feature and more so around the

two micron feature. This was possibly due to the larger amounts of orthopyroxene and olivine in

the mixture that overpowered the plagioclase. For both the one micron and two micron features

the positions moved to shorter wavelengths with decreasing olivine and increasing plagioclase,

orthopyroxene, and clinopyroxene, with orthopyroxene having the most influence. In comparison

to these results, in figure 81 the one micron feature of olivine and the pyroxenes did not move as

far to shorter wavelengths, possibly due to the higher impact from clinopyroxene. Instead the

feature got wider than and not as distorted as in figure 80. This was probably due to the

combination of the features around one micron, particularly olivine and clinopyroxene,

especially because these mixtures had less orthopyroxene as well. The two micron feature was

shallower and had a straight slope around 2.3 µm, both like in the mixtures with higher

clinopyroxene amounts above. While the orthopyroxene was at the same amount as

clinopyroxene it still had a stronger spectral signature and the two micron main feature was

strongest around 1.9 µm. The two micron feature lowered in reflectance with decreases in olivine

and increases in plagioclase, orthopyroxene, and clinopyroxene, while the one micron feature

increased in reflectance from 90/5/2.5/2.5 to 80/10/5/5, and then stayed near the same for

70/15/7.5/7.5 and then decreased again for 60/20/10/10. These mixtures are good examples of

the complex forces that can be at play by just adding a bit more clinopyroxene in addition to the

other three minerals.
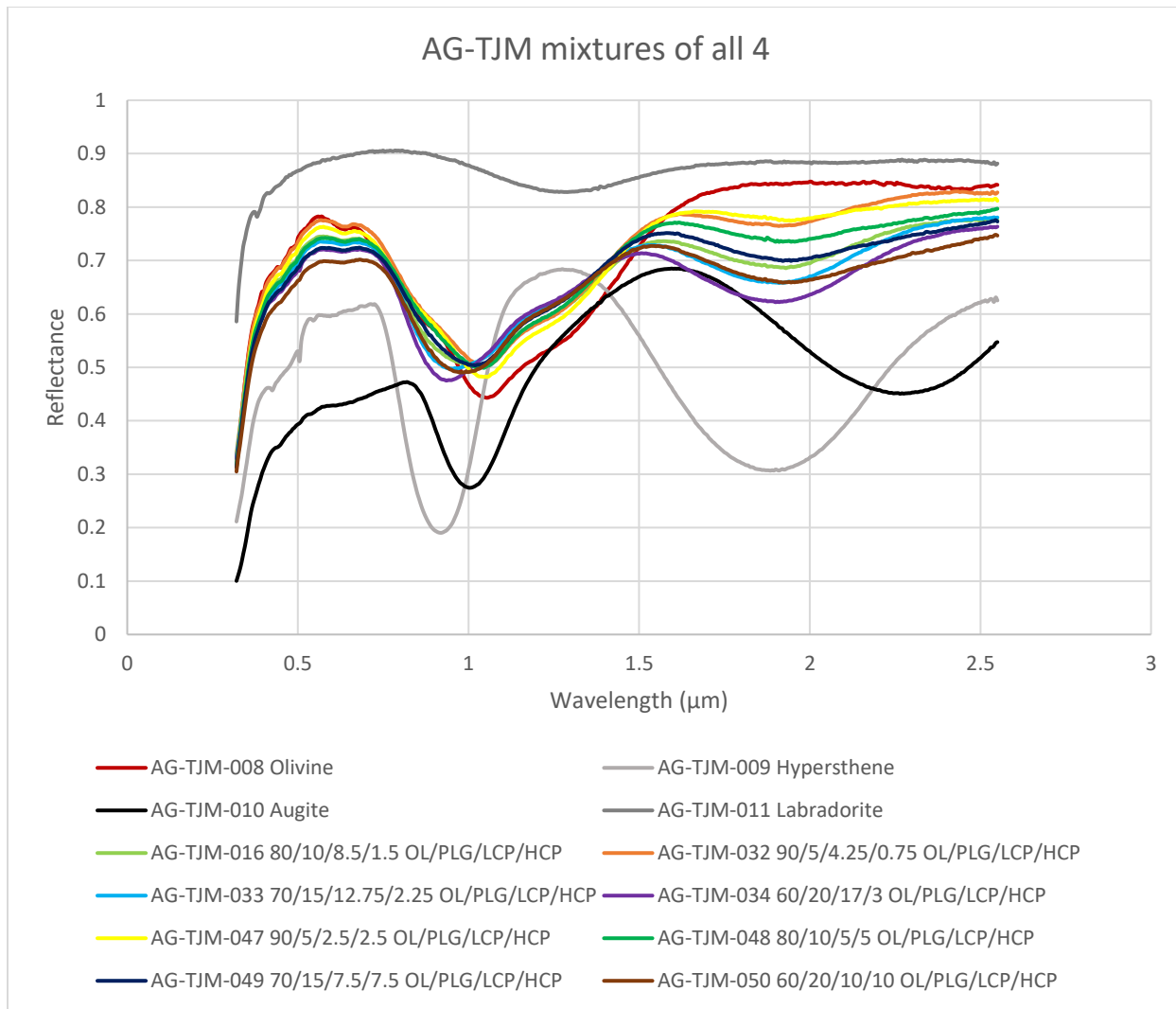
Figure 79. Olivine-plagioclase-orthopyroxene-clinopyroxene mixtures from AG-TJM. Source: RELAB.
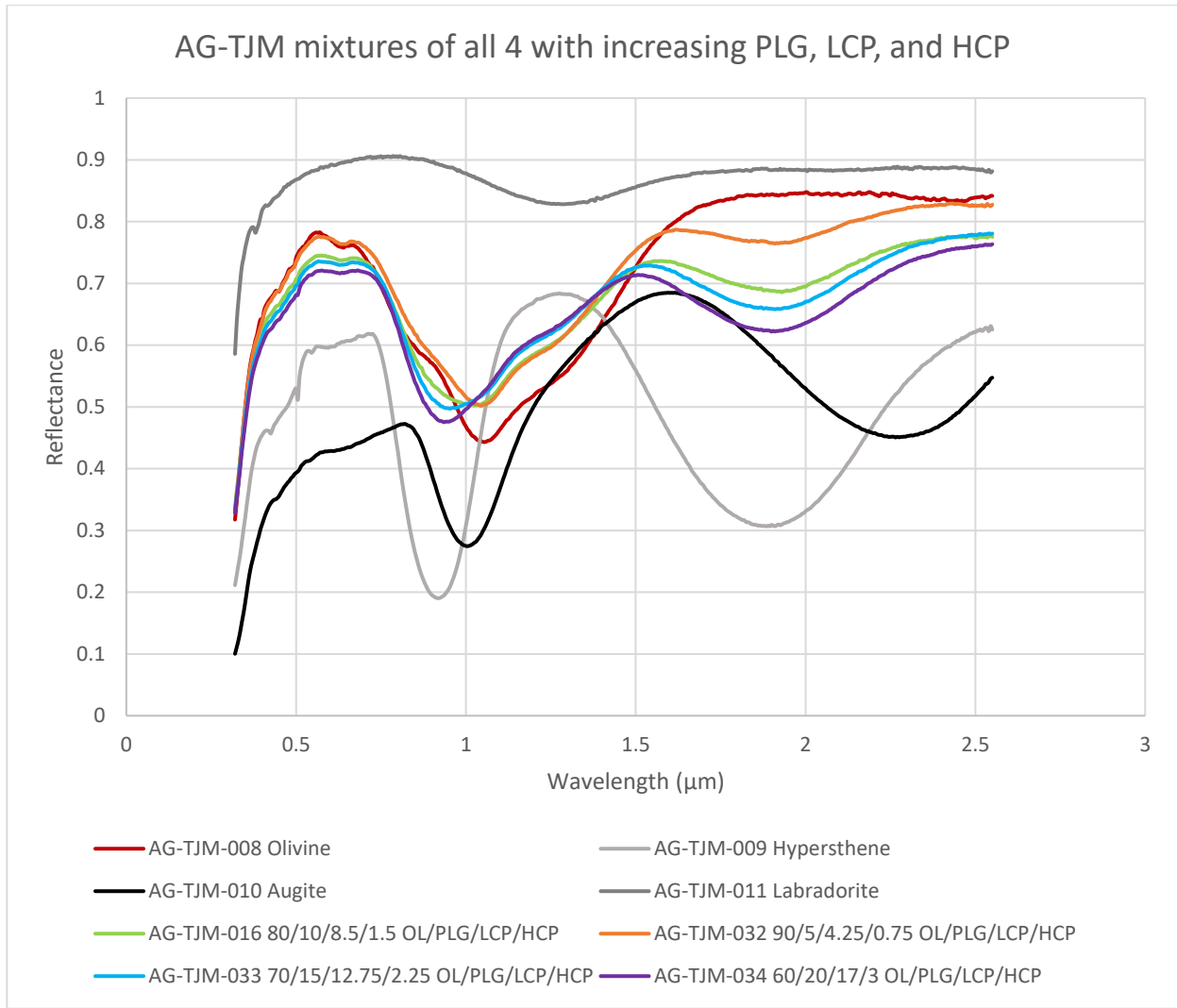
Figure 80. Same as figure 79 but only the mixtures with smaller amounts of clinopyroxene. Source: RELAB.
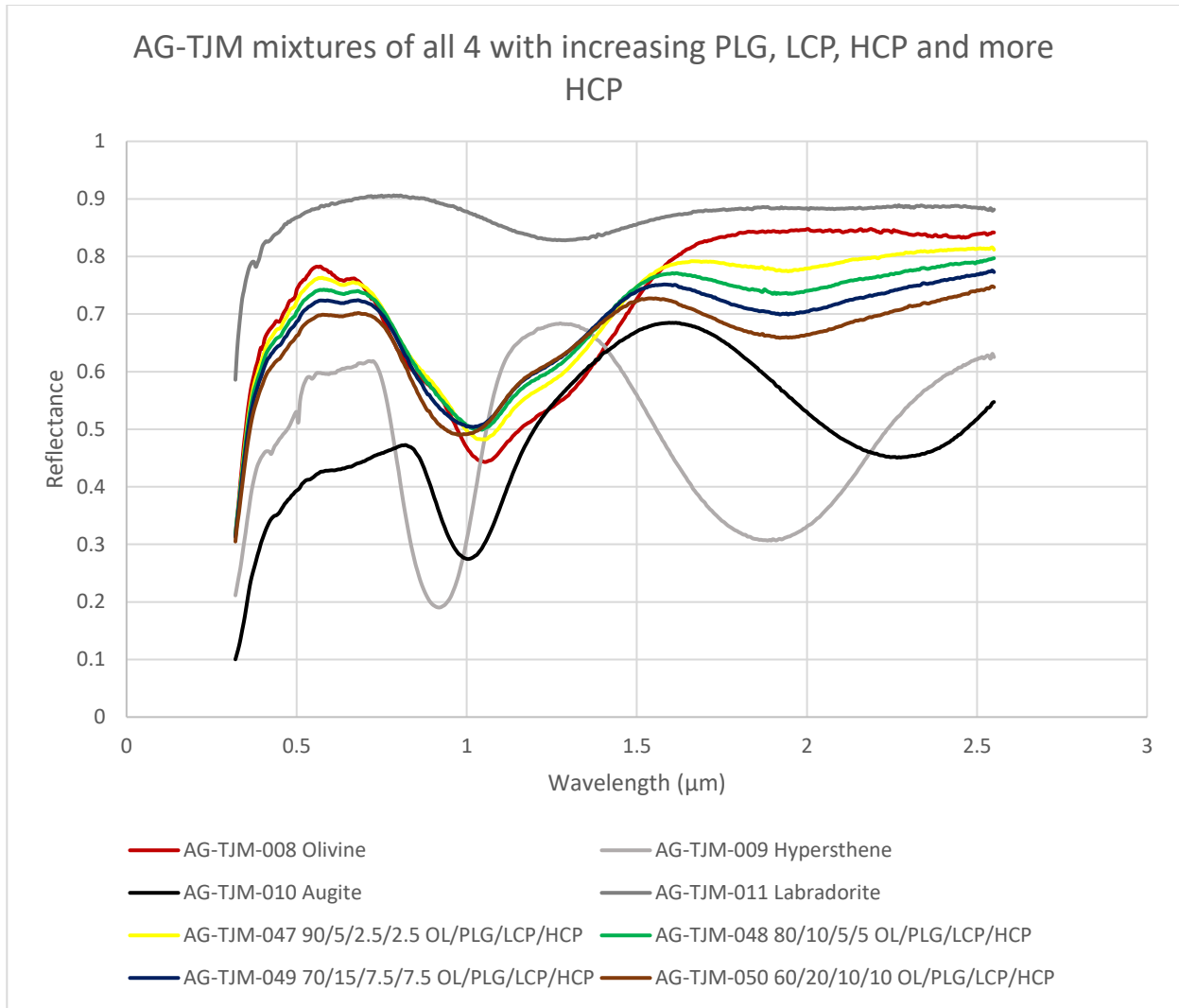
Figure 81. Same as figure 79 but only the mixtures with larger amounts of clinopyroxene. Source: RELAB.

The AG-TJM mixtures were polynomial fitted for their myriad minima. The olivine

sample, AG-TJM-008, had a zero-crossing point that was a little below the x-axis. The mixture

AG-TJM-012 had a similar issue as AG-TJM-008 for its one micron feature. The one micron

feature for the AG-TJM-014 mixture had a zero-crossing point a bit above the x-axis, while the

two micron feature was a tad below. AG-TJM-016 had its askew one micron feature's zero-

crossing point decently below the x-axis. Its two micron feature's zero-crossing point was a tad

under the x-axis as well. The one micron feature for the mixture AG-TJM-017 had a zero-

crossing point slightly below the x-axis, as did the mixtures AG-TJM-018, AG-TJM-019, AG-TJM-020, AG-TJM-021, AG-TJM-022, AG-TJM-027, AG-TJM-028, AG-TJM-030, AG-TJM-031, AG-TJM-032, AG-TJM-035, AG-TJM-036, AG-TJM-039, AG-TJM-041, AG-TJM-042, AG-TJM-044, AG-TJM-045, AG-TJM-046, AG-TJM-047, AG-TJM-048, AG-TJM-049, and AG-TJM-050. The one micron feature's zero-crossing was a bit above for the mixtures AG-TJM-023, AG-TJM-024, AG-TJM-025, AG-TJM-026, AG-TJM-033, AG-TJM-034, AG-TJM-037, AG-TJM-038, and AG-TJM-040. The two micron zero-crossing point was also slightly below the x-axis for AG-TJM-024, AG-TJM-026, AG-TJM-034, AG-TJM-043, AG-TJM-047, and AG-TJM-049. The two micron zero-crossing point was slightly above the x-axis for AG-TJM-035. Overall, the minima differences between the lowest reflectances and polynomial fits were small. The only mixture spectra that had one micron feature minima differences greater than 5 nm were AG-TJM-011 at 10 nm, AG-TJM-016 at -25 nm, AG-TJM-037 at -10 nm, AG-TJM-047 at 10 nm, AG-TJM-048 at 10 nm, and AG-TJM-050 at 25 nm. For the two micron feature minima differences, the ones that had greater than 5 nm minima differences were AG-TJM-017 at 10 nm, AG-TJM-018 at 10 nm, AG-TJM-020 at 15 nm, AG-TJM-027 at -30 nm, AG-TJM-028 at -10 nm, AG-TJM-030 at -10 nm, AG-TJM-031 at -20 nm, AG-TJM-035 at -25 nm, AG-TJM-036 at -15 nm,  AG-TJM-037 at -10 nm, AG-TJM-038 at -10 nm, AG-TJM-039 at -20 nm, AG-TJM-040 at -10 nm, AG-TJM-041 at -15 nm, AG-TJM-044 at 15 nm, AG-TJM-048 at -25 nm, AG-TJM-050 at -15 nm, and AG-TJM-051 at 15 nm. These minima are compared in figures 82 through 86. The spectra that had only one feature have been graphed against 1 µm.
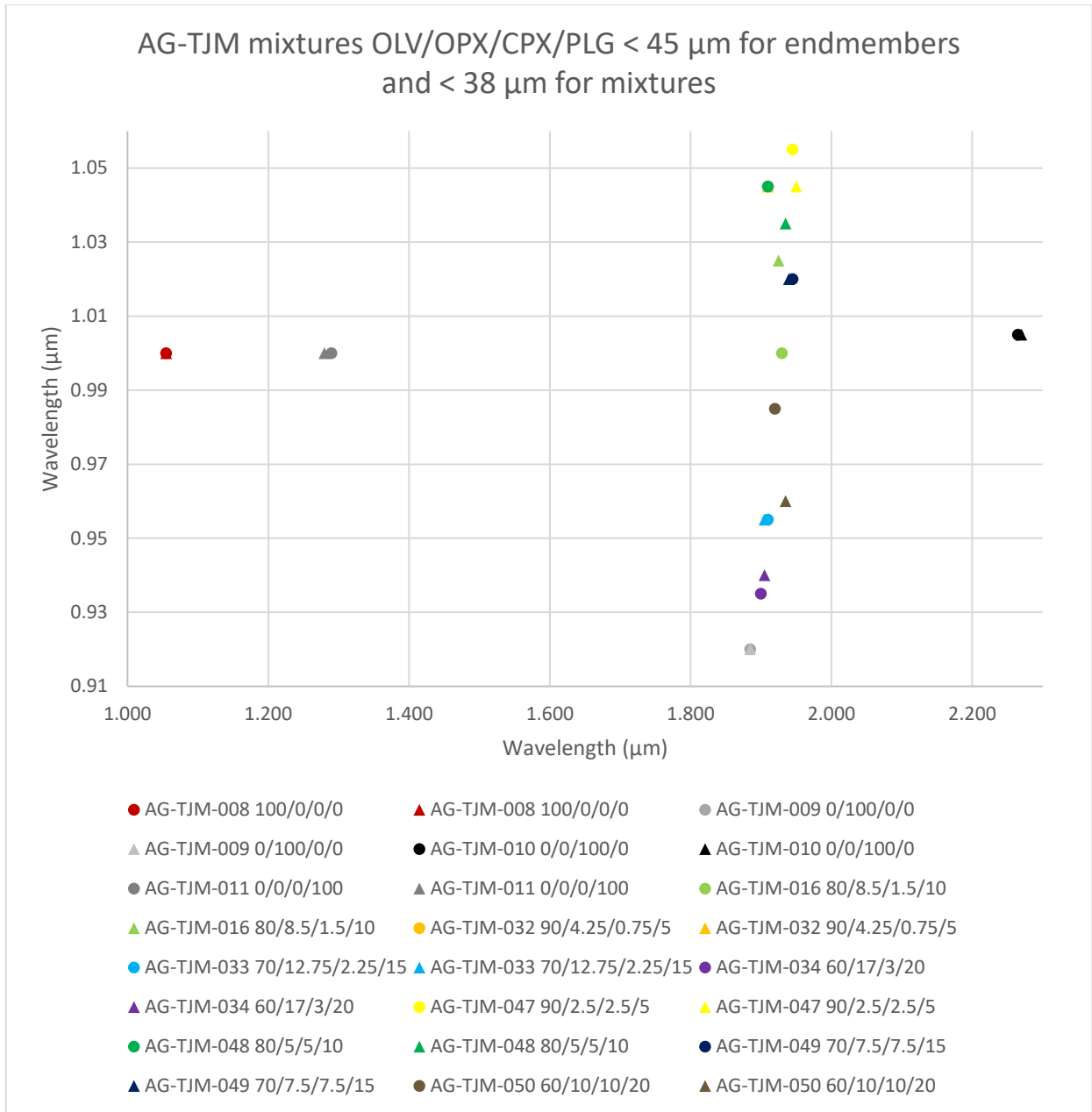
Figure 82. Minima comparisons for the AG-TJM mixture spectra of AG-TJM-008, AG-TJM-009, AG-TJM-010, and AG-TJM-011. The circles are the minima I originally found while the triangles are the minima I found using polynomial fitting. Sources: RELAB, McCraig et al. 2017.
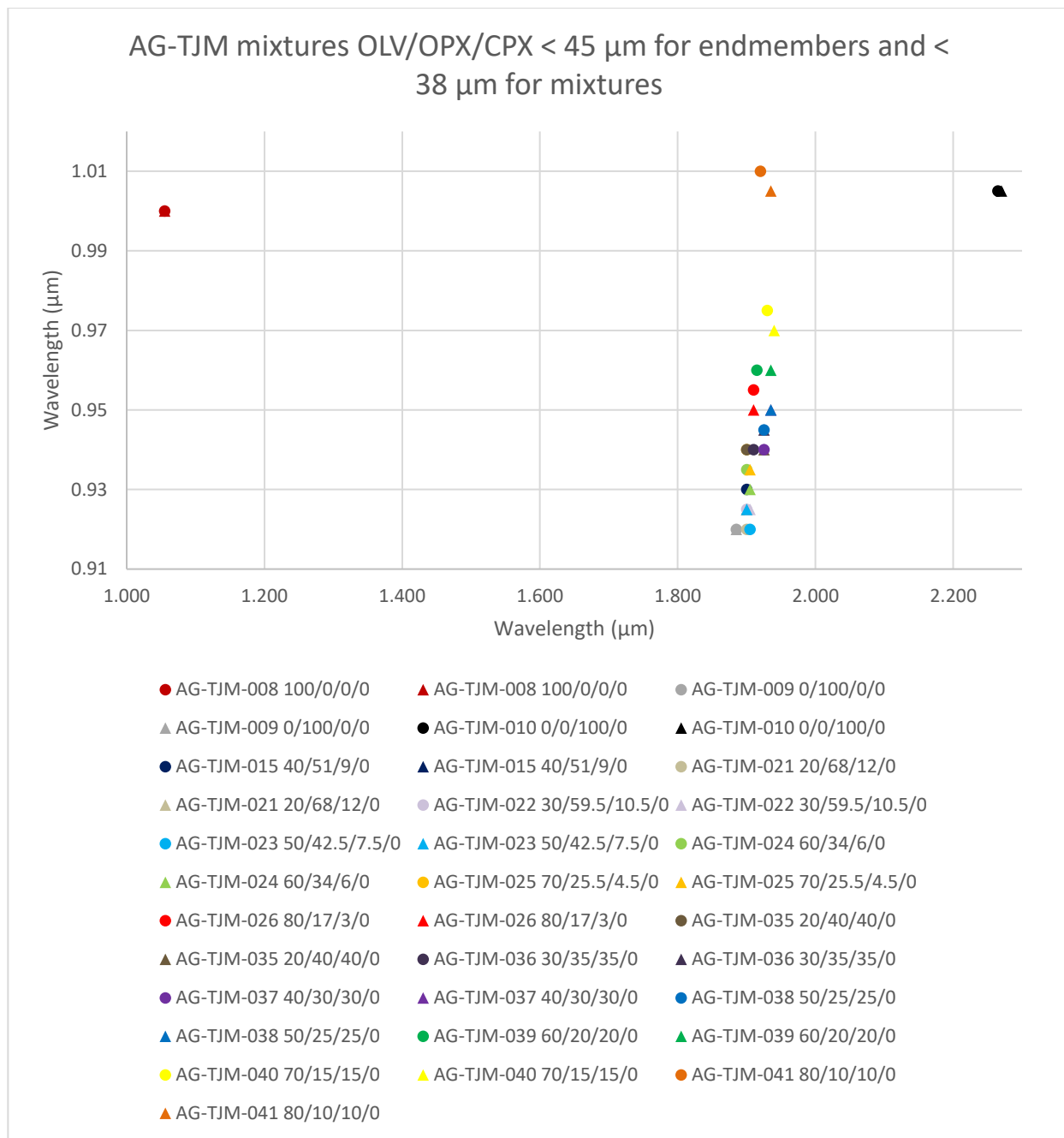
Figure 83. Minima comparisons for the AG-TJM mixture spectra of AG-TJM-008, AG-TJM-009, and AG-TJM-010. The circles are the minima I originally found while the triangles are the minima I found using polynomial fitting. Sources: RELAB, McCraig et al. 2017.
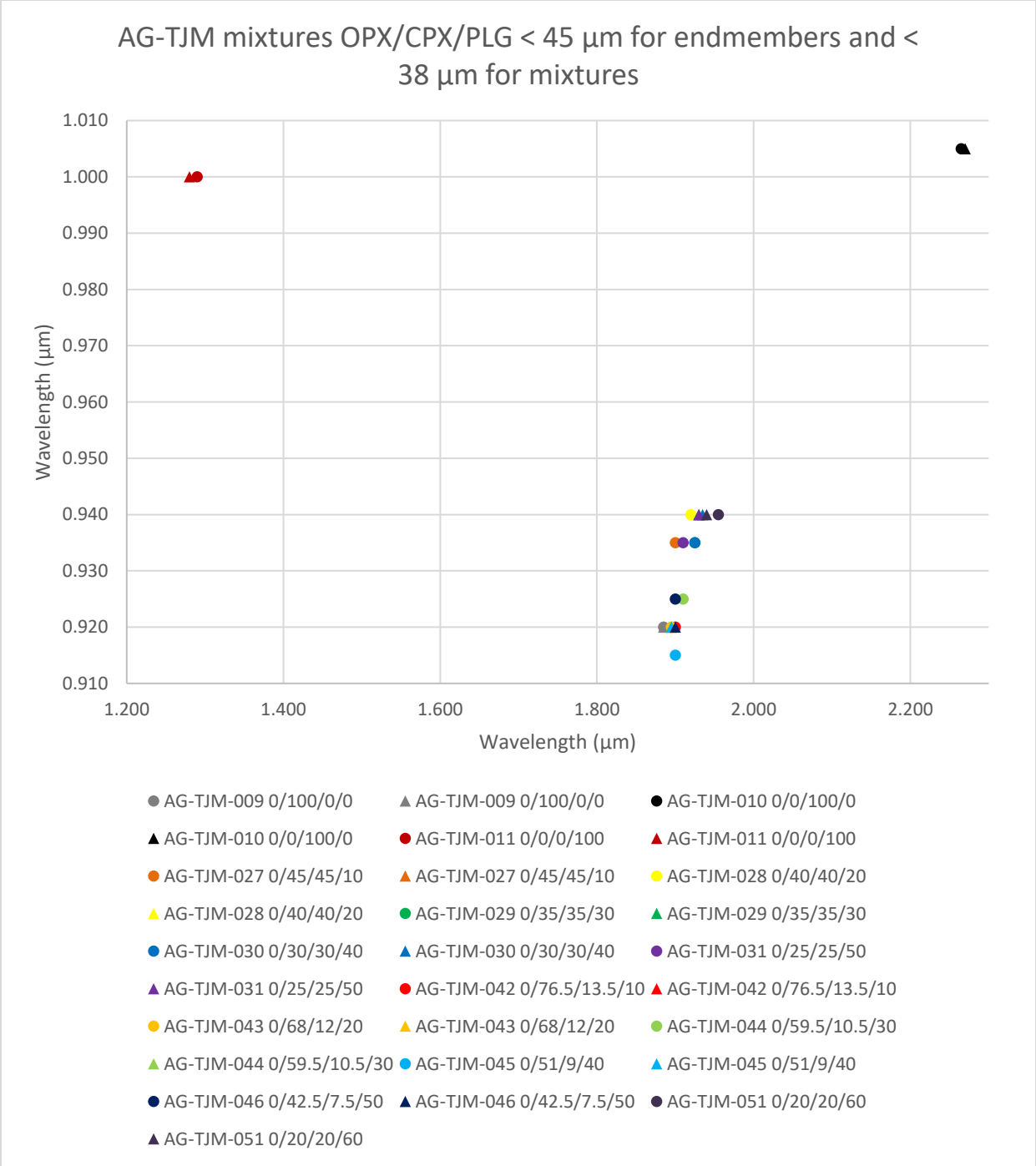
Figure 84. Minima comparisons for the AG-TJM mixture spectra of AG-TJM-009, AG-TJM-010, and AG-TJM-011. The circles are the minima I originally found while the triangles are the minima I found using polynomial fitting. Sources: RELAB, McCraig et al. 2017.

166
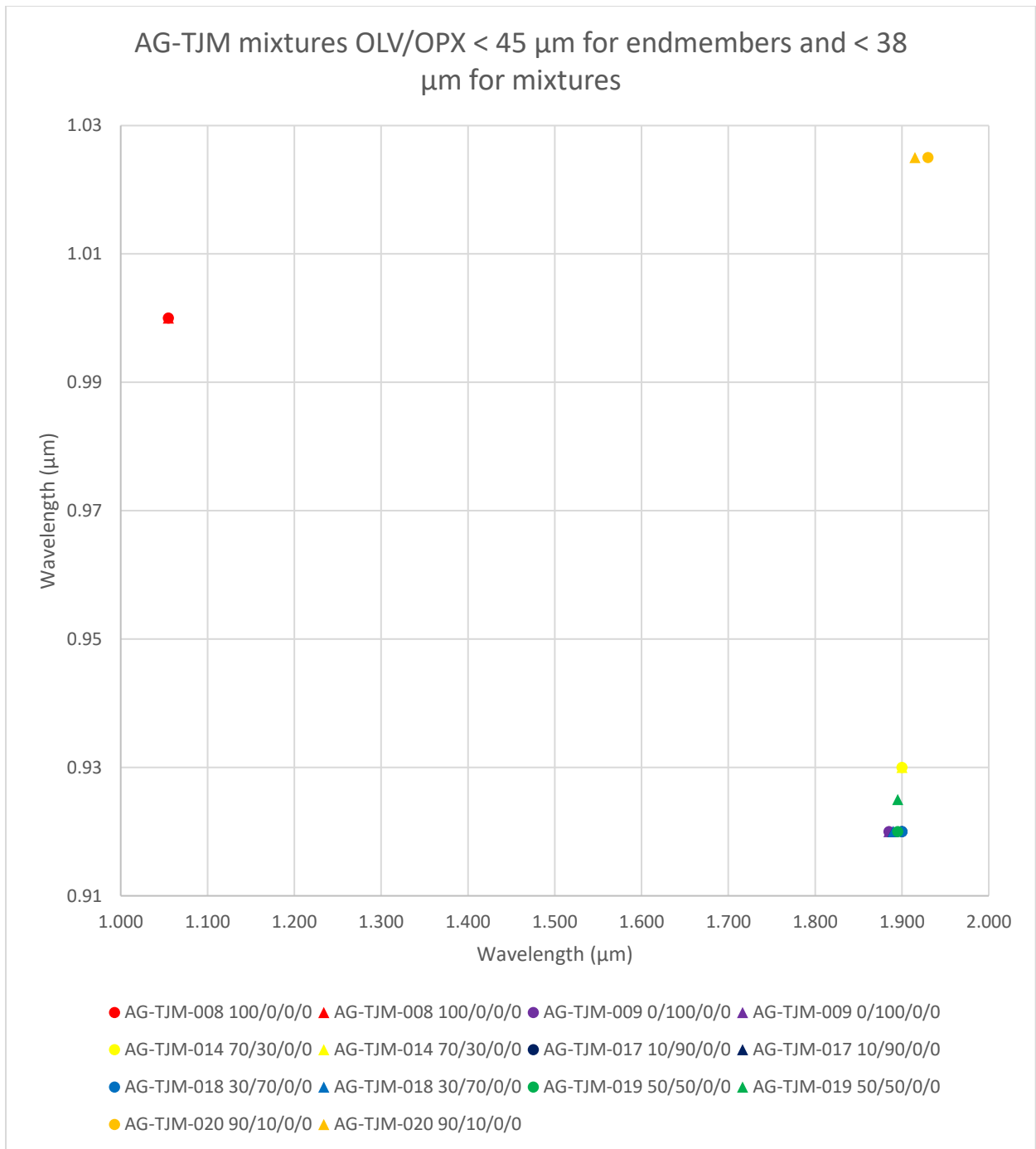
Figure 85. Minima comparisons for the AG-TJM mixture spectra of AG-TJM-008 and AG-TJM-009. The circles are the minima I originally found while the triangles are the minima I found using polynomial fitting. Sources: RELAB, McCraig et al. 2017.
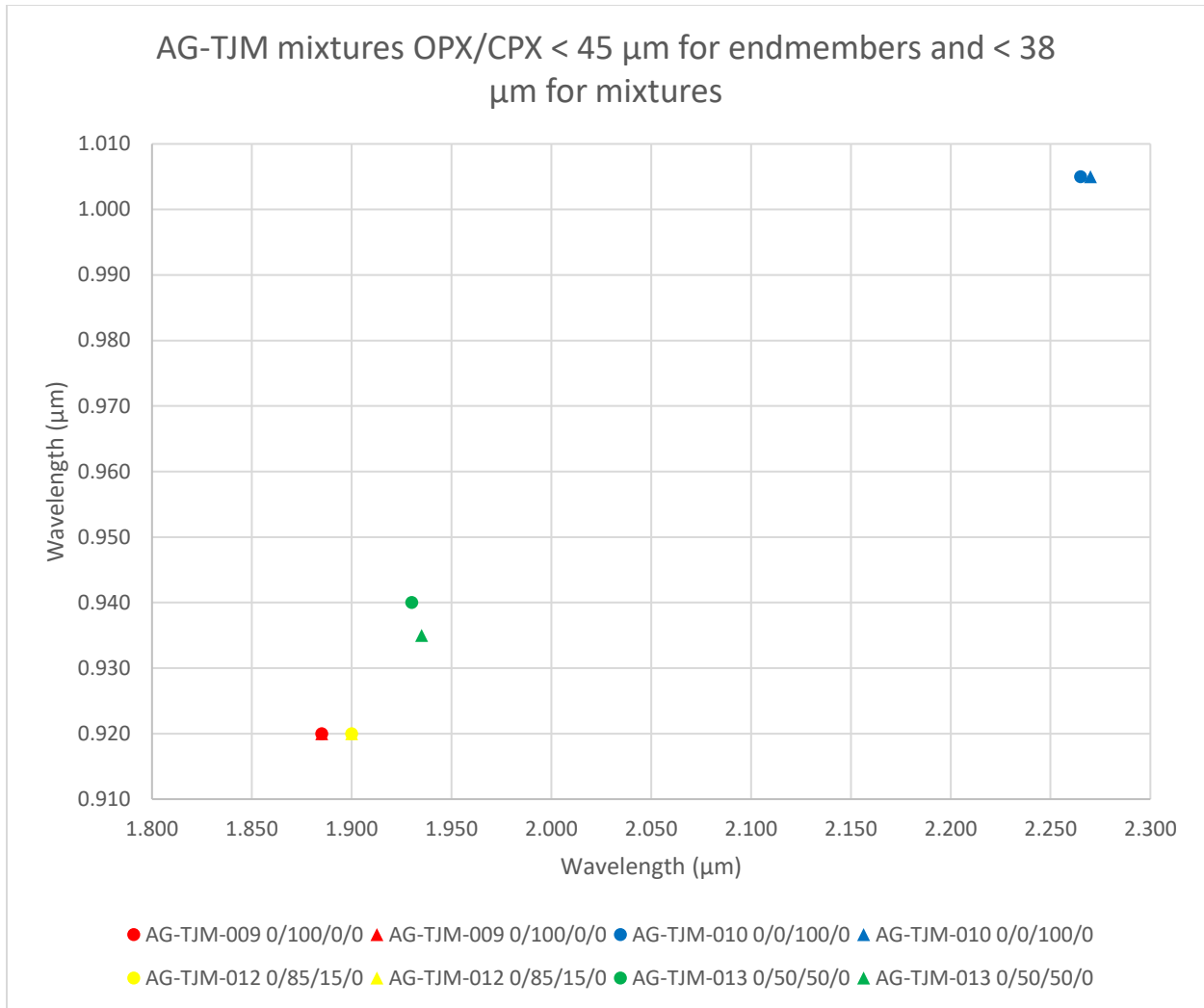
Figure 86. Minima comparisons for the AG-TJM mixture spectra of AG-TJM-009 and AG-TJM-010. The circles are the minima I originally found while the triangles are the minima I found using polynomial fitting. Sources: RELAB, McCraig et al. 2017.

Another set of mixtures from MX-CMP showed the effects of plagioclase, a labradorite, on diopside. They were measured at varying intervals at 45-75 µm grain sizes. These spectra are in figure 87. The samples with the most plagioclase had the highest reflectances and this decreased with increasing diopside. The ~ 1.25 µm feature from plagioclase was strong until after 10 % clinopyroxene where the clinopyroxene feature started to become much stronger as it increased in abundance. By 25 % clinopyroxene the plagioclase feature had disappeared and it looked like the pure clinopyroxene feature, albeit at a higher reflectance. The clinopyroxene one

micron feature was obvious by 5 % clinopyroxene and 95 % plagioclase, as was the two micron feature. However at close glance both features were faintly visible in 2 % clinopyroxene and 98 % plagioclase as well. This shows how weakly plagioclase affects spectra and that there needs to be a significant amount in order to make large changes in the spectra.
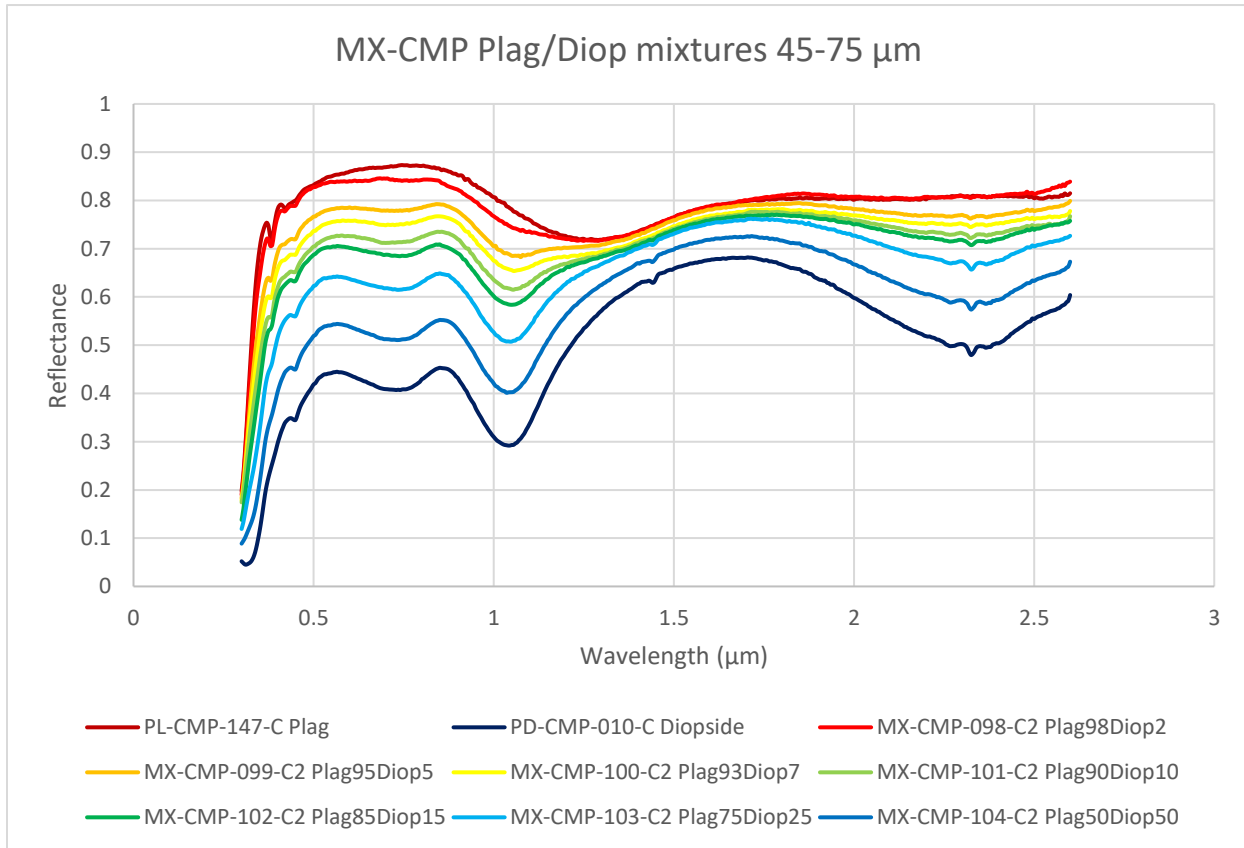


Figure 87. Diopside and labradorite mixtures from MX-CMP. Source: RELAB.

The polynomial fitted minima overall were fairly similar, with the two micron feature possibly having different minima than from lowest reflectance due to water features. Both had their ~ 1 µm features decrease in wavelength position with increasing clinopyroxene; the biggest decrease was in the mixtures from 2 % to 5 % clinopyroxene. There was also a decrease from 0 % to 2 % clinopyroxene for the polynomial fitted minima. The two micron feature in the lowest reflectance minima did not move with increasing clinopyroxene after 5 % clinopyroxene, while

the polynomial fitted minima didn't move much after 10 % clinopyroxene. I was not able to fit the ~ 1.25 µm features at 5 % and beyond with increasing clinopyroxene. Both main features of PD-CMP-010-C had their zero-crossing points below the x-axis and the second feature was a bit noisy. The combination ~ 1.2 µm feature in MX-CMP-098-C2 had a zero-crossing point slightly below the x-axis, while the ~ 1 µm features in MX-CMP-099-C2, MX-CMP-100-C2, MX-CMP-101-C2, and MX-CMP-102-C2 had ones slightly above. The ~ 2.3 µm feature in MX-CMP-101-C2 had a zero-crossing point a little below the x-axis and a second inflection point that was not where the minimum was, possibly due to noise. MX-CMP-102-C2 also had its 2.3 µm feature's zero-crossing point a little below the x-axis. MX-CMP-103-C2 had its zero-crossing point for its 1 and 2 µm features a small amount below the x-axis. MX-CMP-104-C2 had the same as MX-CMP-103-C2, although its 1 µm zero-crossing point was further from the x-axis. The one micron features that had minima differences greater than 5 nm were PL-CMP-147-C at 10 nm, MX-CMP-098-C2 at 25 nm, and MX-CMP-104-C2 at -10 nm. The two micron features that had minima differences greater than 5 nm were PD-CMP-010-C at -10 nm, MX-CMP-098-C2 at 30 nm, MX-CMP-099-C2 at 20 nm, MX-CMP-101-C2 at -10 nm, MX-CMP-103-C2 at -10 nm, and MX-CMP-104-C2 at -10 nm. The comparisons of the minima are shown in figure 88. The spectra that have only one feature are graphed against one micron.
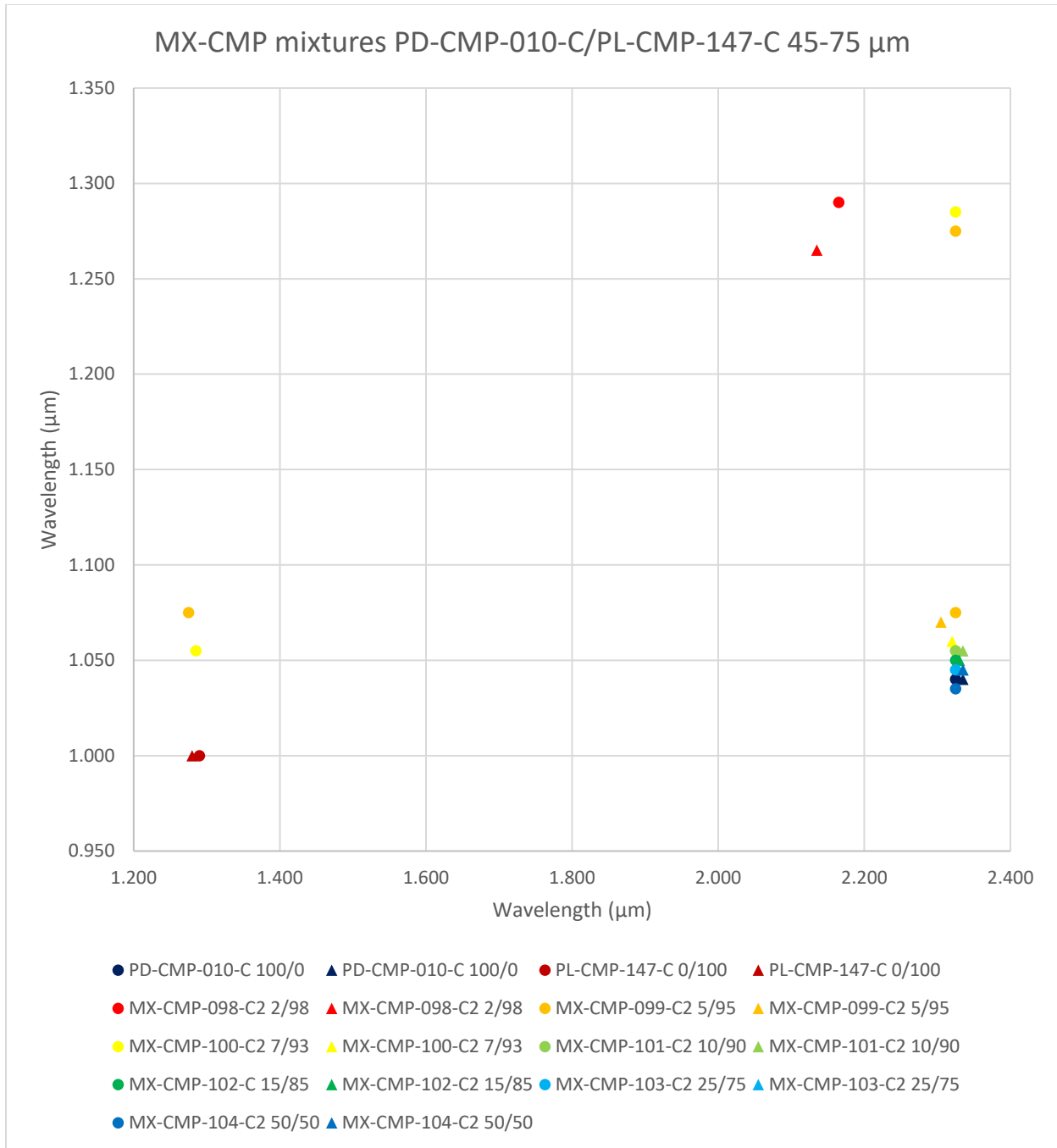
Figure 88. Minima comparisons for the MX-CMP mixture spectra of PD-CMP-010-C and PL-CMP-147-C. The circles are the minima I originally found while the triangles are the minima I found using polynomial fitting. The numbers are in percentages. Sources: RELAB, McCraig et al. 2017.

With the exception of the angrite-like mixtures mentioned in the section below, the last groups of mixtures were another orthopyroxene-clinopyroxene mixture from XP-CMP and were broken up into three groups of different grain sizes and intervals. The grain sizes were 75-125

µm, < 45 µm, and 45-75 µm in the first, second, and third groups, respectively. These mixtures used the diopside PP-CMP-021 and the orthopyroxene PE-CMP-030; their compositions are located in the sample appendices table 1. These graphs are in figures 89 to 91 below.

Figure 89, in rainbow order with decreasing orthopyroxene, started out resembling the pure orthopyroxene sample. The pure samples were at < 45 µm grain sizes, which could explain the reflectance and width differences. The 85/15 orthopyroxene to clinopyroxene and 75/25 spectra had the features resembling orthopyroxene and barely moved in position from each other, although both were at slightly longer wavelengths than the pure orthopyroxene. They were curved more around 1.2 to 1.4 µm than the pure orthopyroxene sample. The 75/25 spectrum started to straighten out past 2.3 µm which, as in other mixtures above, was likely from the influence of increasing clinopyroxene. The rest of the mixtures until 15/85 had two 2 µm features from the influences of the two different pyroxenes. With increasing clinopyroxene after 50/50 the orthopyroxene contribution lessened, being very faint in 25/75 until 15/85 where there was only one 2 µm feature again. The 15/85 one micron feature was slightly distorted from both of the pyroxenes and it was still at shorter wavelengths than the pure clinopyroxene. The one micron feature in general increased slightly with each mixture to longer wavelengths as more clinopyroxene was added, with a larger jump from 40/60 to 25/75 and then from 15/85 to 0/100. The two micron feature did not appreciably start to move to longer wavelengths until 60/40. The two micron feature was also "stretched" more, was not as deep as the pure clinopyroxene endmember, and was also at a shorter wavelength. The ~ 0.65 µm feature in the clinopyroxene started to appear prominently at 75/25 and continued to get stronger after, although even at 85/15 there was a slight dent from the feature. In general the spectra decreased in reflectance with increasing clinopyroxene.

172

Figure 90 had spectra with < 45 µm grain sizes that were at higher reflectances than figure 91 with 45-75 µm grain sizes. The ~ 0.65 µm feature in the clinopyroxene again started to appear at 85/15 orthopyroxene/clinopyroxene. In general, the mixture spectra decreased in reflectance again with increasing clinopyroxene with the exception of the 25/75 mixtures which were both at a lower reflectance than 15/85. 85/15 resembled the pure orthopyroxene sample and was at nearly the same wavelength for both main features. At 75/25 there started to become two 2 µm features which again continued to 25/75 and was nearly gone by 15/85. The one micron feature started at nearly the same wavelength position as the pure orthopyroxene and steadily moved to longer wavelengths with a larger jump again from 40/60 to 25/75. 60/40, 50/50, and 40/60 had distorted to longer one micron features until 25/75 when the spectra features rounded out and started to resemble the pure clinopyroxene one micron feature more. Generally the two micron features, and both when there were two, moved to longer wavelengths steadily, as well.

The last group, in figure 91 at 45-75 µm grain sizes, had reflectances in between the two grain sizes, as lower grain sizes usually have higher reflectances. This set of mixtures had similar results to the other two. There were two 2 µm features at 60/40 orthopyroxene/clinopyroxene and they were nearly gone by 25/75, when the orthopyroxene feature was faint. The 75/25 spectrum had a straight slope after 2.3 µm indicating a contribution from the clinopyroxene. The 0.65 µm clinopyroxene feature again appeared by 15/85. The one micron feature steadily increased to longer wavelengths with increasing clinopyroxene and there was a larger jump from 25/75 to 15/85. The two micron features steadily increased in wavelength position with increasing clinopyroxene as well.
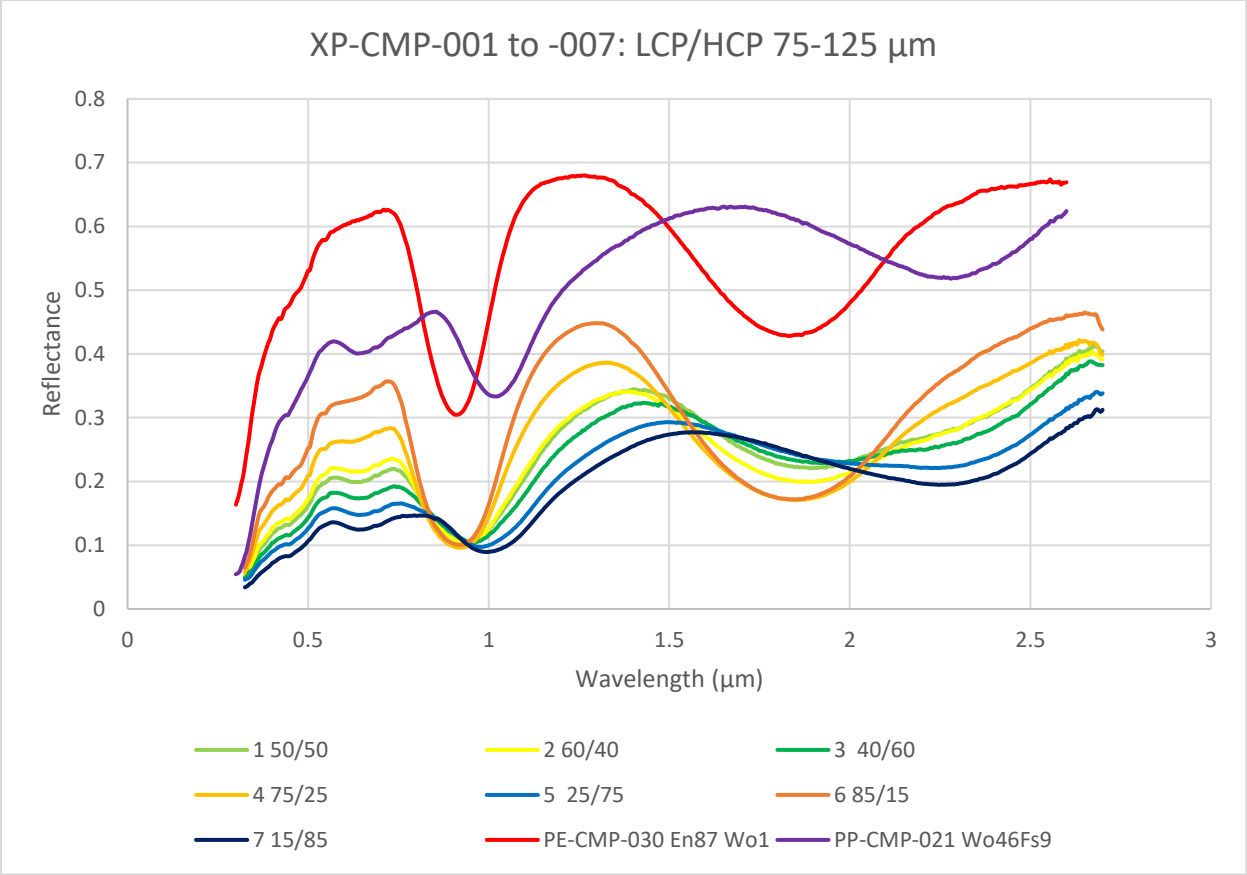
Figure 89. Orthopyroxene-clinopyroxene from XP-CMP at 75-125 µm grain sizes. Source: RELAB.
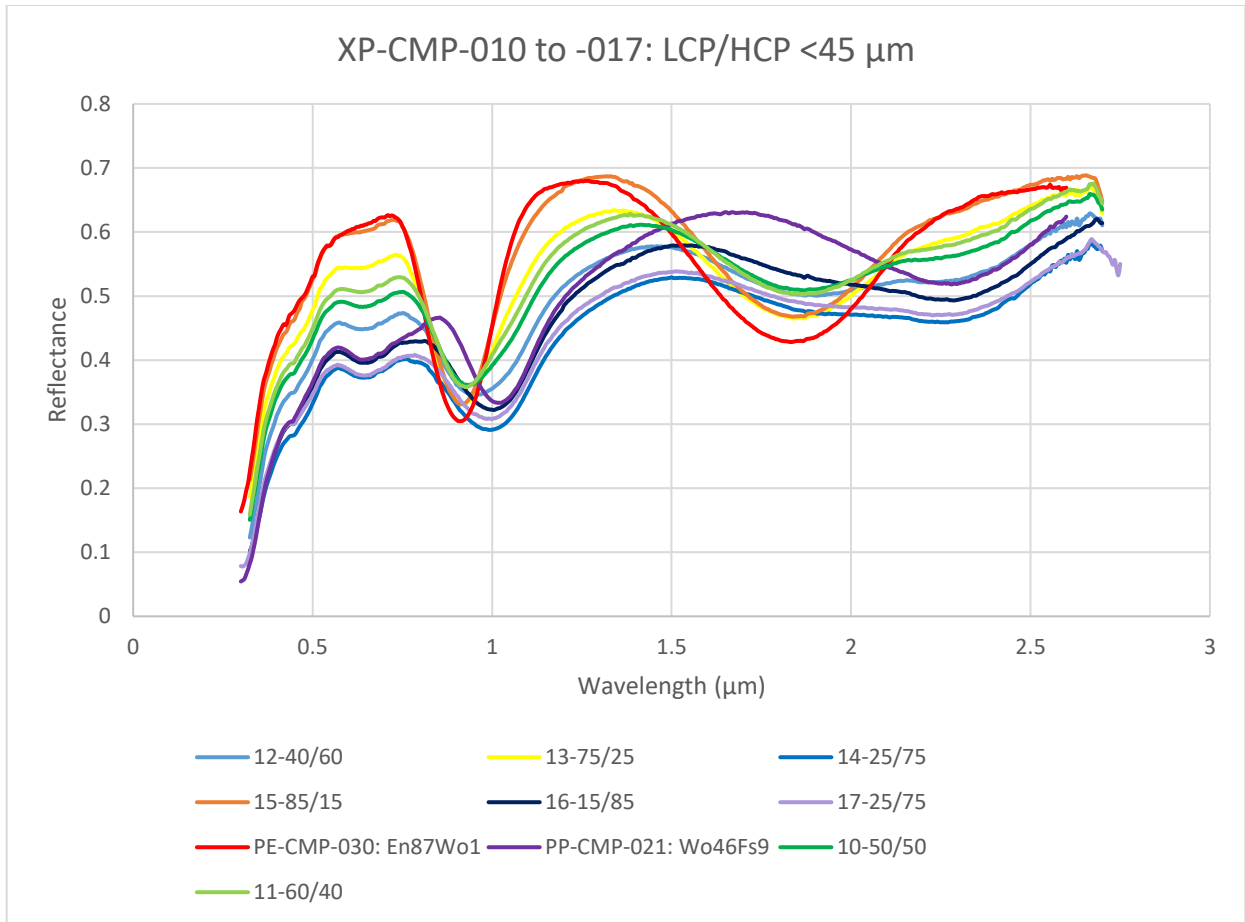
Figure 90. Orthopyroxene-clinopyroxene from XP-CMP at < 45 µm grain sizes. Source: RELAB.
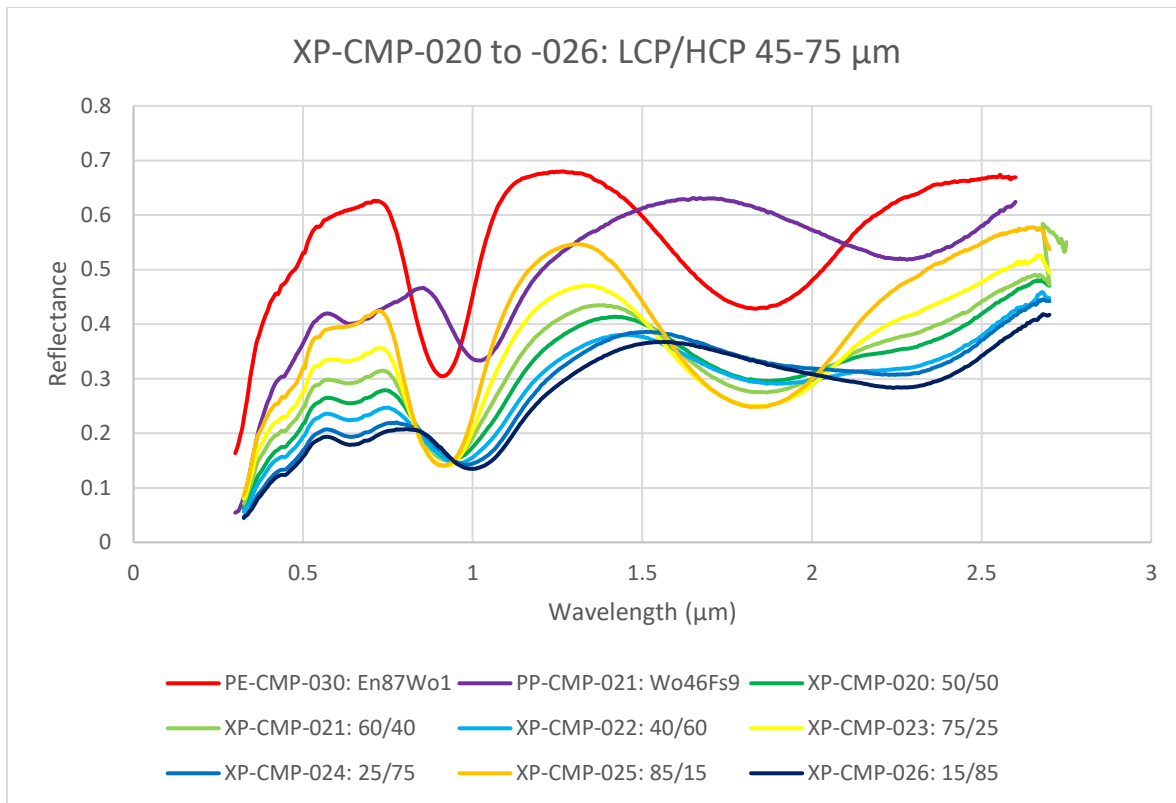
Figure 91. Orthopyroxene-clinopyroxene from XP-CMP at 45-75 µm grain sizes. Source: RELAB.

The first seven mixtures at 75-125 µm grain sizes were polynomial fitted. The polynomial fitted minima were similar to the lowest reflectance minima, in that both the one micron and two micron features decreased with increasing orthopyroxene. XP-CMP-001 is a 50/50 orthopyroxene/clinopyroxene mixture that had two features around 2 µm from the two different pyroxenes. The feature around 2.3 µm was too weak to get a polynomial fitted minimum however. A similar problem occurred with a weaker feature around 2.3 µm in XP-CMP-002, which was 60/40. XP-CMP-003 at 40/60 also had two features around 2 µm and even though the 2.3 µm feature was stronger than in the previous two mixtures, I still was unable to fit it. The 1 µm feature had a zero-crossing point that is slightly below the x-axis, as does XP-CMP-002, XP-CMP-003, XP-CMP-004, and XP-CMP-006. XP-CMP-005 is 25/75 and appeared to have two features around 2 µm but the first one was too weak to fit because there was less

orthopyroxene. The 1 µm feature had a zero-crossing point that was slightly above the x-axis, as did XP-CMP-007. All of the one micron features had minima differences less than or equal to 5 nm. The two micron features that had minima differences greater than 5 nm were PP-CMP-021 at 15 nm, XP-CMP-002 at -10 nm, XP-CMP-006 at 10 nm, and XP-CMP-007 at -7 nm. The comparisons of the minima are in figure 92.

The next mixtures from XP-CMP-010 to -017 had < 45 µm grain sizes. The polynomial fitted minima were also similar to the lowest reflectance minima, in that both the one micron and two micron features generally decreased with increasing orthopyroxene. XP-CMP-010 had 50/50 orthopyroxene/clinopyroxene and had a zero-crossing point a little above the x-axis. Like in the previous group of mixtures, there were visually two features around 2 µm from the two pyroxenes. However, I was only able to get the first of the two features and that one also had a zero-crossing point a little above the x-axis and a lower but still decent $R^2$ value. XP-CMP-011 was 60/40 OPX/CPX and had two visible 2 µm features like before and I was only able to get the first of the two fitted. The one micron feature also had a zero-crossing point a bit above the x-axis. Again, as above, XP-CMP-012 at 40/60 OPX/CPX had two features near two microns but this time I was able to fit both of the features. The 1 µm feature had a zero-crossing point that was a bit above the x-axis, as did the second 2 µm feature but that was only slightly above the x-axis. The two features were weakly visible in XP-CMP-013 and -014 at 75/25 and 25/75 OPX/CPX, respectively, but both were not able to be fitted. The latter had a one micron feature that had a zero-crossing point slightly below the x-axis, as did XP-CMP-015, XP-CMP-016, and XP-CMP-017. That last one also had two features around 2 µm but only the second one was able to be fitted. All of the one micron features had minima differences less than 5 nm. The two micron features that had minima differences greater than 5 nm were PP-CMP-021 at 10 nm, XP-

CMP-011 at 10 nm, XP-CMP-012 at 15 nm, XP-CMP-013 at -15 nm, XP-CMP-014 at 20 nm, XP-CMP-016 at 15 nm, and XP-CMP-017 at -25 nm. The one mixture spectrum that had another feature, XP-CMP-012, had a minimum difference of 30 nm. The comparisons of these minima are in figure 93.

The final six spectra of this group of mixtures from XP-CMP-020 to -026 were the same pyroxenes but at 45-75 µm grain sizes. The polynomial fitted minima were also similar to the lowest reflectance minima, in that both the one micron and two micron features generally decreased with increasing orthopyroxene. XP-CMP-020 had 50/50 orthopyroxene/clinopyroxene and two visible features near 2 µm, although only the first one was able to be fitted. The one micron feature had a zero-crossing point that was slightly below the x-axis. XP-CMP-021 at 60/40 also had two visible 2 µm features with only the first one able to be fitted. It had a one micron feature that had a zero-crossing point that was a bit below the x-axis. XP-CMP-022 at 40/60 again had two visible 2 µm features with only the first one able to be fitted. XP-CMP-023 had a one micron feature zero-crossing point a bit below the x-axis, as did XP-CMP-026. XP-CMP-024 also had a one micron feature zero-crossing point a bit above the x-axis. None of the mixture spectra had one micron feature minima differences greater than 5 nm. For the two micron feature differences, the minima spectra that were greater than 5 nm were PP-CMP-021 at 10 nm, XP-CMP-021 at 15 nm, XP-CMP-025 at -15 nm, and XP-CMP-026 at -15 nm. The comparisons of these minima are in figure 94.
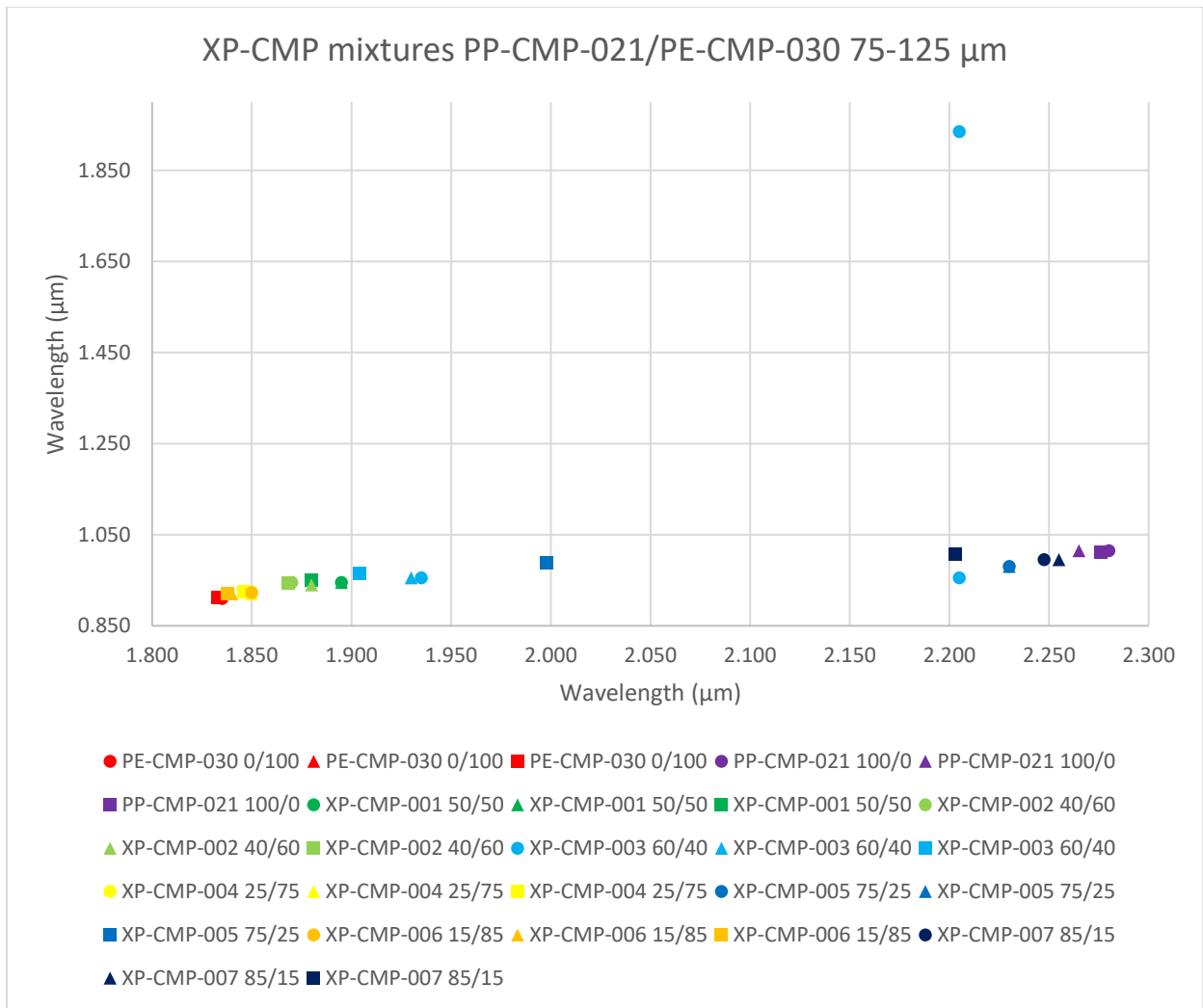
Figure 92. Minima comparisons for the XP-CMP mixture spectra of PE-CMP-030 and PP-CMP-021. The circles are the minima I originally found, the triangles are the minima I found using polynomial fitting, and the squares are centers found in the literature (Sunshine & Pieters 1993, Duffard et al. 2005). Sources: RELAB, McCraig et al. 2017.
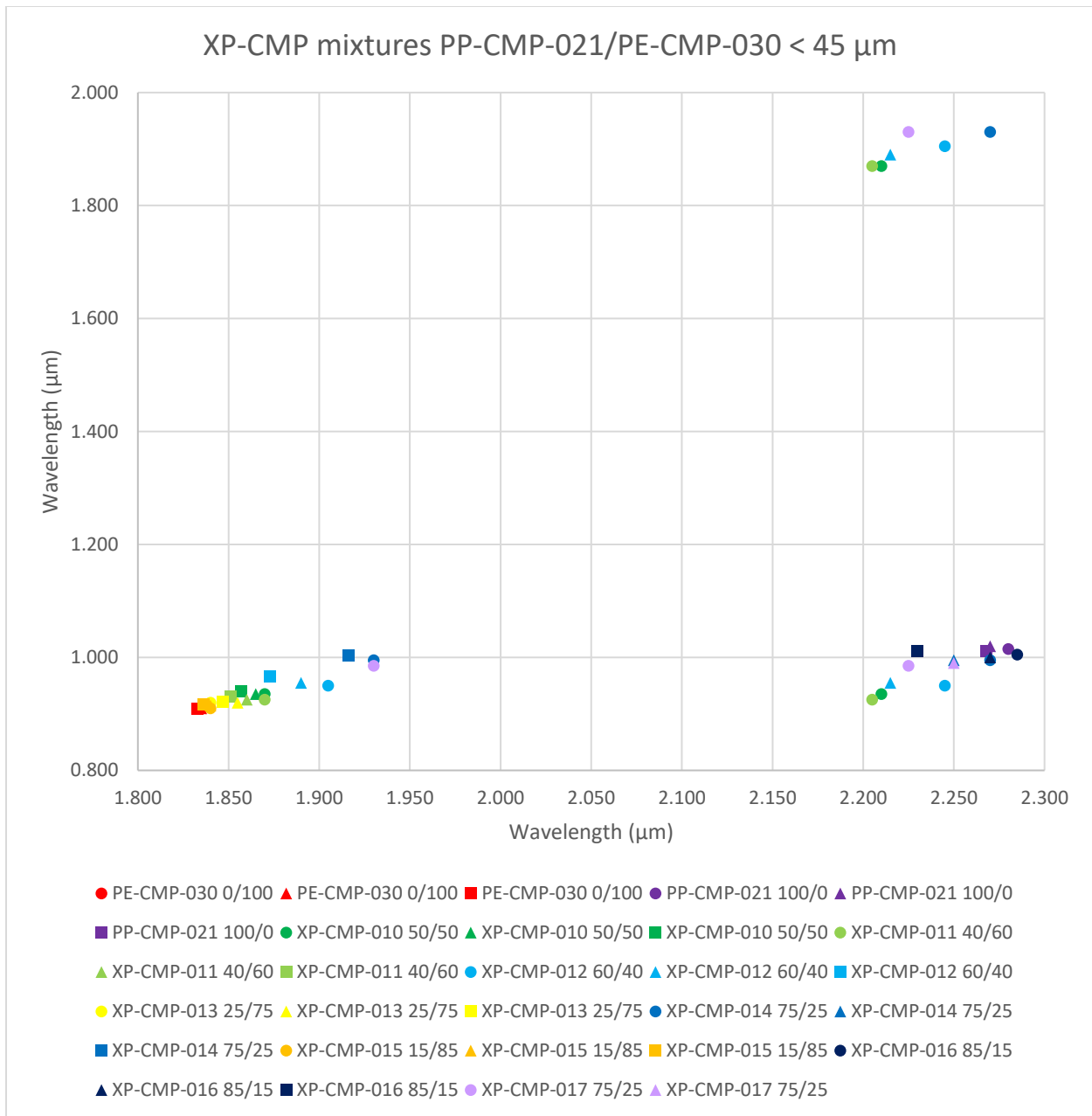
Figure 93. Minima comparisons for the XP-CMP mixture spectra of PE-CMP-030 and PP-CMP-021. The circles are the minima I originally found, the triangles are the minima I found using polynomial fitting, and the squares are centers found in the literature (Sunshine & Pieters 1993, Duffard et al. 2005). Sources: RELAB, McCraig et al. 2017.
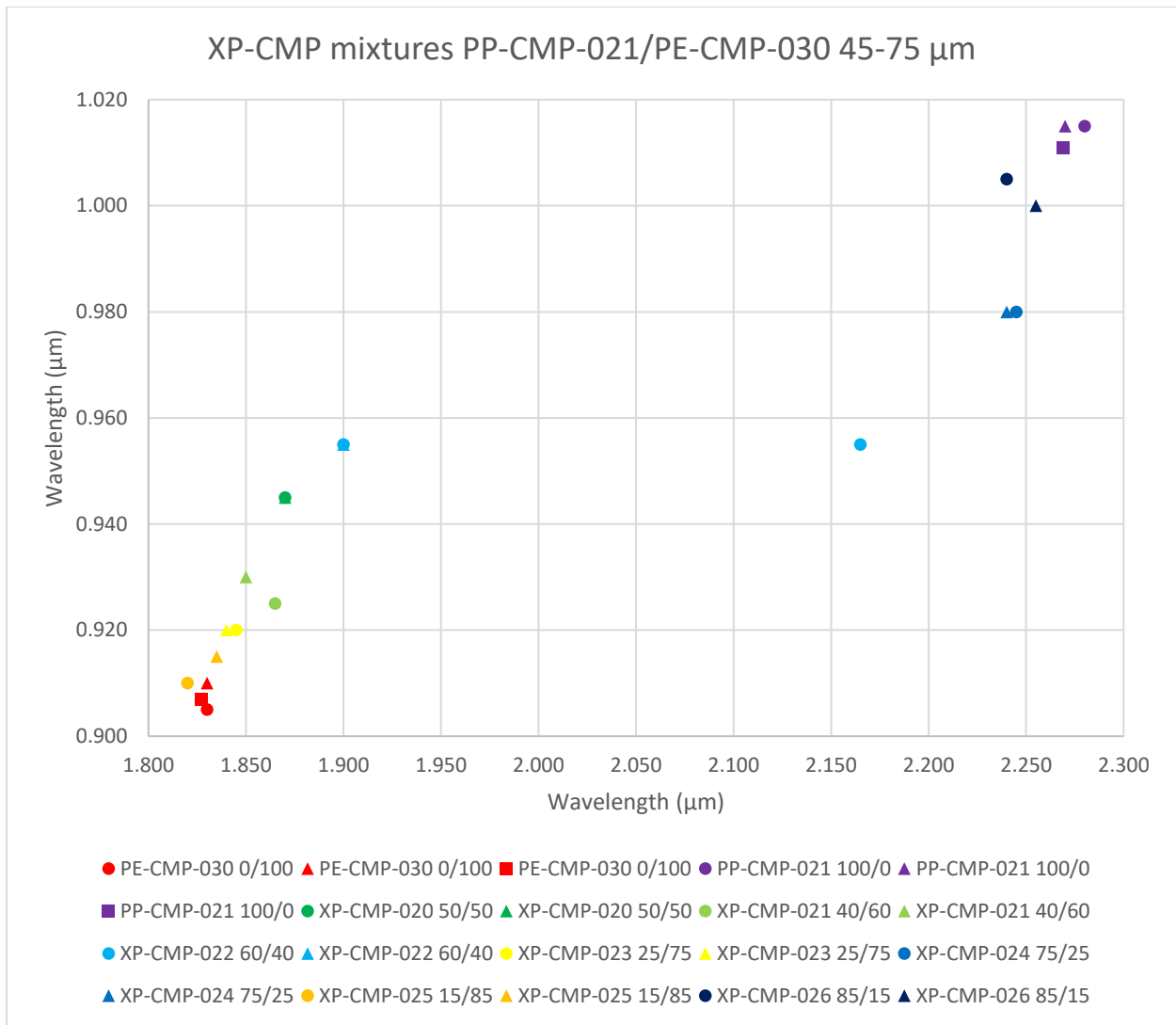
Figure 94. Minima comparisons for the XP-CMP mixture spectra of PE-CMP-030 and PP-CMP-021. The circles are the minima I originally found, the triangles are the minima I found using polynomial fitting, and the squares are centers found in the literature (Sunshine & Pieters 1993, Duffard et al. 2005). Sources: RELAB, McCraig et al. 2017.

There were even fewer mixtures available that had band centers in the literature; there were no band minima. Some mixtures from Sunshine & Pieters 1993 and Duffard et al. (2005) were the only ones that had them. The results were again not as ideal as hoped, but it was hard to compare centers to minima, especially centers that were found via the MGM like in Sunshine & Pieters 1993. The results are in table 7 in the appendices.

# Discussion of angrite band minima and centers

After examining the different mixtures with clinopyroxenes, I looked at some angrite spectra. As a reminder, angrites are a rare meteorite type with abundant amounts of high-calcium clinopyroxene. Since they include olivine and plagioclase as well, I was interested to see how their spectra compared to the previous mixtures, as well as the two mixtures in the next section that were made specifically for comparing with angrites. There were six angrite spectra examined in this study. Three of these spectra were of Angra dos Reis, while the other three were of D'Orbigny, LEW 86010, and Sahara 99555. These are in figure 95 below. As mentioned above, Angra dos Reis appeared to have type B clinopyroxene in its spectra, while the rest seemed to consist of more type A clinopyroxene. The information for these are located in tables 12 through 15 in the appendices.

Angra dos Reis is 90 % aluminum-titanium diopside, with homogeneous endmember compositions around $Fs_{12}Wo_{55}$ (McSween 1999; Floss et al. 2003-ref McKay et al. 1988a; Burbine et al. 2006-ref Prinz et al. 1977; Grady et al. 2015 p.252 ref 10.3). Angra dos Reis has reddened spectra as well. It also appears to have the one micron feature at the shortest wavelength of the angrite group here after finding the minima both with lowest reflectances and polynomial fittings. There were some type B clinopyroxene-olivine mixtures above, in figure 69. PYX016 had less iron and calcium, at $Fs_{2.5}Wo_{48.9}$, and hardly any titanium or aluminum than average Angra dos Reis pyroxenes. However, the olivine, OLV003, is used below in two angritic mixtures. Even at 80 % clinopyroxene and 20 % olivine, the mixture spectrum appeared to be very similar to pure clinopyroxene. Due to the lack of other cations, PYX016 had a much flatter slope than Angra dos Reis. There were no other clinopyroxene-olivine mixtures looked at in Excel with majority type B clinopyroxene. However, Singer (1981) looked at an olivine-type B

clinopyroxene mixture in 25 % intervals, as mentioned in the previous work section above. The clinopyroxene was a diopside with lesser titanium (0.66 wt. %) and aluminum (2.71 wt. %), and more ferric iron (1.11 wt. %) than average angrites. It had much lower calcium and lower iron than in Angra dos Reis, at $Wo_{41}Fs_8$. The olivine was $Fo_{85}$, in comparison to the $Fo_{90}$ olivine in OLV003. It did have more calcium in it, 0.41 wt. % than OLV003, at 0.07 wt. %. At 25/75 olivine/clinopyroxene, the mixture looked nearly the same as the pure clinopyroxene sample, with the exception of the longer wavelength sidelobe from olivine being faintly apparent around 1.3 µm.

LEW 86010 appeared to have a more reddened slope than the other samples. It also had ~ 60 % clinopyroxene, ~ 20 % anorthite, and ~ 20 % olivine with calcium (Burbine et al. 2006-ref Delaney & Sutton 1988, Goodrich 1988, Prinz et al. 1988), while another paper had it as ~ 43 % clinopyroxene and ~ 32 % anorthite (Burbine et al. 2006-ref McKay et al. 1988). The pyroxene endmember compositions typically ranged from $Fs_{13-20}Wo_{52-57}$ and were zoned (Burbine et al. 2006-ref Goodrich 1988, Prinz et al. 1988, Crozaz & McKay 1990, Mittlefehldt et al. 1998, Mikouchi & McKay 2001).

D'Orbigny, had the broadest one micron feature out of all the spectra. Usually this occurs because of the olivine and clinopyroxene in the mixtures. This can be seen in the angrite-like mixtures in the next section in figure 97, which used large amounts of clinopyroxene. The previous mixtures of type A clinopyroxene with olivine did not display this as much until there was a large amount of clinopyroxene, such as 70 %, as can be seen in figure 58. The type A clinopyroxene sample used in that mixture, PYX150, was found to have no ferric iron, also similar to most angrites. However, there was a possible feature around 0.75 µm that usually is from ferric iron. This sample was also extremely low in titanium and aluminum, unlike most

angritic pyroxenes. D'Orbigny and Sahara 99555 are "compositionally indistinguishable" and had around 33 % anorthite, 33 % calcic olivine, and 20-25 % clinopyroxene (Burbine et al. 2006-ref Mikouchi et al. 2000a, 2000b, Mikouchi & McKay 2001, Mittlefehldt et al. 2002). They had pyroxene endmember compositions of around $Fs_{20-49}Wo_{51-54}$ and were zoned (Burbine et al. 2006-ref Mittlefehldt et al. 2002, Mikouchi personal communication). There were possibly some faint two micron features in the type A clinopyroxene-appearing spectra but Angra dos Reis had the most defined two micron feature of the set, being predominantly type B clinopyroxene.
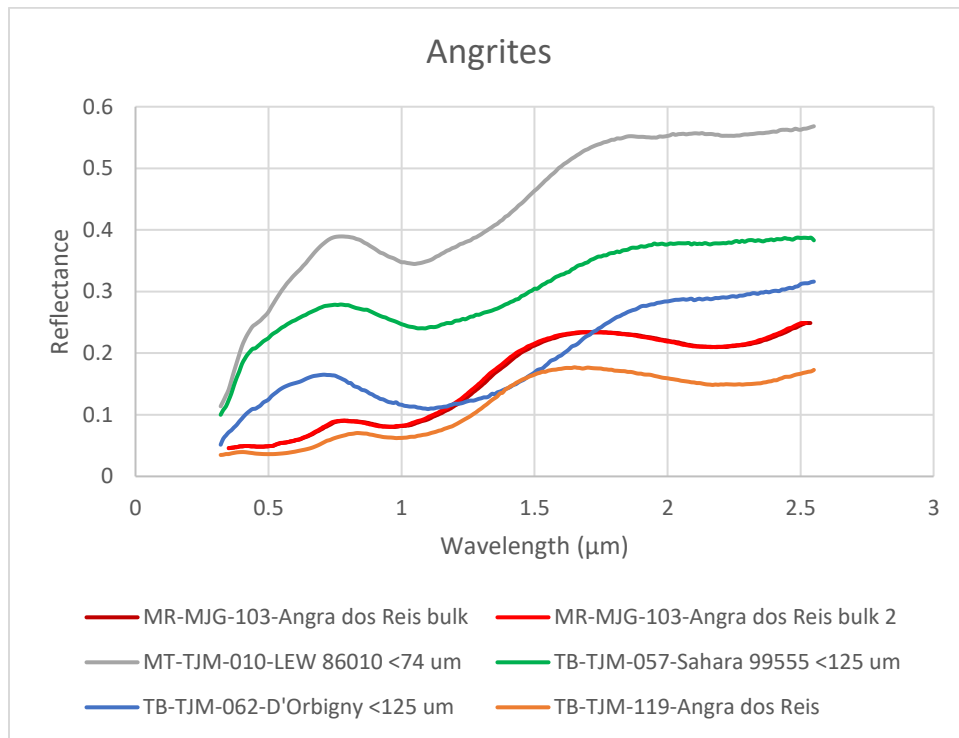


Figure 95. Angrite samples looked at in this study. Source: RELAB.

There were only two angrite samples that had wavelength positions in the literature: TB-TJM-057 and TB-TJM-062. These samples were of Sahara 99555 and D'Orbigny, respectively, both of which were believed to have pyroxenes of predominantly type A, although there were some possible faint two micron features present. Unfortunately, since there were only two samples and only one band center for each from the literature, it did not leave much to compare.

Also, as mentioned above, it can be hard to compare band centers with band minima due to the different methods and spectral slopes.

I decided to find minima again using polynomial fitting. When fitting the first MR-MJG-103 spectrum of Angra dos Reis, it looked like there were possibly two features around one micron, but that may have been noise. The best fitting result seemed to come from fitting it as one feature around one micron. The one micron feature's zero-crossing point was a tad above the x-axis, as was the same feature in the second spectrum of MR-MJG-103. Everything else looked fine. MT-TJM-010, LEW 86010, also had a one micron feature zero-crossing point that was slightly above the x-axis. There was a weak feature around 1.25 µm that was unable to be fitted. A possible weak feature around 2.2 µm was fitted as well. TB-TJM-057, as Sahara 99555, had a one micron feature with a zero-crossing point that was slightly above the x-axis. Its possible two micron feature was too faint and noisy to fit. TB-TJM-062, D'Orbigny, also had a two micron feature that couldn't be fit because of weakness, noise, and slope. Its one micron feature had a zero-crossing point that was a bit below the x-axis. TB-TJM-119, as another Angra dos Reis spectrum, had a one micron feature with a zero-crossing point that was a fair bit below the x-axis but everything else seemed fine. When comparing the ~ 1 µm feature differences in minima from lowest reflectances and polynomial fittings, all but one had differences greater than 5 nm: MR-MJG-103 first spectrum had 8 nm, MR-MJG-103 second spectrum had 13 nm, MT-TJM-010 had 10 nm, TB-TJM-057 had 10 nm, TB-TJM-062 had 0 nm, and TB-TJM-119 had -10 nm. For the samples that had second features, two out of the four had minima differences less than or equal to 5 nm: MR-MJG-103 first spectrum had 5 nm, MR-MJG-103 second spectrum had 0 nm, MT-TJM-010 had 20 nm, and TB-TJM-119 had 20 nm. These minima comparisons are in figure 96.

It is interesting to note that even though D'Orbigny and Sahara 99555 had nearly identical endmember compositions and modal mineralogies, they also had similar appearing spectra. However, the minima were fairly different throughout the three different methods, although they were still in the same general area. The asymmetry of the one micron feature could have potentially contributed to those differences, as could possible pyroxene zoning. All three spectra for Angra dos Reis appeared to be similar spectrally but varied a bit with the minima as well. They had the least reflectance of all the samples, possibly because they had the least amount of anorthite. These minima can be found in tables 12 and 14 below.
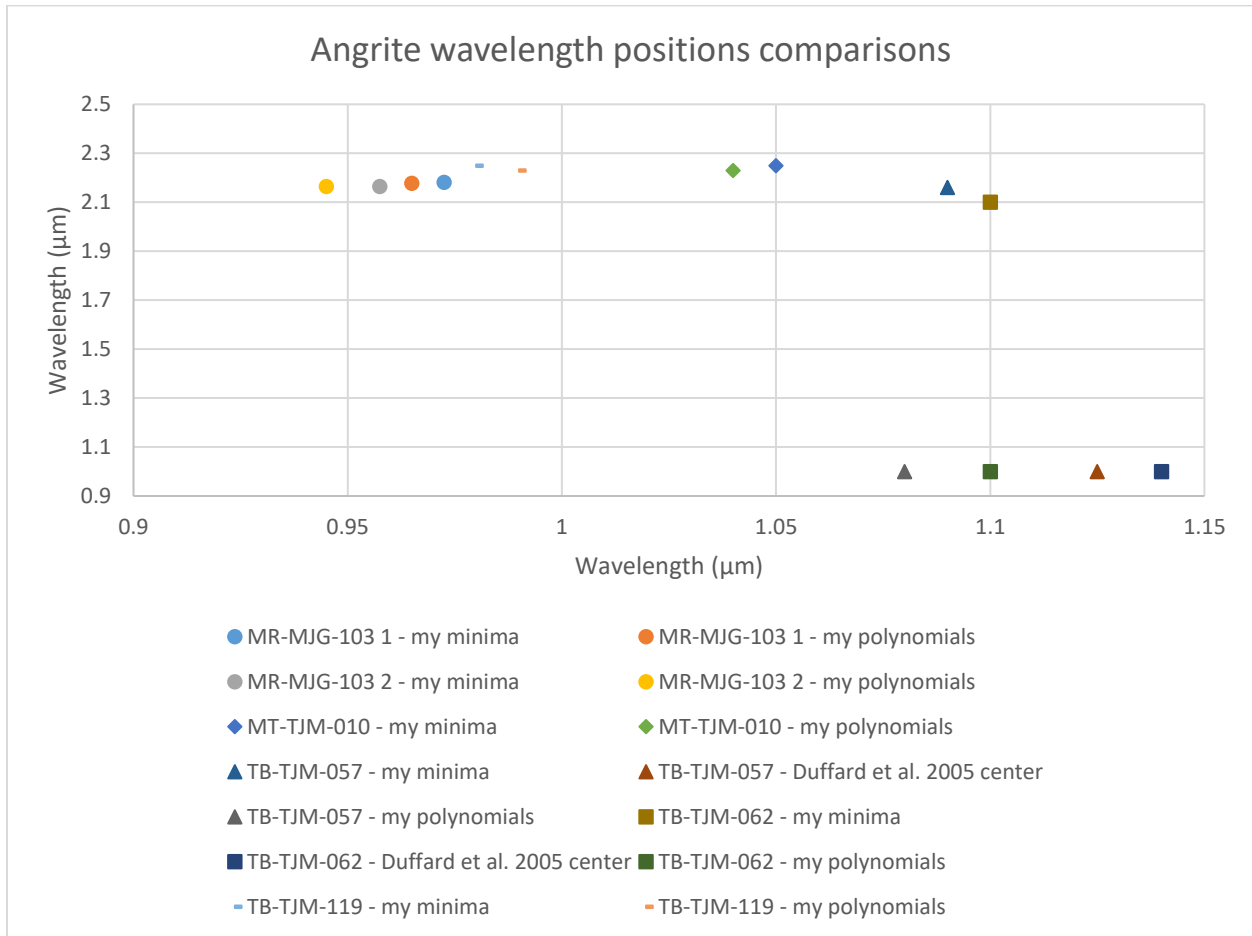


Figure 96. Angrite spectra minima from original minima I found, minima I found from polynomial fitting, and centers from the literature. The different shapes stand for the different samples. Sources: RELAB, Duffard et al. 2005, McCraig et al. 2017.

# Using this information to compare with angrites and potential asteroid parent bodies

Angrites have been touched upon before in the meteorites and angrite sections above. While these are enigmatic meteorites, there are a few ideas of possible parent bodies, as it is believed that they all came from the same body or area in the solar system (Burbine et al. 2006-ref Greenwood et al. 2005). However, none have even been termed a plausible parent body so far. Some of the rarer asteroid classes and groups might provide some clues, such as the O-type class from the Binzel classification (Cloutis et al. 2006a-ref Binzel et a. 1993). There are few asteroids assigned to this class, one being 3628 Božněmcová. While this class is thought to be related to LL-chondrites, there is also a possibility that Božněmcová is related to angrites (Cloutis et al. 2006a; Burbine et al. 2011-ref Binzel et al. 1993). Asteroid 7472 Kumakiri is also similar to Božněmcová (Burbine et al. 2011). However, no known meteorite seems to spectrally match either of these asteroids (Cloutis et al. 2006a; Burbine et al. 2011). Another potential asteroid for comparison to angrites is the L5 Mars Trojan, 5261 Eureka. This is mainly made up of olivine and is likely in the A or S(I) class in the DeMeo et al. taxonomy and the $S_r$ class in the Bus and Binzel taxonomy, all of which are rarer classes (Borisov et al. 2016-ref Bus & Binzel 2002, Rivkin et al. 2007, DeMeo et al. 2009, Lim et al. 2011). It does not appear to have a 2 μm feature (Rivkin et al. 2007). Rivkin et al. (2007-ref Burbine et al. 2006) consider it to be similar to angrites LEW 86010 and Sahara 99555 especially. In addition, they modeled the asteroid using Hapke's bi-directional scattering model with five angrites and a neutral phase, which aided this meteoritic analog hypothesis (Rivkin et al. 2007). They also consider R chondrites to be a potential match, albeit not as strongly, as it matched less in the shorter wavelength regions and the R chondrite used for comparison had heterogeneous spectra (Rivkin et al. 2007-ref Berlin et

al. 2003). Asteroids 289 Nenetta and 3819 Robinson are also under consideration, both being S(I) from the Gaffey et al. (1993) taxonomy, while being A and S$_r$, respectively, from the Bus and Binzel taxonomies (Burbine et al. 2006-ref Bus & Binzel 2002b; Borisov et al. 2016-ref Gaffey et al. 1993, Bus & Binzel 2002, Sanchez et al. 2014). While A types are mainly olivine, there are possibly some related to angrites with type A clinopyroxenes as well (Golubeva & Shestopalov 2006). Golubeva and Shestopalov (2006) found using the 0.5 µm feature of Nenetta that there was pyroxene on the surface spectrally. A-type and S(I) asteroids 2501 Lohja and 3819 Robinson do have a detectable 2 µm feature, indicating some pyroxene and are therefore considered to be olivine-rich asteroids (Sanchez et al. 2014-ref Sunshine et al. 2007). Burbine et al. (2006) found that Robinson was similar to some angrites in visible wavelength spectra but not in the infrared, however. They are considered to possibly be related to pyroxene pallasites, brachinites, ureilites, and R-chondrites (Burbine et al. 2006; Sanchez et al. 2014-ref Mittlefehldt et al. 1998). Sanchez et al. (2014) refer to Nenetta and Eureka as being monomineralic-olivine asteroids, but that generally just means that they do not have a 2 µm feature. However, Sanchez et al. (2014) think that Nenetta's meteorite analogs are brachinites or maybe R chondrites. This conclusion is based off of the information they gathered about the olivine from the spectra, as well as the albedo. Eureka was found to possibly match angrites mainly due to the "broad absorption feature centered around 1 µm, "(Sanchez et al. 2014-ref Burbine et al. 2006 quote, Rivkin et al. 2007). Other possibilities for this asteroid is it being related to brachinites and R chondrites, which was considered after also examining thermal spectra (Sanchez et al. 2014-ref Rivkin et al. 2007).

Previous angrite-like mixtures have been made in order to compare laboratory spectra to an angrite-like asteroid, 3628 Božněmcová (Cloutis et al. 2006a). These are in figure 97 and

188

further info on the samples and mixtures are in tables 1, 6, 9, and 10 in the appendices. Since the mixtures were hard to see because most were at the same reflectance, I added them in 0.25 intervals to separate them. Using anorthitic plagioclase feldspar PLG108 of $An_{85}$ with a type A clinopyroxene PYX009 of $En_{39.8}Fs_{9.7}Wo_{50.5}$, they found that plagioclase feldspar did not contribute much spectrally until it was at a ratio of 1:1 plagioclase feldspar to clinopyroxene. Otherwise, at modest amounts it slightly increased reflectance and decreased one micron absorption feature depths. This lack of spectral influence was apparent in that the pyroxene features barely or did not at all move for the first two mixtures and the pure clinopyroxene, when there was still no olivine. When the mixture included olivine OLV003 at $Fa_{10}$, an increase in plagioclase feldspar also decreased the full width half maximum of the band width (Cloutis et al. 2006a). With olivine, increasing it widened the one micron feature and it looked more like the olivine one micron feature (Burbine et al. 2006; Cloutis et al. 2006a). In figure 97 this appeared to start occurring particularly around BOZ005, when the pyroxene features were at their faintest before becoming the broad combined one micron feature. It was actually in this spectrum that the one micron combined feature started to go to shorter wavelengths, likely due to the increases in olivine. In the previous two spectra, BOZ003 and BOZ004, there were more defined separate features. The 0.9 µm pyroxene feature moved to longer wavelengths, while the 1.1 µm feature moved to shorter wavelengths. In mixture BOZ008 there was an equal amount of olivine and clinopyroxene and the one micron feature resembled olivine, albeit one with weaker features. With additional calcic olivine, which are present in angrites, the 0.95 µm feature's depth would increase, in comparison to the 1.15 µm feature of a Type A clinopyroxene (Cloutis et al. 2006a-ref Burbine et al. 2001). Finally, in BOZ009, the combined one micron feature actually went to a longer wavelength again, possibly because the plagioclase, whose minimum was at a longer

wavelength, was present in the same amounts as the olivine and clinopyroxene. It is worth noting that the clinopyroxene used in this study did have slightly less ferrous iron than typical angrites (Cloutis et al. 2006a).
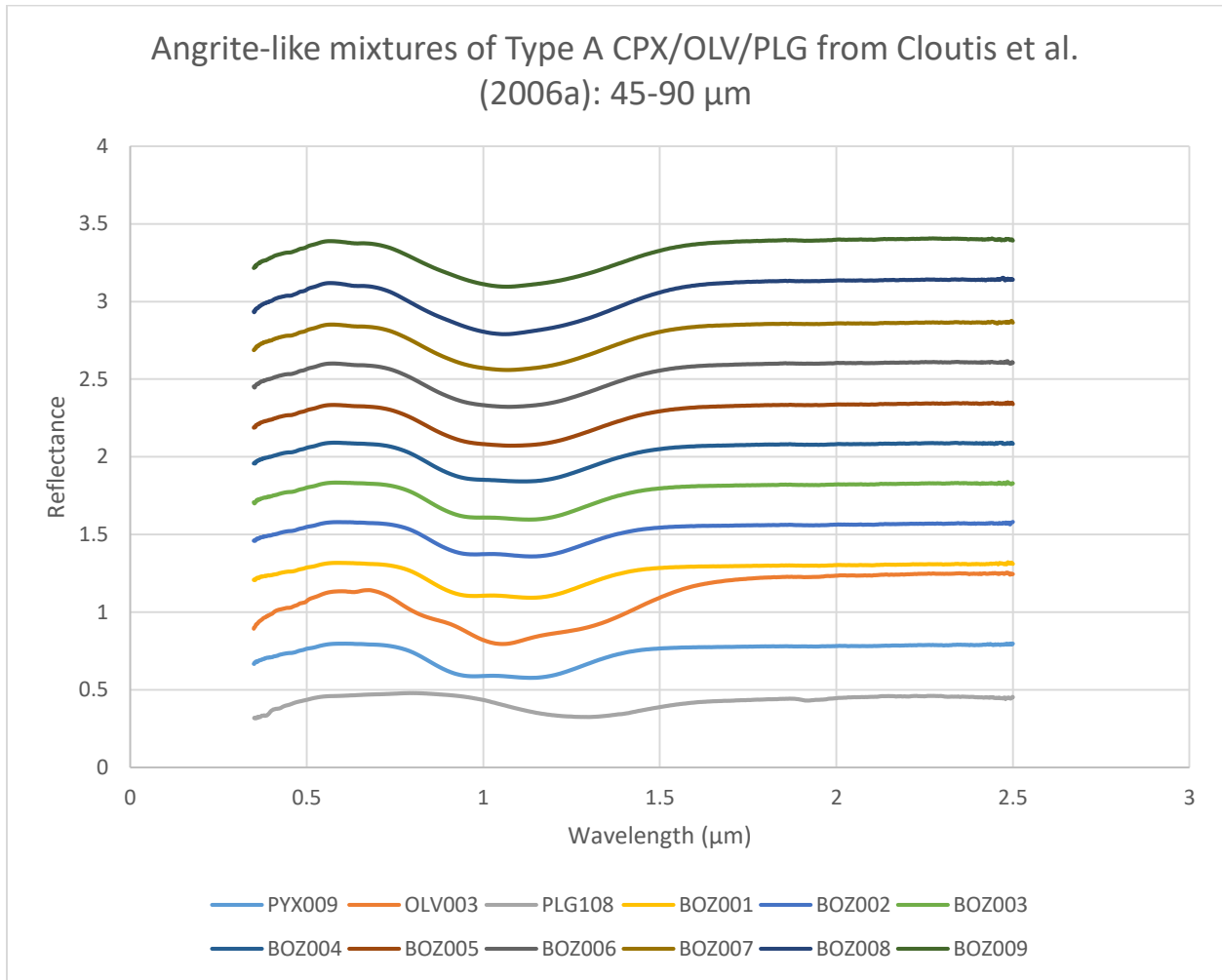


Figure 97. Mixtures from Cloutis et al. (2006a). The different spectra have all been added 0.25 reflectance except for PLG108. Sources: HOSERLab, Cloutis et al. (2006a).

Cloutis et al. (2006a) noted that "because absorption bands in the 1 um region of many type A clinopyroxenes and in the spectrum of Božněmcová are broad and shallow, our determination of absorption band positions was limited to a visually determined minimum position or the point of most abrupt slope change." As mentioned several times previously in the samples and mixtures sections above, this presented a problem to me as well, which is why I

found polynomial fitted minima of these mixtures. As with the minima found by lowest reflectance, there was nearly no change in either the 0.9 or 1.1 µm features for the first two mixtures of BOZ001 and BOZ002. With BOZ003, again the 0.9 µm feature jumped to a longer wavelength, while the 1.1 µm feature decreased. This continued with BOZ004, although the lowest reflectance minima had two features and I was only able to polynomial fit one feature. In BOZ005 there again was an increase in wavelength in the first 1 µm feature for the lowest reflectance minimum. For the polynomial fitted minimum, BOZ005 had a 1 µm feature that decreased, but that is because there was only one fitted feature for BOZ004. For both sets of minima, BOZ006 through BOZ008 had minima that decreased in wavelength until BOZ009, where the minimum increased slightly.

The fitting of BOZ003 had the first of the two 1 µm features as fainter than the previous two mixtures of BOZ001 and BOZ002, although there were no apparent issues with the fitting besides a lower but still decent $R^2$ value. I was not able to fit that feature in any of the following mixtures because it became too faint. There were no other issues with the polynomial fitting. The mixture spectra that had differences of the polynomial fitting and lowest reflectance 0.9-1 µm minima greater than 5 nm were PLG108 at 17 nm, BOZ004 at -9 nm, and BOZ005 at -7 nm. None of the mixture spectra with features around 1.1 µm had minima differences greater than 3 nm. These minima are compared in figure 98, where the spectra with only one feature are graphed against one micron.
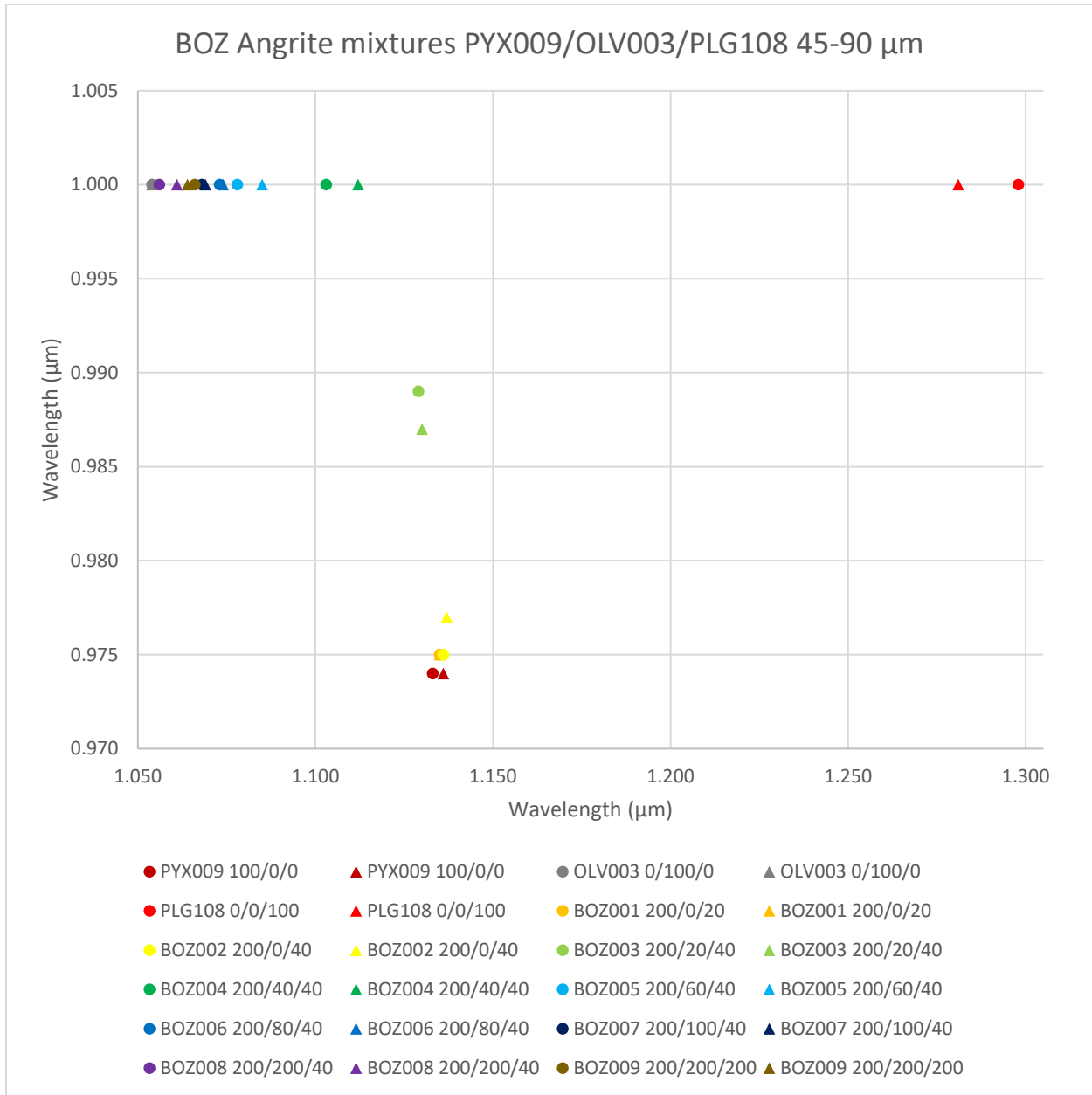
Figure 98. Minima comparisons for the BOZ mixture spectra of PYX009, OLV003, and PLG108. The circles are the minima I originally found and the triangles are the minima I found using polynomial fitting. Sources: HOSERLab, Cloutis et al. 2006a, McCraig et al. 2017.

To build off of Cloutis et al. (2006a), I worked with Dr. Ed Cloutis to make some more

angrite-like mixtures, using PYX009, OLV003, and PLG122. The first two were used in Cloutis

et al. (2006a) and because of limited quality type A clinopyroxene samples, PYX009 had to be

used again. While it had low amounts of titanium and aluminum, and lower amounts of iron in

comparison to angrites, it did have the right calcium amounts. It did not have any measured ferric iron as well. There was also enough sample remaining to make mixtures. In addition, it was the type A clinopyroxene sample with the least amount of slope and noise affecting the two main features; it was easy to find the minima using both the lowest reflectance and polynomial fitting methods. OLV003 was used because there was enough of the sample available and it did not have impurities. I tried to find an olivine sample with angritic amounts of calcium but that was not an available option. PLG122 was not used in the previous mixtures. There was enough of the sample remaining so I decided to use it in these mixtures. It was not included in every mixture spectra, as plagioclase has less of an impact on spectra than the olivine and pyroxene. I also chose this sample because it had a close match to anorthitic plagioclase feldspar in angrites. This sample is weathered but it was used in small amounts so it likely it is not an issue. For their chemical compositions and endmember compositions, see tables 10 and 11 in the appendices.

There are many holes in the literature when it comes to olivine and type A clinopyroxene mixtures so I had eighteen different spectra done to approximate some angritic mixtures. The intervals for olivine and clinopyroxene were 10 % until 70/30 olivine/clinopyroxene, where after the intervals were 5 % with increasing olivine. I was hoping to see if I could catch any changes with the increasing addition of clinopyroxene. For example, other meteorite types have lower amounts of type A clinopyroxene. In this way, it differs from Cloutis et al. (2006a) as well. The addition of plagioclase was in four spectra. It stayed constant at 10 %, while the clinopyroxene was added to the plagioclase and olivine at 5 % intervals starting at 5 % clinopyroxene, with the olivine decreasing respectively. I kept the plagioclase amount constant because it is present in angrites but does not contribute its own minima spectrally unless there is a large amount. This could be seen in the mixtures section above, particularly the AG-TJM and MX-CMP mixtures.

This was also seen in the BOZ mixtures. A graph of the different spectra from this series is in

figures 99 to 101, where I show all mixtures, the olivine and clinopyroxene mixtures, and the

mixtures that include plagioclase, respectively. The color scheme is ROYGBV, with red starting

as 100 % clinopyroxene and continuing with decreasing clinopyroxene.
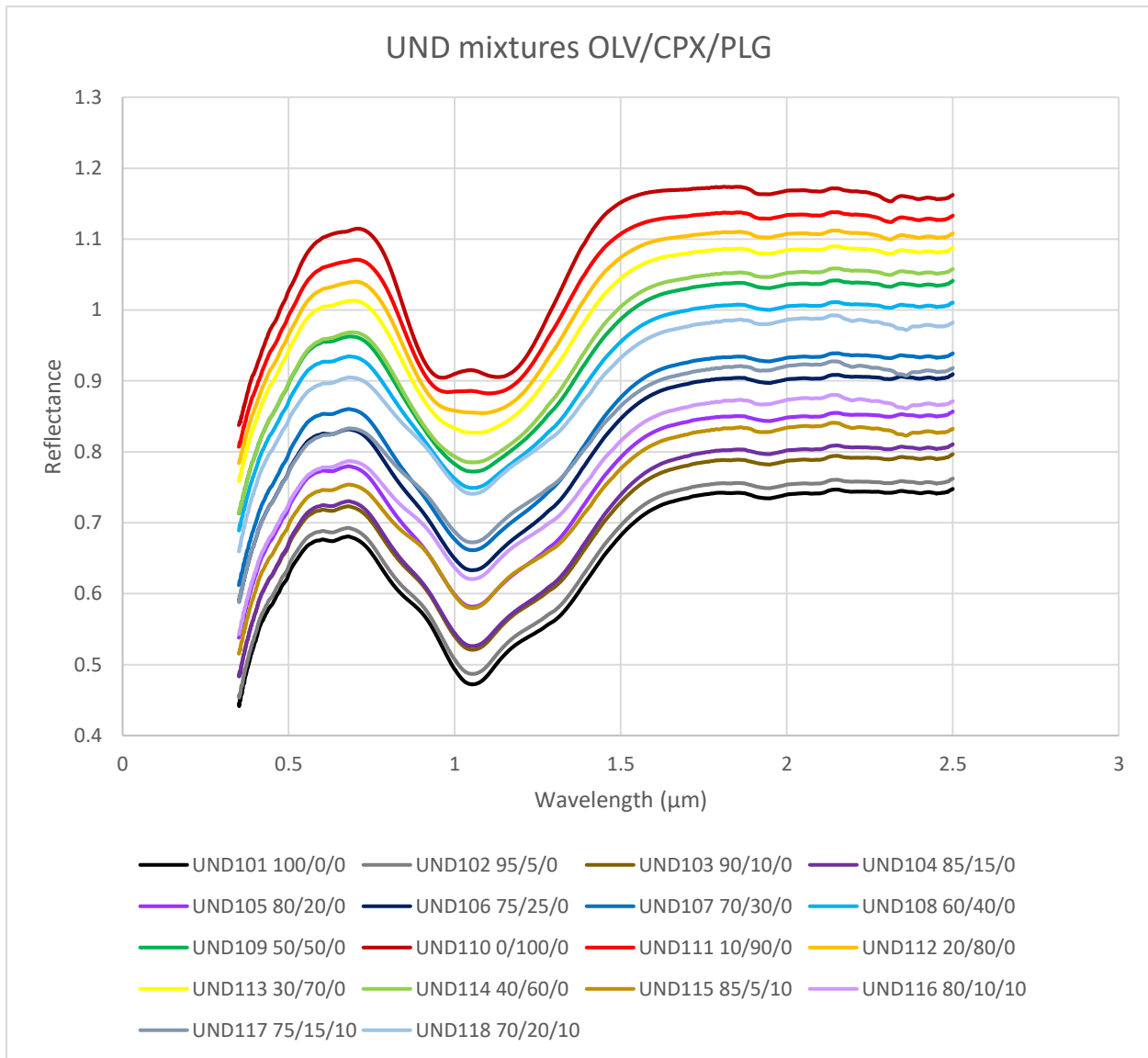


Figure 99. All UND spectra of type A clinopyroxene PYX009, olivine OLV003, and plagioclase PLG108. Spectra are offset by +0.025 in order to make them easier to view. Source: HOSERLab.
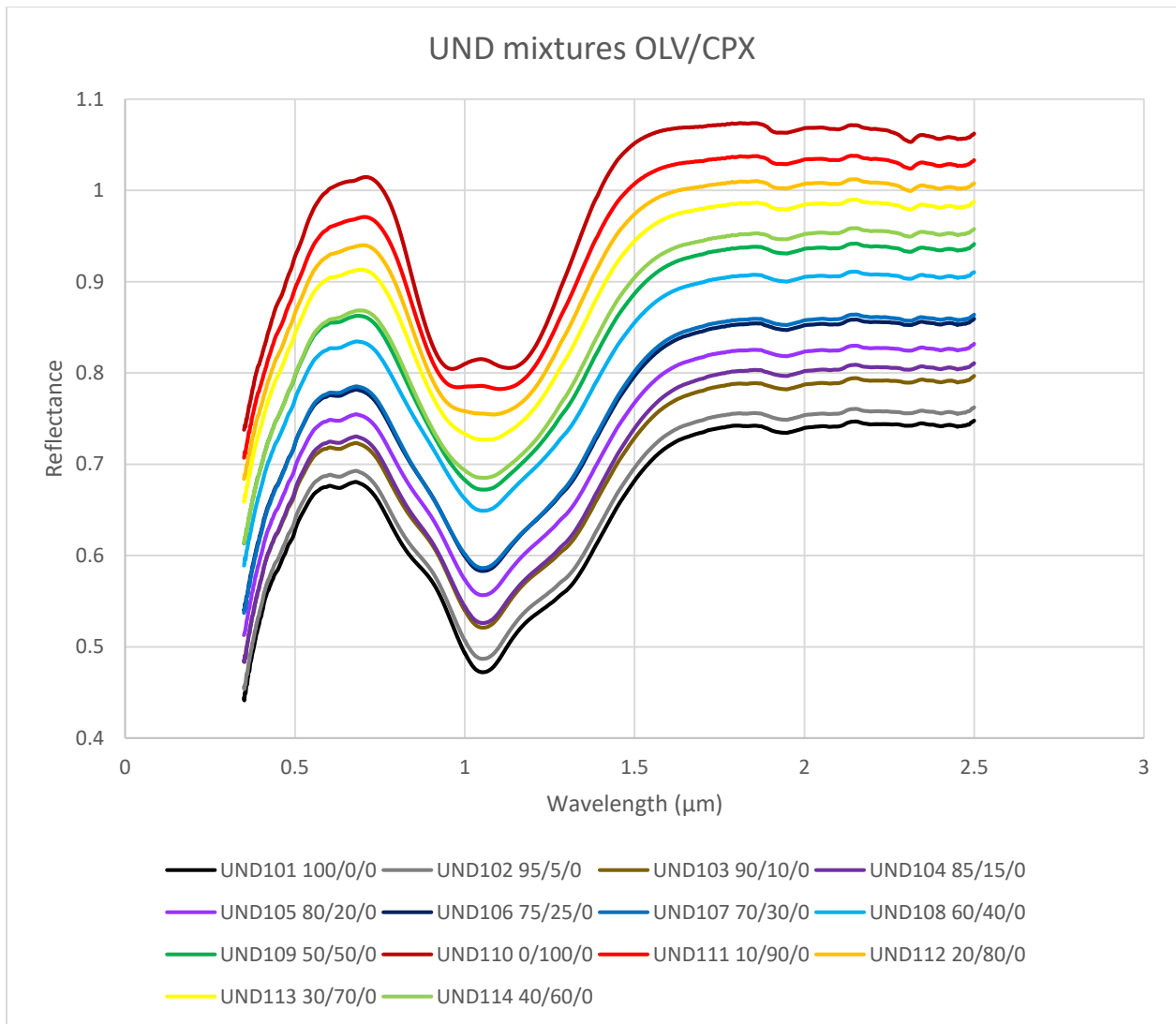
Figure 100. UND spectra of type A clinopyroxene PYX009 and olivine OLV003. Spectra are offset by +0.025 from figure 99 in order to make them easier to view. Source: HOSERLab.
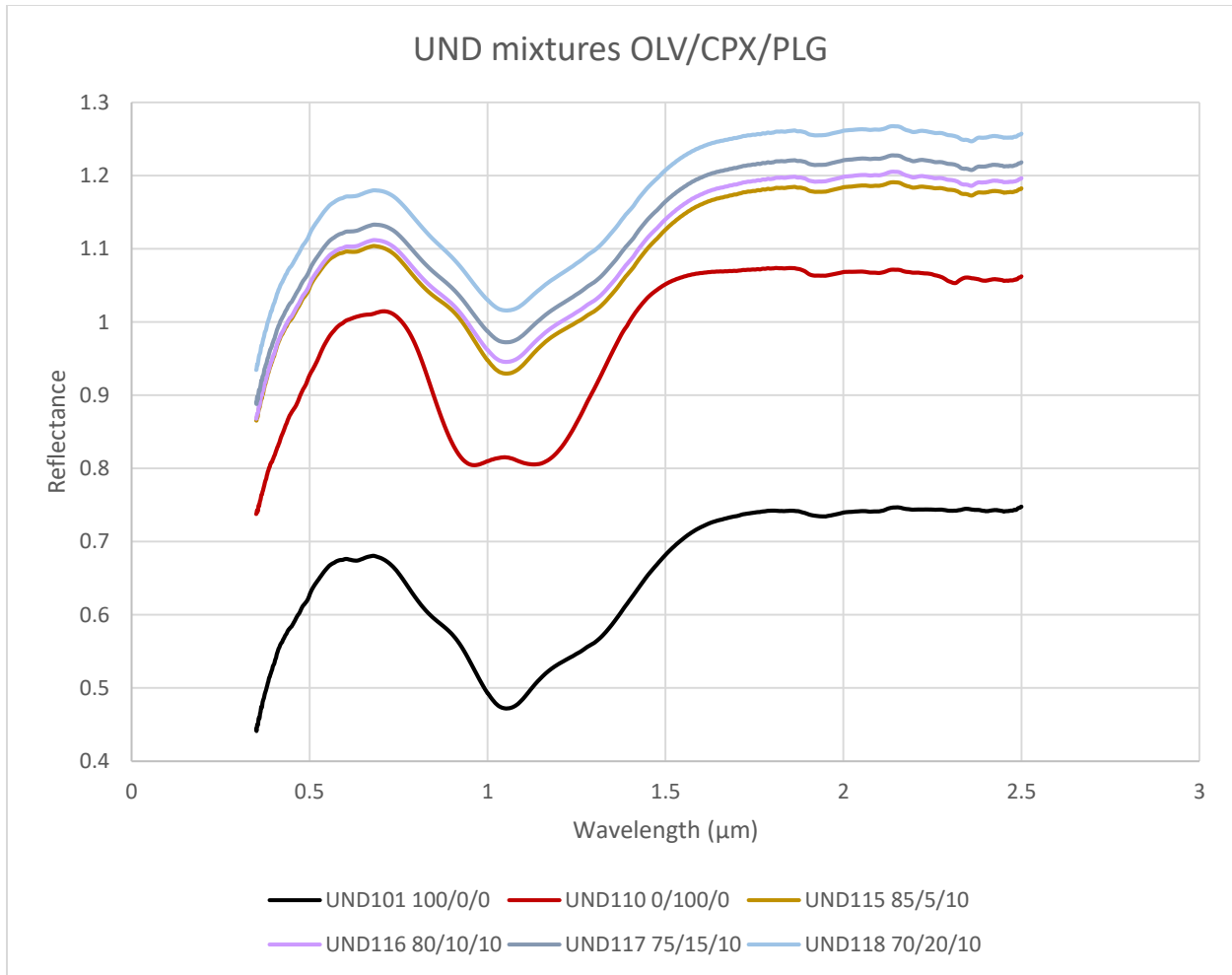
Figure 101. All UND spectra of type A clinopyroxene PYX009, olivine OLV003, and plagioclase PLG108. Spectra are offset by +0.025 from figure 99 in order to make them easier to view. Source: HOSERLab.

As was to be expected, olivine dominated the spectra until clinopyroxene was around fifty percent. That was when one can start seeing the main olivine feature around 1 µm widen. I was interested to see if there were any changes in the olivine 1 µm feature position with the increase in clinopyroxene. I found minima using both lowest reflectance and polynomial fitting, in the same methods as previously used. Figure 102 shows the first method while figure 103 shows the latter. There were no issues with the polynomial fitting. I was only able to fit two main features when the mixtures included at least 90 % clinopyroxene. For the spectra that only had one main feature I graphed the minima versus one micron.
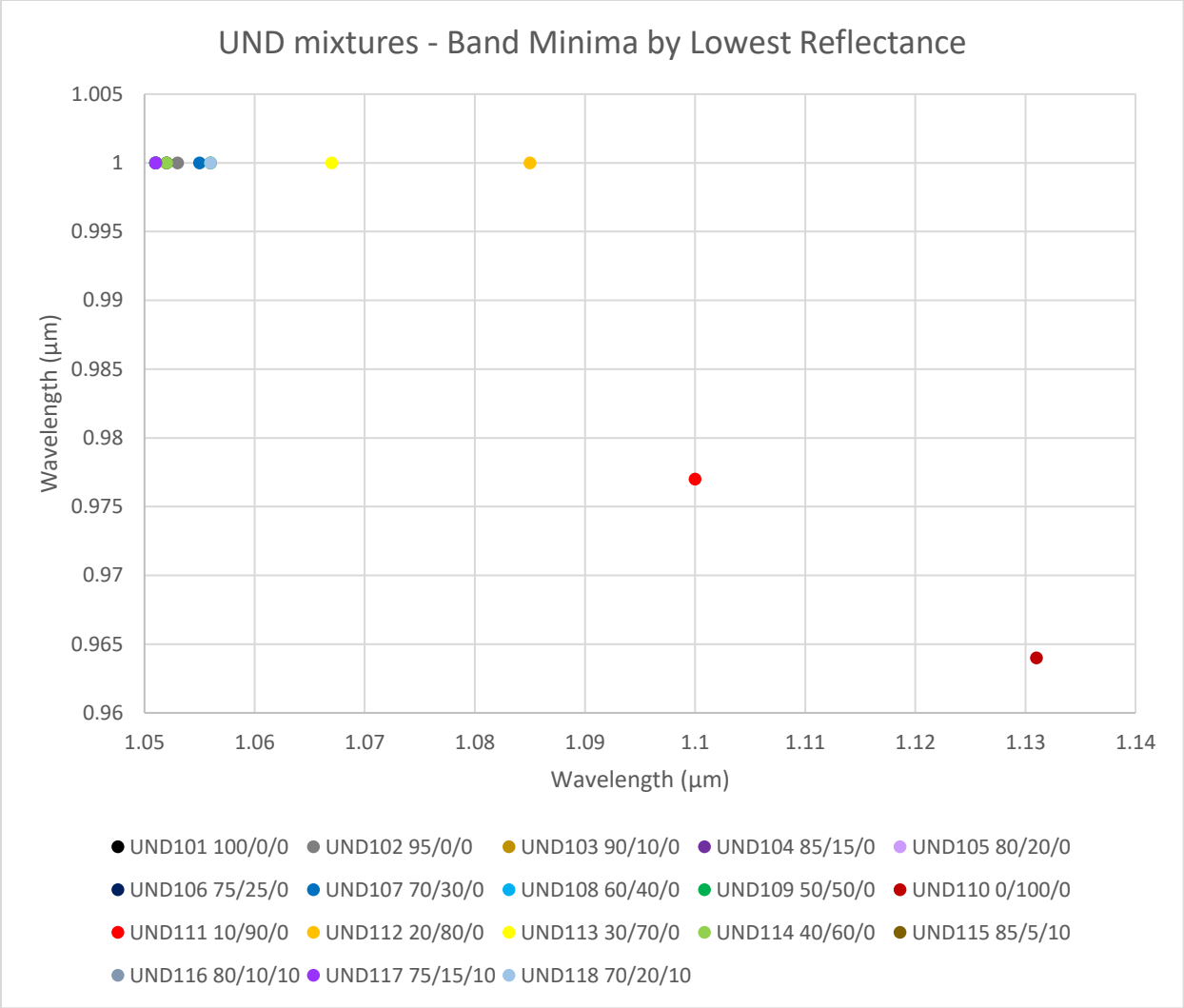
Figure 102. Minima of the UND mixtures found using lowest reflectance. Source: HOSERLab.
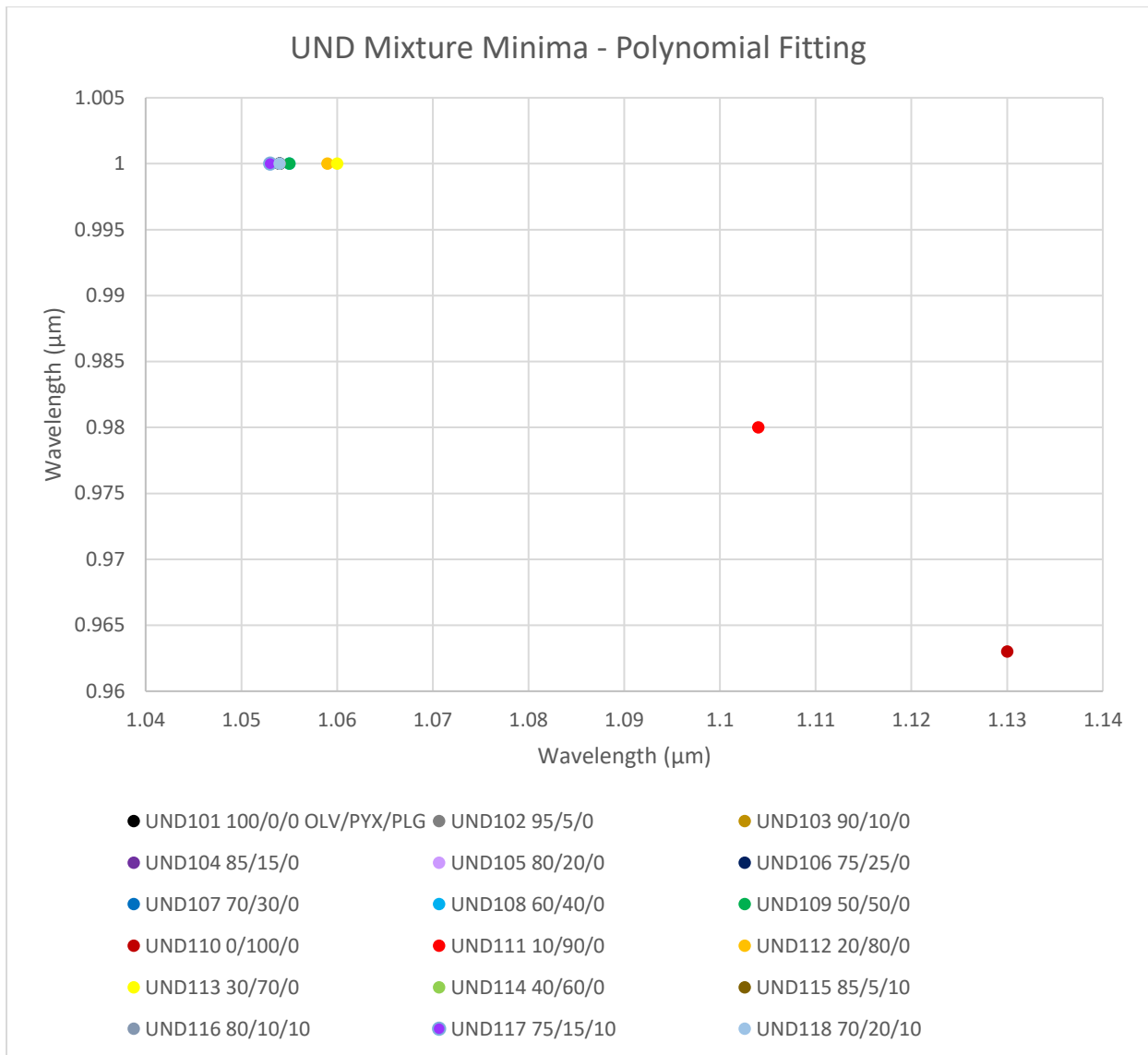
Figure 103. Minima of the UND mixtures found using third order polynomial fitting. Source: HOSERLab, McCraig et al. (2017).

When comparing the minima found from both methods, only two minima had differences between the different methods greater than 5 nm: UND112 at 26 nm and UND113 at 7 nm. UND112 was so high because it was a transition mixture where the amount of high-calcium clinopyroxene was finally high enough that two distinct features around 1 μm started to become visible. So it was useful to see that both methods generally seemed to work. However, caution needs to be used for the lowest reflectance method if there is large asymmetry and/or noisy

features, as can be seen in the previous sections. In those cases, polynomial fitting is better. For

the mixtures of only olivine and clinopyroxene, the polynomial fitting showed a constant

minimum for all until 60/40 olivine/clinopyroxene, where it increased one nanometer. It

decreased two nanometers and then jumped seven nanometers for the 40/60 spectrum. The

changes of a couple nanometers were within the resolution of 2 to 7 nm, so I cannot attribute

such a small amount to mean anything. The jump from 1.059 µm to splitting to 0.98 µm and

1.104 µm from 20/80 to 10/90 was a big jump from the two different clinopyroxene features

becoming discernable. They then decreased in wavelength position to 0.963 µm and increased to

1.13 µm for 0/100. The lowest reflectance minima jumped around several nanometers for the

first few spectra of the mixtures where olivine was at 100 % and then started to decrease with

increasing clinopyroxene. These minima generally acted similarly to the polynomial fitted

minima in that the changes were usually only a few nanometers until higher amounts of

clinopyroxene. These changes and minima can all be seen in table 11 in the appendices, as well

as the spectra graphs above. For an easier comparison, the graphs of both kinds of minima are

shown together in figure 104, with circles being my original lowest reflectance minima and the

triangles being the minima from polynomial fitting.

For the four spectra that included plagioclase, there did not seem to be much changing in

wavelength position with an increase in clinopyroxene. This could be because of the limited

spectra available. The lowest reflectance minima were steady from UND115 to UND117 then

increased in five nanometers from 75/15/10 to 70/20/10 olivine/clinopyroxene/plagioclase. The

polynomial fitting showed basically no changes, as the minima were going back and forth one

nanometer. Therefore, I do not think there were any visible changes from the addition of

clinopyroxene in these limited three-mineral mixtures.
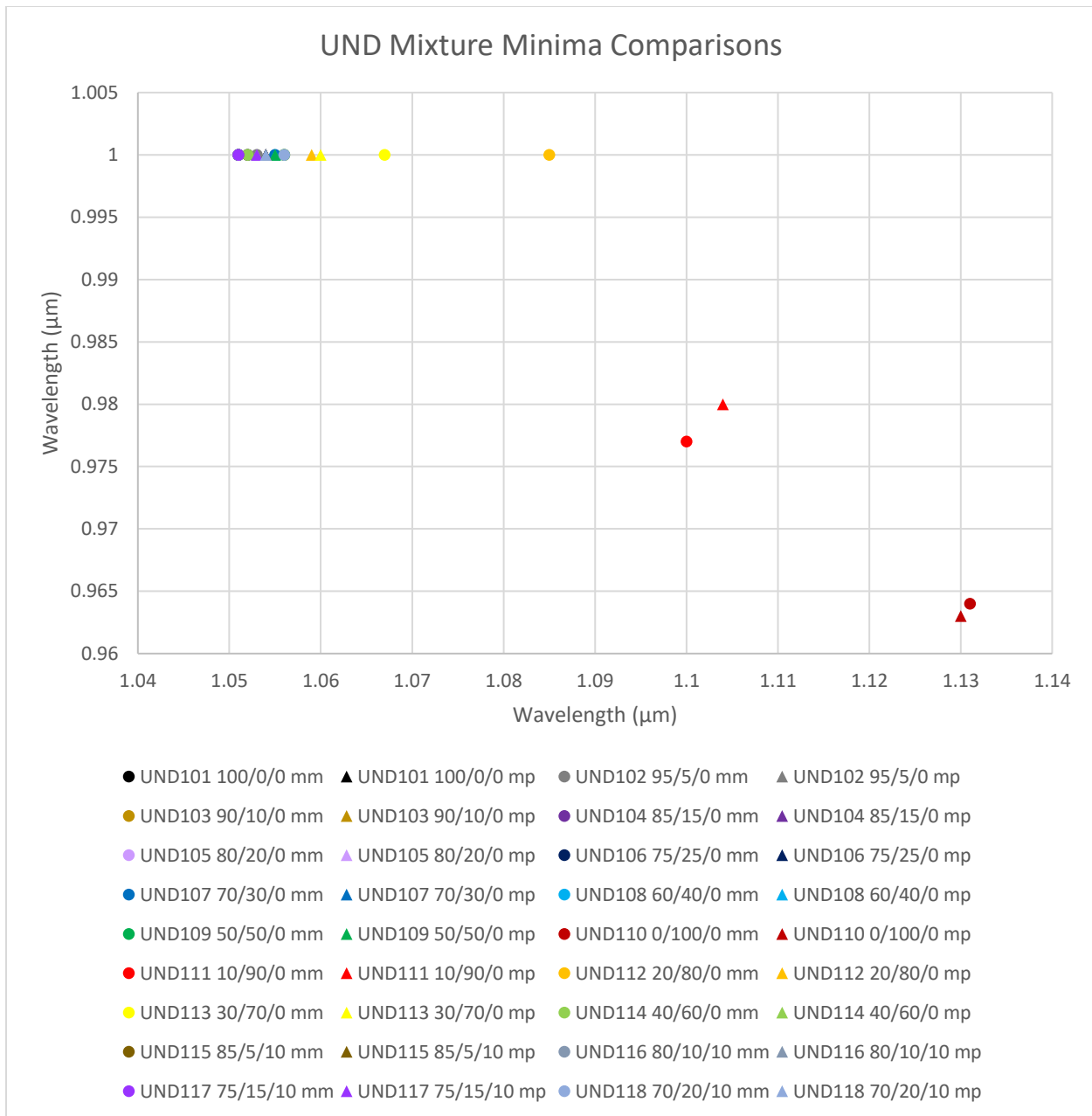
Figure 104. Minima of the UND mixtures found using lowest reflectances (circles) and third order polynomial fitting (triangles).
Source: HOSERLab, McCraig et al. (2017).

## Conclusions and Future Work

For this paper, I tried to examine high calcium clinopyroxenes to try and see if there was

a possible relationship between band positions and iron and calcium contents. I particularly was

interested in examining the type A clinopyroxenes because of their rarity in the literature and

their prevalence in angrites. I also looked at mixtures that included calcic pyroxenes along with orthopyroxenes, olivines, and/or plagioclase feldspar. I used these mixtures to observe spectral changes when abundances of certain minerals were varied. Finally, I also looked at some angrite spectra and angrite-like mixtures to observe additional spectral changes when applied to a specific meteorite group.

As a reminder, the two major pyroxene features are around approximately 0.9 and 1.8 µm for orthopyroxenes, 0.9 and 2 µm for pigeonites, 0.9 and 1.15 µm for type A clinopyroxenes, and 1 and 2.3 µm for type B clinopyroxenes. I first found the minima for the selected samples in this paper using the lowest reflectances around the band absorption features, specifying the range in Excel for each one. I attempted to find the minima using this method for all the smaller absorption features as well, although there was much more error due to the weakness and slope of these features. For both of these steps, I wanted to see if there was any kind of trend line from the different types of pyroxenes, such as found in Cloutis et al. (1991) for the orthopyroxenes and type B clinopyroxenes.

The possible issues with finding the minima from lowest reflectances mainly arose when there were noisy features, features on a slope, or asymmetrical features. Unfortunately, the type A clinopyroxenes in particular had minima that were usually difficult to get because many samples had reddened slopes from ferric iron and titanium. They also typically had much weaker features than the other types of pyroxenes. The orthopyroxenes and type B clinopyroxenes had cleaner spectra, although the two micron features sometimes had water features that interfered with the lowest reflectance. Because of this I either had to change the wavelength range for finding the minimum of a feature or accept that there was likely some error; the latter happened when the noise was around the minimum and could not be taken out of the wavelength range. In

cases like those, the polynomial fitted minima were more useful, as they were usually able to ignore the noise and find minima in a fitted curve. However, if the noise was especially strong, the curve was more twisted and the fitting was not as good as hoped. Luckily, those occasions were rare. The polynomial fitting also used specific wavelength ranges around the absorption features. I used equations and spreadsheets from McCraig et al. (2017) for those minima. Unfortunately, they did not necessarily seem to be much better for sloped minima than the lowest reflectance minima, as part of the process for the fitting involved picking a range that was generally symmetrical, with the ends of the ranges having similar reflectances. The polynomial fittings rounded out asymmetrical features, although those were mainly seen in spectra of mixtures. In general, the band I features had the most similar minima when compared from both of these methods, while the band II had larger differences due to the slope and water features impacting lowest reflectance minima.

I chose these two methods because they are the most repeatable. Other papers have used many different methods, such as dividing or subtracting the continuum or models. While these can be useful, they are not as repeatable because of the processes and inputs involved. The lowest reflectance method of finding minima is easier and more repeatable with the same spectra, as it is the same process each time. Unfortunately, the method does have weaknesses with noisy and sloped spectra, as just described. The polynomial fitted method of finding minima was useful for the features that had problems with the lowest reflectance minima, such as previously stated. They as a whole appeared to be more accurate, as even tiny amounts of noise could affect the minima found from lowest reflectances. It required more work, as it used equations in addition to selected wavelength ranges, but as long as the methods and steps used

are shared, it is generally repeatable as well. The wavelength ranges for the minima found by lowest reflectance are also important to share for repeatability.

I hoped to find some possible trends and to include samples that are underrepresented in the literature, like type A clinopyroxenes and pigeonites. As previously stated, there are a lack of these types of samples in mineral databases due to rarity and/or exsolution issues. I continued work on the Cloutis et al. (1991) apparent trendline between orthopyroxene and type B clinopyroxene. As expected, the orthopyroxenes were at the bottom of the line, followed by some pigeonites mixed in between, and then the type B clinopyroxenes at the top with the longest wavelength positions. The orthopyroxene area was straighter, suggesting a more linear relationship between iron content and band position. The type B clinopyroxene area was more curved and random, suggesting less linearity between iron and calcium contents and band position. In general the features for type B clinopyroxenes did weakly appear to be at longer wavelengths with increasing calcium and more so at longer wavelengths with decreasing iron. The one micron feature appeared to follow these trends more so than the two micron feature, possibly contributing to the more random appearance than the orthopyroxenes. As a reminder, the one micron features usually had less error too, however. The orthopyroxenes did appear to have a much stronger linear relationship with iron content than calcium, as both features had positions that increased with increasing iron. This had been discussed in the literature before (Klima et al. 2011). The type A clinopyroxenes had less of a semblance of any possible trend, as there were too few samples and most had minima that were difficult or impossible to find. The minima graphed were scattered when compared to both iron and calcium amounts.

The mixtures I looked at generally went along with previous trends in the literature for both kinds of high-calcium clinopyroxenes. While there were not many examples of type A

clinopyroxene-olivine mixtures in the literature, I still found similar results with the

PYX150/OLV003 mixture in figures 58 and 61, the BOZ mixtures in figures 97 and 98, and the

UND mixtures in figures 99-104. Even though the latter two mixtures also have plagioclase in

them, the amount of plagioclase is usually small enough that it did not contribute spectrally, with

the exception of higher reflectances. In all of these mixtures, the olivine and clinopyroxene

features were combined into one broadened one micron feature until there was nearly all

pyroxene, typically more than 80 %. The one micron feature also did not appear to move much

in wavelength position from the olivine minimum until there were large amounts of

clinopyroxene as well, where it finally split into two features around 0.9 and 1.15 µm. When

type A clinopyroxene was mixed with orthopyroxene, which happened in only two mixtures in

figures 56 and 57, PYX150 with PYX032, the orthopyroxene also dominated the spectra until the

mixtures were predominantly clinopyroxene. In these mixtures, which were done with two

different grain sizes, the one micron combined feature generally decreased in wavelength with

increasing orthopyroxene, hovering around the same point once there was at least 50 %

orthopyroxene in the mixture. For the other two features, the clinopyroxene feature around 1.15

µm was visible until there was 30 % orthopyroxene in the mixture. After that, the ~ 1.8 µm

feature varied a bit around the same spot. The 1.8 µm feature also was visible even when there

was only five percent orthopyroxene in the mixture. These two kinds of mixtures of olivine and

orthopyroxene with type A clinopyroxene show that while the clinopyroxene does make an

important impact in the different mixtures, it was only able to be measured when there were high

levels of clinopyroxene, usually at least around 70 %. Hopefully more mixtures will be made in

the future, perhaps with varying iron, calcium, and other cation contents, in order to continue

these studies and make stronger conclusions.

The type B clinopyroxenes examined from the databases also agreed with the literature. When type B clinopyroxene was mixed with orthopyroxene, there were eight groups of mixtures. Since both of these pyroxenes have two main features, mixtures of them sometimes included two features near 2 µm; others sometimes had straighter slopes near 2.3 µm that indicated the presence of clinopyroxene. Usually these two features or straighter slopes occurred when the mixtures were from 25/75 to 75/25 orthopyroxene/clinopyroxene, although not all of these minima were able to be found due to faintness or slope. This was also seen in Singer (1981), where the one micron feature was a bit asymmetrical when the mixture included both pyroxenes. In these mixtures, orthopyroxene generally was spectrally stronger than the clinopyroxene.

When type B clinopyroxenes were mixed with olivine, there was one group of mixtures, between PYX016 and OLV003. This group had mixtures separated by 20 weight percent, so there was less detail. The one micron combined feature for PYX016 and OLV003 hovered around the same spot, as they were also both located near the same location. The two micron feature that was only from the clinopyroxene stayed around the same spot with the lowest reflectance minima. However, with the polynomial fitted minima it decreased with increasing clinopyroxene, until the pure clinopyroxene spectrum, where it increased in wavelength again. While there was only one group of these mixtures in the databases, there were some in the literature. In Singer (1981), where the olivine and clinopyroxene were measured in 25 weight percent intervals, the olivine longer wavelength lobe was present even at 75/25 clinopyroxene/olivine, while the two micron clinopyroxene feature was present at 25/75. The pyroxene was spectrally stronger in those mixtures.

When type B clinopyroxene was mixed with plagioclase, there was one group of mixtures, MX-CMP. The main note from these, as talked about in the literature and as seen in

other mixtures here, was that the plagioclase will only contribute spectral features when it is abundant. Even with only 5 % diopside, the spectrum mostly resembled clinopyroxene. By 75/25 plagioclase/clinopyroxene the plagioclase spectral feature was gone. The main impact on the spectra was that the plagioclase increased the reflectance of the mixtures.

There were also some mixtures that examined multiple minerals, including a group of with type B clinopyroxene, orthopyroxene, and olivine, and a group that included type B clinopyroxene, orthopyroxene, and plagioclase. For the first group, the one micron feature was distorted with higher amounts of olivine and the longer wavelength side lobe for olivine was present until there was less than 50 % olivine. When there were lower amounts of clinopyroxene, the mixture mostly resembled an olivine-orthopyroxene mixture, with the exception of some straighter slopes forming past 2.3 µm with increasing clinopyroxene. For higher amounts of clinopyroxene, the slopes were much stronger and appeared to be close to becoming second 2 µm features like in the orthopyroxene-type B clinopyroxene mixtures above. For the group of type B clinopyroxene, orthopyroxene, and plagioclase, the mixtures looked mostly like the pure orthopyroxene sample, as there was little clinopyroxene in most and there was not enough plagioclase to cause changes, as it ranged from 0 to 60 %. Some mixtures that had more clinopyroxene, up to 45 %, had the straight slope past 2.3 µm, indicating its presence. Finally, there was one mixture group of all four: type B clinopyroxene, orthopyroxene, olivine, and plagioclase. It is hard to come to conclusions because there are four different variables, but olivine did appear to dominate the spectra. This was likely because there was not less than 60 % olivine in any of these mixtures. Due to the lack of plagioclase, there were no features from it and even the reflectance didn't seem to increase with increasing plagioclase, possibly because there was orthopyroxene and clinopyroxene increasing in abundance as well. The features

around 2 µm were dominated by the orthopyroxene, because there was more of it than the clinopyroxene. In the samples that had higher amounts of clinopyroxene, there were straight slopes past 2.3 µm, however, indicating their presence.

In addition to the mixtures, I also looked at angrite and angrite-like mixture spectra. The actual angrite spectra had more reddened slopes than the angrite-like mixtures, due to additional titanium cations, but these still had similar results to the lone type A clinopyroxene and olivine mixture studied. They all had broadened one micron features that were a combination of the clinopyroxene and olivine features. The individual pyroxene features were only present when olivine was in low amounts, usually < 20 %. The mixtures showed that the one micron combined feature did not move much in wavelength until that point either, showing that there needs to be a large amount of the type A clinopyroxene to make changes that can actually be fitted from $3^{rd}$ order polynomials.

For future work with type A clinopyroxenes, one could examine and create more samples. There were few type A clinopyroxene samples available in the databases, which made it hard to find possible trends and compare. Even if I had found more certain minima for these samples, there were not enough available to make any possible conclusions. Since they are important in meteorites and asteroids, it would therefore be useful if the sample catalog could grow to provide more opportunities to study the band minima.

I briefly looked at the thermal spectra that were available for some of the samples. Some possible future work is to look at high-calcium clinopyroxenes in more depth at longer wavelengths. The reason I did not go into this is because the band positions at longer wavelengths are affected by other factors than the cations available, such as the grain size and

temperature. It would be interesting to see in future research how the different features from type A and type B clinopyroxenes compare with each other and their calcium and iron amounts. It is hard to do that currently with all of the other factors influencing their minima positions, but it would still be a worthwhile project. Potentially finding a calibration for pyroxenes in mixtures and the thermal infrared would also be very valuable.

Another area of research that could be looked at with examining more high-calcium pyroxenes is the angrite group. While rare, these meteorites are still an important piece in figuring out the evolution of our solar system, especially since they are thought to be one of the oldest meteorites types (McSween 1999 p.147). There are still no plausible parent bodies identified for them. Identifying type A clinopyroxenes, as well as type B, in asteroids that also have olivine is an important area of study for finding plausible parent bodies. Very few mixtures with type A clinopyroxene and olivine have been studied, however. As stated previously, the type A clinopyroxenes in particular were not even mentioned in the literature for many years. It would therefore be worthwhile to continue making more mixtures in order to compare with other known and unknown meteorites and asteroids.

Additionally, there is also another group of meteorites that have a high prevalence of high-calcium clinopyroxene. The Martian meteorites include shergottites, nakhlites, and chassignites, with a couple of other anomalous ones as well (McSween 1994). The Martian meteorite types with high amounts of clinopyroxene are basaltic shergottites and nakhlites, the latter being in plutonic rocks (McSween 1994; McSween 1999 p. 131, 134, 178). Since they are not from asteroids and have differing conditions on Mars, I did not delve into these types here. Mars, being much larger than asteroids, has an atmosphere and more sorting of grain sizes. It also has an abundance of dust that can affect spectra by weakening spectral features, but also has

some dark areas that may include soils (McSween 1994; McSween 1999 p.178). However, they

are interesting groups that can tell more about the surface of Mars and the impact of high-

calcium clinopyroxenes on spectra.

## Sources

1. Abe, M., Takagi, Y., Kitazato, K., Abe, S., Hiroi, T., Vilas, F., ... & Nimura, T. (2006). Near-infrared spectral results of asteroid Itokawa from the Hayabusa spacecraft. *Science*, *312*(5778), 1334-1338.
2. Adams, J. B. (1974), Visible and near-infrared diffuse reflectance spectra of pyroxenes as applied to remote sensing of solid objects in the solar system, J. Geophys. Res., 79, 4829-4836.
3. Adams, J. B. (1975), Interpretation of visible and near-infrared diffuse reflectance spectra of pyroxenes and other rock forming minerals, in Infrared and Raman Spectroscopy of Lunar and Terrestrial Materials (C. Karr, ed.), Academic, New York, 91-116.
4. Beck A. W. and McSween H. Y. 2010. Diogenites as polymict breccias composed of orthopyroxenite and harzburgite. *Meteoritics & Planetary Science***45**:850–872, doi:10.1111/j.1945-5100.2010.01061.x.
5. Binns, R. A. (1970). Pyroxenes from non-carbonaceous chondritic meteorites. *Mineral. Mag*, *37*, 649-669.
6. Bischoff, A. (2000). Mineralogical characterization of primitive, type-3 lithologies in rumuruti chondrites. *Meteoritics & Planetary Science, 35*(4), 699-706. doi:10.1111/j.1945-5100.2000.tb01453.x
7. Bischoff, A., Vogel, N., & Roszjar, J. (2011). The rumuruti chondrite group. *Chemie Der Erde - Geochemistry, 71*(2), 101-133. doi:http://dx.doi.org/10.1016/j.chemer.2011.02.005
8. Blaire, B. R. (2000). The role of near-Earth asteroids in long-term platinum supply. EB535 Metals Economics. Colorado School of Mines.
9. Borisov, G., Christou, A., Bagnulo, S., Cellino, A., Kwiatkowski, T., & Dell'Oro, A. (2016). The olivine-dominated composition of the Eureka family of Mars Trojan asteroids. *Monthly Notices of the Royal Astronomical Society*, *466*(1), 489-495.
10. Brearley, A. J. & Jones, R. H. (1998). Chondritic meteorites. In J. J. Papike (Ed.). *Planetary materials*. (p.3-01-3-398). Washington, D.C.: Mineralogical Society of America.
11. Burbine, T. H., McCoy, T. J., & Binzel, R. P. (2001, March). Spectra of angrites and possible parent bodies. In *Lunar and Planetary Science Conference* (Vol. 32).
12. Burbine, T. H., McCoy, T. J., Hinrichs, J. L., & Lucey, P. G. (2006). Spectral properties of angrites. *Meteoritics & Planetary Science*, *41*(8), 1139-1145.
13. Burbine, T. H., Buchanan, P. C., & Binzel, R. P. (2007, March). Deriving formulas from HED spectra for determining the pyroxene mineralogy of Vesta and Vestoids. In *Lunar and Planetary Science Conference* (Vol. 38, p. 2117).
14. Burbine, T. H., Buchanan, P. C., Dolkar, T., & Binzel, R. P. (2009). Pyroxene mineralogies of near-Earth vestoids. *Meteoritics & planetary science*, *44*(9), 1331-1341.

15. Burbine, T. H., Duffard, R., Buchanan, P. C., Cloutis, E. A., & Binzel, R. P. (2011, March). Spectroscopy of O-type asteroids. In *Lunar and Planetary Science Conference* (Vol. 42, p. 2483).
16. Burns, R. G. (1970). Mineralogical applications of crystal field theory. Cambridge University Press, Cambridge.
17. Burns, R. G. (1993). *Mineralogical applications of crystal field theory* (Vol. 5). Cambridge University Press, Cambridge.
18. Buseck, P.R., Nord, G.L., & Veblen, D. R. (1980). Subsolidus phenomena in pyroxenes. In C. T. Prewitt & Mineralogical Society of America (Ed.). Pyroxenes. (p.117-211). Washington, D.C.: Mineralogical Society of America.
19. Cameron M. & Papike, J. J. (1980). Crystal chemistry of silicate pyroxenes. In C. T. Prewitt & Mineralogical Society of America (Ed.). Pyroxenes. (p.5-92). Washington, D.C.: Mineralogical Society of America.
20. Cecchi, V. M., & Caporali, S. (2015). Petrologic and Minerochemical Trends of Acapulcoites, Winonaites and Lodranites: New Evidence from Image Analysis and EMPA Investigations. *Geosciences*, *5*(3), 222-242.
21. Clark, R. N. (1995). Reflectance spectra. *Rock Physics & Phase Relations: A Handbook of Physical Constants*, 178-188.
22. Clark, R.N., Swayze, G.A., Wise, R., Livo, E., Hoefen, T., Kokaly, R., Sutley, S.J., 2007, USGS digital spectral library splib06a: U.S. Geological Survey, Digital Data Series 231, http://speclab.cr.usgs.gov/spectral.lib06.
23. Cloutis, E., Gaffey, M., Jackowski, T., & Reed, K. (1986). Calibrations of phase abundance, composition, and particle size distribution for olivine-orthopyroxene mixtures from reflectance spectra. *Journal of Geophysical Research*, *91*(11), 641-11.
24. Cloutis, E. A., & Gaffey, M. J. (1991). Pyroxene spectroscopy revisited: Spectral-compositional correlations and relationship to geothermometry. *Journal of Geophysical Research: Planets*, *96*(E5), 22809-22826.
25. Cloutis, E. A. (2002). Pyroxene reflectance spectra: Minor absorption bands and effects of elemental substitutions. *Journal of Geophysical Research: Planets*, *107*(E6).
26. Cloutis, E. A., Binzel, R. P., Burbine, T. H., Gaffey, M. J., & McCoy, T. J. (2006a). Asteroid 3628 Božněmcová: Covered with angrite-like basalts?. *Meteoritics & Planetary Science*, *41*(8), 1147-1161.
27. Cloutis, E., Craig, M., Kaletzke, L., McCormack, K., & Stewart, L. (2006b, March). HOSERLab: A new planetary spectrophotometer facility. In *37th Annual Lunar and Planetary Science Conference* (Vol. 37).
28. Cloutis, E. A., Hiroi, T., Gaffey, M. J., Alexander, C. M. O., & Mann, P. (2011a). Spectral reflectance properties of carbonaceous chondrites: 1. CI chondrites. *Icarus, 212*(1), 180-209. doi:10.1016/j.icarus.2010.12.009
29. Cloutis, E. A., Hudon, P., Hiroi, T., Gaffey, M. J., & Mann, P. (2011b). Spectral reflectance properties of carbonaceous chondrites: 2. CM chondrites. *Icarus, 216*(1), 309-346. doi:http://dx.doi.org/10.1016/j.icarus.2011.09.009
30. Cloutis, E. A., Hudon, P., Hiroi, T., & Gaffey, M. J. (2011c). Spectral reflectance properties of carbonaceous chondrites: 3. CR chondrites. *Icarus,* doi:10.1016/j.icarus.2011.11.004
31. Cloutis, E. A., Hudon, P., Hiroi, T., & Gaffey, M. J. (2012a). Spectral reflectance properties of carbonaceous chondrites 4: Aqueously altered and thermally

metamorphosed meteorites. *Icarus, 220*(2), 586-617. doi:http://dx.doi.org/10.1016/j.icarus.2012.05.018

32. Cloutis, E. A., Hudon, P., Hiroi, T., Gaffey, M. J., & Mann, P. (2012b). Spectral reflectance properties of carbonaceous chondrites – 5: CO chondrites. *Icarus, 220*(2), 466-486. doi:10.1016/j.icarus.2012.05.019

33. Cloutis, E. A., Hudon, P., Hiroi, T., Gaffey, M. J., Mann, P., & Bell III, J. F. (2012c). Spectral reflectance properties of carbonaceous chondrites: 6. CV chondrites. *Icarus, 221*(1), 328-358. doi:http://dx.doi.org/10.1016/j.icarus.2012.07.007

34. Cloutis, E. A., Hudon, P., Hiroi, T., & Gaffey, M. J. (2012d). Spectral reflectance properties of carbonaceous chondrites: 7. CK chondrites. *Icarus, 221*(2), 911-924. doi:http://dx.doi.org/10.1016/j.icarus.2012.09.017

35. Cloutis, E. A., Hudon, P., Hiroi, T., Gaffey, M. J., & Mann, P. (2012e). Spectral reflectance properties of carbonaceous chondrites: 8. "Other" carbonaceous chondrites: CH, ungrouped, polymict, xenolithic inclusions, and R chondrites. *Icarus, 221*(2), 984-1001. doi:http://dx.doi.org/10.1016/j.icarus.2012.10.008

36. Delaney, J. S., Prinz, M., & Takeda, H. (1984). The polymict eucrites. *Journal of Geophysical Research: Solid Earth*, *89*(S01), C251-C288.

37. Duffard, R., Lazzaro, D., & León, J. (2005). Revisiting spectral parameters of silicate-bearing meteorites. *Meteoritics & Planetary Science*, *40*(3), 445-459.

38. Dunn, T.L. (2012) Meteorites and the Asteroidal Parent Bodies. In Meteorites and Asteroids: Characteristics, Geology and Exploration, edited by A. Dementieva & D. Ostrogorsky. NOVA Science Publishing, New York, pp. 1-38.

39. Floss, C., Crozaz, G., McKay, G., Mikouchi, T., & Killgore, M. (2003). Petrogenesis of angrites. *Geochimica et Cosmochimica Acta*, *67*(24), 4775-4789.

40. Gaffey, M. J., Bell, J. F., Brown, R. H., Burbine, T. H., Piatek, J. L., Reed, K. L., & Chaky, D. A. (1993a). Mineralogical variations within the S-type asteroid class. *Icarus*, *106*(2), 573-602.

41. Gaffey, M. J., Burbine, T. H., & Binzel, R. P. (1993b). Asteroid spectroscopy: Progress and perspectives. *Meteoritics*, *28*(2), 161-187.

42. Gaffey, M. J. (1997). The early solar system. In *Planetary and Interstellar Processes Relevant to the Origins of Life* (pp. 185-203). Springer Netherlands.

43. Gaffey, M. J., Cloutis, E. A., Kelley, M. S., & Reed, K. L. (2002). Mineralogy of asteroids. *Asteroids III*, *183*.

44. Gaffey, M. J. (2010). Space weathering and the interpretation of asteroid reflectance spectra. *Icarus*, *209*(2), 564-574.

45. Gaffey, M. J. (2011, September). Mineralogy of Asteroids. In E. Telles, R. Dupke, & D. Lazzaro (Eds.), *AIP Conference Proceedings* (Vol. 1386, No. 1, pp. 129-169). AIP.

46. Gardner-Vandy, K. G., Lauretta, D. S., & McCoy, T. J. (2013). A petrologic, thermodynamic and experimental study of brachinites: Partial melt residues of an R chondrite-like precursor. *Geochimica Et Cosmochimica Acta, 122*, 36-57. doi:http://dx.doi.org/10.1016/j.gca.2013.07.035

47. Gertsch, R., Gertsch, L. S., & Remo, J. L. (1997). Mining near- earth resources. *Annals of the New York Academy of Sciences, 822*(1), 511-537. doi:10.1111/j.1749-6632.1997.tb48362.x

48. Golubeva, L., & Shestopalov, D. (2006, March). Are There Pyroxenes on A-Asteroid Surfaces?. In *37th Annual Lunar and Planetary Science Conference* (Vol. 37).

49. Goodrich, C. A., Fioretti, A. M., & Van Orman, J. (2009). Petrogenesis of augite-bearing ureilites Hughes 009 and FRO 90054/93008 inferred from melt inclusions in olivine, augite and orthopyroxene. *Geochimica et Cosmochimica Acta*, *73*(10), 3055-3076.

50. Grady, M., Pratesi, G. & Cecchi, V. M. (2015) *Atlas of Meteorites*. Cambridge University Press: Cambridge, United Kingdom.

51. Granahan, J. C. (2011). Spatially resolved spectral observations of Asteroid 951 Gaspra. *Icarus*, *213*(1), 265-272.

52. Gietzen, K. M., Lacy, C. H., Ostrowski, D. R., & Sears, D. W. (2012). IRTF observations of S complex and other asteroids: Implications for surface compositions, the presence of clinopyroxenes, and their relationship to meteorites. *Meteoritics & Planetary Science*, *47*(11), 1789-1808.

53. Grossman J.N. (2011) Classification of ordinary chondrites based on mean and standard deviation of Fa and Fs contents of mafic silicates. Unpublished whitepaper.

54. Hamilton, V. E. (2000). Thermal infrared emission spectroscopy of the pyroxene mineral series. *Journal of Geophysical Research: Planets*, *105*(E4), 9701-9716.

55. Hamilton, V. E. (2003). Thermal infrared emission spectroscopy of titanium-enriched pyroxenes. *Journal of Geophysical Research: Planets*, *108*(E8).

56. Harris, A. W., Boslough, M., Chapman, C. R., Drube, L., Michel, P., & Harris, A. W. (2015). Asteroid Impacts and Modern Civilization: Can We Prevent a Catastrophe?. *Asteroids IV*, 835-854.

57. Holsapple, K. A. (2002). The deflection of menacing rubble pile asteroids. Extended Abstracts Volume of the Workshop on Scientific Requirements for Mitigation of Hazardous Comets and Asteroids, Arlington, Virginia, on September 3-6, 2002. National Optical Astronomy Observatory, Tucson, Ariz. Originally available on http://www.noao.edu/meetings/mitigation/media/arlington.extended.pdf, found on http://keith.aa.washington.edu/papers/mitigation.pdf.

58. Huebner, J. S. (1980). Pyroxene phase equilibria at low pressure. In C. T. Prewitt & Mineralogical Society of America (Ed.). Pyroxenes. (p.213-288). Washington, D.C.: Mineralogical Society of America.

59. Hunt, G. R. (1977). Spectral signatures of particulate minerals in the visible and near infrared. *Geophysics*, *42*(3), 501-513.

60. Hunt, A. C., Benedix, G. K., Hammond, S. J., Bland, P. A., Rehkämper, M., Kreissig, K., & Strekopytov, S. (2017). A geochemical study of the winonaites: Evidence for limited partial melting and constraints on the precursor composition. *Geochimica Et Cosmochimica Acta, 199*, 13-30. doi:http://dx.doi.org/10.1016/j.gca.2016.10.043

61. Jurewicz, A. J. G., Mittlefehldt, D. W., & Jones, J. H. (1991). Partial melting of the aliende (CV3) meteorite: implications for origins of basaltic meteorites. *Science*, *252*(5006), 695-698.

62. Keil, K. (2010). Enstatite achondrite meteorites (aubrites) and the histories of their asteroidal parent bodies. *Chemie Der Erde - Geochemistry - Interdisciplinary Journal for Chemical Problems of the Geosciences and Geoecology, 70*(4), 295-317. doi:10.1016/j.chemer.2010.02.002

63. Keil, K. (2014). Brachinite meteorites: Partial melt residues from an FeO-rich asteroid. *Chemie Der Erde - Geochemistry, 74*(3), 311-329. doi:http://dx.doi.org/10.1016/j.chemer.2014.02.001

64. King, T. V., & Ridley, W. I. (1987). Relation of the spectroscopic reflectance of olivine to mineral chemistry and some remote sensing implications. *Journal of Geophysical Research: Solid Earth*, *92*(B11), 11457-11469.

65. King, A.J., Solomon, J.R., Schofield, P.F., & Russell, S.S. (2015). Characterising the CI and CI-like carbonaceous chondrites using thermogravimetric analysis and infrared spectroscopy. *Earth, Planets and Space* 67, 198.

66. Klima, R. L., Pieters, C. M., & Dyar, M. D. (2008). Characterization of the 1.2 μm M1 pyroxene band: Extracting cooling history from near-IR spectra of pyroxenes and pyroxene-dominated rocks. *Meteoritics & Planetary Science*, *43*(10), 1591-1604.

67. Klima, R. L., Dyar, M. D., & Pieters, C. M. (2011). Near-infrared spectra of clinopyroxenes: Effects of calcium content and crystal structure. *Meteoritics & Planetary Science*, *46*(3), 379-395.

68. Kokaly, R.F., Clark, R.N., Swayze, G.A., Livo, K.E., Hoefen, T.M., Pearson, N.C., Wise, R.A., Benzel, W.M., Lowers, H.A., Driscoll, R.L., and Klein, A.J., 2017, USGS Spectral Library Version 7: U.S. Geological Survey Data Series 1035, 61 p., https://doi.org/10.3133/ds1035.

69. Li, S., & Milliken, R. E. (2015). Estimating the modal mineralogy of eucrite and diogenite meteorites using visible–near infrared reflectance spectroscopy. *Meteoritics & Planetary Science*, *50*(11), 1821-1850.

70. Lorenzetti, S., Eugster, O., Busemann, H., Marti, K., Burbine, T. H., & McCoy, T. (2003). History and origin of aubrites. *Geochimica Et Cosmochimica Acta, 67*(3), 557-571. doi:10.1016/S0016-7037(02)01085-2

71. Lu, E. T. & Love, S. G. (2005). Gravitational tractor for towing asteroids. *Nature, 438*(7065), 177. doi:10.1038/438177a

72. Lucey, P. G. (1998). Model near-infrared optical constants of olivine and pyroxene as a function of iron content. *Journal of Geophysical Research: Planets*, *103*(E1), 1703-1713.

73. Lunning, N. G., McSween Jr., H. Y., Tenner, T. J., Kita, N. T., & Bodnar, R. J. (2015). Olivine and pyroxene from the mantle of asteroid 4 vesta. *Earth and Planetary Science Letters, 418*, 126-135. doi:http://dx.doi.org/10.1016/j.epsl.2015.02.043

74. Marshall, D. (1996). Ternplot: An Excel spreadsheet for ternary diagrams. *Computers and Geosciences, 22*(6), 697-699.

75. Mayne, R. G., Sunshine, J. M., McSween, H. Y., McCoy, T. J., Corrigan, C. M., & Gale, A. (2010). Petrologic insights from the spectra of the unbrecciated eucrites: Implications for Vesta and basaltic asteroids. *Meteoritics & Planetary Science*, *45*(7), 1074-1092.

76. McCoy, T. J., Keil, K., Muenow, D. W., & Wilson, L. (1997). *Partial melting and melt migration in the acapulcoite-lodranite parent body.* doi:http://dx.doi.org/10.1016/S0016-7037(96)00365-1

77. McCoy, T. J., Mittlefehldt, D. W., & Wilson, L. (2006). Asteroid differentiation. *Meteorites and the early solar system II*, 733-745.

78. McCraig, M. A., Osinski, G. R., Cloutis, E. A., Flemming, R. L., Izawa, M. R., Reddy, V., ... & Bramble, M. S. (2017). Fitting the curve in Excel®: Systematic curve fitting of laboratory and remotely sensed planetary spectra. *Computers & geosciences*, *100*, 103-114.

79. McSween, H. Y., Bennett, M. E., & Jarosewich, E. (1991). The mineralogy of ordinary chondrites and implications for asteroid spectrophotometry. *Icarus*, *90*(1), 107-116.

80. McSween Jr, H. Y. (1994). What we have learned about Mars from SNC meteorites. *Meteoritics*, *29*(6), 757-779.

81. McSween, H. Y. (1999). *Meteorites and their parent planets* (2nd ed.). Cambridge; New York: Cambridge University Press.

82. Mittlefehldt, D. W. et al. (1998). Non-chondritic meteorites from asteroidal bodies In J. J. Papike (Ed.). *Planetary materials*. (p.4-01-4-195). Washington, D.C.: Mineralogical Society of America.

83. Moriarty, D. P., & Pieters, C. M. (2016). Complexities in pyroxene compositions derived from absorption band centers: Examples from Apollo samples, HED meteorites, synthetic pure pyroxenes, and remote sensing data. *Meteoritics & Planetary Science*, *51*(2), 207-234.

84. Morimoto, N., Fabries, J., Ferguson, A. K., Ginzburg, I. V., Ross, M., Seifert, F. A., Zussman, J., Aoki, K. & Gottardi, G. (1988). Nomenclature of pyroxenes. *American Mineralogist*, *73*(9-10), 1123-1133.

85. Nesse, W. D. (2012). *Introduction to mineralogy* (2nd ed.). New York: Oxford University Press.

86. Ohashi Y., Burnham C. W., and Finger L. W. 1975. The effect of Ca-Fe substitution on the clinopyroxene crystal structure. *American Mineralogist* **60**:423–434.

87. Papike, J. J. (1996). Pyroxene as a recorder of cumulate formational processes in asteroids, Moon, Mars, Earth: Reading the record with the ion microprobe. *American Mineralogist*, *81*(5-6), 525-544.

88. Papike, J. J. (1998). *Planetary materials*. Washington, D.C.: Mineralogical Society of America.

89. Pieters, C. M., & Hiroi, T. (2004, March). RELAB (Reflectance Experiment Laboratory): A NASA multiuser spectroscopy facility. In *Lunar and Planetary Science Conference* (Vol. 35).

90. Pinilla-Alonso, N., Lorenzi, V., Campins, H., de Leon, J., & Licandro, J. (2013). Near-infrared spectroscopy of 1999 JU3, the target of the Hayabusa 2 mission. *Astronomy & Astrophysics*, *552*, A79.

91. Pompilio, L., Sgavetti, M., & Pedrazzi, G. (2007). Visible and near-infrared reflectance spectroscopy of pyroxene-bearing rocks: New constraints for understanding planetary surface compositions. *Journal of Geophysical Research: Planets*, *112*(E1).

92. Reddy, V., Cloutis, E. A., Craig, M. A., & Gaffey, M. J. (2008, March). Spectral calibration of orthopyroxene-type A clinopyroxene mixtures: Implications for interpreting asteroid spectra. In *Lunar and Planetary Science Conference* (Vol. 39, p. 2007).

93. Reddy, V., Sanchez, J. A., Bottke, W. F., Cloutis, E. A., Izawa, M. R., O'Brien, D. P., ... & Fujihara, G. (2014). Chelyabinsk meteorite explains unusual spectral properties of Baptistina Asteroid Family. *Icarus*, *237*, 116-130.

94. Rivkin, A. S., Trilling, D. E., Thomas, C. A., DeMeo, F., Spahr, T. B., & Binzel, R. P. (2007). Composition of the L5 Mars Trojans: Neighbors, not siblings. *Icarus*, *192*(2), 434-441.

95. Rossman, G. R. (1980). Pyroxene spectroscopy. In C. T. Prewitt & Mineralogical Society of America (Ed.). Pyroxenes. (p.93-115). Washington, D.C.: Mineralogical Society of America.

96. Rubin, A. E. (1997). Mineralogy of meteorite groups. *Meteoritics & Planetary Science*, *32*(2), 231-247.
97. Sanchez, J. A., Reddy, V., Kelley, M. S., Cloutis, E. A., Bottke, W. F., Nesvorný, D., ... & Le Corre, L. (2014). Olivine-dominated asteroids: Mineralogy and origin. *Icarus*, *228*, 288-300.
98. Schade, U., Wäsch, R., & Moroz, L. (2004). Near-infrared reflectance spectroscopy of Ca-rich clinopyroxenes and prospects for remote spectral characterization of planetary surfaces. *Icarus*, *168*(1), 80-92.
99. Schweickart, R., Chapman, C., Durda, D., & Hut, P. (2003). Threat mitigation: The asteroid tugboat. *Scientific American*. November 2003. P.54-61.
100. Scott, E. R. D., and J. Taylor (1985), Petrology of types 4–6 carbonaceous chondrites, J. Geophys. Res., 90(S02), C699–C709, doi:10.1029/JB090iS02p0C699.
101. Singer, R. B. (1981). Near-infrared spectral reflectance of mineral mixtures: Systematic Combinations of pyroxenes, olivine, and iron oxides. *Journal of Geophysical Research: Solid Earth*, *86*(B9), 7967-7982.
102. Shearer, C. K., Papike, J. J. & Rietmeijer, F. J. M. (1998). The planetary sample suite and environments of origin. In J. J. Papike (Ed.). *Planetary materials*. (p.1-01-1-28). Washington, D.C.: Mineralogical Society of America.
103. Sunshine, J. M., Pieters, C. M., & Pratt, S. F. (1990). Deconvolution of mineral absorption bands: An improved approach. *Journal of Geophysical Research: Solid Earth*, *95*(B5), 6955-6966.
104. Sunshine, J. M., & Pieters, C. M. (1993). Estimating modal abundances from the spectra of natural and laboratory pyroxene mixtures using the modified Gaussian model. *Journal of Geophysical Research: Planets*, *98*(E5), 9075-9087.
105. Sunshine, J. M., Bus, S. J., McCoy, T. J., Burbine, T. H., Corrigan, C. M., & Binzel, R. P. (2004). High-calcium pyroxene as an indicator of igneous differentiation in asteroids and meteorites. *Meteoritics & Planetary Science*, *39*(8), 1343-1357.
106. Weisberg, M. K., Prinz, M., Clayton, R. N., Mayeda, T. K., Grady, M. M., Franchi, I., Pillinger, C. T., & Kallemeyn, G. W. (1996). *The K (kakangari) chondrite grouplet*. doi:http://dx.doi.org/10.1016/S0016-7037(96)00233
107. Winter, J. D. (2010). *Principles of igneous and metamorphic petrology*. New York: Prentice Hall.
108. Zolensky, M. E., Nakamura, K., Gounelle, M., Mikouchi, T., Kasama, T., Tachikawa, O., & Tonui, E. (2002). Mineralogy of tagish lake: An ungrouped type 2 carbonaceous chondrite. *Meteoritics & Planetary Science, 37*(5), 737-761. doi:10.1111/j.1945-5100.2002.tb00852.x

# Appendices

### 1. Samples

Table 1. Samples used in this study and their minima found by lowest reflectance. 1=USGS Spectral Library, 2=RELAB, 3=HOSERLab, 4=Klima et al. 2011, 5=Sunshine & Pieters 1993, and 6=Gietzen et al. 2012.

| Sample name | Grain size (µm) | Wo | En | Fs | Band I minimum (µm) | Band I fitting range (µm) | Band II minimum (µm) | Band II fitting range (µm) | Source |
|---|---|---|---|---|---|---|---|---|---|
| NMNH120049 | 35 | 34 | 45 | 21 | 1.006 | 0.9-1.2 | 2.295 | 2.1-2.5 | 1 |
| NMNHR18685 | 263 | | | | 1.054 | 0.9-1.2 | 2.315 | 2-2.5 | 1 |
| NMNH119197 | 20-150 | | | | 0.994 | 0.98-1.02 | 1.149 | 1.15-1.2 | 1 |
| HS199 | < 5 | | | | 0.949 | 0.9-1 | 1.994 | 1.9-2 | 1 |
| PYX003 | < 45 | 3.3 | 68.5 | 28.2 | 0.919 | 0.9-1 | 1.817 | 1.8-2 | 2, 3 |
| | < 45 | | | | 0.920 | 0.9-1 | 1.815 | 1.8-2 | |
| | 45-90 | | | | 0.916 | 0.9-1 | 1.818 | 1.8-2 | |
| PYX005 | 45-90 | 49.1 | 41 | 9.9 | 1.025 | 0.9-1.1 | 2.320 | 2.2-2.4 | 2, 3 |
| | < 45 | | | | 1.022 | 0.9-1.1 | 2.321 | 2.2-2.4 | |
| | 90-180 | | | | 1.028 | 0.9-1.1 | 2.318 | 2.2-2.4 | |
| | < 45 | | | | 1.023 | 0.9-1.1 | 2.320 | 2.2-2.4 | |
| PYX007 | 45-90 | 53.1 | 35.7 | 11.2 | 0.920 | 0.9-1 | 1.100 | 1-1.3 | 2, 3 |
| PYX009 | 45-90 | 50.5 | 39.8 | 9.7 | 0.960 | 0.9-1 | 1.135 | 1-1.3 | 2, 3 |
| | < 45 | | | | 0.975 | 0.9-1 | 1.135 | 1-1.3 | |
| | 45-90 | | | | 0.974 | 0.9-1 | 1.133 | 1-1.3 | |
| PYX010 | 45-90 | 50.9 | 30.4 | 18.7 | 0.970 | 0.96-1 | 1.155 | 1.15-2 | 2, 3 |
| PYX015 | < 45 | 43.4 | 51 | 5.6 | 0.915 | 0.8-1 | 1.795 | 1.75-1.9 | 2, 3 |
| PYX016 | 45-90 | 48.9 | 48.6 | 2.5 | 1.050 | 0.9-1.2 | 2.315 | 2-2.5 | 2, 3 |
| | < 45 | | | | 1.049 | 0.9-1.2 | 2.310 | 2-2.5 | |
| | < 45 | | | | 1.049 | 0.9-1.2 | 2.310 | 2-2.5 | |
| | < 250 | | | | 1.047 | 0.9-1.2 | 2.310 | 2-2.5 | |
| | < 45 | | | | 1.050 | 0.9-1.2 | 2.312 | 2-2.5 | |
| | 45-90 | | | | 1.056 | 0.9-1.2 | 2.308 | 2-2.5 | |
| PYX017 | 45-90 | 44.4 | 47.5 | 8.1 | 1.025 | 0.9-1.2 | 2.290 | 2.2-2.4 | 2, 3 |
| | 90-180 | | | | 1.022 | 0.9-1.2 | 2.289 | 2.2-2.4 | |
| | < 45 | | | | 1.024 | 0.9-1.2 | 2.310 | 2.2-2.4 | |
| PYX019 | 45-90 | 50.1 | 39 | 10.9 | 1.020 | 0.9-1.2 | 2.265 | 2.1-2.4 | 2, 3 |
| PYX020 | 45-90 | 48.7 | 48 | 3.3 | 0.950 | 0.9-1 | 1.100 | 1-1.3 | 2, 3 |
| | < 45 | | | | 0.992 | 0.9-1 | 1.093 | 1-1.3 | |
| | 45-90 | | | | 0.973 | 0.9-1 | 1.114 | 1-1.3 | |
| PYX021 | 45-90 | 52.1 | 4.2 | 43.7 | 0.975 | 0.97-0.99 | 1.150 | 1.15-1.2 | 2, 3 |
| PYX023 | 45-90 | 1.3 | 89.3 | 9.4 | 0.915 | 0.9-1 | 1.850 | 1.8-1.9 | 2, 3 |
| | < 45 | | | | 0.913 | 0.9-1 | 1.841 | 1.75-1.85 | |
| | 90-180 | | | | 0.913 | 0.9-1 | 1.861 | 1.8-1.9 | |
| PYX026 | 45-90 | 60.9 | 10.4 | 28.7 | 0.996 | 0.9-1 | 1.150 | 1.15-1.2 | 2, 3 |
| PYX029 | 45-90 | 51.6 | 41.5 | 6.9 | 1.025 | 1-1.1 | 2.315 | 2.2-2.4 | 2, 3 |
| PYX032 | 45-90 | 3.6 | 54.9 | 41.5 | 0.920 | 0.8-1 | 1.955 | 1.8-2 | 2, 3 |
| | 45-90 | | | | 0.920 | 0.8-1 | 1.950 | 1.8-2 | |
| | < 45 | | | | 0.916 | 0.9-1 | 1.903 | 1.8-2 | |
| | 90-180 | | | | 0.932 | 0.8-1 | 1.978 | 1.8-2 | |
| PYX034 | 45-90 | 43.7 | 47.4 | 8.9 | 1.015 | 0.9-1.2 | 2.250 | 2.2-2.4 | 2, 3 |

| | | | | | | | | | |
|---|---|---|---|---|---|---|---|---|---|
| PYX035 | 45-90 | 48.7 | 40.5 | 10.8 | 1.010 | 0.9-1.2 | 2.250 | 2.1-2.4 | 2, 3 |
| PYX036 | 45-90 | 43.3 | 43.3 | 13.4 | 1.020 | 0.9-1.1 | 2.290 | 2-2.5 | 2, 3 |
| PYX038 | 45-90 | 53.8 | 11 | 35.2 | 1.000 | 0.98-1.02 | | | 2, 3 |
| PYX039 | 45-90 | 50.3 | 29.6 | 20.1 | 0.980 | 0.98-1.02 | | | 2, 3 |
| PYX040 | 45-90 | 48.8 | 42.7 | 8.5 | 1.005 | 0.9-1.2 | 2.245 | 2-2.5 | 2, 3 |
| PYX042 | 45-90 | 0.4 | 86.8 | 12.8 | 0.915 | 0.9-1 | 1.855 | 1.8-2 | 2, 3 |
| PYX052 | < 45 | 50.5 | 43.8 | 5.8 | 1.060 | 0.9-1.2 | 2.312 | 2.1-2.4 | 2, 3 |
| | < 45 | | | | 1.058 | 0.9-1.2 | 2.314 | 2.1-2.4 | |
| PYX053 | < 45 | 47.9 | 48.2 | 3.9 | 0.956 | 0.9-1 | 1.032 | 1-1.3 | 2, 3 |
| | < 45 | | | | 0.967 | 0.9-1 | 1.044 | 1-1.3 | |
| PYX054 | < 45 | 45.9 | 41.9 | 12.2 | 1.017 | 0.9-1.2 | 2.202 | 2.2-2.4 | 2, 3 |
| | < 45 | | | | 1.019 | 0.9-1.2 | 2.229 | 2.2-2.4 | |
| PYX057 | < 45 | 41 | 34.1 | 24.9 | 0.892 | 0.85-1 | 1.005 | 1.05-1.3 | 2, 3 |
| | < 45 | | | | 0.888 | 0.85-1 | 1.007 | 1.05-1.3 | |
| PYX101 | 45-90 | 43.3 | 34.7 | 22 | 1.010 | 0.9-1.2 | 2.330 | 2.2-2.5 | 2, 3 |
| | < 45 | | | | 0.995 | 0.9-1.2 | 2.403 | 2.2-2.5 | |
| PYX102 | 45-90 | 49.2 | 48.7 | 2.1 | 1.050 | 1-1.2 | 2.315 | 2.2-2.4 | 2, 3 |
| PYX103 | < 45 | 40.5 | 40.8 | 18.7 | 0.990 | 0.9-1.1 | 2.030 | 2-2.2 | 2, 3 |
| PYX105 | 45-90 | 48.6 | 43.9 | 7.5 | 1.030 | 0.9-1.2 | 2.320 | 2.1-2.4 | 2, 3 |
| PYX108 | 45-90 | 1.1 | 91.1 | 7.8 | 0.910 | 0.9-1 | 1.885 | 1.8-2 | 2, 3 |
| PYX109 | 45-90 | 49.7 | 30.6 | 19.7 | 0.975 | 0.95-1.05 | 1.180 | 1.18-1.2 | 2, 3 |
| PYX110 | 45-90 | 0.5 | 86.3 | 13.2 | 0.915 | 0.8-1 | 1.855 | 1.8-2 | 2, 3 |
| PYX111 | < 45 | 49.8 | 46 | 4.2 | 1.050 | 0.9-1.2 | 2.320 | 2.1-2.6 | 2, 3 |
| PYX112 | < 45 | 8.3 | 64.8 | 26.9 | 0.920 | 0.8-1.1 | 1.840 | 1.6-2.1 | 2, 3 |
| | < 45 | | | | 0.923 | 0.8-1.1 | 1.905 | 1.6-2.1 | |
| | < 45 | | | | 0.922 | 0.8-1.1 | 1.899 | 1.6-2.1 | |
| | 45-90 | | | | 0.921 | 0.8-1.1 | 1.901 | 1.6-2.1 | |
| PYX117 | < 45 | 0.7 | 74.7 | 24.6 | 0.920 | 0.9-1 | 1.870 | 1.8-2 | 2, 3 |
| PYX120 | 45-90 | 49.8 | 45.4 | 4.8 | 0.990 | 0.9-1.1 | 1.100 | 1.1-1.3 | 2, 3 |
| PYX126 | 45-90 | 51.3 | 39.8 | 8.9 | 0.995 | 0.98-1.02 | 2.230 | 2.2-2.3 | 2, 3 |
| PYX135 | < 45 | 49.9 | 48.5 | 1.6 | 1.055 | 0.9-1.1 | 2.320 | 2.1-2.6 | 2, 3 |
| PYX136 | < 45 | 49.6 | 48.8 | 1.6 | 1.050 | 0.9-1.1 | 2.315 | 2.1-2.6 | 2, 3 |
| | | | | | 1.055 | | 2.320 | | |
| PYX150 | < 45 | 51.1 | 44.9 | 4 | 0.975 | 0.9-1.1 | 1.115 | 1.1-1.3 | 2, 3 |
| | < 45 | | | | 0.967 | | 1.129 | | |
| | 45-90 | | | | 0.966 | | 1.132 | | |
| | < 45 | | | | 0.961 | | 1.131 | | |
| PYX160 | 45-90 | 50.7 | 35.3 | 14 | 0.985 | 0.9-1.1 | 1.100 | 1.1-1.3 | 2, 3 |
| PYX170 | < 45 | 49.1 | 46.4 | 4.5 | 1.030 | 0.9-1.2 | 2.330 | 2.1-2.4 | 2, 3 |
| DL-CMP-008-A | < 45 | 5 | 38 | 57 | 0.945 | 0.9-1 | 2.035 | 2-2.1 | 2 |
| DL-CMP-009 | < 45 | 10 | 43 | 47 | 0.960 | 0.9-1 | 2.030 | 1.9-2.2 | 2 |
| DL-CMP-010 | < 45 | 10 | 63 | 27 | 0.945 | 0.8-1.1 | 1.960 | 1.7-2.1 | 2, 4 |
| DL-CMP-011- | < 45 | 14 | 36 | 50 | 0.960 | 0.9-1 | 2.100 | 2-2.2 | 2, 4 |

| | | | | | | | | | |
|---|---|---|---|---|---|---|---|---|---|
| A | | | | | | | | | |
| DL-CMP-012 | < 45 | 5 | 47.5 | 47.5 | 0.945 | 0.9-1 | 1.955 | 1.8-2 | 2 |
| DL-CMP-013 | < 45 | 8 | 46 | 46 | 0.945 | 0.9-1 | 1.990 | 1.9-2.2 | 2 |
| DL-CMP-015 | < 45 | 5 | 66.5 | 28.5 | 0.935 | 0.9-1 | 1.860 | 1.7-1.9 | 2 |
| DL-CMP-016 | < 45 | 5 | 76 | 19 | 0.920 | 0.9-1 | 1.895 | 1.7-1.9 | 2 |
| DL-CMP-017-A | < 45 | 20 | 64 | 16 | 0.990 | 0.9-1.1 | 2.235 | 2-2.5 | 2 |
| DL-CMP-018-A | < 45 | 10 | 72 | 18 | 0.945 | 0.8-1.1 | 1.905 | 1.7-2.1 | 2 |
| DL-CMP-019-A | < 45 | 20 | 56 | 24 | 0.995 | 0.9-1.1 | 2.235 | 2-2.5 | 2 |
| DL-CMP-032-A | < 45 | 46.2 | 53.8 | 0 | 1.050 | 0.9-1.2 | 2.380 | 2.1-2.4 | 2 |
| DL-CMP-033-A | < 45 | 49 | 42 | 8 | 1.050 | 1-1.2 | 2.365 | 2.1-2.5 | 2, 4 |
| DL-CMP-035-A | < 45 | 50 | 10 | 40 | 1.075 | 0.9-1.2 | 1.735 | 1.7-2 | 2 |
| DL-CMP-036-A | < 45 | 49 | 27 | 24 | 1.060 | 1-1.1 | 2.250 | 2.1-2.4 | 2, 4 |
| DL-CMP-037-A | < 45 | 49 | 16 | 35 | 1.055 | 1-1.1 | 2.260 | 2.1-2.4 | 2, 4 |
| DL-CMP-039-A | < 45 | 49 | 29 | 22 | 1.050 | 1-1.1 | 2.330 | 2.1-2.4 | 2, 4 |
| DL-CMP-040-A | < 45 | 50 | 5 | 45 | 1.060 | 0.9-1.2 | 1.760 | 1.7-2 | 2, 4 |
| DL-CMP-041-A | < 45 | 50 | 0 | 50 | 0.960 | 0.9-1.2 | 2.100 | 2.1-2.4 | 2 |
| DL-CMP-043-A | < 45 | 49 | 45 | 6 | 1.055 | 1-1.2 | 2.355 | 2.1-2.5 | 2, 4 |
| DL-CMP-044-A | < 45 | 49 | 43 | 8 | 1.050 | 0.9-1.2 | 2.325 | 2.1-2.5 | 2, 4 |
| DL-CMP-047-A | < 45 | 25 | 30 | 45 | 1.015 | 0.9-1.1 | 2.340 | 2.3-2.4 | 2 |
| DL-CMP-048-A | < 45 | 10 | 14 | 77 | 0.945 | 0.8-1.1 | 2.110 | 1.9-2.4 | 2, 4 |
| DL-CMP-049-A | < 45 | 19 | 11 | 70 | 0.965 | 0.8-1.1 | 2.185 | 2-2.4 | 2, 4 |
| DL-CMP-050-A | < 45 | 23 | 19 | 58 | 0.985 | 0.9-1.1 | 2.260 | 2.2-2.4 | 2, 4 |
| DL-CMP-051-A | < 45 | 27 | 39 | 34 | 1.000 | 0.9-1.1 | 2.285 | 2.2-2.4 | 2, 4 |
| DL-CMP-053-A | < 45 | 9 | 23 | 68 | 0.970 | 0.8-1.1 | 2.185 | 2-2.4 | 2, 4 |
| DL-CMP-054-A | < 45 | 23 | 6 | 70 | 0.995 | 0.9-1.1 | 2.290 | 2.2-2.4 | 2, 4 |
| DL-CMP-055-A | < 45 | 26 | 18 | 56 | 1.005 | 0.9-1.1 | 2.300 | 2.2-2.4 | 2, 4 |
| DL-CMP-056-A | < 45 | 22 | 18 | 60 | 0.975 | 0.9-1.1 | 2.180 | 2.1-2.3 | 2, 4 |
| DL-CMP-057-A | < 45 | 25 | 36 | 39 | 1.000 | 0.9-1.1 | 2.275 | 2.2-2.4 | 2, 4 |
| DL-CMP-058-A | < 45 | 27 | 28 | 45 | 1.005 | 0.9-1.1 | 2.315 | 2.2-2.4 | 2, 4 |
| DL-CMP-059-A | < 45 | 25 | 11 | 64 | 1.070 | 1-1.2 | 1.200 | 1.2-1.4 | 2 |
| DL-CMP-066-A | < 45 | 38 | 15 | 58 | 1.020 | 0.9-1.1 | 2.315 | 2.3-2.4 | 2, 4 |
| DL-CMP-067-A | < 45 | 39 | 52 | 9 | 1.015 | 0.9-1.1 | 2.355 | 2.3-2.4 | 2, 4 |
| DL-CMP-068-A | < 45 | 38 | 29 | 33 | 1.015 | 0.9-1.1 | 2.325 | 2.2-2.4 | 2, 4 |
| DL-CMP-069-A | < 45 | 35 | 20 | 46 | 1.025 | 1-1.1 | 2.320 | 2.2-2.4 | 2 |
| DL-CMP-070-A | < 45 | 45 | 14 | 41 | 1.030 | 1-1.1 | 2.320 | 2.2-2.4 | 2, 4 |

| DL-CMP-071-A | < 45 | 43 | 26 | 31 | | 1.025 | 1-1.1 | | 2.315 | 2.2-2.4 | 2, 4 |
|---|---|---|---|---|---|---|---|---|---|---|---|
| DL-CMP-073-A | < 45 | 39 | 36 | 25 | | 1.015 | 1-1.1 | | 2.325 | 2.2-2.4 | 2, 4 |
| DL-CMP-074-A | < 45 | 39 | 24 | 37 | | 1.020 | 0.9-1.1 | | 2.320 | 2.2-2.4 | 2, 4 |
| DL-CMP-075-A | < 45 | 45 | 46 | 9 | | 1.030 | 0.9-1.2 | | 2.335 | 2.2-2.5 | 2, 4 |
| DL-CMP-076-A | < 45 | 46 | 18 | 35 | | 1.035 | 1-1.1 | | 2.280 | 2.2-2.4 | 2, 4 |
| DL-CMP-077-A | < 45 | 45 | 52 | 3 | | 1.025 | 0.9-1.2 | | 2.355 | 2.2-2.5 | 2, 4 |
| DL-CMP-079-A | < 45 | 47 | 38 | 15 | | 1.030 | 1-1.1 | | 2.325 | 2.2-2.4 | 2, 4 |
| DL-CMP-080-A | < 45 | 40 | 20 | 40 | | 1.040 | 1-1.1 | | 2.330 | 2.2-2.4 | 2 |
| DL-CMP-081-A | < 45 | 35 | 26 | 39 | | 1.020 | 0.9-1.1 | | 2.315 | 2.2-2.4 | 2 |
| DL-CMP-082-A | < 45 | 49 | 1 | 50 | | 1.060 | 1-1.1 | | 2.315 | 2.2-2.4 | 2, 4 |
| DL-CMP-083-A | < 45 | 51 | 0 | 49 | | 0.975 | 0.96-0.98 | | 1.060 | 1.05-1.1 | 2, 4 |
| | | | | | | | | | 2.310 | 2.2-2.4 | |
| DL-CMP-084-A | < 45 | 35 | 0 | 65 | | 1.035 | 1-1.1 | | 2.285 | 2.2-2.4 | 2 |
| DL-CMP-085-A | < 45 | 39 | 0 | 61 | | 1.025 | 1-1.1 | | 2.290 | 2.2-2.4 | 2, 4 |
| DL-CMP-086-A | < 45 | 25 | 0 | 75 | | 1.020 | 1-1.1 | | 2.285 | 2.2-2.4 | 2 |
| DL-CMP-087-A | < 45 | 29 | 0 | 71 | | 1.015 | 0.9-1.1 | | 2.295 | 2.2-2.4 | 2, 4 |
| DL-CMP-088-A | < 45 | 10 | 0 | 90 | | 0.990 | 0.8-1.11 | | 2.200 | 1.9-2.4 | 2, 4 |
| | < 45 | | | | | 0.995 | 0.8-1.11 | | 2.200 | 1.9-2.4 | |
| DL-CMP-089-A | < 45 | 7 | 0 | 93 | | 0.970 | 0.9-1.1 | | 2.145 | 2.1-2.3 | 2 |
| DL-CMP-090-A | < 45 | 5 | 0 | 95 | | 0.955 | 0.9-1 | | 2.100 | 2-2.3 | 2 |
| PE-CMP-030 | < 45 | 1 | 87 | 12 | | 0.910 | 0.9-1 | | 1.835 | 1.8-2 | 2, 5 |
| | < 45 | | | | | 0.910 | 0.9-1 | | 1.835 | 1.8-2 | |
| | < 45 | | | | | 0.910 | 0.9-1 | | 1.825 | 1.8-2 | |
| | < 45 | | | | | 0.910 | 0.9-1 | | 1.840 | 1.8-2 | |
| | < 45 | | | | | 0.910 | 0.9-1 | | 1.840 | 1.8-2 | |
| | 45-75 | | | | | 0.905 | 0.9-1 | | 1.830 | 1.8-2 | |
| | 45-75 | | | | | 0.905 | 0.9-1 | | 1.830 | 1.8-2 | |
| | 45-75 | | | | | 0.915 | 0.9-1 | | 1.845 | 1.8-2 | |
| | 45-75 | | | | | 0.905 | 0.9-1 | | 1.830 | 1.8-2 | |
| | 75-125 | | | | | 0.905 | 0.9-1 | | 1.845 | 1.8-2 | |
| | 75-125 | | | | | 0.905 | 0.9-1 | | 1.845 | 1.8-2 | |
| | 75-125 | | | | | 0.915 | 0.9-1 | | 1.845 | 1.8-2 | |
| PP-CMP-021 | < 45 | 45.59 | 45.89 | 8.52 | | 1.015 | 0.9-1.2 | | 2.280 | 2.1-2.5 | 2, 5 |
| | < 45 | | | | | 1.015 | 0.9-1.2 | | 2.280 | 2.1-2.5 | |
| | < 45 | | | | | 1.020 | 0.9-1.2 | | 2.280 | 2.1-2.5 | |
| | < 45 | | | | | 1.015 | 0.9-1.2 | | 2.275 | 2.1-2.5 | |
| | < 250 | | | | | 1.020 | 0.9-1.2 | | 2.270 | 2.1-2.5 | |
| | 45-75 | | | | | 1.015 | 0.9-1.2 | | 2.280 | 2.1-2.5 | |

| Sample name | Grain size | Wo | En | Fs | Band I min | Band I center | Band II min | Band II center | Source |
|---|---|---|---|---|---|---|---|---|---|
| | 45-75 | | | | 1.015 | 0.9-1.2 | 2.280 | 2.1-2.5 | |
| | 45-75 | | | | 1.015 | 0.9-1.2 | 2.290 | 2.1-2.5 | |
| | 75-125 | | | | 1.020 | 0.9-1.2 | 2.255 | 2.1-2.5 | |
| | 75-125 | | | | 1.020 | 0.9-1.2 | 2.255 | 2.1-2.5 | |
| | 75-125 | | | | 1.020 | 0.9-1.2 | 2.280 | 2.1-2.5 | |
| | < 25 | | | | 1.020 | 0.9-1.2 | 2.280 | 2.1-2.5 | |
| | 25-63 | | | | 1.020 | 0.9-1.2 | 2.280 | 2.1-2.5 | |
| | 63-125 | | | | 1.010 | 0.9-1.2 | 2.260 | 2.1-2.5 | |
| CP-JJG-001 | < 25 | | | | 1.030 | 1-1.1 | 2.320 | 2.2-2.4 | 2 |
| | 25-45 | | | | 1.030 | 1-1.1 | 2.320 | 2.2-2.4 | |
| | 45-53 | | | | 1.020 | 1-1.1 | 2.320 | 2.2-2.4 | |
| | 53-63 | | | | 1.030 | 1-1.1 | 2.320 | 2.2-2.4 | |
| | 63-75 | | | | 1.030 | 1-1.1 | 2.320 | 2.2-2.4 | |
| | 75-150 | | | | 1.040 | 1-1.1 | 2.320 | 2.2-2.4 | |
| ER-TGS-014 | 75-106-particulate | | | | 0.980 | 0.95-1 | 1.150 | 1.15-1.2 | 2 |
| | 75-106-pellet | | | | 0.980 | 0.95-1 | 1.150 | 1.15-1.2 | |
| FB-JFM-031-3CP | 125-150 | | | | 1.030 | 1-1.1 | 2.320 | 2.2-2.4 | 2 |
| PA-RGB-024 | < 250 | 46 | 42 | 11 | 1.000 | 0.95-1.05 | 2.360 | 2.35-2.36 | 2 |
| PP-ALS-108 | < 45 | | | | 1.050 | 1-1.1 | 2.310 | 2.2-2.4 | 2 |
| | < 45 | | | | 1.050 | 1-1.1 | 2.320 | 2.2-2.4 | |
| | < 45 | | | | 1.040 | 1-1.1 | 2.320 | 2.2-2.4 | |
| | < 45 | | | | 1.050 | 1-1.1 | 2.320 | 2.2-2.4 | |
| | < 45 | | | | 1.050 | 1-1.1 | 2.320 | 2.2-2.4 | |
| | < 45 | | | | 1.050 | 1-1.1 | 2.310 | 2.2-2.4 | |
| | < 45 | | | | 1.050 | 1-1.1 | 2.320 | 2.2-2.4 | |
| PX-DWS-012 | 50-100 | 14.6 | | | 0.960 | 0.9-1 | 1.970 | 1.9-2 | 2, 6 |
| PX-RGM-018 | < 25 | 37.6 | 28.4 | 33 | 1.030 | 1-1.1 | 2.325 | 2.2-2.4 | 2 |
| SB-RGB-001 | | 16 | 48 | 37 | 0.925 | 0.9-1 | 1.945 | 1.8-2 | 2 |
| SB-RGB-015 | < 75 | | | | 0.950 | 0.9-1 | 1.145 | 1.14-2 | 2 |
| SB-RGB-021 | < 75 | | | | 0.970 | 0.9-1 | 1.140 | 1.1-1.2 | 2 |
| SB-RGB-055 | < 500 | | | | 0.975 | 0.9-1 | 2.205 | 2.2-2.4 | 2 |
| SR-JFM-042 | 710-1000 | | | | 1.075 | 1-1.5 | 2.315 | 2.3-2.33 | 2 |

Table 2. Samples with band minima and centers found in the literature. All are band centers except for the HOSERLab minima found in the University of Winnipeg Samples Directory.

| Sample name | Grain size (μm) | Wo | En | Fs | Band I min/center (μm) | Band II min/center (μm) | Source |
|---|---|---|---|---|---|---|---|
| PYX003 | 45-90 | 3.3 | 68.5 | 28.2 | 0.93 | 1.825 | Cloutis et al. 2006a |
| | 45-90 | | | | 0.915 | 1.784 | HOSERLab |
| | < 45 | | | | 0.918 | 1.819 | |

| | | | | | | | |
|---|---|---|---|---|---|---|---|
| | < 45 | | | | 0.926 | 1.863 | |
| | < 45 | | | | 0.925 | | |
| PYX009 | 45-90 | 50.5 | 39.8 | 9.7 | | 1.105 | Cloutis et al. 2006a |
| | 45-90 | | | | 0.962 | 1.121 | HOSERLab |
| | 45-90 | | | | 0.982 | 1.118 | |
| | 45-90 | | | | 0.983 | 1.123 | |
| | 45-90 | | | | | 2.492 | |
| PYX015 | 45-90 | 43.4 | 51 | 5.6 | 0.925 | 1.82 | Cloutis et al. 2006a |
| | < 45 | | | | 0.916 | 1.797 | HOSERLab |
| | < 45 | | | | 0.92 | 1.835 | |
| | < 45 | | | | 0.919 | | |
| PYX016 | 45-90 | 48.9 | 48.6 | 2.5 | 1.05 | 2.345 | Cloutis et al. 2006a |
| PYX017 | 45-90 | 44.4 | 47.5 | 8.1 | 1.035 | 2.295 | Cloutis et al. 2006a |
| PYX019 | 45-90 | 50.1 | 39 | 10.9 | 1.05 | 2.29 | Cloutis et al. 2006a |
| PYX020 | 45-90 | 48.7 | 48 | 3.3 | | 1.115 | Cloutis et al. 2006a |
| | 45-90 | | | | 0.977 | 1.088 | HOSERLab |
| | 45-90 | | | | 1.014 | 1.127 | |
| | 45-90 | | | | | 2.286 | |
| PYX021 | < 45 | 52.1 | 4.2 | 43.7 | 0.96 | 1.15 | HOSERLab |
| PYX023 | 45-90 | 1.3 | 89.3 | 9.4 | 0.92 | 1.845 | Cloutis et al. 2006a |
| | 45-90 | | | | 0.912 | 1.856 | HOSERLab |
| PYX026 | 45-90 | 60.9 | 10.4 | 28.7 | 1.035 | | Cloutis et al. 2006a |
| | 45-90 | | | | 0.97 | 1.125 | HOSERLab |
| | 45-90 | | | | | 2.28 | |
| PYX029 | 45-90 | 51.6 | 41.5 | 6.9 | 1.055 | 2.35 | Cloutis et al. 2006a |
| | 45-90 | | | | 1.011 | 2.296 | HOSERLab |
| PYX032 | 45-90 | 3.6 | 54.9 | 41.5 | 0.935 | 1.955 | Cloutis et al. 2006a |
| | 45-90 | | | | | 1.96 | |
| | 45-90 | | | | 0.928 | 1.958 | HOSERLab |
| PYX034 | 45-90 | 43.7 | 47.4 | 8.9 | 1.045 | 2.28 | Cloutis et al. 2006a |
| | 45-90 | | | | 1.005 | 2.243 | HOSERLab |
| PYX035 | 45-90 | 48.7 | 40.5 | 10.8 | 1.05 | 2.29 | Cloutis et al. 2006a |
| PYX036 | 45-90 | 43.3 | 43.3 | 13.4 | 1.04 | 2.29 | Cloutis et al. 2006a |
| | 45-90 | | | | 1.011 | 2.28 | HOSERLab |
| | 45-90 | | | | 1.031 | 2.339 | |
| PYX038 | 45-90 | 53.8 | 11 | 35.2 | 1.05 | | Cloutis et al. 2006a |
| | < 45 | | | | 0.95 | 1.15 | HOSERLab |
| PYX039 | 45-90 | 50.3 | 29.6 | 20.1 | 1.03 | 2.265 | Cloutis et al. 2006a |
| | < 45 | | | | 0.938 | 1.145 | HOSERLab |
| PYX040 | 45-90 | 48.8 | 42.7 | 8.5 | 1.045 | 2.255 | Cloutis et al. 2006a |
| | 45-90 | | | | 1.011 | 2.214 | HOSERLab |
| PYX042 | 45-90 | 0.4 | 86.8 | 12.8 | 0.915 | 1.855 | Cloutis et al. 2006a |
| | 45-90 | | | | 0.917 | 1.878 | HOSERLab |

| | | | | | | | |
|---|---|---|---|---|---|---|---|
| PYX101 | 45-90 | 43.3 | 34.7 | 22 | 1.025 | 2.33 | Cloutis et al. 2006a |
| PYX102 | 45-90 | 49.2 | 48.7 | 2.1 | 1.05 | 2.355 | Cloutis et al. 2006a |
| PYX103 | 45-90 | 40.5 | 40.8 | 18.7 | 1.005 | 2.1 | Cloutis et al. 2006a |
| | < 45 | | | | 0.989 | 2.023 | HOSERLab |
| | < 45 | | | | 0.997 | | |
| PYX105 | 45-90 | 48.6 | 43.9 | 7.5 | 1.045 | 2.35 | Cloutis et al. 2006a |
| PYX108 | 45-90 | 1.1 | 91.1 | 7.8 | 0.92 | 1.85 | Cloutis et al. 2006a |
| PYX110 | 45-90 | 0.5 | 86.3 | 13.2 | 0.915 | 1.855 | Cloutis et al. 2006a |
| | 45-90 | | | | | 1.86 | |
| PYX111 | 45-90 | 49.8 | 46 | 4.2 | 1.05 | 2.355 | Cloutis et al. 2006a |
| | < 45 | | | | 1.042 | 2.468 | HOSERLab |
| | < 45 | | | | 1.047 | | |
| PYX112 | 45-90 | 8.3 | 64.8 | 26.9 | 0.93 | 1.84 | Cloutis et al. 2006a |
| | < 45 | | | | 0.918 | 1.837 | HOSERLab |
| | < 45 | | | | 0.926 | 1.888 | |
| | < 45 | | | | 0.925 | | |
| PYX117 | 45-90 | 0.7 | 74.7 | 24.6 | 0.925 | 1.865 | Cloutis et al. 2006a |
| | 45-90 | | | | 0.92 | 1.875 | |
| | < 45 | | | | 0.917 | 1.873 | HOSERLab |
| | < 45 | | | | 0.907 | 1.873 | |
| | < 45 | | | | 0.92 | 1.897 | |
| | < 45 | | | | 0.921 | | |
| | 45-90 | | | | 0.92 | 1.87 | |
| PYX126 | 45-90 | 51.3 | 39.8 | 8.9 | 1.05 | 2.275 | Cloutis et al. 2006a |
| PYX135 | 45-90 | 49.9 | 48.5 | 1.6 | 1.06 | | Cloutis et al. 2006a |
| | < 45 | | | | 1.043 | | HOSERLab |
| | < 45 | | | | 1.058 | | |
| PYX136 | 45-90 | 49.6 | 48.8 | 1.6 | 1.055 | 2.325 | Cloutis et al. 2006a |
| | < 45 | | | | 1.043 | | HOSERLab |
| | < 45 | | | | 1.049 | | |
| PYX150 | 45-90 | 51.1 | 44.9 | 4 | | 1.1 | Cloutis et al. 2006a |
| | < 45 | | | | 0.982 | 1.112 | HOSERLab |
| | < 45 | | | | 0.987 | 1.131 | |
| PYX160 | 45-90 | 50.7 | 35.3 | 14 | | 2.35 | Cloutis et al. 2006a |
| PYX170 | 45-90 | 49.1 | 46.4 | 4.5 | 1.04 | 2.285 | Cloutis et al. 2006a |
| DL-CMP-009 | < 45 | 10 | 43 | 47 | 0.951 | 2.042 | Klima et al. 2011 |
| DL-CMP-011-A | < 45 | 14 | 36 | 50 | 0.954 | 2.089 | Klima et al. 2011 |
| DL-CMP-033-A | < 45 | 49 | 42 | 8 | 1.05 | 2.321 | Klima et al. 2011 |
| DL-CMP-036-A | < 45 | 49 | 27 | 24 | 1.061 | 2.35 | Klima et al. 2011 |
| DL-CMP-037-A | < 45 | 49 | 16 | 35 | 1.049 | 2.35 | Klima et al. 2011 |
| DL-CMP-039- | < 45 | 49 | 29 | 22 | 1.066 | 2.322 | Klima et al. 2011 |

| A | | | | | | | |
|---|---|---|---|---|---|---|---|
| DL-CMP-043-A | < 45 | 49 | 45 | 6 | 1.055 | 2.29 | Klima et al. 2011 |
| DL-CMP-050-A | < 45 | 23 | 19 | 58 | 0.983 | 2.262 | Klima et al. 2011 |
| DL-CMP-051-A | < 45 | 27 | 39 | 34 | 0.988 | 2.283 | Klima et al. 2011 |
| DL-CMP-053-A | < 45 | 9 | 23 | 68 | 0.964 | 2.164 | Klima et al. 2011 |
| DL-CMP-054-A | < 45 | 23 | 6 | 70 | 0.993 | 2.298 | Klima et al. 2011 |
| DL-CMP-055-A | < 45 | 26 | 18 | 56 | 0.994 | 2.303 | Klima et al. 2011 |
| DL-CMP-056-A | < 45 | 22 | 18 | 60 | 0.969 | 2.188 | Klima et al. 2011 |
| DL-CMP-057-A | < 45 | 25 | 36 | 39 | 0.992 | 2.268 | Klima et al. 2011 |
| DL-CMP-058-A | < 45 | 27 | 28 | 45 | 0.995 | 2.289 | Klima et al. 2011 |
| DL-CMP-066-A | < 45 | 38 | 15 | 58 | 1.01 | 2.309 | Klima et al. 2011 |
| DL-CMP-067-A | < 45 | 39 | 52 | 9 | 1.01 | 2.316 | Klima et al. 2011 |
| DL-CMP-068-A | < 45 | 38 | 29 | 33 | 1.01 | 2.332 | Klima et al. 2011 |
| DL-CMP-070-A | < 45 | 45 | 14 | 41 | 1.028 | 2.303 | Klima et al. 2011 |
| DL-CMP-071-A | < 45 | 43 | 26 | 31 | 1.023 | 2.308 | Klima et al. 2011 |
| DL-CMP-073-A | < 45 | 39 | 36 | 25 | 1.009 | 2.313 | Klima et al. 2011 |
| DL-CMP-074-A | < 45 | 39 | 24 | 37 | 1.011 | 2.308 | Klima et al. 2011 |
| DL-CMP-075-A | < 45 | 45 | 46 | 9 | 1.022 | 2.314 | Klima et al. 2011 |
| DL-CMP-076-A | < 45 | 46 | 18 | 35 | 1.032 | 2.275 | Klima et al. 2011 |
| DL-CMP-077-A | < 45 | 45 | 52 | 3 | 1.022 | 2.309 | Klima et al. 2011 |
| DL-CMP-079-A | < 45 | 47 | 38 | 15 | 1.023 | 2.311 | Klima et al. 2011 |
| DL-CMP-082-A | < 45 | 49 | 1 | 50 | 1.065 | 2.29 | Klima et al. 2011 |
| DL-CMP-083-A | < 45 | 51 | 0 | 49 | 1.07 | 2.338 | Klima et al. 2011 |
| DL-CMP-085-A | < 45 | 39 | 0 | 61 | 1.024 | 2.29 | Klima et al. 2011 |
| DL-CMP-087-A | < 45 | 29 | 0 | 71 | 1.006 | 2.294 | Klima et al. 2011 |
| DL-CMP-088-A | < 45 | 10 | 0 | 90 | 0.979 | 2.194 | Klima et al. 2011 |
| PE-CMP-030 | 45-75 | 1 | 87 | 12 | 0.91 | 1.83 | Sunshine & Pieters 1993 |
| | < 45 | | | | 0.909 | 1.833 | |

| | 45-75 | | | | 0.907 | | 1.827 | |
|---|---|---|---|---|---|---|---|---|
| | 75-125 | | | | 0.907 | | 1.83 | |
| | < 45 | | | | 0.911 | | 1.833 | Duffard et al. 2005 |
| PP-CMP-021 | | 45.59 | 45.89 | 8.52 | 1.02 | | 2.29 | Sunshine & Pieters 1993 |
| | < 45 | | | | 1.012 | | 2.268 | |
| | 45-75 | | | | 1.011 | | 2.269 | |
| | 75-125 | | | | 1.012 | | 2.276 | |
| PX-DWS-012 | 50-100 | 14.6 | | | 1 | | 1.98 | Gietzen et al. 2012 |

Table 3. Select samples with polynomial fitted minima with the methods and spreadsheets from McCraig et al. 2017. 1=RELAB, 2=HOSERLab, 3=Sunshine et al. 1990, 4=Sunshine & Pieters 1993, 5=Klima et al. 2011, and 6=Gietzen et al. 2012.

| Sample name | Grain size (µm) | Wo | En | Fs | Band I minimum (µm) | Band I fitting range (µm) | Band II minimum (µm) | Band II fitting range (µm) | Source |
|---|---|---|---|---|---|---|---|---|---|
| PYX005 | < 45 | 49.1 | 41 | 9.9 | 1.023 | 0.95-1.084 | 2.347 | 2.23-2.425 | 1, 2 |
| | 45-90 | | | | 1.025 | 0.95-1.1 | 2.310 | 2.15-2.45 | |
| | 90-180 | | | | 1.033 | 0.96-1.1 | 2.337 | 2.21-2.41 | |
| PYX007 | 45-90 | 53.1 | 35.7 | 11.2 | 0.915 | 0.89-0.925 | | | 1, 2 |
| PYX009 | 45-90 | 50.5 | 39.8 | 9.7 | 0.974 | 0.95-1 | 1.136 | 1.1-1.163 | 1, 2 |
| PYX010 | 45-90 | 50.9 | 30.4 | 18.7 | 0.975 | 0.935-1.03 | 1.130 | 1.08-1.17 | 1, 2 |
| PYX016 | < 45 | 48.9 | 48.6 | 2.5 | 1.049 | 1.006-1.09 | 2.348 | 2.18-2.492 | 1, 2 |
| | 45-90 | | | | 1.050 | 1-1.1 | 2.345 | 2.16-2.49 | |
| PYX017 | 45-90 | 44.4 | 47.5 | 8.1 | 1.020 | 0.95-1.095 | 2.300 | 2.1-2.48 | 1, 2 |
| | 90-180 | | | | 1.022 | 0.942-1.1 | 2.287 | 2.1-2.45 | |
| PYX020 | 45-90 | 48.7 | 48 | 3.3 | 0.960 | 0.935-0.985 | 1.085 | 1.05-1.1 | 1, 2 |
| PYX021 | 45-90 | 52.1 | 4.2 | 43.7 | 0.970 | 0.93-1.025 | | | 1, 2 |
| PYX023 | < 45 | 1.3 | 89.3 | 9.4 | 0.913 | 0.855-0.97 | 1.864 | 1.167-2.032 | 1, 2 |
| | 45-90 | | | | 0.910 | 0.86-0.96 | 1.855 | 1.72-1.975 | |
| | 90-180 | | | | 0.913 | 0.85-0.974 | 1.864 | 1.69-2.018 | |
| PYX026 | 45-90 | 60.9 | 10.4 | 28.7 | 0.955 | 0.91-1 | | | 1, 2 |
| PYX032 | < 45 | 3.6 | 54.9 | 41.5 | 0.930 | 0.86-1 | 1.961 | 1.758-2.15 | 1, 2 |
| | 45-90 | | | | 0.925 | 0.82-1.02 | 1.950 | 1.68-2.2 | |
| | 90-180 | | | | 0.929 | 0.86-1 | 1.972 | 1.78-2.15 | |
| PYX053 | < 45 | 47.9 | 48.2 | 3.9 | 0.958 | 0.94-0.98 | 1.037 | 1.009-1.065 | 1, 2 |
| PYX057 | < 45 | 41 | 34.1 | 24.9 | 0.897 | 0.85-0.95 | 2.341 | 2.29-2.457 | 1, 2 |
| PYX102 | 45-90 | 49.2 | 48.7 | 2.1 | 1.050 | 0.99-1.1 | 2.345 | 2.17-2.59 | 1, 2 |
| PYX105 | 45-90 | 48.6 | 43.9 | 7.5 | 1.035 | 0.98-1.08 | 2.325 | 2.21-2.45 | 1, 2 |
| PYX109 | 45-90 | 49.7 | 30.6 | 19.7 | 0.980 | 0.94-1.03 | 1.155 | 1.1-1.2 | 1, 2 |
| PYX111 | 45-90 | 49.8 | 46 | 4.2 | 1.050 | 0.99-1.1 | 2.345 | 2.27-2.55 | 1, 2 |
| PYX112 | < 45 | 8.3 | 64.8 | 26.9 | 0.920 | 0.86-0.98 | 1.840 | 1.66-2 | 1, 2 |

| Sample name | Grain size | Wo | En | Fs | Band I min | Band I range | Band II min | Band II range | Sources |
|---|---|---|---|---|---|---|---|---|---|
| PYX120 | 45-90 | 49.8 | 45.4 | 4.8 | 0.990 | 0.95-1.03 | | | 1, 2 |
| PYX135 | < 45 | 49.9 | 48.5 | 1.6 | 1.055 | 1-1.1 | 2.345 | 2.2-2.55 | 1, 2 |
| PYX136 | < 45 | 49.6 | 48.8 | 1.6 | 1.055 | 1-1.1 | 2.360 | 2.2-2.61 | 1, 2 |
| PYX150 | < 45 | 51.1 | 44.9 | 4 | 0.970 | 0.93-1.02 | 1.130 | 1.06-1.17 | 1, 2 |
| | 45-90 | | | | 0.968 | 0.95-0.99 | 1.132 | 1.1-1.157 | |
| PYX160 | 45-90 | 50.7 | 35.3 | 14 | 0.985 | 0.94-1.035 | | | 1, 2 |
| PE-CMP-030 | < 45 | 1 | 87 | 12 | 0.910 | 0.86-0.96 | 1.835 | 1.64-2.03 | 1, 3 |
| | 45-75 | | | | 0.910 | 0.86-0.96 | 1.830 | 1.64-2.015 | |
| | 75-125 | | | | 0.910 | 0.86-0.96 | 1.830 | 1.64-2.015 | |
| PP-CMP-021 | < 45 | 45.59 | 45.89 | 8.52 | 1.020 | 0.94-1.1 | 2.270 | 2.12-2.41 | 1, 4 |
| | 45-75 | | | | 1.015 | 0.94-1.1 | 2.270 | 2.12-2.41 | |
| | 75-125 | | | | 1.015 | 0.94-1.1 | 2.265 | 2.12-2.41 | |
| DL-CMP-083-A | < 45 | 51 | 0 | 49 | 0.990 | 0.97-1.01 | 1.070 | 1.05-1.1 | 1, 5 |
| | | | | | | | 2.305 | 2.2-2.44 | |
| ER-TGS-014 | 75-106 | | | | 1.010 | 0.97-1.03 | 1.150 | 1.11-1.18 | 1 |
| FB-JFM-031-3CP | 125-250 | | | | 1.030 | 0.96-1.1 | 2.310 | 2.18-2.42 | 1 |
| PA-RGB-024 | <250 | 46 | 42 | 11 | 1.015 | 0.95-1.07 | 2.320 | 2.2-2.4 | 1 |
| PP-ALS-108 | < 45 | | | | 1.050 | 1-1.09 | 2.320 | 2.2-2.46 | 1 |
| PX-DWS-012 | < 50-100 | 14.6 | | | 0.960 | 0.9-1.02 | 2.000 | 1.85-2.25 | 1, 6 |
| SB-RGB-015 | < 75 | | | | 0.960 | 0.93-1 | 1.105 | 1.095-1.14 | 1 |
| SB-RGB-021 | < 75 | | | | 0.970 | 0.94-1.01 | 1.130 | 1.06-1.17 | 1 |
| SR-JFM-042 | 45-150 | | | | 1.050 | 1-1.09 | 2.310 | 2.2-2.4 | 1 |

Table 4. Original spectral groupings that I found using the first samples and lowest reflectance minima. Sources: HOSERLab, RELAB, USGS Spectral Library.

| Sample name | Grain size (μm) | Wo | En | Fs | Band I minimum (μm) | Band II minimum (μm) | Original groupings | Possible notes | Other notes |
|---|---|---|---|---|---|---|---|---|---|
| PYX120 | 45-90 | 49.8 | 45.4 | 4.8 | 0.990 | 1.100 | Possible with PYX150. | Possible with PYX150: Both have similar endmember compositions, are diopsides, and are type A clinopyroxenes. Band minima are a little different. Chemical compositions are overall | Hard to get 2 μm feature. |

| | | | | | | | | | |
|---|---|---|---|---|---|---|---|---|---|
| | | | | | | | | similar, with the main exceptions of $Fe_2O_3$ (0.68 wt. %, 0 wt. %) and $Na_2O$ (0.69 wt. %, 0.05 wt. %). | |
| PYX150 | < 45 | 51.1 | 44.9 | 4 | 0.975 | 1.115 | Possible with PYX120. | Possible with PYX120: Both have similar endmember compositions, are diopsides, and are type A clinopyroxenes. Band minima are a little different. Chemical compositions are overall similar, with the main exceptions of $Fe_2O_3$ (0.68 wt. %, 0 wt. %) and $Na_2O$ (0.69 wt. %, 0.05 wt. %). | Has multiple spectra. |
| PYX160 | 45-90 | 50.7 | 35.3 | 14 | 0.985 | 1.100 | | | Hard to get 2 µm feature. |
| PYX007 | 45-90 | 53.1 | 35.7 | 11.2 | 0.920 | 1.100 | | | |
| PYX009 | 45-90 | 50.5 | 39.8 | 9.7 | 0.960 | 1.135 | | | |
| PYX020 | 45-90 | 48.7 | 48 | 3.3 | 0.950 | 1.100 | | | |
| PYX053 | < 45 | 47.9 | 48.2 | 3.9 | 0.956 | 1.032 | | | |

| | | | | | | | | |
|---|---|---|---|---|---|---|---|---|
| PYX057 | < 45 | 41 | 34.1 | 24.9 | 0.892 | 1.005 | | |
| PYX112 | < 45 | 8.3 | 64.8 | 26.9 | 0.920 | 1.840 | | |
| DL-CMP-035-A | < 45 | 50 | 10 | 40 | 1.075 | 1.735 | Probable with DL-CMP-040-A. | | No chemical analyses available. Maybe a mixture, so it is a problem sample. |
| DL-CMP-040-A | < 45 | 50 | 5 | 45 | 1.060 | 1.760 | Probable with DL-CMP-035-A. | | No chemical analyses available. Maybe a mixture, so it is a problem sample. |
| DL-CMP-048-A | < 45 | 10 | 14 | 77 | 0.945 | 2.110 | | | No chemical analyses. |
| DL-CMP-049-A | < 45 | 19 | 11 | 70 | 0.965 | 2.185 | Possible with DL-CMP-053-A. | Possible with DL-CMP-053-A: Have similar iron amounts in the endmember compositions and similar band I and II minima. | No chemical analyses. |
| DL-CMP-053-A | < 45 | 9 | 23 | 68 | 0.970 | 2.185 | Possible with DL-CMP-049-A. | Possible with DL-CMP-049-A: Have similar iron amounts in the endmember compositions and similar band I and II minima. | No chemical analyses. |
| DL-CMP-088-A | < 45 | 10 | 0 | 90 | 0.990 | 2.200 | | | No chemical analyses. |

| | | | | | | | | |
|---|---|---|---|---|---|---|---|---|
| | | | | | | | | |
| DL-CMP-009 | < 45 | 10 | 43 | 47 | 0.960 | 2.030 | Possible with DL-CMP-013. | Possible with DL-CMP-013: Similar endmember compositions, short wavelength features, and spectral shapes. | No chemical analyses. Has 0.5 % glass. |
| DL-CMP-013 | < 45 | 8 | 46 | 46 | 0.945 | 1.990 | Possible with DL-CMP-009. | Possible with DL-CMP-009: Similar endmember compositions, short wavelength features, and spectral shapes. | No chemical analyses. Has 0.5 % glass, cristobalite. |
| | | | | | | | | |
| DL-CMP-010 | < 45 | 10 | 63 | 27 | 0.945 | 1.960 | Possible with DL-CMP-018-A. | Possible with DL-CMP-018-A: Similar calcium amounts in the endmember compositions, similar band I minima. | No chemical analyses. Appears to be a mixture, so it is a problem sample. Has trace cristobalite. |
| DL-CMP-018-A | < 45 | 10 | 72 | 18 | 0.945 | 1.905 | Possible with DL-CMP-010. | Possible with DL-CMP-010-A: Similar calcium amounts in the endmember compositions, similar band I minima. | No chemical analyses. Appears to be a mixture, so it is a problem sample. |
| | | | | | | | | |
| PYX016 | 45-90 | 48.9 | 48.6 | 2.5 | 1.050 | 2.315 | Probable with NMNH1R8685. Possible with PYX102. | Possible with PYX102: Both are diopsides and have similar endmember compositions and band I and II minima. PYX016 has a stronger feature around 0.8 µm. The only main difference in chemical compositions is $Al_2O_3$ (0.23 wt. %, 0.94 wt. %). | Has multiple spectra. |
| PYX102 | 45-90 | 49.2 | 48.7 | 2.1 | 1.050 | 2.315 | Possible with PYX016, NMNHR18685, PYX135, PYX136. | Possible with PYX016: Both are diopsides and have similar endmember compositions and band I and II minima. PYX016 has a stronger feature around 0.8 µm. The only main | |

| | | | | | | | | | |
|---|---|---|---|---|---|---|---|---|---|
| | | | | | | | | difference in chemical compositions is $Al_2O_3$ (0.23 wt. %, 0.94 wt. %). Possible with NMNHR18685: Both have similar band I and II minima. NMNHR18685 has shorter wavelength features. Possible with PYX135: Both have similar endmember compositions, band I and II minima, and chemical compositions. PYX135 has much weaker 1 and 2 µm features. Possible with PYX136: Both have similar endmember compositions, band I and II minima, and chemical compositions, however $Al_2O_3$ is (0.94 wt. %, 0.06 wt. %). PYX136 has weaker 1 and 2 µm features, and a much noisier 2 µm feature. | |
| NMNHR18685 | 263 | | | | 1.054 | 2.315 | Probable with PYX016. Possible with PYX102. | Possible with PYX102: Both have similar band I and II minima. NMNHR18685 has shorter wavelength features. | No endmember or full chemical compositions. Noisy spectra near 2 µm, which makes me consider it more of a problem sample. |
| | | | | | | | | | |
| PYX101 | 45-90 | 43.3 | 34.7 | 22 | 1.010 | 2.330 | | | |
| | | | | | | | | | |

| | | | | | | | | | |
|---|---|---|---|---|---|---|---|---|---|
| PYX052 | < 45 | 50.5 | 43.8 | 5.8 | 1.060 | 2.312 | | | |
| PYX105 | 45-90 | 48.6 | 43.9 | 7.5 | 1.030 | 2.320 | | | |
| PYX170 | < 45 | 49.1 | 46.4 | 4.5 | 1.030 | 2.330 | | | |
| DL-CMP-041-A | < 45 | 50 | 0 | 50 | 0.960 | 2.100 | | | No chemical analyses. |
| | | | | | | | | | |
| DL-CMP-033-A | < 45 | 49 | 42 | 8 | 1.050 | 2.365 | Possible with DL-CMP-043-A. | Possible with DL-CMP-043-A: Both have similar endmember compositions and band I and II minima. | No chemical analyses. Has 1 % cristobalite. |
| DL-CMP-036-A | < 45 | 49 | 27 | 24 | 1.060 | 2.250 | Possible with DL-CMP-037-A & DL-CMP-039-A, DL-CMP-044-A. | Possible with DL-CMP-037-A & DL-CMP-039-A: DL-CMP-036-A and DL-CMP-039-A have similar endmember compositions, while DL-CMP-037-A has the same calcium endmember amount but more iron. All three have similar 1 µm band minima, and DL-CMP-036-A and DL-CMP-037-A have similar 2 µm band minima. DL-CMP-036-A and DL-CMP-039-A are both augites. DL- | No chemical analyses. Has 5 % bustamite. |

| | | | | | | | | | |
|---|---|---|---|---|---|---|---|---|---|
| | | | | | | | | CMP-037-A and DL-CMP-039-A have stronger features ~ 0.8 µm. Possible with DL-CMP-044-A: Both have similar calcium endmember amounts and band I minima. Iron and magnesium endmember amounts are different. | |
| DL-CMP-037-A | < 45 | 49 | 16 | 35 | 1.055 | 2.260 | Possible with DL-CMP-036-A & DL-CMP-039-A. | Possible with DL-CMP-036-A & DL-CMP-039-A: DL-CMP-036-A and DL-CMP-039-A have similar endmember compositions, while DL-CMP-037-A has the same calcium endmember amount but more iron. All three have similar 1 µm band minima, and DL-CMP-036-A and DL-CMP-037-A have similar 2 µm band minima. DL-CMP-036-A and DL-CMP-039-A are both augites. DL-CMP-037-A and DL-CMP-039-A have stronger features ~ 0.8 µm. | No chemical analyses. |
| DL-CMP-039-A | < 45 | 49 | 29 | 22 | 1.050 | 2.330 | Possible with DL-CMP-036-A & DL-CMP-037-A, DL-CMP-044-A, DL-CMP-037-A. | Possible with DL-CMP-036-A & DL-CMP-037-A: DL-CMP-036-A and DL-CMP-039-A have similar endmember compositions, while DL-CMP-037-A has the same calcium endmember amount but more iron. All three have | No chemical analyses. 99 % augite. |

| | | | | | | | | | |
|---|---|---|---|---|---|---|---|---|---|
| | | | | | | | | similar 1 µm band minima, and DL-CMP-036-A and DL-CMP-037-A have similar 2 µm band minima. DL-CMP-036-A and DL-CMP-039-A are both augites. DL-CMP-037-A and DL-CMP-039-A have stronger features ~ 0.8 µm. Possible with DL-CMP-044-A: Both have similar calcium endmember amounts and band I and band II minima. Iron and magnesium endmember amounts are different. | |
| DL-CMP-043-A | < 45 | 49 | 45 | 6 | 1.055 | 2.355 | Possible with DL-CMP-033-A, DL-CMP-044-A. | Possible with DL-CMP-033-A: Both have similar endmember compositions and band I and II minima. | No chemical analyses. |
| DL-CMP-044-A | < 45 | 49 | 43 | 8 | 1.050 | 2.325 | Possible with DL-CMP-036-A, DL-CMP-039-A. | Possible with DL-CMP-036-A: Both have similar calcium endmember amounts and band I minima. Iron and magnesium endmember amounts are different. Possible with DL-CMP-039-A: Both have similar calcium endmember amounts and band I and band II minima. Iron and magnesium endmember amounts are different. | No chemical analyses. |
| | | | | | | | | | |

| | | | | | | | | |
|---|---|---|---|---|---|---|---|---|
| DL-CMP-075-A | < 45 | 45 | 46 | 9 | 1.030 | 2.335 | Possible with DL-CMP-077-A. | Possible with DL-CMP-077-A: Both have similar endmember compositions, band I minima, and shorter wavelength features. | No chemical analyses. |
| DL-CMP-077-A | < 45 | 45 | 52 | 3 | 1.025 | 2.355 | Possible with DL-CMP-075-A. | | No chemical analyses. |
| | | | | | | | | | |
| PYX017 | 45-90 | 44.4 | 47.5 | 8.1 | 1.025 | 2.290 | Possible with PYX034. | Possible with PYX034: Both are endiopsides and have similar endmember compositions. Chemical analyses are somewhat similar, with differences in $Al_2O_3$ (4.09 wt. %, 5.63 wt. %), $Fe_2O_3$ (1.25 wt. %, 2.03 wt. %), $Na_2O$ (0.32 wt. %, 1.06 wt. %), $TiO_2$ (1.04 wt. %, 1.55 wt. %), and $Cr_2O_3$ (0.78 wt. %, 0.12 wt. %). | Has multiple Spectra. |
| PYX019 | 45-90 | 50.1 | 39 | 10.9 | 1.020 | 2.265 | Probable with PYX035. | | |
| PYX034 | 45-90 | 43.7 | 47.4 | 8.9 | 1.015 | 2.250 | Possible with PYX017, PYX035. | Possible with PYX017: Both are endiopsides and have similar endmember compositions. Chemical analyses are somewhat similar, with differences in $Al_2O_3$ (4.09 wt. %, 5.63 wt. %), $Fe_2O_3$ (1.25 wt. %, 2.03 wt. %), $Na_2O$ (0.32 wt. %, 1.06 wt. %), $TiO_2$ (1.04 wt. %, 1.55 wt. %), and $Cr_2O_3$ (0.78 wt. %, 0.12 wt. | |

| | | | | | | | | | |
|---|---|---|---|---|---|---|---|---|---|
| | | | | | | | | %). Possible with PYX035: Both have similar endmember compositions and band I and II minima. PYX034 is an endiopside while PYX035 is a salite. The chemical compositions are similar with the exception of the lower iron amounts in PYX034, $Fe_2O_3$ (2.03 wt. %, 2.56 wt. %), $Na_2O$ (1.06 wt. %, 0.53 wt. %). | |
| PYX035 | 45-90 | 48.7 | 40.5 | 10.8 | 1.010 | 2.250 | Probable with PYX019. Possible with PYX054, PYX034. | Possible with PYX054: PYX035 is a salite, while PYX054 is an augite. Both have similar endmember compositions. Chemical analyses are similar with differences in $Al_2O_3$ (5.15 wt. %, 6.56 wt. %), FeO (6.29 wt. %, 7.08 wt. %), $Fe_2O_3$ (2.56 wt. %, 3.50 wt. %), and $TiO_2$ (1.73 wt. %, 1.12 wt. %). Possible with PYX035: Both have similar endmember compositions and band I and II minima. PYX034 is an endiopside while PYX035 is a salite. The chemical compositions are similar with the exception of the lower iron amounts in PYX034, Fe2O3 (2.03 wt. %, 2.56 wt. %), Na2O (1.06 wt. %, 0.53 wt. %). | |

| | | | | | | | | |
|---|---|---|---|---|---|---|---|---|
| PYX036 | 45-90 | 43.3 | 43.3 | 13.4 | 1.020 | 2.290 | | |
| PYX040 | 45-90 | 48.8 | 42.7 | 8.5 | 1.005 | 2.245 | | |
| PYX054 | < 45 | 45.9 | 41.9 | 12.2 | 1.017 | 2.202 | Possible with PYX035. | Possible with PYX035: PYX035 is a salite, while PYX054 is an augite. Both have similar endmember compositions. Chemical analyses are similar with differences in $Al_2O_3$ (5.15 wt. %, 6.56 wt. %), FeO (6.29 wt. %, 7.08 wt. %), $Fe_2O_3$ (2.56 wt. %, 3.50 wt. %), and $TiO_2$ (1.73 wt. %, 1.12 wt. %). | |
| DL-CMP-017-A | < 45 | 20 | 64 | 16 | 0.990 | 2.235 | Possible with DL-CMP-019-A. | Possible with DL-CMP-019-A: Both have similar calcium endmember compositions and similar band I and II minima. | No chemical analyses. Is 99.5 % cpx. |
| DL-CMP-019-A | < 45 | 20 | 56 | 24 | 0.995 | 2.235 | Possible with DL-CMP-017-A. | Possible with DL-CMP-017-A: Both have similar calcium endmember compositions and similar band I and II minima. | No chemical analyses. Is 99.5 % cpx. |
| PYX111 | < 45 | 49.8 | 46 | 4.2 | 1.050 | 2.320 | Probable with PYX135. Possible with PYX135 & PYX136. | Possible with PYX135 & PYX136: All three have similar endmember compositions, band I and II minima, weak 2 | Noisy, weak 2 µm area. |

| | | | | | | | | | |
|---|---|---|---|---|---|---|---|---|---|
| | | | | | | | | µm features, and are diopsides. PYX111 does not have a 0.8 µm feature like the other two. Chemical analyses are similar, with differences in $Al_2O_3$ (0.72 wt. %, 0.54 wt. %, 0.06 wt. %), FeO (2.67 wt. %, 1.03 wt. %, 1.05 wt. %), and $Na_2O$ (0.40 wt. %, 0.35 wt. %, 0.02 wt. %). | |
| PYX135 | < 45 | 49.9 | 48.5 | 1.6 | 1.055 | 2.320 | Probable with PYX136, PYX111. Possible with PYX111 & PYX136, PYX102. | Possible with PYX111 & PYX136: All three have similar endmember compositions, band I and II minima, weak 2 µm features, and are diopsides. PYX111 does not have a 0.8 µm feature like the other two. Chemical analyses are similar, with differences in $Al_2O_3$ (0.72 wt. %, 0.54 wt. %, 0.06 wt. %), FeO (2.67 wt. %, 1.03 wt. %, 1.05 wt. %), and $Na_2O$ (0.40 wt. %, 0.35 wt. %, 0.02 wt. %). Possible with PYX102: Both have similar endmember compositions, band I and II minima, and chemical compositions. PYX135 has much weaker 1 and 2 µm features. | Noisy, weak 2 µm area. |
| PYX136 | < 45 | 49.6 | 48.8 | 1.6 | 1.050 | 2.315 | Probable with PYX135. Possible with PYX111 & PYX135, PYX102. | Possible with PYX111 & PYX135: All three have similar endmember compositions, band I and II | Noisy, weak 2 µm area. |

| | | | | | | | | | |
|---|---|---|---|---|---|---|---|---|---|
| | | | | | | | | | minima, weak 2 µm features, and are diopsides. PYX111 does not have a 0.8 µm feature like the other two. Chemical analyses are similar, with differences in $Al_2O_3$ (0.72 wt. %, 0.54 wt. %, 0.06 wt. %), FeO (2.67 wt. %, 1.03 wt. %, 1.05 wt. %), and $Na_2O$ (0.40 wt. %, 0.35 wt. %, 0.02 wt. %). Possible with PYX102: Both have similar endmember compositions, band I and II minima, and chemical compositions, however $Al_2O_3$ is (0.94 wt. %, 0.06 wt. %). PYX136 has weaker 1 and 2 µm features, and a much noisier 2 µm feature. | |
| DL-CMP-032-A | < 45 | 46.2 | 53.8 | 0 | 1.050 | 2.380 | | | No chemical analyses. Problem sample because endmember composition has no iron. |
| PP-CMP-021 | < 45 | 45.59 | 45.9 | 8.52 | 1.015 | 2.280 | | | |
| NMNH120049 | 35 | 34 | 45 | 21 | 1.006 | 2.295 | | | |

Table 5. Samples with available compositions from their previous sources of USGS Spectral Library, RELAB, and HOSERLab.

| Wt. % | NMNH120049 | NMNHR18685 | HS199 | PYX003 | PYX005 | PYX007 | PYX009 | PYX010 |
|---|---|---|---|---|---|---|---|---|
| SiO$_2$ | 48.93 | 54.77 | | 50.33 | 49.70 | 44.46 | 53.90 | 51.94 |
| Al$_2$O$_3$ | 8.44 | 0.49 | | 5.46 | 4.12 | 8.08 | 0.51 | 0.50 |
| FeO | 8.59 | 0.87 | 25.31 | 17.30 | 5.93 | 6.11 | 6.20 | 10.18 |
| Fe$_2$O$_3$ | | | | 1.43 | 0.77 | 2.07 | 0.00 | 4.83 |
| MgO | 14.37 | 18.26 | | 23.58 | 13.80 | 10.92 | 14.18 | 9.31 |
| CaO | 16.87 | 25.60 | 33.93 | 1.59 | 22.94 | 22.64 | 25.08 | 21.65 |
| Na$_2$O | 1.57 | 0.39 | | 0.05 | 0.57 | 0.94 | 0.05 | 1.39 |
| TiO$_2$ | 1.38 | 0.05 | | 0.41 | 1.48 | 3.92 | 0.01 | tr. |
| Cr$_2$O$_3$ | | | | 0.11 | 0.17 | 0.05 | 0.04 | 0.03 |
| MnO | 0.21 | 0.06 | 40.86 | 0.29 | 0.11 | 0.27 | 0.26 | 0.52 |
| K$_2$O | 0.02 | 0.01 | | | | | | |
| V$_2$O$_5$ | | | | 0.02 | 0.00 | 0.00 | 0.02 | tr. |
| CoO | | | | 0.04 | 0.04 | 0.04 | 0.05 | 0.02 |
| NiO | | | | 0.01 | 0.04 | 0.02 | 0.15 | 0.01 |
| ZrO$_2$ | | | | 0.00 | 0.00 | 0.00 | 0.00 | 0.00 |
| ZnO | | | | | | | | |
| Nb$_2$O$_5$ | | | | | | | | |
| P$_2$O$_5$ | | | | | | | | |
| Total | 100.38 | 100.49 | | 100.62 | 99.67 | 99.52 | 100.45 | 100.38 |

| Wt. % | PYX015 | PYX016 | PYX017 | PYX019 | PYX020 | PYX021 | PYX023 | PYX026 |
|---|---|---|---|---|---|---|---|---|
| SiO$_2$ | 52.07 | 55.08 | 50.57 | 48.41 | 55.23 | 48.35 | 56.86 | 49.37 |
| Al$_2$O$_3$ | 6.34 | 0.23 | 4.09 | 5.29 | 0.59 | 0.54 | 0.76 | 0.61 |
| FeO | 3.25 | 1.69 | 4.88 | 6.15 | 2.07 | 23.25 | 6.36 | 13.62 |
| Fe$_2$O$_3$ | 0.01 | 0.10 | 1.25 | 3.79 | 0.00 | 3.81 | 0.83 | 5.07 |
| MgO | 16.42 | 17.82 | 16.05 | 12.37 | 17.06 | 1.25 | 34.04 | 2.79 |
| CaO | 19.38 | 24.96 | 20.85 | 22.15 | 24.08 | 21.66 | 0.65 | 22.54 |
| Na$_2$O | 1.31 | 0.13 | 0.32 | 0.36 | 0.52 | 0.18 | 0.00 | 0.13 |
| TiO$_2$ | 0.21 | 0.07 | 1.04 | 1.05 | 0.09 | 0.00 | 0.01 | 0.01 |
| Cr$_2$O$_3$ | 1.39 | 0.03 | 0.78 | 0.03 | 0.96 | 0.02 | 0.45 | 0.03 |
| MnO | 0.10 | 0.07 | 0.13 | 0.26 | 0.10 | 1.17 | 0.17 | 6.71 |
| K$_2$O | | | | | | | | |
| V$_2$O$_5$ | 0.03 | 0.00 | 0.02 | 0.03 | 0.05 | tr. | tr. | 0.01 |
| CoO | 0.03 | 0.04 | 0.03 | 0.05 | 0.05 | 0.06 | 0.03 | 0.05 |
| NiO | 0.07 | 0.03 | 0.06 | 0.02 | 0.06 | 0.02 | 0.08 | 0.03 |
| ZrO$_2$ | 0.00 | 0.00 | 0.00 | 0.00 | 0.00 | 0.00 | 0.00 | 0.00 |
| ZnO | n.d. | n.d. | n.d. | n.d. | n.d. | n.d. | n.d. | 0.00 |
| Nb$_2$O$_5$ | | | | | | | | |
| P$_2$O$_5$ | | | | | | | | |

| Wt. % | | | | | | PYX038 | PYX039 | |
|---|---|---|---|---|---|---|---|---|
| Total | 100.61 | 100.25 | 100.07 | 99.96 | 100.86 | 100.31 | 100.24 | 100.97 |
| | PYX029 | PYX032 | PYX034 | PYX035 | PYX036 | | | PYX040 |
| $SiO_2$ | 51.56 | 50.21 | 49.80 | 48.05 | 50.54 | 49.40 | 51.45 | 47.27 |
| $Al_2O_3$ | 3.48 | 1.24 | 5.63 | 5.15 | 2.99 | 0.31 | 1.16 | 8.28 |
| $FeO$ | 4.20 | 23.65 | 5.21 | 6.29 | 8.18 | 17.49 | 10.26 | 4.69 |
| $Fe_2O_3$ | 1.39 | 5.11 | 2.03 | 2.56 | 1.71 | 8.70 | 6.47 | 2.77 |
| $MgO$ | 14.01 | 17.57 | 14.58 | 13.12 | 14.64 | 3.06 | 8.47 | 13.19 |
| $CaO$ | 24.22 | 1.59 | 19.86 | 21.95 | 20.35 | 20.80 | 20.03 | 20.90 |
| $Na_2O$ | 0.40 | 0.00 | 1.06 | 0.53 | 0.27 | 0.61 | 2.14 | 0.63 |
| $TiO_2$ | 0.38 | 0.19 | 1.55 | 1.73 | 0.86 | 0.00 | 0.05 | 1.73 |
| $Cr_2O_3$ | 0.03 | 0.04 | 0.12 | 0.03 | 0.07 | 0.02 | 0.02 | 0.43 |
| $MnO$ | 0.31 | 0.53 | 0.12 | 0.19 | 0.25 | 0.61 | 0.67 | 0.11 |
| $K_2O$ | | | | | | | | |
| $V_2O_5$ | 0.00 | tr. | 0.01 | 0.02 | 0.08 | 0.00 | tr. | tr. |
| $CoO$ | 0.03 | 0.06 | 0.03 | 0.04 | 0.04 | 0.08 | 0.05 | 0.03 |
| $NiO$ | 0.03 | 0.01 | 0.05 | 0.02 | 0.02 | 0.01 | 0.02 | 0.03 |
| $ZrO_2$ | 0.00 | 0.00 | 0.00 | 0.00 | 0.00 | 0.00 | 0.00 | 0.00 |
| $ZnO$ | n.d. | n.d. | n.d. | n.d. | n.d. | n.d. | n.d. | n.d. |
| $Nb_2O_5$ | | | | | | | | n.d. |
| $P_2O_5$ | | | | | | | | |
| Total | 100.04 | 100.20 | 100.05 | 99.68 | 100.00 | 101.09 | 100.79 | 100.06 |
| Wt. % | PYX042 | PYX052 | PYX053 | PYX054 | PYX057 | PYX101 | PYX102 | PYX103 |
| $SiO_2$ | 56.59 | 51.84 | 55.57 | 46.40 | 53.81 | 50.63 | 54.72 | 52.06 |
| $Al_2O_3$ | 0.09 | 0.49 | 0.65 | 6.56 | 14.02 | 1.49 | 0.94 | 0.98 |
| $FeO$ | 8.93 | 3.81 | 2.41 | 7.08 | 7.57 | 12.99 | 1.40 | 11.38 |
| $Fe_2O_3$ | 0.84 | 0.36 | 0.63 | 3.50 | 2.76 | 1.44 | 0.02 | 1.32 |
| $MgO$ | 33.88 | 16.22 | 16.69 | 13.68 | 5.84 | 11.52 | 17.79 | 13.96 |
| $CaO$ | 0.22 | 26.02 | 23.03 | 20.83 | 9.76 | 19.99 | 25.00 | 19.31 |
| $Na_2O$ | 0.00 | 0.39 | 0.30 | 0.60 | 3.17 | 0.16 | 0.16 | 0.22 |
| $TiO_2$ | 0.04 | 0.03 | 0.01 | 1.12 | 1.41 | 0.67 | 0.08 | 0.35 |
| $Cr_2O_3$ | 0.04 | 10 ppm | 4350 ppm | 90 ppm | 20 ppm | 0.14 | 0.04 | 0.07 |
| $MnO$ | 0.04 | 0.20 | 0.09 | 0.23 | 0.16 | 0.38 | 0.06 | 0.29 |
| $K_2O$ | | 0.00 | 0.01 | 0.05 | 0.85 | | | |
| $V_2O_5$ | tr. | | | | | 0.05 | 0.02 | 0.06 |
| $CoO$ | 0.02 | | | | | 0.05 | 0.03 | 0.05 |
| $NiO$ | 0.01 | | | | | 0.09 | 0.04 | 0.04 |
| $ZrO_2$ | 0.00 | | | | | 0.00 | 0.00 | 0.00 |
| $ZnO$ | n.d. | | | | | | | |

| Wt. % | | | | | | | | |
|---|---|---|---|---|---|---|---|---|
| $Nb_2O_5$ | 0.00 | | | | | | | |
| $P_2O_5$ | | 0.02 | 0.02 | 0.04 | 0.33 | | | |
| Total | 100.70 | 99.68 | 99.41 | 100.09 | 99.68 | 99.60 | 100.30 | 100.09 |

| Wt. % | PYX105 | PYX108 | PYX109 | PYX110 | PYX111 | PXY112 | PYX117 | PYX120 |
|---|---|---|---|---|---|---|---|---|
| $SiO_2$ | 54.17 | 56.97 | 52.48 | 56.65 | 54.83 | 49.99 | 53.54 | 54.83 |
| $Al_2O_3$ | 0.79 | 0.82 | 0.51 | 0.03 | 0.72 | 6.21 | 1.54 | 0.57 |
| $FeO$ | 4.47 | 5.29 | 10.37 | 9.19 | 2.67 | 16.56 | 16.17 | 3.05 |
| $Fe_2O_3$ | 2.09 | 1.13 | 4.45 | 0.44 | 0.00 | 0.58 | 1.02 | 0.68 |
| $MgO$ | 14.58 | 34.82 | 8.99 | 33.92 | 16.59 | 22.31 | 27.53 | 15.84 |
| $CaO$ | 22.41 | 0.54 | 20.36 | 0.30 | 25.01 | 3.99 | 0.35 | 24.20 |
| $Na_2O$ | 1.39 | 0.00 | 2.13 | 0.00 | 0.40 | 0.06 | 0.00 | 0.69 |
| $TiO_2$ | 0.05 | 0.02 | 0.06 | 0.03 | 0.02 | 0.53 | 0.03 | 0.04 |
| $Cr_2O_3$ | 0.07 | 0.38 | 0.06 | 0.05 | 0.07 | 0.13 | 0.07 | 0.02 |
| $MnO$ | 0.06 | 0.18 | 1.29 | 0.04 | 0.15 | 0.26 | 0.44 | 0.35 |
| $K_2O$ | | | | | | | | |
| $V_2O_5$ | 0.02 | 0.00 | 0.01 | 0.01 | 0.02 | 0.00 | 0.00 | 0.00 |
| $CoO$ | 0.03 | 0.02 | 0.05 | 0.01 | 0.04 | 0.04 | 0.01 | 0.04 |
| $NiO$ | 0.02 | 0.05 | 0.02 | 0.02 | 0.04 | 0.03 | 0.05 | 0.04 |
| $ZrO_2$ | 0.00 | 0.00 | 0.00 | 0.00 | 0.00 | 0.00 | 0.00 | 0.00 |
| $ZnO$ | | | | | | | | n.d. |
| $Nb_2O_5$ | n.d. | 0.00 | n.d. | 0.00 | n.d. | | | n.d. |
| $P_2O_5$ | | | | | | | | |
| Total | 100.15 | 100.22 | 100.78 | 100.69 | 100.56 | 100.69 | 100.75 | 100.35 |

| Wt. % | PYX126 | PYX135 | PYX136 | PYX150 | PYX160 | PYX170 | PE-CMP-030 | PP-CMP-021 |
|---|---|---|---|---|---|---|---|---|
| $SiO_2$ | 47.83 | 55.39 | 55.07 | 55.75 | 53.31 | 52.49 | 56.23 | 49.69 |
| $Al_2O_3$ | 6.44 | 0.54 | 0.06 | 0.24 | 0.06 | 4.48 | 1.02 | 6.40 |
| $FeO$ | 5.22 | 1.03 | 1.05 | 2.56 | 8.53 | 2.62 | 8.53 | 6.29 |
| $Fe_2O_3$ | 3.80 | 0.00 | 0.05 | 0.00 | 2.24 | 0.34 | 0.00 | n.d. |
| $MgO$ | 12.38 | 17.38 | 18.02 | 16.26 | 12.07 | 15.28 | 32.81 | 15.14 |
| $CaO$ | 22.20 | 24.88 | 25.45 | 25.70 | 24.10 | 22.47 | 0.41 | 20.92 |
| $Na_2O$ | 0.28 | 0.35 | 0.02 | 0.05 | n.d. | n.d. | 0.01 | 0.40 |
| $TiO_2$ | 1.32 | 0.02 | 0.05 | 0.00 | 0.04 | 0.04 | 0.02 | 0.79 |
| $Cr_2O_3$ | 0.08 | 0.05 | 0.04 | tr. | 0.14 | 0.99 | 0.00 | 0.91 |
| $MnO$ | 0.16 | 0.05 | 0.08 | 0.11 | 0.37 | 0.00 | 0.19 | 0.12 |
| $K_2O$ | | n.d. | n.d. | 0.00 | 0.02 | n.d. | 0.00 | 0.01 |
| $V_2O_5$ | 0.03 | 0.01 | 0.03 | 0.00 | 0.00 | 0.16 | | n.d. |
| $CoO$ | 0.05 | 0.04 | 0.02 | 0.05 | 0.00 | 0.00 | | n.d. |
| $NiO$ | 0.04 | 0.02 | 0.03 | tr. | 0.07 | 0.20 | | n.d. |

| | | | | | | | |
|---|---|---|---|---|---|---|---|
| ZrO$_2$ | 0.00 | 0.00 | 0.00 | tr. | n.d. | | | |
| ZnO | n.d. | n.d. | n.d. | 0.03 | 0.00 | 0.00 | | n.d. |
| Nb$_2$O$_5$ | n.d. | | | | | | | |
| P$_2$O$_5$ | | | | | | | 0.00 | |
| Total | 99.83 | 99.76 | 99.97 | 100.75 | 100.95 | 99.07 | 99.22 | 99.76 |

| Wt. % | CP-JJG-001 | ER-TGS-014 | FB-JFM-031-3CP | PA-RGB-024 | PP-ALS-108 | PX-DWS-012 | SB-RGB-001 | SB-RGB-015 |
|---|---|---|---|---|---|---|---|---|
| SiO$_2$ | 50.31 | 53.88 | 51.95 | 53.85 | 53.78 | 50.56 | 50.46 | 47.79 |
| Al$_2$O$_3$ | 4.78 | 1.19 | 4.65 | 0.66 | 0.72 | 1.41 | 1.41 | 0.50 |
| FeO | 4.34 | 1.58 | 2.39 | 6.55 | 2.16 | 23.17 | 23.17 | 23.72 |
| Fe$_2$O$_3$ | 0.00 | 0.00 | 0.00 | 0.00 | 0.88 | 0.12 | 0.12 | 0.00 |
| MgO | 15.87 | 18.12 | 16.50 | 14.92 | 16.43 | 16.10 | 16.10 | 0.72 |
| CaO | 22.57 | 24.76 | 22.95 | 23.50 | 25.74 | 7.05 | 7.05 | 22.28 |
| Na$_2$O | 0.45 | 0.41 | 0.53 | 1.10 | 0.00 | 0.26 | 0.26 | 0.10 |
| TiO$_2$ | 1.43 | 0.06 | 0.08 | 0.04 | 0.08 | 0.58 | 0.58 | 0.02 |
| Cr$_2$O$_3$ | 0.46 | 0.00 | 1.09 | 0.04 | 0.00 | 0.00 | 0.00 | 0.00 |
| MnO | 0.08 | 0.08 | 0.09 | 0.05 | 0.18 | 0.00 | 0.54 | 3.90 |
| K$_2$O | 0.00 | 0.00 | 0.00 | 0.03 | 0.00 | 0.23 | 0.03 | 0.00 |
| V$_2$O$_5$ | | | | | | | | |
| CoO | | | | | | | | |
| NiO | | | | | | | | |
| ZrO$_2$ | | | | | | | | |
| ZnO | | | | | | | | |
| Nb$_2$O$_5$ | | | | | | | | |
| P$_2$O$_5$ | 0.00 | 0.00 | 0.00 | 0.00 | 0.00 | 0.00 | 0.00 | 0.00 |
| Total | 100.29 | 100.08 | 100.24 | 100.74 | 99.97 | 99.48 | 99.72 | 99.03 |

| Wt. % | SB-RGB-021 | SB-RGB-055 | SR-JFM-042 | | | | | |
|---|---|---|---|---|---|---|---|---|
| SiO$_2$ | 48.24 | 41.89 | 53.36 | | | | | |
| Al$_2$O$_3$ | 0.09 | 8.81 | 0.85 | | | | | |
| FeO | 23.17 | 0.69 | 0.00 | | | | | |
| Fe$_2$O$_3$ | 0.00 | 10.31 | 5.42 | | | | | |
| MgO | 0.10 | 11.63 | 15.81 | | | | | |
| CaO | 22.24 | 21.35 | 22.95 | | | | | |
| Na$_2$O | 0.01 | 1.11 | 1.42 | | | | | |
| TiO$_2$ | 0.00 | 3.42 | 0.03 | | | | | |
| Cr$_2$O$_3$ | 0.03 | 0.00 | 0.14 | | | | | |
| MnO | 5.43 | 0.12 | 0.18 | | | | | |
| K$_2$O | 0.00 | 0.01 | 0.07 | | | | | |

| | | | |
|---|---|---|---|
| $V_2O_5$ | | | |
| CoO | | | |
| NiO | | | |
| $ZrO_2$ | | | |
| ZnO | | | |
| $Nb_2O_5$ | | | |
| $P_2O_5$ | 0.00 | 0.00 | 0.00 |
| Total | 99.31 | 99.34 | 100.23 |

## 2. Mixtures

Table 6. Mixtures looked at in this study and their minima found by lowest reflectance. 1=HOSERLab, 2=Sunshine & Pieters 1993, 3=RELAB, and 4=Duffard et al. 2005.

| Sample Name | Description | Band I Minimum (μm) | Band I fitting range (μm) | Band II Minimum (μm) | Band II fitting range (μm) | Other (μm) | Other fitting range (μm) | Source |
|---|---|---|---|---|---|---|---|---|
| COMIX1101 | Type A CPX/OPX PYX150/PYX032 0/100 < 45 μm | 0.916 | 0.9-1 | 1.903 | 1.8-2 | | | 1 |
| COMIX1102 | 10/90 | 0.916 | 0.9-1 | 1.901 | 1.8-2 | | | 1 |
| COMIX1103 | 20/80 | 0.915 | 0.9-1 | 1.901 | 1.8-2 | | | 1 |
| COMIX1104 | 30/70 | 0.914 | 0.9-1 | 1.907 | 1.8-2 | | | 1 |
| COMIX1105 | 40/60 | 0.914 | 0.9-1 | 1.901 | 1.8-2 | | | 1 |
| COMIX1106 | 50/50 | 0.916 | 0.9-1 | 1.907 | 1.8-2 | | | 1 |
| COMIX1107 | 60/40 | 0.916 | 0.9-1 | 1.905 | 1.8-2 | | | 1 |
| COMIX1108 | 70/30 | 0.919 | 0.9-1 | 1.907 | 1.8-2 | | | 1 |
| COMIX1108.5 | 75/25 | 0.917 | 0.9-1 | 1.100 | 1.1-1.2 | 1.908 | 1.8-2 | 1 |
| COMIX11 | 80/20 | 0.921 | 0.9-1 | 1.907 | 1.8-2 | | | 1 |

242

| | | | | | | | |
|---|---|---|---|---|---|---|---|
| 09 | | | | | | | |
| COMIX11 09.5 | 85/15 | 0.918 | 0.9-1 | 1.914 | 1.8-2 | | | 1 |
| COMIX11 10 | 90/10 | 0.927 | 0.9-1 | 1.114 | 1.1-1.15 | 1.912 | 1.8-2 | 1 |
| COMIX11 10.5 | 95/5 | 0.930 | 0.9-1 | 1.120 | 1.1-1.15 | 1.925 | 1.8-2 | 1 |
| COMIX11 11 | 100/0 | 0.949 | 0.9-1 | 1.128 | 1.1-1.15 | 1.942 | 1.8-2 | 1 |
| | | | | | | | | |
| COMIX21 01 | Type A CPX/OPX PYX150/PYX 032 0/100 45-90 µm | 0.911 | 0.9-1 | 1.865 | 1.8-2 | | | 1 |
| COMIX21 02 | 10/90 | 0.913 | 0.9-1 | 1.867 | 1.8-2 | | | 1 |
| COMIX21 03 | 20/80 | 0.914 | 0.9-1 | 1.865 | 1.8-2 | | | 1 |
| COMIX21 04 | 30/70 | 0.915 | 0.9-1 | 1.859 | 1.8-2 | | | 1 |
| COMIX21 05 | 40/60 | 0.915 | 0.9-1 | 1.872 | 1.8-2 | | | 1 |
| COMIX21 06 | 50/50 | 0.917 | 0.9-1 | 1.865 | 1.8-1.9 | | | 1 |
| COMIX21 07 | 60/40 | 0.918 | 0.9-1 | 1.843 | 1.8-1.9 | | | 1 |
| COMIX21 08 | 70/30 | 0.920 | 0.9-1 | 1.840 | 1.8-1.9 | | | 1 |
| COMIX21 08.5 | 75/25 | 0.925 | 0.9-1 | 1.834 | 1.8-2 | | | 1 |
| COMIX21 09 | 80/20 | 0.925 | 0.9-1 | 1.838 | 1.8-2 | | | 1 |
| COMIX21 09.5 | 85/15 | 0.932 | 0.9-1 | 1.109 | 1.1-1.15 | 1.836 | 1.8-1.85 | 1 |
| COMIX21 10 | 90/10 | 0.939 | 0.9-1 | 1.124 | 1.1-1.15 | 1.824 | 1.8-1.85 | 1 |
| COMIX21 10.5 | 95/5 | 0.946 | 0.9-1 | 1.131 | 1-1.15 | 1.752 | 1.75-1.85 | 1 |
| COMIX21 11 | 100/0 | 0.966 | 0.9-1 | 1.135 | 1-1.15 | | | 1 |
| | | | | | | | | |
| OCMIX10 01 | Type A CPX/OLV PYX150/OLV | 1.060 | 1-1.2 | | | | | 1 |

| | | | | | | | | |
|---|---|---|---|---|---|---|---|---|
| | 003 0/100 < 45 µm | | | | | | | |
| OCMIX1002 | 10/90 | 1.052 | 1-1.2 | | | | | 1 |
| OCMIX1003 | 20/80 | 1.058 | 1-1.2 | | | | | 1 |
| OCMIX1004 | 30/70 | 1.062 | 1-1.2 | | | | | 1 |
| OCMIX1005 | 40/60 | 1.062 | 1-1.2 | | | | | 1 |
| OCMIX1006 | 50/50 | 1.062 | 1-1.2 | | | | | 1 |
| OCMIX1007 | 60/40 | 1.062 | 1-1.2 | | | | | 1 |
| OCMIX1008 | 70/30 | 1.056 | 1-1.2 | | | | | 1 |
| OCMIX1009 | 80/20 | 1.064 | 1-1.2 | | | | | 1 |
| OCMIX1010 | 90/10 | 1.032 | 0.9-1.2 | | | | | 1 |
| OCMIX1011 | 100/0 | 0.961 | 0.9-1 | 1.131 | 1.1-1.15 | | | 1 |
| | | | | | | | | |
| PMIX1101 | Type B CPX/OPX PYX005/PYX023 100/0 < 45 µm | 1.023 | 1-1.2 | 2.320 | 2-2.5 | | | 1 |
| PMIX1102 | 90/10 | 1.011 | 0.9-1.2 | 2.324 | 2-2.5 | | | 1 |
| PMIX1103 | 80/20 | 0.950 | 0.9-1.1 | 2.320 | 2-2.5 | | | 1 |
| PMIX1104 | 70/30 | 0.935 | 0.9-1.1 | 1.938 | 1.8-2 | 2.318 | 2.3-2.5 | 1 |
| PMIX1105 | 60/40 | 0.923 | 0.9-1.1 | 1.907 | 1.8-2 | 2.320 | 2.3-2.5 | 1 |
| PMIX1106 | 50/50 | 0.919 | 0.9-1 | 1.912 | 1.8-2 | | | 1 |
| PMIX1107 | 40/60 | 0.918 | 0.9-1 | 1.903 | 1.8-2 | | | 1 |
| PMIX1108 | 30/70 | 0.916 | 0.9-1 | 1.843 | 1.75-1.85 | | | 1 |
| PMIX1109 | 20/80 | 0.914 | 0.9-1 | 1.842 | 1.75-1.85 | | | 1 |
| PMIX1110 | 10/90 | 0.914 | 0.9-1 | 1.850 | 1.75-1.85 | | | 1 |
| PMIX1111 | 0/100 | 0.913 | 0.9-1 | 1.841 | 1.75-1.85 | | | 1 |
| | | | | | | | | |

| ID | Description | | | | | | | |
|---|---|---|---|---|---|---|---|---|
| PMIX2001 | Type B CPX/OPX PYX017/PYX 032 100/0 90-180 µm | 1.022 | 1-1.1 | 2.289 | 2.2-2.4 | | | 1 |
| PMIX2002 | 80/20 | 1.004 | 0.9-1.1 | 2.202 | 2-2.3 | | | 1 |
| PMIX2003 | 60/40 | 0.979 | 0.9-1.1 | 2.100 | 2-2.25 | | | 1 |
| PMIX2004 | 40/60 | 0.972 | 0.9-1.1 | 2.080 | 2-2.2 | | | 1 |
| PMIX2005 | 20/80 | 0.949 | 0.9-1.1 | 1.993 | 1.9-2.1 | | | 1 |
| PMIX2006 | 0/100 | 0.932 | 0.8-1 | 1.978 | 1.8-2 | | | 1 |
| | | | | | | | | |
| PMIX2101 | Type B CPX/OPX PYX005/PYX 023 100/0 90-180 µm | 1.028 | 1-1.2 | 2.318 | 2.2-2.5 | | | 1 |
| PMIX2102 | 80/20 | 0.932 | 0.9-1.1 | 1.910 | 1.8-2 | | | 1 |
| PMIX2103 | 60/40 | 0.922 | 0.9-1 | 1.900 | 1.8-1.9 | | | 1 |
| PMIX2104 | 40/60 | 0.918 | 0.9-1 | 1.899 | 1.8-1.9 | | | 1 |
| PMIX2105 | 20/80 | 0.918 | 0.9-1 | 1.900 | 1.8-1.9 | | | 1 |
| PMIX2106 | 0/100 | 0.913 | 0.9-1 | 1.861 | 1.8-1.9 | | | 1 |
| | | | | | | | | |
| c1xp14 | Type B CPX/OPX PP-CMP-021/PE-CMP-030 75/25 < 45 µm | 0.995 | 0.9-1.1 | 2.270 | 2.2-2.5 | | | 2, 3, 1 |
| c1xp24 | 75/25 45-75 µm | 0.980 | 0.9-1.1 | 2.245 | 2.2-2.4 | | | 2, 3, 1 |
| c1xp05 | 75/25 75-125 µm | 0.980 | 0.9-1.1 | 2.230 | 2.2-2.4 | | | 2, 3, 1 |
| c1xp12 | 60/40 < 45 µm | 0.950 | 0.9-1.1 | 1.905 | 1.8-2 | 2.200 | 2.2-2.4 | 2, 3, 1 |
| c1xp22 | 60/40 45-75 µm | 0.955 | 0.9-1.1 | 1.900 | 1.8-2 | 2.200 | 2.2-2.4 | 2, 3, 1 |
| c1xp03 | 60/40 75-125 µm | 0.955 | 0.9-1 | 1.935 | 1.8-2 | 2.205 | 2.2-2.4 | 2, 3, 1 |
| | | | | | | | | |

| | | | | | | | | |
|---|---|---|---|---|---|---|---|---|
| PYX016 | Type B CPX/OLV PYX016/OLV 003 100/0 < 45 μm | 1.049 | 1-1.2 | 2.310 | 2.2-2.5 | | | 1 |
| OLV003 | 0/100 | 1.053 | 1-1.1 | | | | | 1 |
| MIX031 | 20/80 | 1.053 | 1-1.1 | 2.312 | 2.2-2.5 | | | 1 |
| MIX032 | 40/60 | 1.050 | 1-1.1 | 2.310 | 2.2-2.5 | | | 1 |
| MIX033 | 60/40 | 1.051 | 1-1.1 | 2.310 | 2.2-2.5 | | | 1 |
| MIX034 | 80/20 | 1.049 | 1-1.1 | 2.311 | 2.2-2.5 | | | 1 |
| | | | | | | | | |
| AG-TJM-008 | OLV (Fo90)/OPX (Hyp)/Type B CPX (Aug)/PLG (Lab) 100/0/0/0 < 45 μm | 1.055 | 1-1.2 | | | | | 3 |
| AG-TJM-009 | 0/100/0/0 | 0.920 | 0.8-1 | 1.885 | 1.8-2 | | | 3 |
| AG-TJM-010 | 0/0/100/0 | 1.005 | 0.9-1.1 | 2.265 | 2.2-2.4 | | | 3 |
| AG-TJM-011 | 0/0/0/100 | 1.290 | 1.2-1.4 | | | | | 3 |
| AG-TJM-012 | 0/85/15/0 < 38 μm (for the rest) | 0.920 | 0.9-1 | 1.900 | 1.8-2 | | | 3 |
| AG-TJM-013 | 0/50/50/0 | 0.940 | 0.9-1 | 1.930 | 1.8-2 | | | 3 |
| AG-TJM-014 | 70/30/0/0 | 0.930 | 0.9-1 | 1.900 | 1.8-2 | | | 3 |
| AG-TJM-015 | 40/51/9/0 | 0.930 | 0.9-1 | 1.900 | 1.8-2 | | | 3 |
| AG-TJM-016 | 80/8.5/1.5/10 | 1.000 | 0.9-1.1 | 1.930 | 1.8-2 | | | 3 |
| AG-TJM-017 | 10/90/0/0 | 0.920 | 0.8-1 | 1.900 | 1.8-2 | | | 3 |
| AG-TJM-018 | 30/70/0/0 | 0.920 | 0.8-1 | 1.900 | 1.8-2 | | | 3 |
| AG-TJM-019 | 50/50/0/0 | 0.920 | 0.9-1 | 1.895 | 1.8-2 | | | 3 |

| AG-TJM-020 | 90/10/0/0 | 1.025 | 0.9-1.1 | 1.930 | 1.8-2 | | | 3 |
|---|---|---|---|---|---|---|---|---|
| AG-TJM-021 | 20/68/12/0 | 0.920 | 0.9-1 | 1.900 | 1.8-2 | | | 3 |
| AG-TJM-022 | 30/59.5/10.5/0 | 0.925 | 0.9-1 | 1.900 | 1.8-2 | | | 3 |
| AG-TJM-023 | 50/42.5/7.5/0 | 0.920 | 0.9-1 | 1.905 | 1.8-2 | | | 3 |
| AG-TJM-024 | 60/34/6/0 | 0.935 | 0.9-1 | 1.900 | 1.8-2 | | | 3 |
| AG-TJM-025 | 70/25.5/4.5/0 | 0.940 | 0.9-1 | 1.900 | 1.8-2 | | | 3 |
| AG-TJM-026 | 80/17/3/0 | 0.955 | 0.9-1 | 1.910 | 1.8-2 | | | 3 |
| AG-TJM-027 | 0/45/45/10 | 0.935 | 0.9-1 | 1.900 | 1.8-2 | | | 3 |
| AG-TJM-028 | 0/40/40/20 | 0.940 | 0.9-1 | 1.920 | 1.8-2 | | | 3 |
| AG-TJM-029 | 0/35/35/30 | 0.935 | 0.9-1 | 1.925 | 1.8-2 | | | 3 |
| AG-TJM-030 | 0/30/30/40 | 0.935 | 0.9-1 | 1.925 | 1.8-2 | | | 3 |
| AG-TJM-031 | 0/25/25/50 | 0.935 | 0.9-1 | 1.910 | 1.8-2 | | | 3 |
| AG-TJM-032 | 90/4.25/0.75/5 | 1.045 | 1-1.1 | 1.910 | 1.8-2 | | | 3 |
| AG-TJM-033 | 70/12.75/2.25/15 | 0.955 | 0.9-1.1 | 1.910 | 1.8-2 | | | 3 |
| AG-TJM-034 | 60/17/3/20 | 0.935 | 0.9-1 | 1.900 | 1.8-2 | | | 3 |
| AG-TJM-035 | 20/40/40/0 | 0.940 | 0.9-1 | 1.900 | 1.8-2 | | | 3 |
| AG-TJM-036 | 30/35/35/0 | 0.940 | 0.9-1 | 1.910 | 1.8-2 | | | 3 |
| AG-TJM-037 | 40/30/30/0 | 0.940 | 0.9-1 | 1.925 | 1.8-2 | | | 3 |
| AG-TJM-038 | 50/25/25/0 | 0.945 | 0.9-1 | 1.925 | 1.8-2 | | | 3 |
| AG-TJM-039 | 60/20/20/0 | 0.960 | 0.9-1 | 1.915 | 1.8-2 | | | 3 |
| AG-TJM-040 | 70/15/15/0 | 0.975 | 0.9-1 | 1.930 | 1.8-2 | | | 3 |
| AG-TJM-041 | 80/10/10/0 | 1.010 | 0.9-1.1 | 1.920 | 1.8-2 | | | 3 |
| AG-TJM-042 | 0/76.5/13.5/10 | 0.920 | 0.9-1 | 1.900 | 1.8-2 | | | 3 |

| | | | | | | | | |
|---|---|---|---|---|---|---|---|---|
| AG-TJM-043 | 0/68/12/20 | 0.920 | 0.9-1 | 1.895 | 1.8-2 | | | 3 |
| AG-TJM-044 | 0/59.5/10.5/30 | 0.925 | 0.9-1 | 1.910 | 1.8-2 | | | 3 |
| AG-TJM-045 | 0/51/9/40 | 0.915 | 0.9-1 | 1.900 | 1.8-2 | | | 3 |
| AG-TJM-046 | 0/42.5/7.5/50 | 0.925 | 0.9-1 | 1.900 | 1.8-2 | | | 3 |
| AG-TJM-047 | 90/2.5/2.5/5 | 1.055 | 1-1.1 | 1.945 | 1.8-2 | | | 3 |
| AG-TJM-048 | 80/5/5/10 | 1.045 | 1-1.1 | 1.910 | 1.8-2 | | | 3 |
| AG-TJM-049 | 70/7.5/7.5/15 | 1.020 | 0.9-1.1 | 1.945 | 1.8-2 | | | 3 |
| AG-TJM-050 | 60/10/10/20 | 0.985 | 0.9-1.1 | 1.920 | 1.8-2 | | | 3 |
| AG-TJM-051 | 0/20/20/60 | 0.940 | 0.9-1 | 1.955 | 1.8-2 | | | 3 |
| | | | | | | | | |
| PD-CMP-010-C | Type B CPX (Dio)/PLG (Lab) 100/0 45-75 µm | 1.040 | 1-1.1 | 2.325 | 2.2-2.4 | | | 3 |
| PL-CMP-147-C | 0/100 | 1.290 | 1.2-1.4 | | | | | 3 |
| MX-CMP-098-C2 | 2/98 | 1.290 | 1.2-1.4 | 2.165 | 2-2.4 | | | 3 |
| MX-CMP-099-C2 | 5/95 | 1.075 | 1-1.1 | 1.275 | 1.27-1.3 | 2.325 | 2.2-2.4 | 3 |
| MX-CMP-100-C2 | 7/93 | 1.055 | 1-1.1 | 1.285 | 1.27-1.3 | 2.325 | 2.2-2.4 | 3 |
| MX-CMP-101-C2 | 10/90 | 1.055 | 1-1.1 | 2.325 | 2.2-2.4 | | | 3 |
| MX-CMP-102-C2 | 15/85 | 1.050 | 1-1.1 | 2.325 | 2.2-2.4 | | | 3 |
| MX-CMP-103-C2 | 25/75 | 1.045 | 1-1.1 | 2.325 | 2.2-2.4 | | | 3 |
| MX-CMP-104-C2 | 50/50 | 1.035 | 1-1.1 | 2.325 | 2.2-2.4 | | | 3 |
| | | | | | | | | |
| PE-CMP-030 | Type B CPX/OPX PP-CMP-021/PE-CMP-030 0/100 75-125 µm | 0.910 | 0.9-1 | 1.835 | 1.7-2 | | | 3, 4 |

| ID | Ratio | | | | | | | |
|---|---|---|---|---|---|---|---|---|
| PP-CMP-021 | 100/0 | 1.015 | 0.9-1.1 | 2.280 | 2.2-2.4 | | | 3, 4 |
| XP-CMP-001 | 50/50 | 0.945 | 0.9-1 | 1.895 | 1.8-2 | | | 3, 4 |
| XP-CMP-002 | 40/60 | 0.945 | 0.9-1 | 1.870 | 1.8-2 | | | 3, 4 |
| XP-CMP-003 | 60/40 | 0.955 | 0.9-1 | 1.935 | 1.8-2 | 2.205 | 2.18-2.23 | 3, 4 |
| XP-CMP-004 | 25/75 | 0.925 | 0.9-1 | 1.850 | 1.8-2 | | | 3, 4 |
| XP-CMP-005 | 75/25 | 0.980 | 0.9-1 | 2.230 | 2.2-2.4 | | | 3, 4 |
| XP-CMP-006 | 15/85 | 0.923 | 0.9-1 | 1.850 | 1.8-2 | | | 3, 4 |
| XP-CMP-007 | 85/15 | 0.995 | 0.95-1.05 | 2.248 | 2.2-2.4 | | | 3, 4 |
| XP-CMP-010 | 50/50 < 45 µm now | 0.935 | 0.9-1 | 1.870 | 1.8-2 | 2.210 | 2.2-2.25 | 3, 4 |
| XP-CMP-011 | 40/60 | 0.925 | 0.9-1 | 1.870 | 1.8-2 | 2.205 | 2.2-2.25 | 3, 4 |
| XP-CMP-012 | 60/40 | 0.950 | 0.9-1 | 1.905 | 1.8-2 | 2.245 | 2.2-2.25 | 3, 4 |
| XP-CMP-013 | 25/75 | 0.920 | 0.9-1 | 1.840 | 1.8-2 | | | 3, 4 |
| XP-CMP-014 | 75/25 | 0.995 | 0.9-1.1 | 1.930 | 1.9-1.95 | 2.270 | 2.2-2.4 | 3, 4 |
| XP-CMP-015 | 15/85 | 0.910 | 0.9-1 | 1.840 | 1.8-2 | | | 3, 4 |
| XP-CMP-016 | 85/15 | 1.005 | 0.9-1.1 | 2.285 | 2.2-2.4 | | | 3, 4 |
| XP-CMP-017 | 75/25 | 0.985 | 0.9-1.1 | 1.930 | 1.9-1.94 | 2.225 | 2.2-2.4 | 3, 4 |
| XP-CMP-020 | 50/50 45-75 µm now | 0.945 | 0.9-1 | 1.870 | 1.8-2 | | | 3 |
| XP-CMP-021 | 40/60 | 0.925 | 0.9-1 | 1.865 | 1.8-2 | | | 3 |
| XP-CMP-022 | 60/40 | 0.955 | 0.9-1 | 1.900 | 1.8-2 | 2.165 | 2.16-2.25 | 3 |
| XP-CMP-023 | 25/75 | 0.920 | 0.9-1 | 1.845 | 1.8-2 | | | 3 |
| XP-CMP-024 | 75/25 | 0.980 | 0.95-1.05 | 2.245 | 2.2-2.4 | | | 3 |
| XP-CMP-025 | 15/85 | 0.910 | 0.9-1 | 1.820 | 1.8-2 | | | 3 |
| XP-CMP-026 | 85/15 | 1.005 | 0.95-1.05 | 2.240 | 2.2-2.4 | | | 3 |

| | Type A PYX/OLV (Fa10)/PLG (An93) PYX009/OLV 003/PLG108 100/0/0 45-90 | | | | | | | |
|---|---|---|---|---|---|---|---|---|
| PYX009 | µm | 0.974 | 0.9-1 | 1.133 | 1-1.3 | | | 1 |
| OLV003 | 0/100/0 | 1.054 | 1-1.2 | | | | | 1 |
| PLG108 | 0/0/100 | 1.298 | 1.2-1.4 | | | | | 1 |
| BOZ001 | 200 mg/0 mg/20 mg | 0.975 | 0.9-1 | 1.135 | 1-1.2 | | | 1 |
| BOZ002 | 200 mg/0 mg/40 mg | 0.975 | 0.9-1 | 1.136 | 1-1.2 | | | 1 |
| BOZ003 | 200 mg/20 mg/40 mg | 0.989 | 0.9-1 | 1.129 | 1-1.2 | | | 1 |
| BOZ004 | 200 mg/40 mg/40 mg | 1.000 | 0.9-1 | 1.103 | 1-1.2 | | | 1 |
| BOZ005 | 200 mg/60 mg/40 mg | 1.078 | 1-1.2 | | | | | 1 |
| BOZ006 | 200 mg/80 mg/40 mg | 1.073 | 1-1.2 | | | | | 1 |
| BOZ007 | 200 mg/100 mg/40 mg | 1.068 | 1-1.2 | | | | | 1 |
| BOZ008 | 200 mg/200 mg/ 40 mg | 1.056 | 1-1.2 | | | | | 1 |
| BOZ009 | 200 mg/200 mg/200 mg | 1.066 | 1-1.2 | | | | | 1 |

Table 7. Mixtures with band centers in the literature. 1=Sunshine & Pieters 1993 and 2=Duffard et al. 2005.

| Sample Name | Description | Band I center (µm) | Band II center (µm) | Other center (µm) | Source |
|---|---|---|---|---|---|
| c1xp14 | Type B CPX/OPX PP-CMP-021/PE-CMP-030 75/25 < 45 µm | 1.029 | 1.821 | 2.304 | 1 |
| c1xp24 | 75/25 45-75 µm | 1.023 | 1.842 | 2.303 | 1 |
| c1xp05 | 75/25 75-125 µm | 1.028 | 1.836 | 2.293 | 1 |
| | | | | | |
| PE-CMP-030 | Type B CPX/OPX PP-CMP-021/PE-CMP-030 0/100 75-125 µm | 0.911 | 1.833 | | 2 |

| Sample Name | Description | Band I Minimum (µm) | Band I fitting range (µm) | Band II Minimum (µm) | Band II fitting range (µm) | Other (µm) | Other fitting range (µm) | Source |
|---|---|---|---|---|---|---|---|---|
| PP-CMP-021 | 100/0 | 1.012 | | 2.276 | | | | 1 |
| XP-CMP-001 | 50/50 | 0.951 | | 1.88 | | | | 2 |
| XP-CMP-002 | 40/60 | 0.944 | | 1.868 | | | | |
| XP-CMP-003 | 60/40 | 0.964 | | 1.904 | | | | |
| XP-CMP-004 | 25/75 | 0.924 | | 1.846 | | | | |
| XP-CMP-005 | 75/25 | 0.988 | | 1.998 | | | | |
| XP-CMP-006 | 15/85 | 0.92 | | 1.838 | | | | |
| XP-CMP-007 | 85/15 | 1.008 | | 2.203 | | | | |
| PE-CMP-030 | 0/100 < 45 µm | 0.909 | | 1.833 | | | | 1 |
| PP-CMP-021 | 100/0 | 1.012 | | 2.268 | | | | 2 |
| XP-CMP-010 | 50/50 | 0.94 | | 1.857 | | | | |
| XP-CMP-011 | 40/60 | 0.931 | | 1.851 | | | | |
| XP-CMP-012 | 60/40 | 0.966 | | 1.873 | | | | |
| XP-CMP-013 | 25/75 | 0.921 | | 1.847 | | | | |
| XP-CMP-014 | 75/25 | 1.003 | | 1.916 | | | | |
| XP-CMP-015 | 15/85 | 0.917 | | 1.836 | | | | |
| XP-CMP-016 | 85/15 | 1.012 | | 2.23 | | | | |

Table 8. Mixtures with minima found using polynomial fitting from McCraig et al. 2017. 1=HOSERLab, 2=Sunshine & Pieters 1993, 3=RELAB, and 4=Duffard et al. 2005.

| Sample Name | Description | Band I Minimum (µm) | Band I fitting range (µm) | Band II Minimum (µm) | Band II fitting range (µm) | Other (µm) | Other fitting range (µm) | Source |
|---|---|---|---|---|---|---|---|---|
| COMIX1101 | Type A CPX/OPX PYX150/PYX032 0/100 < 45 µm | 0.915 | 0.857 -0.97 | 1.886 | 1.75-1.992 | | | 1 |

| COMIX1102 | 10/90 | 0.915 | 0.84-0.986 | 1.877 | 1.7-2.032 | | | 1 |
|---|---|---|---|---|---|---|---|---|
| COMIX1103 | 20/80 | 0.915 | 0.85-0.977 | 1.884 | 1.74-2 | | | 1 |
| COMIX1104 | 30/70 | 0.915 | 0.868-0.96 | 1.887 | 1.74-1.997 | | | 1 |
| COMIX1105 | 40/60 | 0.916 | 0.868-0.96 | 1.886 | 1.74-1.992 | | | 1 |
| COMIX1106 | 50/50 | 0.916 | 0.85-0.977 | 1.893 | 1.771-1.97 | | | 1 |
| COMIX1107 | 60/40 | 0.917 | 0.86-0.969 | 1.887 | 1.74-1.988 | | | 1 |
| COMIX1108 | 70/30 | 0.918 | 0.872-0.96 | 1.886 | 1.715-2 | | | 1 |
| COMIX1108.5 | 75/25 | 0.917 | 0.85-0.978 | 1.877 | 1.713-1.99 | | | 1 |
| COMIX1109 | 80/20 | 0.920 | 0.84-0.99 | 1.885 | 1.7-2 | | | 1 |
| COMIX1109.5 | 85/15 | 0.920 | 0.85-0.98 | 1.873 | 1.7-1.99 | | | 1 |
| COMIX1110 | 90/10 | 0.925 | 0.861-0.98 | 1.116 | 1.09-1.14 | 1.881 | 1.66-2 | 1 |
| COMIX1110.5 | 95/5 | 0.932 | 0.888-0.97 | 1.125 | 1.09-1.144 | 1.811 | 1.6-1.989 | 1 |
| COMIX1111 | 100/0 | 0.953 | 0.933-0.98 | 1.128 | 1.09-1.16 | | | 1 |
| | | | | | | | | |
| COMIX2101 | Type A CPX/OPX PYX150/PYX032 0/100 45-90 µm | 0.911 | 0.805-1.019 | 1.861 | 1.63-2.09 | | | 1 |
| COMIX2102 | 10/90 | 0.913 | 0.833-0.99 | 1.862 | 1.657-2.05 | | | 1 |
| COMIX2103 | 20/80 | 0.913 | 0.844-0.98 | 1.863 | 1.7-2.012 | | | 1 |
| COMIX2104 | 30/70 | 0.914 | 0.844-0.98 | 1.864 | 1.7-2.013 | | | 1 |
| COMIX2105 | 40/60 | 0.915 | 0.83-0.995 | 1.863 | 1.71-2 | | | 1 |
| COMIX2106 | 50/50 | 0.917 | 0.84-0.987 | 1.865 | 1.7-2.006 | | | 1 |
| COMIX2107 | 60/40 | 0.918 | 0.84-0.99 | 1.863 | 1.7-2.002 | | | 1 |
| COMIX2108 | 70/30 | 0.920 | 0.84-0.99 | 1.863 | 1.7-1.997 | | | 1 |
| COMIX2108.5 | 75/25 | 0.924 | 0.84-0.994 | 1.860 | 1.7-1.988 | | | 1 |
| COMIX2109 | 80/20 | 0.925 | 0.84-0.996 | 1.860 | 1.7-1.986 | | | 1 |
| COMIX2109.5 | 85/15 | 0.930 | 0.882-0.97 | 1.863 | 1.746-1.95 | | | 1 |
| COMIX2110 | 90/10 | 0.938 | 0.873-0.99 | 1.123 | 1.096-1.14 | 1.809 | 1.7-1.948 | 1 |
| COMIX2110.5 | 95/5 | 0.945 | 0.908-0.98 | 1.129 | 1.102-1.15 | 1.700 | 1.55-1.96 | 1 |
| COMIX2111 | 100/0 | 0.965 | 0.937-1 | 1.136 | 1.073-1.175 | | | 1 |
| | | | | | | | | |
| OCMIX1001 | Type A CPX/OLV PYX150/OLV003 0/100 < 45 µm | 1.057 | 1-1.11 | | | | | 1 |

| | | | | | | | | |
|---|---|---|---|---|---|---|---|---|
| OCMIX1002 | 10/90 | 1.052 | 0.98-1.135 | | | | | 1 |
| OCMIX1003 | 20/80 | 1.053 | 1-1.11 | | | | | 1 |
| OCMIX1004 | 30/70 | 1.058 | 1-1.113 | | | | | 1 |
| OCMIX1005 | 40/60 | 1.057 | 1-1.112 | | | | | 1 |
| OCMIX1006 | 50/50 | 1.059 | 1-1.11 | | | | | 1 |
| OCMIX1007 | 60/40 | 1.058 | 0.98-1.135 | | | | | 1 |
| OCMIX1008 | 70/30 | 1.051 | 1-1.11 | | | | | 1 |
| OCMIX1009 | 80/20 | 1.071 | 1-1.12 | | | | | 1 |
| OCMIX1010 | 90/10 | 1.035 | 0.9-1.197 | | | | | 1 |
| OCMIX1011 | 100/0 | 0.961 | 0.93-0.999 | 1.119 | 1.06-1.159 | | | 1 |
| | | | | | | | | |
| PMIX1101 | Type B CPX/OPX PYX005/PYX023 100/0 < 45 µm | 1.022 | 0.97-1.07 | 2.334 | 2.05-2.5 | | | 1 |
| PMIX1102 | 90/10 | 1.009 | 0.96-1.043 | 2.333 | 2.15-2.462 | | | 1 |
| PMIX1103 | 80/20 | 0.954 | 0.9-1.023 | 1.933 | 1.832-2.031 | 2.322 | 2.141-2.436 | 1 |
| PMIX1104 | 70/30 | 0.930 | 0.87-1.01 | 1.924 | 1.63-2.14 | 2.316 | 2.14-2.41 | 1 |
| PMIX1105 | 60/40 | 0.923 | 0.862-0.99 | 1.905 | 1.7-2.03 | | | 1 |
| PMIX1106 | 50/50 | 0.919 | 0.86-0.98 | 1.902 | 1.716-2.02 | | | 1 |
| PMIX1107 | 40/60 | 0.917 | 0.86-0.976 | 1.894 | 1.75-1.982 | | | 1 |
| PMIX1108 | 30/70 | 0.916 | 0.852-0.98 | 1.878 | 1.673-2.05 | | | 1 |
| PMIX1109 | 20/80 | 0.915 | 0.86-0.969 | 1.887 | 1.794-1.95 | | | 1 |
| PMIX1110 | 10/90 | 0.914 | 0.85-0.976 | 1.872 | 1.74-1.976 | | | 1 |
| PMIX1111 | 0/100 | 0.913 | 0.87-0.956 | 1.870 | 1.744-1.97 | | | 1 |
| | | | | | | | | |
| PMIX2001 | Type B CPX/OPX PYX017/PYX032 100/0 90-180 µm | 1.022 | 0.942-1.1 | 2.287 | 2.105-2.45 | | | 1 |
| PMIX2002 | 80/20 | 1.003 | 0.924-1.08 | 2.196 | 1.97-2.387 | | | 1 |
| PMIX2003 | 60/40 | 0.980 | 0.91-1.042 | 2.102 | 1.889-2.27 | | | 1 |
| PMIX2004 | 40/60 | 0.973 | 0.89-1.04 | 2.066 | 1.904-2.2 | | | 1 |
| PMIX2005 | 20/80 | 0.950 | 0.88-1.01 | 2.002 | 1.75-2.219 | | | 1 |
| PMIX2006 | 0/100 | 0.929 | 0.85-1.004 | 1.972 | 1.78-2.15 | | | 1 |
| | | | | | | | | |

| | | | | | | | | |
|---|---|---|---|---|---|---|---|---|
| PMIX2101 | Type B CPX/OPX PYX005/PYX023 100/0 90-180 µm | 1.033 | 0.98-1.08 | 2.328 | 2.15-2.463 | | | 1 |
| PMIX2102 | 80/20 | 0.932 | 0.85-1.004 | 1.898 | 1.706-2.03 | | | 1 |
| PMIX2103 | 60/40 | 0.923 | 0.839-1 | 1.890 | 1.74-1.998 | | | 1 |
| PMIX2104 | 40/60 | 0.917 | 0.86-0.97 | 1.872 | 1.723-2 | | | 1 |
| PMIX2105 | 20/80 | 0.916 | 0.86-0.97 | 1.873 | 1.757-1.97 | | | 1 |
| PMIX2106 | 0/100 | 0.913 | 0.87-0.955 | 1.865 | 1.76-1.96 | | | 1 |
| | | | | | | | | |
| c1xp14 | Type B CPX/OPX PP-CMP-021/PE-CMP-030 75/25 < 45 µm | 0.995 | 0.91-1.065 | 1.930 | 1.9-1.955 | 2.250 | 2.16-2.335 | 2, 3, 1 |
| c1xp24 | 75/25 45-75 µm | 0.980 | 0.93-1.035 | 2.240 | 2.15-2.32 | | | 2, 3, 1 |
| c1xp05 | 75/25 75-125 µm | 0.980 | 0.92-1.04 | 2.230 | 2.165-2.29 | | | 2, 3, 1 |
| c1xp12 | 60/40 < 45 µm | 0.955 | 0.9-1.015 | 1.890 | 1.825-1.97 | 2.215 | 2.175-2.275 | 2, 3, 1 |
| c1xp22 | 60/40 45-75 µm | 0.955 | 0.9-1.01 | 1.900 | 1.805-2 | | | 2, 3, 1 |
| c1xp03 | 60/40 75-125 µm | 0.955 | 0.91-1 | 1.925 | 1.845-2.02 | | | 2, 3, 1 |
| | | | | | | | | |
| PYX016 | Type B CPX/OLV PYX016/OLV003 100/0 < 45 µm | 1.050 | 0.992-1.1 | 2.341 | 2.174-2.49 | | | 1 |
| OLV003 | 0/100 | 1.053 | 1-1.111 | | | | | 1 |
| MIX031 | 20/80 | 1.052 | 1-1.105 | 2.363 | 2.15-2.486 | | | 1 |
| MIX032 | 40/60 | 1.051 | 1-1.1 | 2.352 | 2.09-2.496 | | | 1 |
| MIX033 | 60/40 | 1.051 | 1-1.098 | 2.343 | 2.17-2.48 | | | 1 |
| MIX034 | 80/20 | 1.050 | 0.995-1.1 | 2.330 | 2.2-2.475 | | | 1 |
| | | | | | | | | |
| AG-TJM-008 | OLV (Fo90)/OPX (Hyp)/Type B CPX (Aug)/PLG (Lab) 100/0/0/0 < 45 µm | 1.055 | 1.015-1.09 | | | | | 3 |
| AG-TJM-009 | 0/100/0/0 | 0.920 | 0.87-0.965 | 1.885 | 1.71-2.065 | | | 3 |
| AG-TJM-010 | 0/0/100/0 | 1.005 | 0.92-1.09 | 2.270 | 2.15-2.4 | | | 3 |
| AG-TJM-011 | 0/0/0/100 | 1.280 | 1.17-1.4 | | | | | 3 |
| AG-TJM-012 | 0/85/15/0 < 38 µm (for the rest) | 0.920 | 0.86-0.98 | 1.900 | 1.725-2.07 | | | 3 |
| AG-TJM-013 | 0/50/50/0 | 0.935 | 0.88-0.995 | 1.935 | 1.845-2.02 | | | 3 |
| AG-TJM-014 | 70/30/0/0 | 0.930 | 0.875-0.985 | 1.900 | 1.79-2 | | | 3 |

| AG-TJM-015 | 40/51/9/0 | 0.925 | 0.875 - 0.975 | 1.900 | 1.8-2 | | | 3 |
|---|---|---|---|---|---|---|---|---|
| AG-TJM-016 | 80/8.5/1.5/10 | 1.025 | 0.965 - 1.065 | 1.925 | 1.8-2.01 | | | 3 |
| AG-TJM-017 | 10/90/0/0 | 0.920 | 0.86-0.975 | 1.890 | 1.75-2.025 | | | 3 |
| AG-TJM-018 | 30/70/0/0 | 0.920 | 0.875 - 0.965 | 1.890 | 1.78-2 | | | 3 |
| AG-TJM-019 | 50/50/0/0 | 0.925 | 0.88-0.965 | 1.895 | 1.8-1.98 | | | 3 |
| AG-TJM-020 | 90/10/0/0 | 1.025 | 0.985 -1.06 | 1.915 | 1.8-2 | | | 3 |
| AG-TJM-021 | 20/68/12/0 | 0.925 | 0.875 -0.97 | 1.900 | 1.805-1.99 | | | 3 |
| AG-TJM-022 | 30/59.5/10.5/0 | 0.925 | 0.89-0.955 | 1.905 | 1.81-1.985 | | | 3 |
| AG-TJM-023 | 50/42.5/7.5/0 | 0.925 | 0.865 -0.99 | 1.900 | 1.8-2 | | | 3 |
| AG-TJM-024 | 60/34/6/0 | 0.930 | 0.89-0.97 | 1.905 | 1.81-1.985 | | | 3 |
| AG-TJM-025 | 70/25.5/4.5/0 | 0.935 | 0.885 -0.99 | 1.905 | 1.81-1.995 | | | 3 |
| AG-TJM-026 | 80/17/3/0 | 0.950 | 0.915 - 0.985 | 1.910 | 1.81-1.995 | | | 3 |
| AG-TJM-027 | 0/45/45/10 | 0.940 | 0.9-0.98 | 1.930 | 1.825-2.035 | | | 3 |
| AG-TJM-028 | 0/40/40/20 | 0.940 | 0.885 -0.99 | 1.930 | 1.815-2.05 | | | 3 |
| AG-TJM-029 | 0/35/35/30 | 0.940 | 0.885 -0.99 | 1.930 | 1.87-2 | | | 3 |
| AG-TJM-030 | 0/30/30/40 | 0.940 | 0.9-0.975 | 1.935 | 1.845-2.02 | | | 3 |
| AG-TJM-031 | 0/25/25/50 | 0.940 | 0.9-0.975 | 1.930 | 1.85-2.02 | | | 3 |
| AG-TJM-032 | 90/4.25/0.75/5 | 1.045 | 0.99-1.095 | 1.910 | 1.755-2.02 | | | 3 |
| AG-TJM-033 | 70/12.75/2.25/15 | 0.955 | 0.92-0.995 | 1.905 | 1.8-1.995 | | | 3 |
| AG-TJM-034 | 60/17/3/20 | 0.940 | 0.89-1 | 1.905 | 1.8-1.995 | | | 3 |
| AG-TJM-035 | 20/40/40/0 | 0.940 | 0.905 - 0.975 | 1.925 | 1.865-1.995 | | | 3 |
| AG-TJM-036 | 30/35/35/0 | 0.945 | 0.9-0.985 | 1.925 | 1.84-2.02 | | | 3 |
| AG-TJM-037 | 40/30/30/0 | 0.950 | 0.905 -0.99 | 1.935 | 1.805-2.07 | | | 3 |
| AG-TJM-038 | 50/25/25/0 | 0.950 | 0.905 - 0.995 | 1.935 | 1.84-2.02 | | | 3 |
| AG-TJM-039 | 60/20/20/0 | 0.960 | 0.935 -0.98 | 1.935 | 1.81-2.05 | | | 3 |
| AG-TJM-040 | 70/15/15/0 | 0.970 | 0.905 -1.05 | 1.940 | 1.84-2.03 | | | 3 |
| AG-TJM-041 | 80/10/10/0 | 1.005 | 0.965 -1.04 | 1.935 | 1.83-2.035 | | | 3 |

| | | | | | | | | |
|---|---|---|---|---|---|---|---|---|
| AG-TJM-042 | 0/76.5/13.5/10 | 0.920 | 0.87-0.97 | 1.895 | 1.76-2.03 | | | 3 |
| AG-TJM-043 | 0/68/12/20 | 0.920 | 0.875-0.965 | 1.895 | 1.845-1.94 | | | 3 |
| AG-TJM-044 | 0/59.5/10.5/30 | 0.920 | 0.88-0.965 | 1.895 | 1.8-1.99 | | | 3 |
| AG-TJM-045 | 0/51/9/40 | 0.920 | 0.88-0.96 | 1.895 | 1.75-2.04 | | | 3 |
| AG-TJM-046 | 0/42.5/7.5/50 | 0.920 | 0.88-0.965 | 1.900 | 1.795-1.995 | | | 3 |
| AG-TJM-047 | 90/2.5/2.5/5 | 1.045 | 1-1.09 | 1.950 | 1.8-2.055 | | | 3 |
| AG-TJM-048 | 80/5/5/10 | 1.035 | 1-1.07 | 1.935 | 1.77-2.08 | | | 3 |
| AG-TJM-049 | 70/7.5/7.5/15 | 1.020 | 0.97-1.06 | 1.940 | 1.845-2.015 | | | 3 |
| AG-TJM-050 | 60/10/10/20 | 0.920 | 0.88-0.96 | 1.935 | 1.8-2.075 | | | 3 |
| AG-TJM-051 | 0/20/20/60 | 0.940 | 0.89-0.99 | 1.940 | 1.855-2.04 | | | 3 |
| | | | | | | | | |
| PD-CMP-010-C | Type B CPX (Dio)/PLG (Lab) 100/0 45-75 µm | 1.040 | 0.98-1.095 | 2.335 | 2.2-2.435 | | | 3 |
| PL-CMP-147-C | 0/100 | 1.280 | 1.16-1.4 | | | | | 3 |
| MX-CMP-098-C2 | 2/98 | 1.265 | 1.15-1.35 | 2.135 | 1.95-2.3 | | | 3 |
| MX-CMP-099-C2 | 5/95 | 1.070 | 1.025-1.12 | 2.305 | 2.09-2.445 | | | 3 |
| MX-CMP-100-C2 | 7/93 | 1.060 | 1.02-1.105 | 2.320 | 2.125-2.445 | | | 3 |
| MX-CMP-101-C2 | 10/90 | 1.055 | 1.005-1.105 | 2.335 | 2.16-2.425 | | | 3 |
| MX-CMP-102-C2 | 15/85 | 1.050 | 0.99-1.11 | 2.330 | 2.22-2.42 | | | 3 |
| MX-CMP-103-C2 | 25/75 | 1.045 | 0.99-1.095 | 2.335 | 2.215-2.42 | | | 3 |
| MX-CMP-104-C2 | 50/50 | 1.045 | 1-1.08 | 2.335 | 2.225-2.42 | | | 3 |
| | | | | | | | | |
| PE-CMP-030 | Type B CPX/OPX PP-CMP-021/PE-CMP-030 0/100 75-125 µm | 0.910 | 0.86-0.96 | 1.830 | 1.64-2.015 | | | 3, 4 |
| PP-CMP-021 | 100/0 | 1.015 | 0.94-1.1 | 2.265 | 2.12-2.41 | | | 3, 4 |
| XP-CMP-001 | 50/50 | 0.945 | 0.85-1.025 | 1.895 | 1.785-2 | | | 3, 4 |
| XP-CMP-002 | 40/60 | 0.940 | 0.835-1.025 | 1.880 | 1.75-2 | | | 3, 4 |
| XP-CMP-003 | 60/40 | 0.955 | 0.88-1.025 | 1.930 | 1.82-2.04 | | | 3, 4 |
| XP-CMP-004 | 25/75 | 0.920 | 0.86-0.975 | 1.850 | 1.74-1.96 | | | 3, 4 |
| XP-CMP-005 | 75/25 | 0.980 | 0.92-1.04 | 2.230 | 2.17-2.275 | | | 3, 4 |
| XP-CMP-006 | 15/85 | 0.920 | 0.855- | 1.840 | 1.785-1.9 | | | 3, 4 |

| | | | 0.975 | | | | | |
|---|---|---|---|---|---|---|---|---|
| XP-CMP-007 | 85/15 | 0.995 | 0.95-1.045 | 2.255 | 2.15-2.35 | | | 3, 4 |
| XP-CMP-010 | 50/50 <45 µm now | 0.935 | 0.885-0.99 | 1.865 | 1.825-1.915 | | | 3, 4 |
| XP-CMP-011 | 40/60 | 0.925 | 0.88-0.975 | 1.860 | 1.785-1.935 | | | 3, 4 |
| XP-CMP-012 | 60/40 | 0.955 | 0.92-0.99 | 1.890 | 1.805-1.99 | 2.215 | 2.16-2.3 | 3, 4 |
| XP-CMP-013 | 25/75 | 0.920 | 0.87-0.965 | 1.855 | 1.75-1.95 | | | 3, 4 |
| XP-CMP-014 | 75/25 | 0.995 | 0.92-1.06 | 2.250 | 2.175-2.325 | | | 3, 4 |
| XP-CMP-015 | 15/85 | 0.915 | 0.855-0.975 | 1.840 | 1.765-1.925 | | | 3, 4 |
| XP-CMP-016 | 85/15 | 1.000 | 0.95-1.05 | 2.270 | 2.155-2.365 | | | 3, 4 |
| XP-CMP-017 | 75/25 | 0.990 | 0.91-1.065 | 2.250 | 2.15-2.335 | | | 3, 4 |
| XP-CMP-020 | 50/50 45-75 µm now | 0.945 | 0.88-1 | 1.870 | 1.765-1.98 | | | 3 |
| XP-CMP-021 | 40/60 | 0.930 | 0.9-0.955 | 1.850 | 1.785-1.92 | | | 3 |
| XP-CMP-022 | 60/40 | 0.955 | 0.9-1.01 | 1.900 | 1.8-2 | | | 3 |
| XP-CMP-023 | 25/75 | 0.920 | 0.855-0.98 | 1.840 | 1.73-1.955 | | | 3 |
| XP-CMP-024 | 75/25 | 0.980 | 0.92-1.05 | 2.240 | 2.17-2.3 | | | 3 |
| XP-CMP-025 | 15/85 | 0.915 | 0.87-0.955 | 1.835 | 1.775-1.9 | | | 3 |
| XP-CMP-026 | 85/15 | 1.000 | 0.97-1.025 | 2.255 | 2.15-2.345 | | | 3 |
| | | | | | | | | |
| PYX009 | Type A PYX/OLV (Fa10)/PLG (An93) PYX009/OLV003/PLG108 100/0/0 45-90 µm | 0.974 | 0.95-1 | 1.136 | 1.1-1.163 | | | 1 |
| OLV003 | 0/100/0 | 1.054 | 1.01-1.1 | | | | | 1 |
| PLG108 | 0/0/100 | 1.281 | 1.155-1.41 | | | | | 1 |
| BOZ001 | 200 mg/0 mg/20 mg | 0.975 | 0.955-1 | 1.135 | 1.1-1.165 | | | 1 |
| BOZ002 | 200 mg/0 mg/40 mg | 0.977 | 0.96-0.993 | 1.137 | 1.09-1.174 | | | 1 |
| BOZ003 | 200 mg/20 mg/40 mg | 0.987 | 0.977-0.998 | 1.130 | 1.08-1.168 | | | 1 |
| BOZ004 | 200 mg/40 mg/40 mg | 1.112 | 1.054-1.16 | | | | | 1 |
| BOZ005 | 200 mg/60 mg/40 mg | 1.085 | 0.955-1.197 | | | | | 1 |
| BOZ006 | 200 mg/80 mg/40 mg | 1.074 | 0.951-1.2 | | | | | 1 |
| BOZ007 | 200 mg/100 mg/40 mg | 1.069 | 0.954-1.2 | | | | | 1 |
| BOZ008 | 200 mg/200 mg/ 40 mg | 1.061 | 1.014-1.11 | | | | | 1 |

| | | | | 1-1.148 | | | | | | | | 1 |
|---|---|---|---|---|---|---|---|---|---|---|---|---|
| BOZ009 | 200 mg/200 mg/200 mg | | 1.064 | 1.148 | | | | | | | | 1 |

Table 9. Information for remaining endmember samples used in mixtures. Included are comparisons of minima from lowest reflectance, minima from polynomial fittings (McCraig et al. 2017), and minima and centers from the literature. 1= minima from University of Winnipeg Samples Directory from HOSERLab, 2=Cloutis et al. 2006, 3=HOSERLab, 4=RELAB.

| Sample name | Grain size (µm) | Endmember composition | Band I my minimum (µm) | Band I fitting range (µm) | Band II my minimum (µm) | Band II fitting range (µm) | Band I my polynomial (µm) | Band I fitting range (µm) | Band II my polynomial (µm) | Band II fitting range (µm) | Band I literature (µm) | Sources |
|---|---|---|---|---|---|---|---|---|---|---|---|---|
| OLV003 | < 45 | Fo90.4 Fa9.6 | 1.053 | 1-1.1 | | | 1.058 | 1.01-1.1 | | | 1.06 | 1,3 |
| | | | | | | | | | | | 1.06 | 1,3 |
| | 45-90 | | 1.054 | 1-1.2 | | | 1.054 | 1.01-1.1 | | | 1.05 | 1,3 |
| | | | | | | | | | | | 1.06 | 1,3 |
| | | | | | | | | | | | 1.060 | 1,3 |
| | | | | | | | | | | | 1.070 | 2,3 |
| PLG108 | 45-90 | Ab15.2 An84.7 Or0.1 | 1.298 | 1.1-1.4 | | | 1.281 | 1.155-1.41 | | | | 3 |
| PLG122 | 45-90 | Ab7.2 An92.8 Or0.0 | 1.150 | 1-1.38 | | | 1.151 | 1.11-1.21 | | | | 3 |
| AG-TJM-008 | < 45 | Fo90 | 1.055 | 1-1.2 | | | 1.055 | 1.015-1.09 | | | | 4 |
| AG-TJM-009 | < 45 | Hypersthene | 0.920 | 0.8-1 | 1.885 | 1.8-2 | 0.920 | 0.87-0.965 | 1.885 | 1.71-2.065 | | 4 |
| AG-TJM-010 | < 45 | Augite | 1.005 | 0.9-1.1 | 2.265 | 2.2-2.4 | 1.005 | 0.92-1.09 | 2.270 | 2.15-2.4 | | 4 |
| AG-TJM-011 | < 45 | Labradorite | 1.290 | 1.2-1.4 | | | 1.280 | 1.17-1.4 | | | | 4 |
| PD-CMP-010-C | 45-75 | Diopside | 1.040 | 1-1.1 | 2.325 | 2.2-2.4 | 1.040 | 0.98-1.095 | 2.335 | 2.2-2.435 | | 4 |
| PL-CMP-147-C | 45-75 | Labradorite | 1.290 | 1.2-1.4 | | | 1.280 | 1.16-1.4 | | | | 4 |

Table 10. Composition graphs of the available remaining endmember samples used in mixtures. Sources: HOSERLab, RELAB.

| Wt. % | OLV003 | PLG108 | PLG122 | AG-TJM-008-Olivine |
|---|---|---|---|---|
| $SiO_2$ | 40.64 | 46.55 | 44.80 | 40.81 |
| $Al_2O_3$ | tr. | 32.70 | 35.05 | 0.00 |
| FeO | 9.25 | | | 9.55 |
| $Fe_2O_3$ | 0.59 | 0.64 | 0.61 | 0.00 |
| MgO | 49.13 | 0.04 | 0.01 | 49.42 |
| CaO | 0.07 | 17.28 | 18.76 | 0.05 |
| $Na_2O$ | 0.00 | 1.71 | 0.81 | 0.00 |
| $TiO_2$ | 0.00 | 0.05 | 0.05 | 0.00 |
| $Cr_2O_3$ | 0.01 | 0.03 | 0.02 | 0.00 |
| MnO | 0.09 | 0.01 | 0.01 | 0.14 |
| $K_2O$ | 0.00 | 0.02 | 0.00 | 0.00 |

| Wt. % | | | | |
|---|---|---|---|---|
| V$_2$O$_5$ | 0.00 | 0.01 | 0.01 | |
| CoO | 0.04 | 0.03 | 0.04 | |
| NiO | 0.33 | 0.09 | 0.08 | |
| ZrO$_2$ | | | | |
| ZnO | 0.00 | 0.02 | 0.03 | |
| Nb$_2$O$_5$ | | | | |
| P$_2$O$_5$ | | | | |
| SrO | | 0.03 | 0.08 | |
| BaO | | 0.03 | 0.05 | |
| Total | 100.15 | 99.24 | 100.41 | 99.97 |
| **Wt. %** | **AG-TJM-009-Hypersthene** | **AG-TJM-010-Augite** | **AG-TJM-011-Labradorite** | |
| SiO$_2$ | 54.09 | 50.73 | 51.25 | |
| Al$_2$O$_3$ | 1.23 | 8.73 | 30.91 | |
| FeO | 15.22 | 5.37 | 0.15 | |
| Fe$_2$O$_3$ | 0.00 | 1.08 | 0.34 | |
| MgO | 26.79 | 16.65 | 0.14 | |
| CaO | 1.52 | 15.82 | 13.64 | |
| Na$_2$O | 0.05 | 1.27 | 3.45 | |
| TiO$_2$ | 0.16 | 0.74 | 0.05 | |
| Cr$_2$O$_3$ | 0.75 | 0.00 | 0.00 | |
| MnO | 0.49 | 0.13 | 0.01 | |
| K$_2$O | 0.05 | 0.00 | 0.18 | |
| V$_2$O$_5$ | | | | |
| CoO | | | | |
| NiO | | | | |
| ZrO$_2$ | | | | |
| ZnO | | | | |
| Nb$_2$O$_5$ | | | | |
| P$_2$O$_5$ | | | | |
| SrO | | | | |
| BaO | | | | |
| Total | 100.35 | 100.52 | 100.12 | |

Table 11. Lowest reflectance and polynomial fitted minima for the UND mixtures made for this paper. Sources: HOSERLab, McCraig et al. 2017.

| Sample name | Description | Band I my minimum (µm) | Band I fitting range (µm) | Band II my minimum (µm) | Band II fitting range (µm) | Band I polynomial (µm) | Band I fitting range (µm) | Band II polynomial (µm) | Band II fitting range (µm) | Difference Band I (µm) | Difference Band II (µm) |
|---|---|---|---|---|---|---|---|---|---|---|---|
| UND101 | 100/0/0 OLV/PYX/PLG | 1.052 | 1-1.1 | | | 1.054 | 1-1.113 | | | -0.002 | |

| | | | | | | | | | | | |
|---|---|---|---|---|---|---|---|---|---|---|---|
| UND102 | 95/5/0 | 1.053 | 1-1.1 | | | 1.054 | 1-1.113 | | | -0.001 | |
| UND103 | 90/10/0 | 1.056 | 1-1.1 | | | 1.054 | 1-1.113 | | | 0.002 | |
| UND104 | 85/15/0 | 1.051 | 1-1.1 | | | 1.054 | 1-1.113 | | | -0.003 | |
| UND105 | 80/20/0 | 1.051 | 1-1.1 | | | 1.054 | 1-1.113 | | | -0.003 | |
| UND106 | 75/25/0 | 1.051 | 1-1.1 | | | 1.054 | 1-1.113 | | | -0.003 | |
| UND107 | 70/30/0 | 1.055 | 1-1.1 | | | 1.054 | 1-1.113 | | | 0.001 | |
| UND108 | 60/40/0 | 1.051 | 1-1.1 | | | 1.055 | 1-1.115 | | | -0.004 | |
| UND109 | 50/50/0 | 1.056 | 1-1.1 | | | 1.055 | 0.97-1.152 | | | 0.001 | |
| UND110 | 0/100/0 | 0.964 | 0.9-1 | 1.131 | 1.05-1.2 | 0.963 | 0.944-0.985 | 1.13 | 1.08-1.17 | 0.001 | 0.001 |
| UND111 | 10/90/0 | 0.977 | 0.9-1 | 1.1 | 1.05-1.2 | 0.98 | 0.965-1 | 1.104 | 1.075-1.134 | -0.003 | -0.004 |
| UND112 | 20/80/0 | 1.085 | 0.9-1.2 | | | 1.059 | 0.9-1.23 | | | 0.026 | |
| UND113 | 30/70/0 | 1.067 | 0.9-1.2 | | | 1.06 | 0.95-1.171 | | | 0.007 | |
| UND114 | 40/60/0 | 1.052 | 0.9-1.2 | | | 1.053 | 0.93-1.2 | | | -0.001 | |
| UND115 | 85/5/10 | 1.051 | 1-1.1 | | | 1.054 | 1-1.112 | | | -0.003 | |
| UND116 | 80/10/10 | 1.051 | 1-1.1 | | | 1.053 | 1-1.111 | | | -0.002 | |
| UND117 | 75/15/10 | 1.051 | 1-1.1 | | | 1.053 | 1-1.111 | | | -0.002 | |
| UND118 | 70/20/10 | 1.056 | 1-1.1 | | | 1.054 | 1-1.113 | | | 0.002 | |

## 3. Angrite Samples

Table 12. Lowest reflectance minima for the angrite spectra looked at in this paper. 1=RELAB, 2=Burbine et al. 2001, 3=Duffard et al. 2005.

| Sample name | Description | Band I minimum (µm) | Band I fitting range (µm) | Band II minimum (µm) | Band II fitting range (µm) | Source |
|---|---|---|---|---|---|---|
| MR-MJG-103 | Angra dos Reis bulk | 0.970-0.975 | 0.8-1.1 | 2.177-2.187 | 2.1-2.4 | 1 |
| | | 0.955-0.960 | 0.8-1.1 | 2.160-2.170 | 2.1-2.4 | 1 |
| MT-TJM-010 | LEW86010 < 74 µm | 1.050 | 1-1.2 | 2.250 | 2.2-2.4 | 1 |
| TB-TJM-057 | Sahara 99555 < 125 µm | 1.090 | 1-1.2 | 2.160 | 2.1-2.3 | 1, 2, 3 |
| TB- | D'Orbigny < | 1.100 | 1-1.2 | 2.100 | 2.1-2.3 | 1, 2, 3 |

| | | | | | |
|---|---|---|---|---|---|
| TJM-062 | 125 µm | | | | |
| TB-TJM-119 | Angra dos Reis | 0.980 | 0.9-1.1 | 2.250 | 2.2-2.4 | 1 |

Table 13. Angrite samples with band centers in the literature. 1=RELAB, 2=Burbine et al. 2001, 3=Duffard et al. 2005.

| Sample name | Description | Band center (µm) | Source |
|---|---|---|---|
| TB-TJM-057 | Sahara 99555 < 125 µm | 1.125 | 1,2,3 |
| TB-TJM-062 | D'Orbigny < 125 µm | 1.14 | 1,2,3 |

Table 14. Polynomial fitted minima for the angrite samples looked at in this paper. 1=RELAB, 2=Burbine et al. 2001, 3=Duffard et al. 2005. Source for the fitting: McCraig et al. 2017.

| Sample name | Description | Band I minimum (µm) | Band I fitting range (µm) | Band II minimum (µm) | Band II fitting range (µm) | Source |
|---|---|---|---|---|---|---|
| MR-MJG-103 | Angra dos Reis bulk | 0.965 | 0.9-1.041 | 2.177 | 2.047-2.327 | 1 |
| | | 0.945 | 0.9-1.005 | 2.165 | 2.01-2.33 | 1 |
| MT-TJM-010 | LEW86010 < 74 µm | 1.040 | 0.97-1.12 | 2.230 | 2.13-2.34 | 1 |
| TB-TJM-057 | Sahara 99555 < 125 µm | 1.080 | 0.99-1.18 | | | 1, 2, 3 |
| TB-TJM-062 | D'Orbigny < 125 µm | 1.100 | 1-1.19 | | | 1, 2, 3 |
| TB-TJM-119 | Angra dos Reis | 0.990 | 0.93-1.03 | 2.230 | 2.06-2.39 | 1 |

Table 15. Available composition graph for one angrite sample. Source: RELAB.

| Sample | MR-MJG-103 - Angra dos Reis |
|---|---|
| $SiO_2$ | 44.64 |
| $Al_2O_3$ | 9.85 |
| FeO | 8.10 |

| | |
|---|---|
| Fe$_2$O$_3$ | 0.00 |
| MgO | 11.40 |
| CaO | 23.30 |
| Na$_2$O | 0.04 |
| TiO$_2$ | 2.30 |
| Cr$_2$O$_3$ | 0.29 |
| MnO | 0.08 |
| Total | 100.00 |